Nonlinear Control and Stability Analysis of Multi-Terminal High Voltage Direct Current Networks

Yijing Chen

Université Paris-Sud

Ecole Doctorale Sciences et Technologies de l'Information, des Télécommunications et des Systèmes (ED STITS)

Laboratoire des Signaux et Systèmes (L2S)

Discipline : Automatique

Thèse de doctorat

Soutenue: le 8 Avril 2015 par

Yijing Chen

Commande Nonlinéaire et Analyse de Stabilité de Réseaux Multi-Terminaux Haute Tension à Courant Continu

(Nonlinear Control and Stability Analysis of Multi-Terminal High Voltage Direct Current Networks)

Composition du jury :

Directeur de thèse	Dr. Françoise LAMNABHI-LAGARRIGUE	Directeur de Recherche, CNRS & L2S
Co-directeur de thèse :	Dr. Gilney DAMM	Maître de Conférences, HDR Université d'Evry-Val-d'Essonn & L2S
	Dr. Abdelkrim BENCHAIB	Ingénieur de Recherche, HDR, Alstom
Rapporteurs :	Dr. Anuradha ANNASWAMY	Senior Research Scientist Massachusetts Institute of Technology
	Prof. Fouad GIRI	Université de Caen Basse-Normandie
Examinateurs	Prof. Alain GLUMINEAU	Ecole Centrale de Nantes
	Prof. Didier GEORGES	ENSE3
	Prof. Riccardo MARINO	Università di Roma Tor Vergata

Acknowledgments

My deepest gratitude is to my three thesis supervisors, Dr. Françoise LAMNABHI-LAGARRIGUE, Dr. Gilney DAMM and Dr. Abdelkrim BENCHAIB, for their guidance, advices and assistance. It is my greatest pleasure to work with them. Thanks a lot to Dr. Gilney DAMM for his unremittingly invaluable guidance and comprehensive assistance. He is always ready to help me whenever I had scientific or personal difficulties. He usually shared his experience with me and gave me constant advice in research and career orientation. He never put undue pressure on me. It was really a great chance to work with him. Thanks a lot to Dr. Abdelkrim BENCHAIB for offering invaluable advice from the point view of industry. After every discussion with him, I acquired a greater depth of understanding of my thesis work. Thanks a lot to Dr. Françoise LAMNABHI-LAGARRIGUE who admitted me as a Ph.D. candidate in L2S. She helped me a lot to deal with all the administrative trivial things. She always tried her best to build a convivial ambiance for work. With her support and trust, my Ph.D. years have become a pleasant life journey.

I would like to thank the members of the jury, Dr. Anuradha ANNASWAMY, Prof. Fouad GIRI, Prof. Alain GLUMINEAU, Prof. Riccardo MARINO and Prof. Didier GEORGES, for their comments, questions and suggestions. Special thanks to Dr. Anuradha ANNASWAMY and Prof. Fouad GIRI, who spent a lot of time and effort to review my thesis and gave advice to improve my work. Thanks a lot to Dr. Anuradha ANNASWAMY who warmly hosted me during my visit to the active adaptive control laboratory (AACLAB) at Massachusetts Institute of Technology (MIT). She introduced me to the domain of adaptive control which is a powerful tool to solve the system uncertainties. Thanks to this visit, I have the opportunity to meet researchers in the Department of Mechanical Engineering and discussed with them to expand my knowledge.

I am indebted to the former and the current faculty, personnel, Ph.D. students from L2S, who constantly helped me. Special thanks to Jing DAI who used to be a post-doc in L2S. He helped me to correct many bad writing habits when I wrote my first paper. He also gave me lots of comments and suggestions on my dissertation and other papers. I will always remember that even during the Christmas holiday, he still corrected my dissertation and gave me feedbacks. Many thanks to Miguel Jiménez Carrizosa for discussing with me. In fact, I did not take many courses in the field of electrical engineering during my undergraduate and master study. Miguel shared his professional knowledge of electrical engineering. I also want to thank Fernando DORADO NAVAS, Mawulikplimi Komlan Crédo PANIAH, Van Cuong NGUYEN, Alessio Iovine, Alexandre Azevedo, Yujun HE $\cdots$ for their helpful discussions. I would like to thank Mme. Maryvonne GIRON and Mme. Laurence ANTUNES for helping me a lot to handle the visa paper work and renew of my "titre de séjour ". I am grateful to my dear friends, Yuling ZHENG, Long CHEN, Chuan XU, Zheng CHEN $\cdots$. I shall evermore cherish the memory that we played badminton together.

Last, my deepest gratitude is undoubtedly to my families who are always beside me and support me. I want to thank my father, my oldest friend, who always supported and encouraged me; my mother who always prayed for me and my sister who always comforted me and straightened me out when I encountered unhappy things. I'm so thankful that I have such wonderful families.

Abstract

Nowadays the world total electricity demand increases year by year while the existing alternating current (AC) transmission grids are operated close to their limits. As it is difficult to upgrade the existing AC grids, high voltage direct current (HVDC) is considered as an alternative solution to several related problems such as: the increase of transmission capability; the interconnection of remote and scattered generation from renewable energy sources (in particular offshore); the interconnection of different asynchronous zones. At present, over one hundred direct current (DC) transmission projects exist in the world, the vast majority for two-terminal HVDC transmission systems and only three for multi-terminal HVDC systems. The traditional two-terminal HVDC transmission system can only carry out point-to-point power transfer. As the economic development and the construction of the power grid require that the DC grid can achieve power exchanges among multiple power suppliers and multiple power consumers, multi-terminal voltage-sourced converter HVDC (MTDC) systems draw more and more attention. As a DC transmission network connecting more than two converter stations, an MTDC transmission system offers a larger transmission capacity than the AC network and also provides a more flexible and efficient transmission method. Most studies in the field of MTDC systems have involved an empirical control approach, namely, vector control approach consisting of several standard proportional-integral (PI) controllers. This control concept is mainly based on the assertion that the system state variables exhibit the performances with different dynamics. However, very rare relevant work has ever presented a theoretically detailed explanation on the validity and the implications of this assertion in the literature.

The research work in this dissertation was started with the intention of filling some gaps between the theory and the practice, in particular: 1) to investigate various control approaches for the purpose of improving the performance of MTDC systems; 2) to establish connections between existing empirical control design and theoretical analysis; 3) to improve the understanding of the multi-time-scale behavior of MTDC systems characterized by the presence of slow and fast transients in response to external disturbances.

The main contributions of this thesis work can be put into three areas, namely nonlinear control design of MTDC systems, analysis of MTDC system's dynamic behaviors and application of MTDC systems for frequency control of AC systems.

In the area of nonlinear control design of MTDC systems, based on different nonlinear control design techniques, new control schemes have been proposed with corresponding theoretical analysis. Besides, the developed control algorithms have been tested by numerical simulations, whose performances are evaluated in comparison to the performance of the conventional vector control method.

The main motivation for the topic on analysis of MTDC system's dynamic behav-

iors is the desire to provide a rigorous theoretical demonstration on the assertion that part of system states' dynamics are much faster than the rest. As a consequence, it is possible to simplify the control design procedure. The contribution in this area consists of three parts: 1) control induced time-scale separation for a class of nonlinear systems; 2) analysis of time-scale separation for an MTDC system with master-slave control configuration; 3) analysis of time-scale separation for an MTDC system with droop control configuration. Theoretical analysis, mainly based on singular perturbation and Lyapunov theories, have been carried out for each of the aforementioned aspects and confirmed by various simulation studies. The study of the first part has been mostly dedicated to propose a time-scale separation control method which can drive a class of nonlinear systems to exhibit a multi-time-scale performance. The theoretical results obtained from the first part have been applied to investigate the dynamic behaviors of MTDC systems where the two main control configurations, i.e. master-slave and droop control configurations, are considered. Empirical vector current control designs have been proposed for each control configuration. Theoretical explanations and fundamental analysis indicate that with the proposed empirical control algorithms, the inductor currents indeed exhibit a dynamic behavior with different dynamics. Furthermore, we have provided more details on how and why these empirical vector current control designs work as well as the rules of tuning the control parameters.

The final contribution relates to the application of MTDC systems where frequency support strategy using MTDC systems has been introduced and analyzed. The principle of the frequency control is to regulate the AC frequency by modulating each AC grid's scheduled (or prescribed) active power. A DC-voltage-based control scheme for the AC frequency regulation is proposed, which achieves the objective of sharing primary reserves between different AC areas interconnected via an MTDC system without using remote information communication.

Contents

List of Abbreviations

AC	Alternating current
CCC	Capacitor-commutated converter
DC	Direct current
DFIG	Doubly fed induction generator
DPC	Direct power control
GTO	Gate turn-off thyristor
HVDC	High voltage direct current
IGBT	Insulated-gate bipolar transistor
IGCT	Integrated gate-commutated thyristor
LCC	Line-commutated current source converter
LMI	Linear matrix inequality
MI	Mineral-insulated
MMC	Modular multilevel converter
MTDC	Multi-terminal voltage-sourced converter high voltage direct current
PCC	Point of common coupling
PI	Proportional-integral
PLL	Phase-locked loop
PWM	Pulse-width modulation
RMS	Root mean square
SAC	Strong AC network
SCR	Short circuit ratio
SRF-PLL	Three-phase synchronous reference frame phase-locked loop
TSO	Transmission system operator
VSC	Voltage-sourced converter
WAC	Weak AC network
XLPE	Cross-linked polyethylene

Liste des Abréviations

AC	Courant alternatif
CCC	Convertisseur de condensateurs à commutation
DC	Courant continu
DFIG	Générateur d'induction à double alimentation
DPC	Contrôle direct de la puissance
GTO	Thyristor à extinction par la gâchette
HVDC	Courant continu haute tension
IGBT	Transistor bipolaire à grille isolée
LCC	Convertisseurs commutés par les lignes
LMI	Inégalité matricielle linéaire
MMC	Convertisseurs multi-niveaux modulaire
MTDC	Réseau multiterminal à courant continu
PCC	Point de couplage commung
PI	Proportionnel intégral
PLL	Boucle à phase asservie
PWM	Modulation de largeur d'impulsion
RMS	Moyenne quadratique
SAC	Réseau AC fort
SCR	Rapport de court-circuit
TSO	Gestionnaire de réseau de transport
VSC	Convertisseurs en source de tension
WAC	Réseau AC faible
XLPE	Polyéthylène réticulé

List of Symbols

t	Time
τ	Time variable for fast dynamics
ε	Small scalar to qualify the time scales
L_{g_i}	i^{th} SAC connected VSC terminal's phase reactor inductance
R_{g_i}	i^{th} SAC connected VSC terminal's phase reactor resistance
f_{g_i}	Frequency of the i_{th} SAC at the PCC
V_{rms,g_i}	AC voltage magnitude of the i_{th} SAC at the PCC
$v_{sg_i,dq}$	$d-$ and $q-$ axis AC voltage of the i^{th} SAC at the PCC
$v_{sg_i,abc}$	$a-$, $b-$ and $c-$ axis AC voltage of the i^{th} SAC at the PCC
$v_{cg_i,dq}$	$d-$ and $q-$ axis AC voltage of the i^{th} SAC at the converter side
$v_{cg_i,abc}$	$a-$, $b-$ and $c-$ axis AC voltage of the i^{th} SAC at the converter side
$i_{g_i,dq}$	$d-$ and $q-$ axis phase reactor current of the i^{th} SAC
$i_{g_i,abc}$	$a-$, $b-$ and $c-$ axis phase reactor current of the i^{th} SAC
P_{g_i}	Active power of the i^{th} SAC at the PCC
Q_{g_i}	Reactive power of the i^{th} SAC at the PCC
ω_{g_i}	i^{th} SAC system's pulsation
δ_{g_i}	Phase angle of the i^{th} SAC connected VSC
m_{g_i}	Modulation ratio of the i^{th} SAC connected VSC
$m_{g_i,dq}$	$d-$ and $q-$ axis modulation index of the i^{th} SAC connected VSC
i_{cg_i}	DC current flowing from the i^{th} SAC connected VSC
R_{equi}, g_i	Equivalent resistance representing the i^{th} SAC connected VSC's loss
L_{w_j}	j^{th} WAC connected VSC terminal's phase reactor inductance
R_{w_j}	j^{th} WAC connected VSC terminal's phase reactor resistance
f_{w_j}	Frequency of the j_{th} WAC at the PCC
C_{fw_j}	j^{th} WAC connected VSC terminal's filter capacitance
V_{rms,w_j}	AC voltage magnitude of the j_{th} WAC at the PCC
$v_{sw_j,dq}$	$d-$ and $q-$ axis AC voltage of the j^{th} WAC at the PCC
$v_{sw_j,abc}$	$a-$, $b-$ and $c-$ axis AC voltage of the j^{th} WAC at the PCC
$v_{cw_j,dq}$	$d-$ and $q-$ axis AC voltage of the j^{th} WAC at the converter side
$v_{cw_j,abc}$	$a-$, $b-$ and $c-$ axis AC voltage of the j^{th} WAC at the PCC
$I_{w_j,dq}$	$d-$ and $q-$ axis controlled current source of the j^{th} WAC network
$i_{w_j,dq}$	$d-$ and $q-$ axis phase reactor current of the j^{th} WAC
$i_{w_j,abc}$	$a-$, $b-$ and $c-$ axis phase reactor current of the j^{th} WAC
P_{w_j}	Active power of the j^{th} WAC at the PCC
Q_{w_j}	Reactive power of the j^{th} WAC at the PCC
ω_{w_j}	j^{th} WAC system's pulsation
δ_{w_j}	Phase angle of the j^{th} WAC connected VSC
m_{w_j}	Modulation ratio of the j^{th} WAC connected VSC

$m_{w_j,dq}$	$d-$ and $q-$ axis modulation index of the j^{th} WAC connected VSC
i_{cw_j}	DC current flowing from the j^{th} WAC connected VSC
R_{equi}, w_j	Equivalent resistance representing the j^{th} WAC connected VSC's loss
C_{g_i}	i^{th} SAC converter node's capacitance
C_{w_j}	j^{th} WAC converter node's capacitance
C_{t_h}	h^{th} intermediate node's capacitance
i_{c_k}	k^{th} transmission line's branch current
R_{c_k}	k^{th} transmission line's resistance
L_{c_k}	k^{th} transmission line's inductance
i_c	Transmission branch circuit current vector: $i_c = [i_{c_1} \ \cdots \ i_{c_L}]^T$
u_{cg_i}	DC voltage of the i_{th} SAC converter node
u_{cw_j}	DC voltage of the j_{th} WAC converter node
u_{ct_h}	DC voltage of the h_{th} intermediate node
u_{cg}	DC voltage vector: $u_{cg} = [u_{cg_1} \ \cdots \ u_{cg_N}]^T$
u_{cw}	DC voltage vector: $u_{cw} = [u_{cw_1} \ \cdots \ u_{cw_M}]^T$
u_{ct}	DC voltage vector: $u_{ct} = [u_{ct_1} \ \cdots \ u_{ct_P}]^T$
u_c	DC voltage vector: $u_c = [u_{cg} \ u_{cw} \ u_{ct}]^T$
z	State variables of the DC grid: $z = [u_c \ i_c]^T$
$u_{c,\min}$	Acceptable minimum value of the DC voltage
$u_{c,\max}$	Acceptable maximum value of the DC voltage
S_{rate}	Rated apparent power of the converter
u_{rate}	Rated DC voltage of the transmission lines
H	Incidence matrix of the weakly connected directed graph that maps to the topology of the DC network
C	Capacitance matrix: $C = \text{diag}(C_{g_1} \cdots C_{g_N} \ C_{W_1} \cdots C_{W_M} \ C_{t_1} \cdots C_{t_P})$
L	Inductance matrix: $L = \text{diag}(L_{c_1} \cdots L_{c_L})$
R	Inductance matrix: $R = \text{diag}(R_{c_1} \cdots R_{c_L})$
N	Number of SAC nodes
M	Number of WAC nodes
P	Number of intermediate nodes
L	Number of branch circuits
$\mathcal{N}$	Set $\mathcal{N} = \{1, \cdots, N\}$
$\mathcal{N}_{-1}$	Set $\mathcal{N}_{-1} = \{2, \cdots, N\}$
$\mathcal{M}$	Set $\mathcal{M} = \{1, \cdots, M\}$
$\mathcal{P}$	Set $\mathcal{P} = \{1, \cdots, P\}$
$\mathcal{L}$	Set $\mathcal{L} = \{1, \cdots, L\}$
$\mathcal{T}$	Set $\mathcal{T} = \{1, \cdots, N+M+P\}$
i	Index $i \in \mathcal{N}$
ρ	Index $\rho \in \mathcal{N}_{-1}$
j	Index $j \in \mathcal{M}$
h	Index $h \in \mathcal{P}$
k	Index $k \in \mathcal{L}$
V_i	i^{th} AC area's DC voltage
P_i^{dc}	i^{th} AC area's DC power injection

R_{ik}	Resistance of the transmission line between the i^{th} and the k^{th} AC areas
P_{m_i}	i^{th} AC area's mechanical power input
J_i	i^{th} AC area's moment of inertia
D_{g_i}	i^{th} AC area's damping factor of the aggregated generator
f_i	i^{th} AC area's frequency
$f_{\text{nom},i}$	i^{th} AC area's nominal frequency
P_{l_i}	i^{th} AC area's load
$T_{sm,i}$	i^{th} AC area's time constant of the servomotor
$P^s_{m_i}$	i^{th} AC area's scheduled mechanical power input
$P_{\text{nom},i}$	i^{th} AC area's nominal mechanical power input
σ_i	i^{th} AC area's generator droop

List of Figures

List of Tables

Chapter 1

Introduction

Contents

This thesis was devoted to the study of Multi-Terminal High Voltage Direct Current networks. The main contributions were in the field of nonlinear automatic control, applied to power systems, power electronics and renewable energy sources. In the current chapter, we first give a general introduction to HVDC technology where its advantages and disadvantages are analyzed. Then, we present the related research work on the control of HVDC. Finally, we elaborate the objectives and the contributions of this dissertation.

1.1 History and background

Direct current (DC) technology was introduced at a very early stage in the field of power systems. The first long-distance electrical energy transmission line was built using DC technology between Miesbach and Munich in Germany in 1882. Since the power losses in the transmission lines are proportional to the square of the current flowing through the conductors, electrical power is usually transmitted at a high voltage level so as to reduce these power losses. In the early days, due to technical limitations, it was difficult and uneconomic to convert the DC voltage between the

low voltage level for consumer's use and the high voltage level for transmission. In alternating current (AC) system, thanks to the invention of AC transformer, it is possible to convert the AC voltage between different levels in a simple and economic way. In addition, a three-phase AC generator is superior to a DC generator in many aspects. For example, the AC generator is more efficient, has a much simpler structure with lower cost and requires easier maintenance. Because of these reasons, AC technology has become dominant in the areas of power generation, transmission and distribution. Although AC provides many benefits, it still has some limitations in practice, mainly in the following aspects [Siemens 2005, Andersen 2002]. :

- The efficiency of power transmission capacity is subject to the capacitive and inductive effects of underground/undersea cables or AC overhead transmission lines. For a long AC transmission system, the current that flows to charge the line (or cable) capacitance could be remarkable, causing a significant amount of energy losses as heat in the wires.

- It is impossible to connect unsynchronized AC networks via an AC transmission link. The latter is only suitable for the connection between synchronized AC networks with the same frequency where the phase difference between these synchronized AC networks is also restricted to certain allowable range.

- AC transmission technology is not a very good choice for integrating massive renewable energy sources into the existing electrical grid. In particular, since the renewable generation outputs are usually intermittent (for example, the energy production of wind farms strongly depends on the wind speed), the power variations seriously affect the AC voltage at the point of common coupling (PCC) when the renewable power occupies a significant share of the total electricity generation.

- For offshore applications, what implies the use of cables instead of overhead lines, the well known limitations of using AC is very expensive while DC is not concerned by these problems.

People have been therefore making efforts to find a satisfactory alternative to AC transmission technology. In the past decades, significant advances have been achieved in the development of high power devices [Long 2007]. This has provided beneficial conditions for DC technology which could come again in sight in the application of power transmission after years of silence.

The invention of mercury-vapor valves which could convert AC current to DC current appeared in 1901 and made HVDC transmission possible [Rudervall 2000]. Several experiments with mercury-arc valves for DC power transmission have been carried out in America and Europe before 1940. In 1941, a commercial HVDC system was designed for supplying Berlin in Germany via a 115 km buried cable using mercury-arc valves. However, it was never put in operation because of the war. The first commercial HVDC transmission used to connect the mainland of Sweden and the island of Gotland was put into service in 1954. Here, we also pay tribute to

the father of HVDC, Uno Lamm, who made a significant contribution towards the application of HVDC in practice [Wollard 1988, Lamm 1966]. Since then, several HVDC transmission systems have been built with mercury arc valves up to 1972, the installation of the last mercury-arc HVDC system in Manitoba, Canada. The solid state semiconductor valves (thyristor valves) first appeared in 1970, and then soon replaced the mercury-arc valves [Karady 1973]. Thyristor valves have many advantages over mercury-arc valves. For example, it is easy to increase the voltage just by connecting thyristors in series. The first HVDC system using thyristor valves were put into operation in 1972. Today, most of existing HVDC projects are still based on thyristor valves [Asplund 2007, Varley 2004]. Since mercury-arc valves and thyristors can not achieve the operation of turn-off by themselves, both of them need an external AC circuit to force the current to zero and hence, the converters based on these two valves are known as line-commutated converters (LCCs) [Daryabak 2014]. During the conversion process of LCCs, the converters need to consume the reactive power which is usually supplied by the AC filters or series capacitors embedded in the converter station [Bahrman 2007]. In the late 1990's, capacitor-commutated converters (CCCs) were introduced where capacitors in series connected between the thyristors and the transformers are used to provide the reactive power. The first CCC based HVDC system was built in 1998 used to connect Argentina and Brazil. In fact, CCCs have not been widely applied in the construction of HVDC systems because of the advent of new power electronics in the mid 1990's. The development of high rated semiconductor devices such as integrated gate-commutated thyristors (IGCTs), insulated-gate bipolar transistors (IGBTs), gate turn-off thyristors (GTOs) etc. has marked the beginning of a new era in the area of HVDC systems [Andersen 2000, Poullain 2001, Flourentzou 2009, Andersen 2000]. The IGBT differs from thyristor in that it has the ability to turn off by itself, which can be used to make self-commutated converters. Converters built with IGBTs are known as voltage-sourced converters (VSCs). The first complete VSC HVDC system was built in Gotland, Sweden, 1999 [Eriksson 2001]. Since then, many VSC HVDC systems have been put into operation [Asplund 2000, Johansson 2004, Stendius 2006, Dodds 2010]. The recent first three-terminal VSC HVDC system operated by China Southern Power Grid has been put into service at the end of 2013, which is used to feed wind power generated from Nanao island into the mainland of Guangdong via a combination of underground cables, submarine cables and overheard lines [Li 2014, Fu 2014].

1.2 Overview of HVDC technology

The most essential process in an HVDC system is the conversion of the energy between AC and DC. The converter station located at the sending end is called the rectifier (to convert the current from AC to DC) while the one at the receiving end is called the inverter (to convert the current from DC to AC). As mentioned in Section 1.1, there are two basic converter technologies in today's HVDC transmission

systems, LCC and VSC.

1.2.1 Line-commutated current source converters

Conventional (or classical) HVDC systems are based on LCCs with thyristor valves which are used to achieve the operation of converting the current between AC and DC [Carlsson 2003, Carlsson 2002, Varley 2004, CIGRE 2014]. The essential component of LCCs is the three-phase or six-pulse bridge composed of six controlled switches or thyristor valves. In order to operate at the desired voltage rating, the thyristors are usually connected in series to build up a suitable thyristor valve. The drawback of the six-pulse bridge is that considerable AC current and DC voltage harmonics are produced due to each phase change every 60°. To deal with this problem, two six-pulse bridges are connected in series to constitute a twelve-pulse bridge. In this manner, with each of the two six-pulse bridges connected to one DC rail, the 30° phase displacement can be achieved so that some harmonics can be eliminated. In fact, the twelve-pulse bridge has become dominant in modern LCC HVDC systems.

Since LCC can not be turned off by itself, an external relatively strong AC voltage source is required to perform the commutation. As a result, it is impossible to change the direction of the current. In an LCC HVDC system, in order to change the power direction, it is necessary to change the polarity of the output voltage. This leads to inherent difficulty when a weak AC system or a passive network is connected to an LCC converter station. As a controlled solid-state semiconductor device, the thyristor can only be turned on by control action and hence, LCC has one degree of freedom, i.e. the firing angle, which represents the phase lag of AC current behind the voltage. The only way to regulate the DC voltage rating across a valve is by means of controlling the firing angle. More details of the control of firing angle are well documented in the literature [Arrillaga 1998, Kimbark 1971, CIGRE 2014].

1.2.2 Voltage-sourced converters

Voltage-sourced converter is built up with fully controlled semiconductor devices such as IGBT and GTO with the ability of turn-off compared to LCC [Flourentzou 2009, Dodds 2010, Wang 2011]. As a result, an external AC voltage is no longer required since the converter based on IGBTs (or GTOs) are self-commutated. The additional controllability (the operation of turn-off) gives many advantages to the VSC:

- Pulse-width modulation (PWM) can be applied to the operation of VSC, which works at higher frequencies than the line frequency and gives rise to high dynamic performance [Trzynadlowski 1996]. With PWM, the VSC can generate any voltage with desired phase angle and amplitude. Less harmonics are produced compared to LCC with PWM.

- Because the AC current always lags behind the voltage in the operation of LCC, the converter needs to consume the reactive power to keep the amplitude

of AC voltage within acceptable range, while the VSC itself has no reactive power need. Therefore, it is flexible to place the VSCs anywhere in the AC system.

- Unlike LCC, a strong AC voltage source is not indispensable for the VSC connected AC system and hence, there is no restriction on the inherent characteristics of the connected AC networks.

- Since the VSC possesses two degrees of freedom, this converter has the ability to control active and reactive power independently. This capability makes the VSC act close to an ideal generator in a transmission network.

- The bidirectional power transmission can be achieved with the VSC by changing the current direct without changing the output voltage polarity.

More details of the operation of VSCs are presented in Section 2.

1.2.3 LCC vs VSC

Although the capability of turn-off produces many benefits for the VSC, it does not mean that VSC can replace LCC. Both of the two converters are applied in modern HVDC systems and they have their respective merits that meet different requirements [Marques 2011, Rudervall 2000]:

- In recent years, significant advances and improvements in the thyristor technology have been achieved. In particular, the thyristor has a large capacity that can withstand high voltage (up to 10 kV) and high current (4 kA) ratings. Therefore, there is no special restriction on the power range of HVDC with LCC since very high voltages can be achieved by connecting the thyristors in series. Besides, the inductive and capacitive elements of the transmission lines have no effect on the HVDC with LCC and hence, the power losses caused by these elements do not limit the transmission distance. For these reasons, LCC HVDC system is well established for long-distance bulk power transmission.

- VSC-HVDC technology is mainly used in medium-capacity power transmission based upon the considerations: 1) Unlike the thyristor, the IGBT has a limit capacity with weak overload capability; 2) Due to the use of PWM at high frequency, the switching losses of the VSC HVDC are higher than the LCC HVDC. 3) A VSC HVDC system usually uses a special cross-linked polyethylene (XLPE) cable which has a lower voltage capability compared to the mineral-insulated (MI) cable used in LCC HVDC system.

- A VSC HVDC system can be used to supply the electrical power to passive or weak AC networks with low short-circuit capacity. Since the semiconductor devices used in the VSC are self-commutating, for the connected AC system, a strong AC voltage source is not necessary.

- At present, the vast majority of existing HVDC links are composed of two converter stations, only carrying out point-to-point power transfer. As the economic development and the construction of the power grid require that the DC grid can achieve power exchanges between multiple power suppliers and multiple power consumers, multi-terminal HVDC system consisting of more than two converter stations have drawn more and more attention. VSC HVDC technology is more appropriate than LCC HVDC to build a multi-terminal HVDC system because of the following reasons: 1) For the LCC HVDC, the only way of reversing the power direction is to change the DC voltage polarity. However, in a multi-terminal HVDC system, the reversal of one terminal's DC voltage polarity gives remarkable disturbances to other terminals and hence, it is essential to arrange the switching operation of each terminals [Reeve 1980]. 2) For the VSC HVDC, the power direction can be changed through the reversal of the current direction while keeping the DC voltage polarity unchanged. Therefore, one terminal's power direction can be changed without considering other terminal's power flow directions.

1.2.4 Advantages of HVDC over AC

As discussed in Section 1.1, the inherent drawbacks of AC encourage the development of DC technology. The rationale for the choice of HVDC instead of AC is often various and complex. The common applications in favor of HVDC are listed as follows:

- **Long-distance transmission:**

  For an AC transmission, the capacitive effect of long overhead lines not only causes the additional power losses but also limits the transmission distance while it has less impact on the HVDC transmission line. For these reasons, HVDC technology provides bulk power transmission solution over very long distances. From economic aspects, the costs of an HVDC transmission line are less that an AC line for the same distance but the construction of a converter station is expensive. A famous diagram as illustrated in Fig. 1.1 shows a typical cost analysis for AC and DC [SIEMENS 2014]. Above the break-even distance, the HVDC transmission line becomes an attractive solution with less costs in comparison to an AC transmission line with the same power capacity. Moreover, DC overhead lines occupy much less space than AC transmission lines with the same power capacity. This reduces the visual impact and the usage of rights-of-way. Therefore, it is possible to realize the power delivery from remote power resources such as offshore wind farms or hydro-power plants using lower visual impact and fewer transmission lines with HVDC.

- **Underground or submarine transmission:**

  From the environment aspects, it is hard to upgrade the electrical grid with overhead AC lines which require large transmission line corridors. It is recommended to use underground cables that can share rights-of-way with other

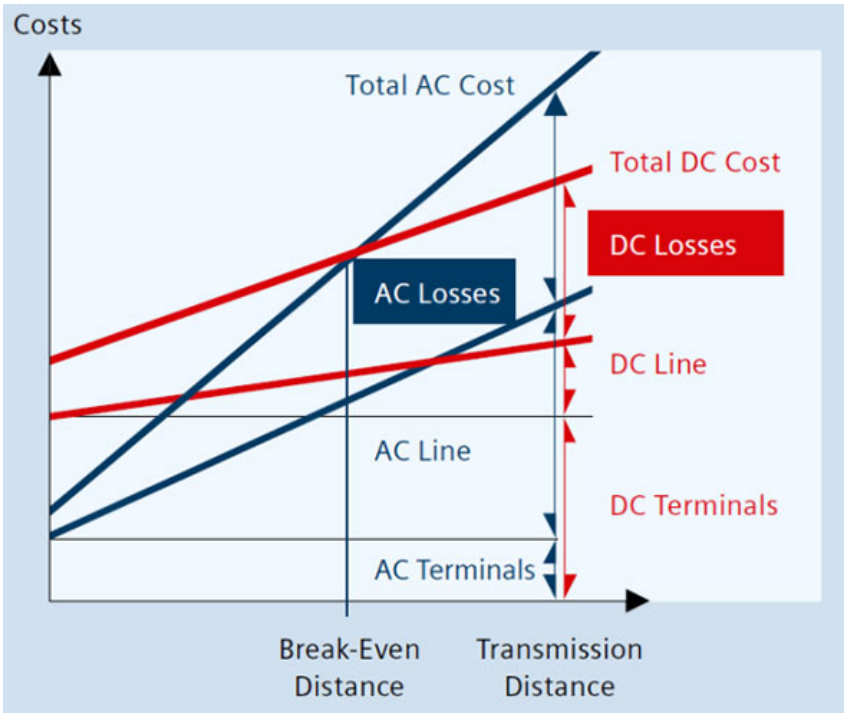

Figure 1.1: AC versus DC cost.

utilities. As discussed above, the main drawback of underground or submarine cable systems with AC lines is the remarkable power losses and transmission distance limits caused by the capacitive effect. The VSC HVDC system with XLPE cables provides a more flexible, efficient and reliable way to carry out the power transfer via long-distance underground or submarine transmission.

- **Asynchronous connection:**

  HVDC technology is the only way that can connect AC networks with different frequencies. The advantage of this application is that a disturbance in one AC area does not affect another, and thus the HVDC link can play the role of a firewall to prevent cascading failure. In addtion, in an asynchronous connection, back-to-back configuration is often used without transmission lines to achieve power exchange.

- **Renewable power transmission:**

  Due to environmental issues and the need to meet the increasing demand of electricity, the development of renewable energy, which comes from continually regenerated resources such as sunlight, wind, tides and waves, is promoted to achieve sustainability. In 2011, about 19% of worldwide electricity generation came from renewable energy, with 19% from hydroelectricity and 3% from other renewable sources such as wind, sun and biomass [Network 2012].

Renewable power generators are spreading across many countries and especially, wind power already occupies a significant share of electricity in Europe, Asia and the United States. At the end of 2012, wind power grew at an annual rate of 30% with a worldwide installed capacity of 282,482 MW. It is expected that wind energy in 2020 should meet 15.7% of EU electricity demand of 230 GW, and by 2030, 28.5% of 400 GW[Zervos 2009]. Large wind farms consist of hundreds of individual turbines which are connected to the electric power transmission network. In general, offshore wind is steadier and stronger than onshore wind farms. However, on the one hand, offshore wind farms are usually located far away from the grid, and on the other hand, wind power is consistent from year to year but has significant variation over short time scales. This inherent characteristic could affect the stability of the interconnected power grid when wind power provides large share of electricity. It is a big challenge to integrate these long-distance scattered offshore wind farms through AC networks [Ayodele 2011]. Based upon the above considerations, multi-terminal VSC HVDC (MTDC) transmission systems consisting of more than two converter stations provide an efficient solution [Chaudhary 2008, Livermore 2010, Kirby 2002].

1.3 Literature review: related studies on control designs

The control design is always one of the most popular research topics in the area of VSC HVDC systems. A large number of studies have been devoted to the control of VSC HVDC systems from different points of view.

1.3.1 Control of a single VSC terminal

For any VSC HVDC system, the converter is the most basic component, whose operation has a great impact on the system's overall performance. Therefore, it is particularly important to develop appropriate control structures for the VSC. There are two most frequently discussed control methods, namely direct control method and vector control method. The direct control approach is very straightforward where the control inputs, the phase angle and the amplitude modulation ratio, are directly derived from the measurements of the currents and the voltages at the PCC [Ooi 1990, Ohnishi 1991, Noguchi 1998, Sood 2010]. The major advantage of this control method is its simple structure easily implementable while the gravest drawback is its incapability of limiting the current through the converter to protect the semiconductor devices.

To overcome this shortcoming, the vector control method is widely used in the context of the control of VSC [Lindberg 1994, Lindberg 1996, Blasko 1997, Li 2010, Thomas 2001, Xu 2005, Beccuti 2010] where the VSC is modeled in a synchronous reference dq frame. The main feature of this method is that it consists of two control loops, namely the fast inner current loop and the slow outer loop, where the slow outer loop provides the reference trajectories to the fast inner current one. Thanks

to the fast inner current loop, this control structure has the ability to limit the current through the converter.

Studies on comparing the direct control method and the vector control method are carried out in [Sood 2010, Zakaria Moustafa 2008]. The conventional vector control method is usually based on several standard PI controllers where a phase-locked loop (PLL) is usually applied to provide a synchronous reference frame [Lindberg 1994, Lindberg 1996, Blasko 1997]. However, several limitations of pure PI control are presented in [Du 2005, Dannehl 2009, Durrant 2003], which show that the maximum transferable power capability with the conventional vector control method is far less than the system's maximum achievable capacity and the system overall performance is remarkably disturbed by the system uncertainties.

Thus, some modified vector control methods are developed. In [Zhao 2013], adaptive backstepping control technique is applied to the DC voltage outer loop and the inner current loop to ensure the global stability. In [Li 2010], an optimal control strategy using a direct current vector control technology is proposed where the current loop can be a combination of different technologies such as PID, adaptive control, etc. In [Beccuti 2010], a nonlinear model predictive control method is applied to the inner current loop without the need of a PLL. Since the conventional vector control does not fully use the potential of the VSC, in particular, in the case of connecting to a weak AC system, several other control methods are developed. In [Zhang 2010], power-synchronization control with a new synchronization method as an alternative to PLL is established, whose control concept is derived from the behaviors of synchronous generators. This method is effective when a very weak AC system is connected to the DC grid via a VSC [Zhang 2011a, Zhang 2011b]. In [Mariethoz 2014], a VSC HVDC decentralized model predictive control method is proposed with the purpose of achieving fast control of active and reactive power, improving power quality, etc. In [Xu 2007b], a new direct power control is proposed where the converter voltage is directly derived from the defined power flux. This method is applied to the control of doubly fed induction generators (DFIG) with good performance [Zhi 2007]. Furthermore, an improved DPC is presented in [Zhi 2009]. In [Durrant 2006], both linear matrix inequality (LMI) and heuristic schemes like genetic algorithm are presented and a comparison is carried out between them.

1.3.2 Control of MTDC systems

As mentioned in the previous section, AC transmission lines are not feasible for carrying out power transfer from large offshore power plants due to the requirement of transmission lines over long distances. In order to connect those large-scale, offshore and scattered energy sources such as wind farms to the grid, MTDC systems provide a flexible, fast and reversible control of power flow. However, the operation and the control of an MTDC system is still an open and challenging problem. For example, since the semiconductor devices in VSC are very sensitive to overvoltage, it is very important to restrict the DC voltage to an acceptable band.

Several research works have proposed different control structures to ensure the normal operation of an MTDC system. Master-slave control strategy (or constant DC voltage control strategy) are applied in [Ekanayake 2009, Zhang 2012, Lu 2003, Lu 2005] where one terminal called master terminal is arranged to control the DC voltage at a constant desired level while the remaining terminals control their respective active power or other variables. The main drawback of this control approach is that N-1 secure operation can not be ensured in case of outage of the master terminal. Besides, since only the master terminal is used to ensure the power balance of the DC grid and keep the DC voltage constant, it is needed a master terminal with large capacity.

To avoid the above problems, some other control strategies are introduced. In [Tokiwa 1993, Haileselassie 2008, Nakajima 1999, Mier 2012], a control strategy called voltage margin method is developed. With this approach, the operation of each converter is characterized by specific active power-DC voltage ($P-V_{DC}$) curve. With the voltage margin method, one VSC terminal, for instance, VSC 1, is initially used to keep the DC voltage constant by adjusting its active power P_1 to counteract disturbances. When P_1 reaches its upper or lower limit, VSC 1 starts to operate in constant active power mode and the DC voltage will rise or decrease until it reaches another VSC terminal's DC voltage reference setting, for instance, VSC 2's DC voltage reference setting. Then, VSC 2 is responsible for the regulation of DC voltage according to its $P - V_{DC}$ characteristic. Furthermore, a modified two-stage voltage margin control is proposed in [Nakajima 1999] by considering each converter's inherent physical features.

Another control scheme, namely, DC voltage droop control method, whose control philosophy is to use more than one converter to regulate the DC voltage, is widely applied in the context of MTDC systems [Karlsson 2003, Prieto-Araujo 2011, Wang 2014a, Chaudhuri 2013, Bianchi 2011, Chen 2014, Haileselassie 2012b, Wang 2014b, Eriksson 2014, Johnson 1993, Liang 2009, Rogersten 2014]. With this control approach, some or all converters are equipped with a droop controller which is characterized by $P - V_{DC}$ or $I - V_{DC}$ (current vs DC voltage) curve with the slope K_{droop} called the droop gain. This control method has the advantage of 1) sharing the duty of eliminating the power imbalance of the DC grid between several terminals; 2) taking actions only based on local information without remote communication. In [Pinto 2011], each of the aforementioned control strategies is tested and moreover, a performance comparison between them is also carried out.

Concerning the power relations between converter terminals, three DC voltage control and power dispatch modes are established in [Xu 2011]. In the first mode, one terminal, for instance, VSC 1, has priority over the other converters in carrying out the power transfer. When VSC achieves its active power's upper limit, another converter takes over the duty of transmitting the energy. In the second mode, two converters transmit the energy according to a power ratio which can be varied in real time. The third mode is the combination of the two mentioned modes. In [Pinto 2013], a novel distributed direct-voltage control strategy is introduced. The main idea of this control approach is to provide a specific voltage

reference to each of the terminals which participate in the regulation of the DC voltage. In [Rodrigues 2013], an optimal power flow control is proposed where the convariance matrix adaptation (CMA) algorithm is applied to solve an optimal DC load-flow problem and then provide the DC voltage references to the distributed voltage control developed in [Pinto 2013].

The use of MTDC systems for connecting offshore wind farms have been studied by a number of papers [Haileselassie 2012a, Li 2014, Karaagac 2014, Haileselassie 2008, Chen 2011, Lie 2008, Prieto-Araujo 2011, Liang 2011, Haileselassie 2009, Xu 2007a, Fu 2014] where the control structures are well established and the simulation results are also carried out.

The above mentioned articles in this section are entirely dedicated to the control design of VSC HVDC systems. There are also a large number of studies that focus on the modeling of the VSC HVDC systems [Cole 2010, Beerten 2014], the protection system [Kong 2014, Xiang 2015], the development of multilevel modular converters (MMC) which generates less harmonics and reduces the losses of the semiconductor devices [Shi 2015, Adam 2015, Ilves 2015], etc.

1.4 Motivations and contributions of the thesis

For years, people have been working on the development of a European supergrid that allows the massive integration of renewable energy sources to meet the ever increasing consumption of electricity. Due to some undesirable inherent characteristics of the renewable energy sources, such as the variability of the generation output, the conventional AC transmission lines are not quite suitable for the connection of large shares of renewable energy sources while VSC HVDC systems provide an alternative solution. Although numerous research studies on VSC HVDC systems have been carried out, there are still many challenges and it is not yet totally feasible to build such a supergrid.

1.4.1 Motivations

This dissertation is motivated by the challenges in the control design of MTDC systems and analysis of MTDC system's dynamic behavior.

1.4.1.1 Control methods

As a system with complex dynamics, any operation of the VSC HVDC system may give rise to both potential dangers of unexpected interaction and improvement of the system performance. Therefore, developing control structures which are capable to keep good performances like fast tracking or small overshoots, during disturbances is always a challenge for the control of VSC HVDC systems.

As presented in Section 1.3.1, many control methods have been developed. However, most of them lack the corresponding theoretical support and usually need significant efforts to adjust the controller. For example, though the traditional vector

control method based on standard PI controllers has a simple structure, we need to tune the PI control gains by using other procedures [Bajracharya 2008]. Reference [Zhang 2011c] gives a stability analysis for power synchronization control method. Nevertheless, this analysis is carried out by linearizing the system around the operating point and hence, the nonlinear behavior of the system can not be well exhibited. Reference [Dannehl 2009] also presents a study on the limitations of vector control method, but, similar to the case of power synchronization control method, this research work is done via linearization and it is only valid for the behavior within a small neighborhood of the operating point. It is worth considering that, when designing a control structure, we should not only focus on the actual results (or performances) of the control strategy but also on the theoretical explanation of the control operating principle.

1.4.1.2 Dynamic behaviors

As discussed in the section of literature review, vector control method, which is composed of two control loops, is the most widely used control approach for VSC HVDC systems due to its simple structure and its capability to limit the current through the converter. The rationale of this method is based on the assertion that the dynamics of the inductor currents are much faster than the dynamics of the capacitor voltages. As a result, the independent control designs of the two control loops are achievable. However, there exist very few relevant studies in the literature that have ever presented a detailed theoretical explanation on the validity and the implications of this assertion. It is not clear if the time-scale separation between the dynamics of the current and the voltage is an inherent characteristics or it exists only under certain conditions. For example, as demonstrated in [Kimball 2008], for some DC-DC converters, the dynamic separation between the system variables exists only when the stability requirement is satisfied. If the time-scale separation exists in a high-order system, this feature has a great significance to the analysis of system's behavior. Based on the time-scale separation, two (or more) subsystems of lower orders can usually be deduced from the original high-order system and then, we can use the behaviors of the low-order subsystems to approximate the behaviors of the high-order original system. This greatly reduces the complexity of analyzing the system's dynamic performance. Therefore, the verification of the existence of the time-scale separation is very desirable.

1.4.2 Contributions

The research work in this dissertation aims at filling some gaps between the theory and the practice, i.e. 1) to investigate various control approaches for the purpose of improving the performance of MTDC systems; 2) to establish connections between existing empirical control designs and theoretical analysis; 3) to increase understanding of the multi-time-scale behavior of MTDC systems characterized by the presence of slow and fast transients in response to external disturbances.

The main contributions of the research work reported in this thesis can be put into three aspects, namely nonlinear control designs of MTDC systems, analysis of MTDC system's dynamic behaviors and application of MTDC systems to provide frequency support for AC networks.

1.4.2.1 Nonlinear control designs

In the area of nonlinear control design of MTDC systems, three nonlinear control design tools, namely feedback linearization control, feedback linearization control with sliding mode control and passivity-based state feedback control, are applied to establish different control schemes with corresponding theoretical analysis. Besides, the developed control algorithms have been tested by detailed and realistic numerical simulations, whose performances are evaluated in comparison to the performance of the conventional vector current algorithm.

1.4.2.2 Analysis of dynamic performances

The main motivation for the research work in the area of analysis of MTDC system's dynamic behaviors is the desire to provide a rigorous theoretical demonstration to verify a common assertion used in the control design of VSC HVDC systems, that is, the dynamics of the inductor currents are much faster than the capacitor voltage. The contribution in this area consists of three parts: 1) development of a general control theory that we named "Control induced time-scale separation" for a class of nonlinear systems; 2) analysis of control induced time-scale separation for an MTDC system with master-slave control configuration; 3) analysis of control induced time-scale separation for an MTDC system with droop control configuration. Theoretical analysis, mainly based on singular perturbation and Lyapunov theories, have been carried out for each of the aforementioned aspects and clarified with various simulation studies. The study of the first part has been mainly performed to propose a time-scale separation control method which can drive a class of nonlinear systems to exhibit a multi-time-scale performance. The theoretical results obtained from the first part have been applied to investigate the dynamic behaviors of MTDC systems under the two main control configurations, i.e. master-slave and droop control. Empirical vector current control designs have been proposed for each control configuration. Theoretical explanations and fundamental analysis indicate that with the currently used empirical control algorithms, the inductor currents indeed perform a dynamic behavior with different dynamics. Furthermore, more details on how and why these empirical vector current control designs work have been also provided.

1.4.2.3 Frequency support

The final contribution relates to analysis of the application of MTDC systems for frequency support strategy. A DC voltage based control scheme for the AC frequency regulation is proposed, achieving the objective of sharing primary reserves between different AC areas interconnected via MTDC system without using remote

information though telecommunication. The frequency control principle is to regulate the AC frequency by modulating each AC grid's scheduled (or prescribed) input of active power.

1.5 Outline of the thesis

This dissertation is organized as follows: In Chapter 2 a brief introduction of VSC HVDC technology is presented. In particular, the possible operation modes of the VSC are discussed, which are essential for the design of a control system. In Chapter 3 the dynamic model of a multi-terminal VSC HVDC system is established based on a synchronous reference dq frame. This MTDC system consists of two different AC networks connected via a generic DC grid. In Chapter 4 two most used conventional control methods, namely direct control method and vector control method, are introduced. In addition, the merits and drawbacks of these two methods are also discussed. In Chapter 5 three different nonlinear control structures are proposed for VSC HVDC systems. With the help of numerical simulations, the advantages claimed for each of the proposed controllers are verified in comparison to the conventional vector current control method. In Chapter 6 the system dynamic behaviors are investigated. We first demonstrate that there exists a control structure that can drive a class of nonlinear systems to exhibit arbitrary multi-time-scale dynamics that were not natural to the system. Then, we apply the obtained theoretical results to the MTDC system under two control configurations, namely master-slave control configuration and droop control configuration. The theoretical analysis of the time-scale separation between the dynamics of the system states are also carried out for each of the aforementioned control configuration. In Chapter 7 the potential of VSC HVDC technology for frequency regulation is investigated where a DC-voltage-based control scheme is proposed to make the interconnected AC networks share their primary reserves. In Chapter 8 conclusions are drawn and future work is discussed.

1.6 Publications

Most of the materials in this thesis have been published in the following articles:

- "Nonlinear Control Design for a Multi-Terminal VSC-HVDC System", Yijing Chen, Jing Dai, Gilney Damm, Françoise Lamnabhi-Lagarrigue, 2013 European Control Conference (ECC), July 17-19, 2013, Zürich, Switzerland.
- "A detailed study on a DC-voltage-based control scheme using a multi-terminal HVDC system for frequency control", Yijing Chen, Jing Dai, Gilney Damm, Françoise Lamnabhi-Lagarrigue, 2013 European Control Conference (ECC), July 17-19, 2013, Zürich, Switzerland.
- "Control Induced Explicit Time-Scale Separation to Attain DC Voltage Stability for a VSC-HVDC Terminal", Yijing Chen, Gilney Damm, Abdelkrim Ben-

chaib, Mariana Netto, Françoise Lamnabhi-Lagarrigue, 19th World Congress of the International Federation of Automatic Control (IFAC), August 24-29, 2014, Cape Town, South Africa.

- "Feedback Linearization for the DC Voltage Control of a VSC-HVDC Terminal", Yijing Chen, Gilney Damm, Abdelkrim Benchaib, Françoise Lamnabhi-Lagarrigue, 2014 European Control Conference (ECC), June 24-27, 2014, Strasbourg, France.

- "Multi-Time-Scale Stability Analysis and Design Conditions of a VSC Terminal with DC Voltage Droop Control for HVDC Networks", Yijing Chen, Gilney Damm, Abdelkrim Benchaib, Françoise Lamnabhi-Lagarrigue, 53rd IEEE Conference on Decision and Control (CDC), December 15-17, 2014, Los Angeles, CA, USA.

- "Multi-Terminal High Voltage Direct Current Networks for Renewable Energy Sources", Miguel Jiménez Carrizosa, Yijing Chen, Gilney Damm, Abdelkrim Benchaib and Françoise Lamnabhi-Lagarrigue, ERCIM News No. 97 special theme: "Cyber-Physical Systems", Link: http://ercim-news.ercim.eu/en97/special/multi-terminal-high-voltage-direct-current-networks-for-renewable-energy-sources

Chapter 2

VSC HVDC technology

Contents

In order to get a good understanding of VSC HVDC technology, this chapter first introduces the main components of a VSC HVDC system in Section 2.1, each performing a different function. Subsequently, the operating principles of VSC are described in Section 2.2. Next, several configurations of HVDC systems are presented in Section 2.3. Finally, various control modes of VSC terminals are discussed in Section 2.4.

2.1 Key components

A simplified representation of a VSC HVDC converter station is depicted in Fig. 2.1. The characteristics and purposes of the main components of a VSC HVDC system are introduced in this section [Siemens 2005, Bahrman 2007, Dodds 2010, Andersen 2002].

Transformer

A bank of transformers are installed to adapt the AC voltage level of the connected AC grid to the rated DC voltage transmission level. Since harmonic filters are located between the phase reactors and the transformers, harmonic currents have little or no effects on the transformers. Therefore, ordinary transformers can be used for VSC HVDC systems.

Harmonic filter

With VSCs, the generated harmonics are usually at high frequencies, which strongly depend on the PWM method and converter topology. In a VSC HVDC system,

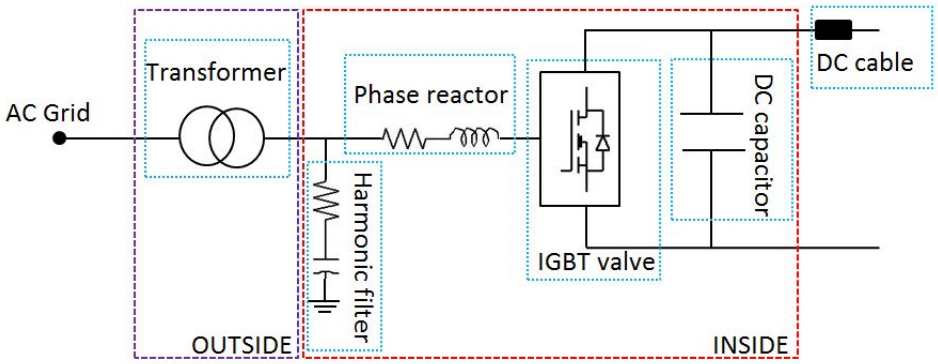

Figure 2.1: A simplified representation of a VSC HVDC converter station. Usually, the harmonic filters, the phase reactors, the converters and the DC capacitors are located indoors while the transformers and the cooling system are outdoors.

shunt filters are used to reduce such high-frequency harmonic currents flowing into the AC system so that the transformers are not exposed to harmonic stress.

Phase reactor

The phase reactors are composed by large inductances with small resistances. On the one hand, the phase reactor can also reduce the harmonic distortions to smoothen the phase currents like the harmonic filters. On the other hand, they play an essential role in determining the dynamics of the converter on the AC side.

Converters

As the most important component in an HVDC system, the converters are used to perform the conversion between AC and DC. Each valve in the VSC bridge consists of series connected semiconductors (such as IGBT) to create a high-level DC voltage. PWM technology is usually employed for the VSC to create the desired voltage and to improve the harmonic distortion of the converter.

DC capacitor

The main purpose of the DC capacitors is to maintain the DC voltage within its acceptable band by charging and discharging the capacitors. Besides, the DC capacitors can also reduce the voltage ripples generated by the converters.

DC cable

Solid-dielectric extrude polymer cables with prefabricated joints are used in VSC HVDC systems. This kind of cables are much lighter, more flexible than mass-

impregnated or gas-filled conductors. In addition, there is no need to worry about the problem of leaking cable oil.

In this section, we just presented the components that have great effects on the system dynamic modeling and steady-state analysis. Hence, some other indispensable elements of VSC HVDC systems, such as high-side breakers, valve coolers etc, are not illustrated in Fig. 2.1.

2.2 Operating principles of VSC

The most common three-phase bidirectional VSC creates two voltage levels at the AC side of each phase with a six pulse bridge as shown in Fig. 2.2. Each valve in the six pulse bridge is made of a fully controllable semiconductor such as IGBT with a diode connected in anti-parallel. The operations of turning on and off of the self-commutated semiconductors result in a square waveform for each phase, which is relevant to the DC voltage u_c. For example, the square waveform of the converter voltage in phase a can be expressed by

$$v_{ca} = \frac{1}{2} u_c m \sin(\omega_e t + \delta) + \text{harmonics} \tag{2.1}$$

where $m \in [0,\ 1]$ is the amplitude modulation ratio, ω_e is the frequency of fundamental AC component and δ is the phase angle between the fundamental component of the converter AC voltage and the AC system voltage at the PCC. However, the two-level bridge in the square wave operation usually produces large unacceptable harmonics. Hence, the application of PWM technology can improve the harmonic distortion of the converter with less low-frequency harmonics and give a fast response [Trzynadlowski 1996]. By using PWM techniques such as sinusoidal PWM (SPWM), δ and m are fed to the pulse width modulator to determine the phase shift and the duration of firing pulses, respectively. Finally, the firing pulses are generated and then sent to the converter to switch the IGBTs [Stijn 2010, Mohan 2003]. With PWM, the IGBTs are usually switched on and off many times in order to create the desired phase angle or amplitude.

2.3 Configurations of HVDC systems

Depending on the applications of HVDC, there are various configurations of HVDC systems.

Monopolar system

Monopolar HVDC link as illustrated in Fig. 2.3 is the simplest and least expensive configuration for HVDC link where a single conductor is used for power transmission while the current return path is earth, water or a metallic conductor. This type of HVDC link is mainly applicable for submarine cable transmission. Because of its low cost, it also has the advantage in connecting two remote AC systems through an overhead line with a distance of 300 to 3000 km and more.

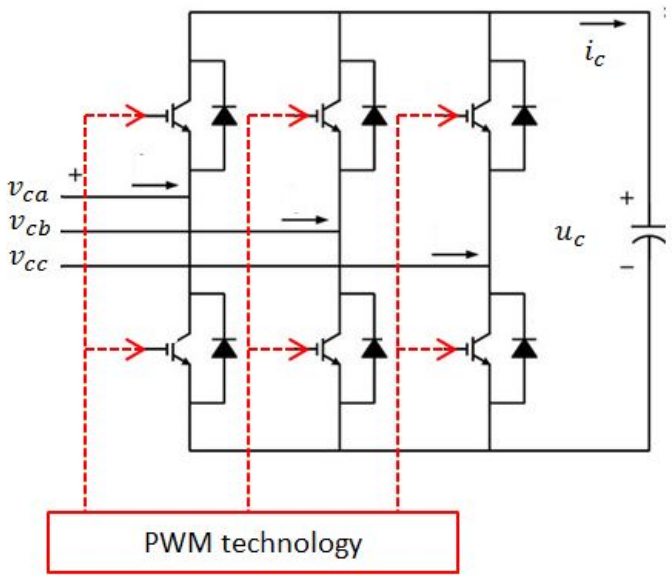

Figure 2.2: Three phase bidirectional VSC.

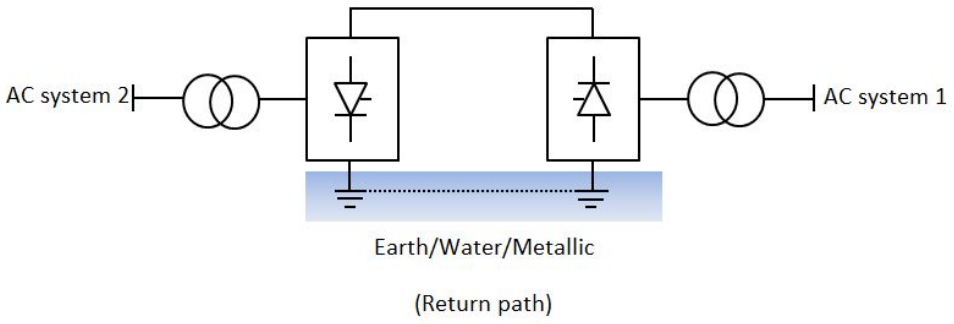

Figure 2.3: Monopolar HVDC link with earth, water or metallic return path.

Bipolar system

With two sets of conductors as shown in Fig. 2.4, bipolar HVDC link is the most common configuration for today's HVDC systems. The current return path is usually provided by two earth electrodes or a metallic return conductor. One pole is positive with respect to earth and the other is negative. Since the two poles are independent of each other, a bipolar can operate as two monopolars. Therefore, in case of outage or scheduled maintenance of one pole, it is still possible to transfer the power by using the other pole with a reduced transmission capacity.

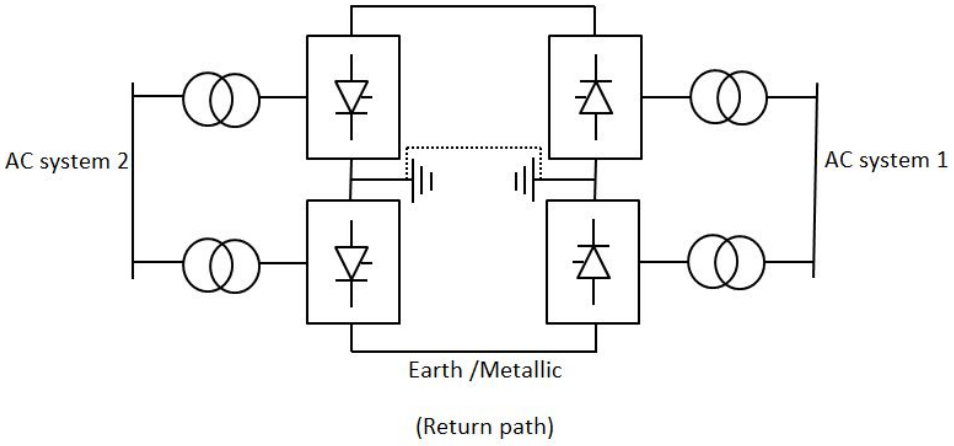

Figure 2.4: Bipolar HVDC link with earth or metallic return path.

Back-to-back system

Back-to-back HVDC link is usually a bipolar HVDC link without earth return as shown in Fig. 2.5. It is especially suitable for connection between two asynchronous AC systems with different system parameters (for example, different frequencies or different voltage level). In a back-to-back HVDC link, the rectifier and the inverter are usually located in the same area or the same building. In addition, the length of the conductor line between the two converters can be kept as short as possible. Therefore, the DC voltage transmission level can be freely chosen. In order to reduce the number of the semiconductors and the size of valve hall, the DC voltage is usually set to a low level and the DC current to a high level.

Multi-terminal system

Multi-terminal HVDC link is used to connect more than two converter terminals in parallel, series or hybrid. Its main advantage is that the power exchange can be fulfilled between multi-suppliers and multi-consumers. An example of three terminals connected in parallel is given by Fig. 2.6.

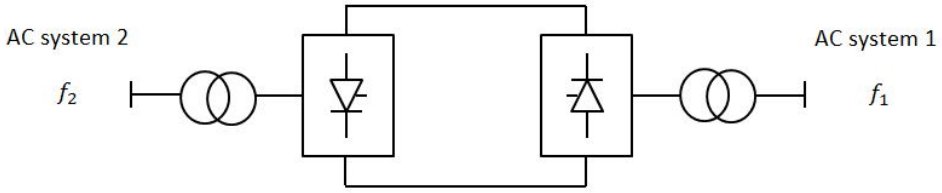

Figure 2.5: Back-to-back HVDC link.

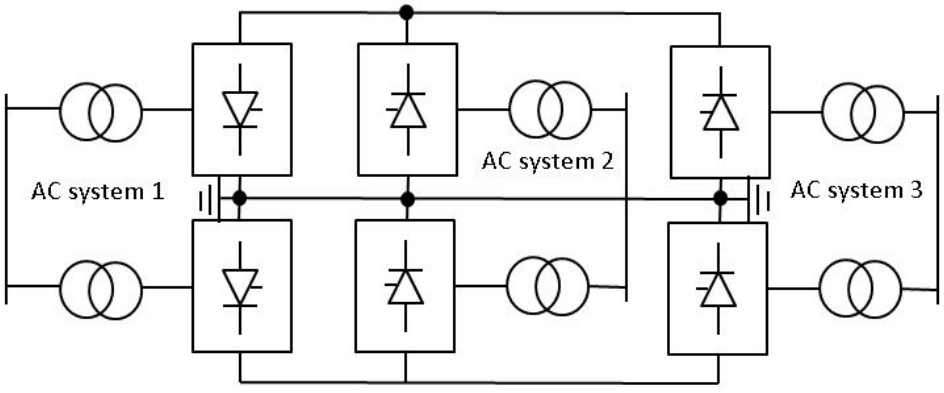

Figure 2.6: Multi-terminal HVDC link with three terminals connected in parallel.

2.4 AC network and control modes of VSC terminals

Before discussing the control modes of a single VSC terminal, we introduce the types of AC grid in the inverter and rectifier side.

2.4.1 AC network connected to VSC terminal

The strength of the AC network connected to the converter station at the PCC has significant impact on the performance of VSC HVDC systems [IEE 1997]. If the AC network gets most of the power from its own generators, the system electromotive force (EMF) can be kept within an acceptable band by the AC network itself in case of power variations in the DC grid. However, if the DC grid is the main source for the AC network or the AC network has a high impedance, the power variation in the DC grid may cause the system voltage and frequency to go beyond their safe operating ranges.

The strength of the AC network relative to DC power at the PCC is commonly described by the short circuit ratio (SCR) [Gavrilovic 1991], i.e. the ratio of the AC network three-phase short circuit power in MVA at the PCC and the rated DC power in MW. In general, three types of AC systems can be distinguished in terms of SCR. A system with SCR larger than 3 is called a high SCR system (or strong system) where an adequate inertia is available to maintain the frequency and amplitude of the AC voltage at the PCC irrespective of the change of active or reactive power. A system is said to be a low SCR system if the SCR is between 2 and 3. If a system has the SCR less than 2, we call it a very low SCR system (or weak system). For example, an isolated island or an offshore platform belongs to the family of weak systems. For this kind of system, any change in power flow at the PCC may lead to AC instability. To avoid this risk, an AC frequency and voltage controller need to be installed. It can be summarized that the interaction between AC and DC becomes more sensitive to disturbances as the SCR of the AC system becomes lower [Thallam 1992].

2.4.2 Control modes of VSC terminals

Consider a single line representation of the AC side of a VSC as illustrated in Fig. 2.7 where the reactance X includes the reactances of the transmission line, the phase reactors, etc. The AC voltages of the AC network at the PCC and the converter are denoted by $V_s = V_{s,\text{rms}}\angle 0$ and $V_c = V_{c,\text{rms}}\angle\delta$, respectively.

The transmitted active power and reactive power at the PCC in steady-state condition are given by

$$\begin{aligned} P_s &= \frac{V_{s,\text{rms}}V_{c,\text{rms}}}{X}\sin\delta = P_{\max}\sin\delta \\ Q_s &= \frac{V_{s,\text{rms}}^2}{X} - \frac{V_{s,\text{rms}}V_{c,\text{rms}}}{X}\cos\delta \end{aligned} \tag{2.2}$$

where $P_{\max} = \dfrac{V_{s,\text{rms}}V_{c,\text{rms}}}{X}$ is the maximum active power that can be transmitted

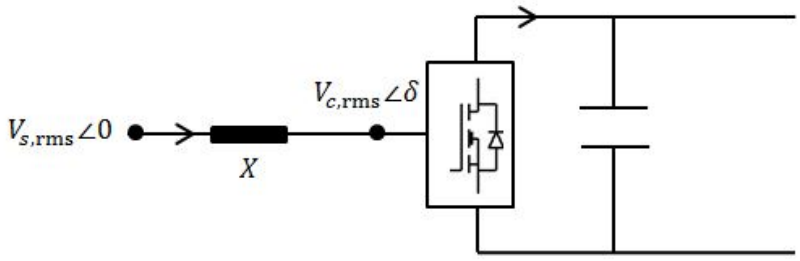

Figure 2.7: A single line representation of the AC side of a VSC.

through the line. In addition, the power angle δ can be deduced as

$$\delta = \arcsin(\frac{P_s}{P_{\max}}) \tag{2.3}$$

From (2.2), it can be seen that P_s and Q_s are determined by $V_{s,\text{rms}}$, $V_{c,\text{rms}}$ and δ. Usually, $V_{s,\text{rms}}$ is considered to be fixed at a constant level[1] and hence, P_s and Q_s are controlled by regulating the phase angle δ and the converter voltage $V_{c,\text{rms}}$. From (2.1), it can be seen that $V_{c,\text{rms}}$ depends on the modulation index m. Therefore, P_s and Q_s are actually controlled by the modulation index m and the angle δ.

Based on the purposes of the converter, four possible control modes (control objectives) exist [Akhmatov 2014, Zakaria Moustafa 2008]:

- **Mode 1: AC voltage control mode**

  This control mode is particularly designed for the VSC connected to a weak AC system. Since the weak AC system with high impedance relative to the DC rated power is susceptible to AC/DC interactions, any disturbances either from the DC side of the converter or the AC side may lead to instability of the AC voltage (for example, voltage collapse, overvoltage, etc). Fortunately, fast AC voltage controller provides an effective support for the operation of the VSC which enables the weak AC system to operate at fixed magnitude.

- **Mode 2: Active power control mode**

  As described in (2.2), it shows that the active power can be controlled by the converter. An active power controller can be designed such that the active power follows its reference which is provided by a higher control level (or a central power dispatching station).

- **Mode 3: Reactive power control mode**

  This control mode is used to regulate the reactive power at its reference. For example, if the reference input for the reactive power controller is set to zero, the reactive power can be kept at this value to obtain an unity-power factor.

[1] In general, this voltage is kept by the Transmission System Operator (TSO).

This action is helpful in improving the power quality. Moreover, unlike LCC HVDC systems, the VSC itself does not need reactive power support. Actually, the VSC can work as a reactive power compensator to regulate the amplitude of the AC system voltage by controlling the reactive power at the PCC.

Because of the ability to fully control the power flow, the VSC has become a very important power flow controlling device [Van Hertem 2005]

- **Mode 4: DC voltage control mode**

  It is very important to keep in mind that, the operation of VSC HVDC system is always constrained by the DC voltage which is only acceptable in a narrow operating band. As a result, for any VSC HVDC system with either conventional two terminals or multi terminals, at least one terminal must be equipped with DC voltage controller to ensure that the DC voltage always remains in its acceptable range, what is obtained by the power flow balance of the DC grid.

The dominant feature of VSC based on IGBTs is that both turn-on and turn-off operations on the valves are available. Therefore, VSC possesses a second degree of freedom compared to LCC. This additional controllability gives many advantages, one of which is that the VSC has the possibility to control two output quantities. According to the applications and the types of VSC connected AC systems, there are possible combinations [Zakaria Moustafa 2008] for a single VSC operation:

- DC voltage and AC voltage control modes
- DC voltage and reactive power control modes
- Active and reactive power power control modes
- Active power and AC voltage control modes.

2.5 Chapter conclusions

In this chapter, we have introduced the key components of a VSC terminal, explained the operating principles of the converter and classified AC systems into three types in terms of SCR. According to various applications of VSC HVDC systems, four different configurations have been presented. Furthermore, four possible control modes for operating a VSC have been discussed. This chapter makes preparations for the system modeling in the following chapter.

Chapter 3

Dynamic model of multi-terminal VSC HVDC systems

Contents

In this chapter, an average state-space model is developed for multi-terminal VSC HVDC systems. In the modeling, a synchronously rotating dq frame is chosen so that the three-phase quantities can be transformed into two-phase quantities. Using basic physical laws, the dynamics of the converter's AC and DC sides are modeled by differential equations. A generic topology for the DC network is considered and the properties of the DC grid are discussed. Furthermore, two most widely used control approaches are also presented.

3.1 Preliminary knowledge

There exist different approaches to modeling VSC HVDC systems. In the detailed modeling approach, every semiconductor device should be treated as an individual unit, where the type of modulation (sinusoidal PMW or optimized PMW), the converter switching level (two-level or multi-level) and harmonics with high frequency need to be analyzed. Such a method results in a very complex model which needs a

lot of memory and CPU times to run simulations. Compared to the detailed modeling approach, the time-averaged modeling approach [Middlebrook 1976] seems much simpler and tractable while still enabling us to study the system behaviors related to the fundamental frequency components of the voltage and the current. In the time-averaged model, the VSC is viewed as a controllable AC voltage source from AC side whereas it is considered as a controllable current source from DC side as depicted in Fig. 2.2. By using the time-averaged modeling approach, there is no need to consider the dynamics of each individual semiconductor device and moreover, high frequency harmonics can also be neglected. This greatly simplifies the modeling process, save simulation memory and accelerates the simulation speed. Based on the above considerations, the time-averaged modeling approach is applied in this thesis work. As a result, according to (2.1), the converter voltage $v_{c,abc}$ and the DC voltage u_c in the time-averaged model satisfy

$$v_{c,abc} = \frac{1}{2} u_c m_{abc} \tag{3.1}$$

where m_a, m_b and $m_c \in [0,\ 1]$ are the modulation indices of the phase a, phase b and phase c, respectively, determined by the amplitude modulation ratio m and the phase angle δ, according to the following expressions

$$\begin{aligned} m_a &= m\sin(\omega_e t + \delta) \\ m_b &= m\sin(\omega_e t - \tfrac{2}{3}\pi + \delta) \\ m_c &= m\sin(\omega_e t + \tfrac{2}{3}\pi + \delta) \end{aligned} \tag{3.2}$$

In the remainder of this thesis, it is assumed that all VSC connected AC systems are under balanced network conditions. Thus, there is no negative sequence component of the three-phase voltage or current, and the three phases have equal voltage amplitudes with a phase angle of 120° between themselves.

3.2 Clarke's and Park's transformations

Clarke's and Park's transformations are widely used in many studies on synchronous and asynchronous machines. Their basic principle is to transform a balanced three-phase system into a two-phase system by simplifying the analysis of three-phase circuit. The difference between both transformations is that Clarke's transformation is to project the three-phase quantities onto a stationary two-axis reference frame, whereas Park's transformation onto a rotating two-axis reference frame.

3.2.1 Clarke's transformation

The stationary two axes of Clarke's transformation are denoted by $\alpha-$ and $\beta-$, which are orthogonal. In order to make the transformation invertible, the zero-sequence component is usually added and then, Clarke's transformation matrix can

be expressed by

$$x_{\alpha\beta 0} = T_{\alpha\beta 0}\; x_{abc} = k_c \begin{bmatrix} 1 & -\frac{1}{2} & -\frac{1}{2} \\ 0 & \frac{\sqrt{3}}{2} & -\frac{\sqrt{3}}{2} \\ \frac{1}{2} & \frac{1}{2} & \frac{1}{2} \end{bmatrix} x_{abc} \tag{3.3}$$

where k_c is a constant and x can represent the AC voltage, current, etc. The inverse Clarke's transformation is given by

$$T^{-1}_{\alpha\beta 0} = \frac{2}{3} k_c^{-1} \begin{bmatrix} 1 & 0 & 1 \\ -\frac{1}{2} & \frac{\sqrt{3}}{2} & 1 \\ -\frac{1}{2} & -\frac{\sqrt{3}}{2} & 1 \end{bmatrix} \tag{3.4}$$

Let us take an example. Consider a balanced three-phase system whose voltages and currents in $a-$, $b-$, and $c-$axis are given by

$$\begin{aligned} v_a &= \sqrt{2} V_{\text{rms}} \cos(\omega t + \delta_a) \\ v_b &= \sqrt{2} V_{\text{rms}} \cos(\omega t - \tfrac{2}{3}\pi + \delta_a) \\ v_c &= \sqrt{2} V_{\text{rms}} \cos(\omega t + \tfrac{2}{3}\pi + \delta_a) \end{aligned} \tag{3.5}$$

and

$$\begin{aligned} i_a &= \sqrt{2} I_{\text{rms}} \cos(\omega t + \delta_a + \phi) \\ i_b &= \sqrt{2} I_{\text{rms}} \cos(\omega t - \tfrac{2}{3}\pi + \delta_a + \phi) \\ i_c &= \sqrt{2} I_{\text{rms}} \cos(\omega t + \tfrac{2}{3}\pi + \delta_a + \phi) \end{aligned} \tag{3.6}$$

where

- V_{rms} and I_{rms} are the root mean square values of the AC voltage and current, respectively.
- $\omega = 2\pi f$ is the angular frequency in rad/s and f is the frequency of the AC system.
- δ_a is the phase of v_a and ϕ is the phase angle between the voltage and the current.

Applying Clarke's transformation to v_{abc} and i_{abc}, we get

$$\begin{aligned} v_\alpha &= \tfrac{3}{2} k_c \sqrt{2} V_{\text{rms}} \cos(\omega t + \delta_a) \\ v_\beta &= \tfrac{3}{2} k_c \sqrt{2} V_{\text{rms}} \sin(\omega t + \delta_a) \end{aligned} \tag{3.7}$$

and

$$\begin{aligned} i_\alpha &= \tfrac{3}{2} k_c \sqrt{2} I_{\text{rms}} \cos(\omega t + \delta_a + \phi) \\ i_\beta &= \tfrac{3}{2} k_c \sqrt{2} I_{\text{rms}} \sin(\omega t + \delta_a + \phi) \end{aligned} \tag{3.8}$$

3.2.2 Park's transformation

By rotating the two-phase $\alpha\beta$ reference frame over an angle θ according to the formula

$$x_{dq} = \begin{bmatrix} \cos\theta & \sin\theta \\ -\sin\theta & \cos\theta \end{bmatrix} x_{\alpha\beta} \tag{3.9}$$

it can be turned into a new reference frame represented by $d-$ and $q-$ axis.

The above transformation from $\alpha\beta$ reference frame to dq reference frame is called Park's transformation and its inverse is given by

$$x_{\alpha\beta} = \begin{bmatrix} \cos\theta & -\sin\theta \\ \sin\theta & \cos\theta \end{bmatrix} x_{dq} \tag{3.10}$$

Applying Park's transformation to $v_{\alpha\beta}$ and $i_{\alpha\beta}$ in (3.7) and (3.8) yields

$$\begin{aligned} v_d &= \tfrac{3}{2} k_c \sqrt{2} V_{\text{rms}} \cos(\omega t + \delta_a - \theta) \\ v_q &= \tfrac{3}{2} k_c \sqrt{2} V_{\text{rms}} \sin(\omega t + \delta_a - \theta) \end{aligned} \tag{3.11}$$

and

$$\begin{aligned} i_d &= \tfrac{3}{2} k_c \sqrt{2} I_{\text{rms}} \cos(\omega t + \delta_a + \phi - \theta) \\ i_q &= \tfrac{3}{2} k_c \sqrt{2} I_{\text{rms}} \sin(\omega t + \delta_a + \phi - \theta) \end{aligned} \tag{3.12}$$

By setting the rotation angle θ to ωt, v_{dq} become

$$\begin{aligned} v_d &= \tfrac{3}{2} k_c \sqrt{2} V_{\text{rms}} \cos\delta_a \\ v_q &= \tfrac{3}{2} k_c \sqrt{2} V_{\text{rms}} \sin\delta_a \end{aligned} \tag{3.13}$$

which are two non time-varying constants.

Actually, the three-phase abc frame can be directly transformed into the two-phase dq frame by

$$x_{dq0} = T_{dq0}\, x_{abc} = k_c \begin{bmatrix} \cos\theta & \cos(\theta - \frac{2\pi}{3}) & \cos(\theta + \frac{2\pi}{3}) \\ -\sin\theta & -\sin(\theta - \frac{2\pi}{3}) & -\sin(\theta + \frac{2\pi}{3}) \\ \frac{\sqrt{2}}{2} & \frac{\sqrt{2}}{2} & \frac{\sqrt{2}}{2} \end{bmatrix} x_{abc} \tag{3.14}$$

and the inverse is given by

$$x_{abc} = T_{dq0}^{-1}\, x_{dqo} = \frac{2}{3} k_c^{-1} \begin{bmatrix} \cos\theta & -\sin\theta & \frac{\sqrt{2}}{2} \\ \cos(\theta - \frac{2\pi}{3}) & -\sin(\theta - \frac{2\pi}{3}) & \frac{\sqrt{2}}{2} \\ \cos(\theta + \frac{2\pi}{3}) & -\sin(\theta + \frac{2\pi}{3}) & \frac{\sqrt{2}}{2} \end{bmatrix} x_{dq0} \tag{3.15}$$

If $k_c = \sqrt{\frac{2}{3}}$, the active power in dq frame has the identical magnitude as in abc frame, i.e. $v_a i_a + v_b i_b + v_c i_c = v_d i_d + v_q i_q$. If $k_c = \frac{2}{3}$, as seen in (3.11), the amplitudes of the AC voltage in abc frame and in dq frame are the same. In the remainder of this

thesis, k_c is equal to $\frac{2}{3}$. In this case, the active power P and the reactive power Q in dq frame satisfy

$$\begin{aligned} P &= \tfrac{3}{2}(v_d i_d + v_q i_q) \\ Q &= \tfrac{3}{2}(v_q i_d - v_d i_q) \end{aligned} \tag{3.16}$$

By comparing the expressions of the AC voltage in abc frame (3.5) and in dq frame (3.13), it can be seen that the application of Park's transformation reduces the complexity of the AC voltage equations, i.e. three time-varying quantities are transformed into two non time-varying quantities. This action favors the analysis of the electrical system and the development of control system. Therefore, an equivalent continuous-time averaged state-space model established in a synchronously rotating dq reference frame will be presented for multi-terminal VSC HVDC systems in the next section.

3.3 Three-phase synchronous reference frame phase-locked loop

As discussed in Section 2.4, a strong AC network itself has the ability to maintain the AC voltage at the PCC. Hence, when a VSC is connected to a strong AC system, it must be synchronized to the frequency of the strong AC system to avoid the risk of instability. This can be achieved with the help of three-phase synchronous reference frame phase-locked loop (SRF-PLL) technology, which is the most widely used technique to synthesize the phase and frequency in electrical systems [Chung 2000].

In the SRF-PLL, the three-phase voltages are transformed into dq reference frame by applying Park's transformation. Then, the rotation angle θ can be controlled via a feedback path. The SRF-PLL system consists of three major parts: the phase detecting device, loop filter, voltage-controlled oscillator (VOC), as illustrated in Fig. 3.1. The phase detecting device is used to generate a voltage, which is designed as a function of the phase difference between the reference input θ and the PLL output $\hat{\theta}$, i.e. $\tilde{\theta} = \theta - \hat{\theta}$. The dynamics of the SRF-PLL system is governed by the loop filter which also enables to eliminate high frequency signals. The design of loop filter is very important, which should consider the trade-off between the filter performance and the system stability. Usually, a typical proportional-integral (PI) filter is chosen.

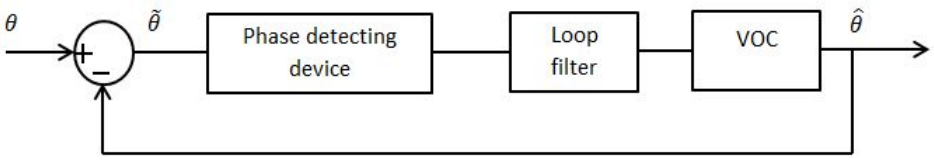

Figure 3.1: A three-phase PLL system.

3.4 Multi-terminal HVDC system model

A general configuration of an MTDC system with N strong AC systems (SAC), M weak AC systems (WAC) and a DC network is depicted in Fig. 3.2 where each AC network is connected by only one VSC converter.

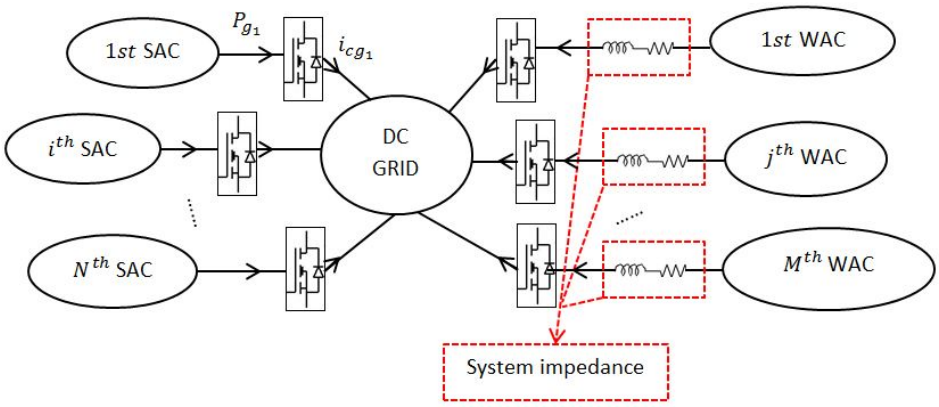

Figure 3.2: A multi-terminal VSC HVDC system with strong and weak AC systems.

By convention, the active power on the AC side and the current through the phase reactor are positive if they flow from the AC side to the DC side via the VSC. The DC current on the DC side is positive if it is injected into the DC grid from the converter. For example, if the active power P_{g_1} (or the DC current i_{cg_1}) of SAC 1 is negative, then SAC 1 absorbs the power from the DC grid as a consumer. Otherwise, it provides the power as a supplier.

3.4.1 Strong AC system side

The configuration of the i^{th} SAC connection terminal is presented in Fig. 3.3 where the currents $i_{g_i,abc}$ flow through the phase reactor made up of an aggregated resistance R_{g_i} and an aggregated inductance L_{g_i}. Since the SAC enables to control its AC voltage at the PCC in case of disturbances, the SAC can be modeled by an ideal three-phase AC source with constant parameters. Consequently, the AC voltage of the i^{th} SAC, i.e. $v_{sg_i,abc}$, can be always maintained at fixed frequency f_{g_i} and amplitude $V_{g_i,\text{rms}}$.

According to Kirchhoff's circuit laws, the dynamics of the currents $i_{g_i,abc}$ can be expressed by

$$L_{g_i}\frac{di_{g_i,abc}}{dt} = v_{sg_i,abc} - v_{cg_i,abc} - R_{g_i}i_{g_i,abc} \tag{3.17}$$

where $v_{cg_i,abc}$ are the converter voltages. Due to the application of PWM, the relation between $v_{cg_i,abc}$ and the DC voltage u_{cg_i} can be provided by the amplitude modulation ratio m_{g_i} and the phase angle δ_{g_i} according to (3.1) and (3.2)

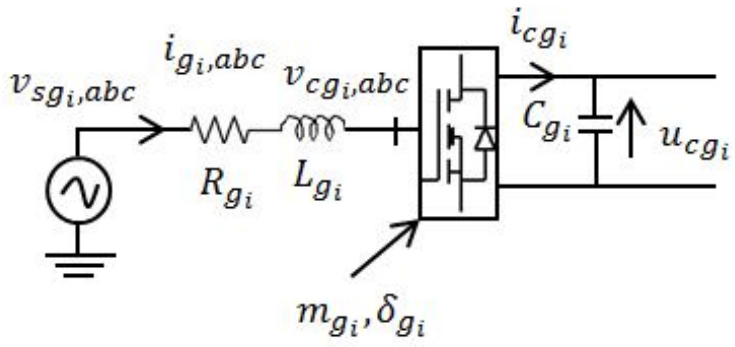

Figure 3.3: A simplified schematic diagram of the i^{th} VSC connected strong grid.

$$v_{cg_i,abc} = \frac{1}{2} u_{cg_i} m_{g_i,abc} \tag{3.18}$$

where

$$\begin{aligned} m_{g_i a} &= m_{g_i} \sin(\omega_{g_i} t + \delta_{g_i}) \\ m_{g_i b} &= m_{g_i} \sin(\omega_{g_i} t - \tfrac{2}{3}\pi + \delta_{g_i}) \\ m_{g_i c} &= m_{g_i} \sin(\omega_{g_i} t + \tfrac{2}{3}\pi + \delta_{g_i}) \end{aligned} \tag{3.19}$$

with $\omega_{g_i} = 2\pi f_{g_i}$.

Substituting (3.18) and (3.19) into (3.17) and then applying Park's transformation (3.14), the dynamics of $i_{g_i,abc}$ in the dq reference frame are described by

$$\begin{aligned} \frac{di_{g_i d}}{dt} &= -\frac{R_{g_i}}{L_{g_i}} i_{g_i d} + \omega_{g_i} i_{g_i q} + \frac{v_{sg_i d}}{L_{g_i}} - \frac{u_{cg_i}}{2L_{g_i}} m_{g_i d} \\ \frac{di_{g_i q}}{dt} &= -\frac{R_{g_i}}{L_{g_i}} i_{g_i q} - \omega_{g_i} i_{g_i d} + \frac{v_{sg_i q}}{L_{g_i}} - \frac{u_{cg_i}}{2L_{g_i}} m_{g_i q} \end{aligned} \tag{3.20}$$

It can be seen that the modulation indices $m_{g_i,abc}$ are turned into $m_{g_i d}$ and $m_{g_i q}$ which satisfy

$$\begin{aligned} m_{g_i} &= \sqrt{m_{g_i d}^2 + m_{g_i d}^2} \leq 1 \\ \delta_{g_i} &= \arctan(\frac{m_{g_i d}}{m_{g_i q}}) \end{aligned} \tag{3.21}$$

For the sake of simplicity, the rotating angle θ_{g_i} of Park's transformation is chosen such that the $d-$axis is aligned to the phase a of AC voltage, which results in $v_{sg_i d} = V_{g_i,\text{rms}}$ and $v_{sg_i q} = 0$. As a result, from (3.16), the instantaneous active power P_{g_i} and reactive power Q_{g_i} at the PCC are given by:

$$\begin{aligned} P_{g_i} &= \frac{3}{2} v_{sg_i d} i_{g_i d} \\ Q_{g_i} &= -\frac{3}{2} v_{sg_i d} i_{g_i q} \end{aligned} \tag{3.22}$$

By virtue of the active power balance on both sides of the converter, the DC current i_{cg_i} can be then deduced as

$$i_{cg_i} = \frac{P_{g_i}}{u_{cg_i}} \tag{3.23}$$

while the losses of the phase reactor and the VSC are neglected [Du 2005, Lee 2000].

3.4.2 Weak AC system side

In this thesis work, we choose VSC HVDC linked wind farm as a study case of weak AC system connection [Chaudhary 2008]. The schematic diagram of wind farm with VSC HVDC integration is illustrated in Fig. 3.4. Wind energy is converted into electrical power by wind turbine generators. Actually, the generation capacity of a single wind turbine is small. For example, the capacity of a large wind turbine is about 5MW. Hence, a wind farm (or wind power plant) usually consists of tens or hundreds of distributed wind turn generators which are connected to the collector bus. Since the voltage operating level of each single wind turbine generator is very low, typically 690V, step-up transformers are needed to increase the AC voltage level of wind turbine generator to the collector bus voltage level. Because system impedance can be viewed as aggregated impedance, which contains the impedances of generators, transformers, transmission lines, etc [Gavrilovic 1991], the use of the step-up transformers causes a high impedance leading to the wind farm with very low SCR. Hence, it is reasonable to consider the VSC connected wind farm as a good study example of weak AC network connection.

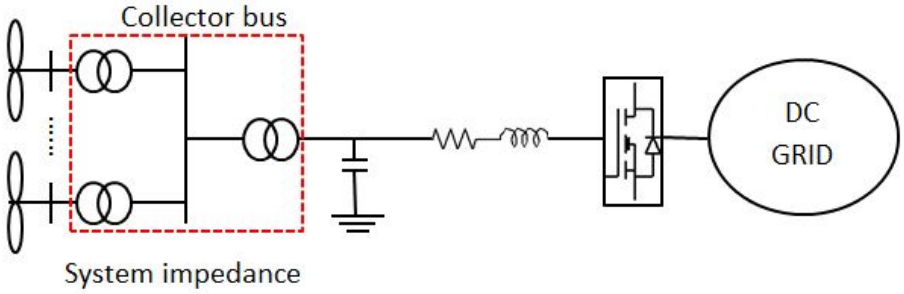

Figure 3.4: A VSC connected to wind farm.

A simplified schematic diagram of the j^{th} VSC connected wind farm is shown in Fig. 3.5. An aggregated output is used to represent all individual wind turbine generator's outputs. In addition, we consider that every wind turbine is based on doubly-fed induction generator (DFIG)[1] [Xu 2007a]. Therefore, the wind farm can be modeled as a controlled source described by $I_{w_j,abc}$ [Pena 1996, Lie 2008]. Due to the use of step-up transformers, some high-order harmonics are produced.

[1] One of the most common technology used for large turbines.

Consequently, the high frequency AC filter represented by a simple capacitor C_{fw_j} is used to eliminate those unacceptable harmonics.

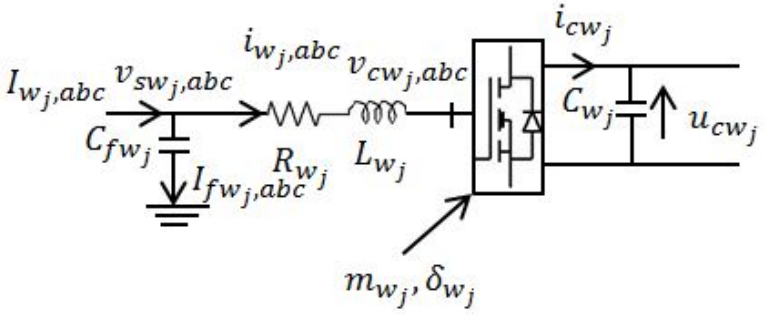

Figure 3.5: A simplified schematic diagram of the j^{th} VSC connected wind farm.

Similar to the modeling of strong AC system connection, the dynamics of the current $i_{w_j,abc}$ flowing into the phase reactor represented by R_{w_j} and L_{w_j} satisfy

$$L_{w_j}\frac{di_{w_j,abc}}{dt} = v_{sw_j,abc} - v_{cw_j,abc} - R_{w_j}i_{w_j,abc} \tag{3.24}$$

where the converter voltages $v_{cw_j,abc}$ are the functions of the DC voltage u_{cw_j}, the amplitude modulation ratio m_{w_j} and the phase angle δ_{w_j} according to (3.1) and (3.2), expressed by

$$v_{cw_j,abc} = \frac{1}{2}u_{cw_j}m_{w_j,abc} \tag{3.25}$$

where

$$\begin{aligned} m_{w_ja} &= m_{w_j}\sin(\omega_{w_j}t + \delta_{w_j}) \\ m_{w_jb} &= m_{w_j}\sin(\omega_{w_j}t - \tfrac{2}{3}\pi + \delta_{w_j}) \\ m_{w_jc} &= m_{w_j}\sin(\omega_{w_j}t + \tfrac{2}{3}\pi + \delta_{w_j}) \end{aligned} \tag{3.26}$$

with $\omega_{w_j} = 2\pi f_{w_j}$. As discussed in Section 2.4, for the WAC connection, the VSC is responsible for assuring the AC voltage at the PCC to operate at fixed frequency and amplitude. So there is no need to synchronize the rotor frequency with the general grid frequency f_{w_j} (usually 50 or 60 Hz), we can freely set ω_{w_j}. For example, we can employ an independent voltage controlled oscillator as an alternative without using PLL technique [Zakaria Moustafa 2008].

The basic equation for the AC voltage $v_{sw_j,abc}$ at the PCC is given by

$$C_{fw_j}\frac{dv_{sw_j,abc}}{dt} = I_{w_j,abc} - i_{w_j,abc} \tag{3.27}$$

After using Park's transformation, the AC side of the VSC connected wind farm in the dq frame is described by

$$\begin{aligned} \frac{di_{w_jd}}{dt} &= -\frac{R_{w_j}}{L_{w_j}}i_{w_jd} + \omega_{w_j}i_{w_jq} + \frac{v_{sw_jd}}{L_{w_j}} - \frac{u_{cw_j}}{2L_{w_j}}m_{w_jd} \\ \frac{di_{w_jq}}{dt} &= -\frac{R_{w_j}}{L_{w_j}}i_{w_jq} - \omega_{w_j}i_{w_jd} + \frac{v_{sw_jq}}{L_{w_j}} - \frac{u_{cw_j}}{2L_{w_j}}m_{w_jq} \end{aligned} \tag{3.28}$$

and

$$\begin{aligned}\frac{dv_{sw_jd}}{dt} &= \omega_{w_j} v_{sw_jq} + \frac{1}{C_{fw_j}}(I_{w_jd} - i_{w_jd}) \\ \frac{dv_{sw_jq}}{dt} &= -\omega_{w_j} v_{sw_jd} + \frac{1}{C_{fw_j}}(I_{w_jq} - i_{w_jq})\end{aligned} \tag{3.29}$$

where the modulation indices m_{w_jd} and m_{w_jq} must satisfy

$$\begin{aligned}m_{w_j} &= \sqrt{m_{w_jd}^2 + m_{w_jd}^2} \leq 1 \\ \delta_{w_j} &= \arctan(\frac{m_{w_jq}}{m_{w_jq}})\end{aligned} \tag{3.30}$$

In addition, according to (3.16), the active and the reactive power at the PCC are given by

$$\begin{aligned}P_{w_j} &= \tfrac{3}{2}(v_{sw_jd} i_{w_jd} + v_{sw_jq} i_{w_jq}) \\ Q_{w_j} &= \tfrac{3}{2}(v_{sw_jq} i_{w_jd} - v_{sw_jd} i_{w_jq})\end{aligned} \tag{3.31}$$

Similarly as in Section 3.4.1, the DC current i_{cw_j} can be deduced as

$$i_{cw_j} = \frac{P_{w_j}}{u_{cw_j}} \tag{3.32}$$

3.4.3 DC network

A generic DC network topology is formed by N SAC converter nodes, M WAC converter nodes, P intermediate nodes and L transmission branches [Prieto-Araujo 2011]. As depicted in Fig. 3.6, the i^{th} SAC converter node, the j^{th} WAC converter node and the h^{th} intermediate node are characterized by their corresponding DC voltages, i.e. u_{cg_i}, u_{cw_j} and u_{ct_h}, and DC capacitors, C_{g_i} and C_{w_j} and C_{t_h}. The k^{th} branch transmission line l_k is modeled by a lumped π-equivalent circuit [Beerten 2014] composed of the aggregated resistance R_{c_k} and inductance L_{c_k}. The branch current of l_k is denoted as i_{c_k}. Every branch circuit is used to connect two adjacent nodes and every node can be connected to a number of transmission lines. As illustrated in Fig. 3.6, the green arrow means that the branch circuit current is fed into the node, whereas the violet one represents the branch circuit current discharges from the node. An example of such DC grid is presented in Fig. 3.7, which consists of two SAC converter nodes ($u_{cg_{1,2}}$), two WAC converter nodes ($u_{cw_{1,2}}$), three intermediate nodes ($u_{ct_{1,2,3}}$) and seven transmission branches (i_{c_k}, $k = 1, \cdots, 7$). It can be seen that the second intermediate node is connected to three transmission branches (l_2, l_5 and l_6). Moreover, it has one incoming current (i_{c_6}) and two outgoing currents (i_{c_1} and i_{c_5}).

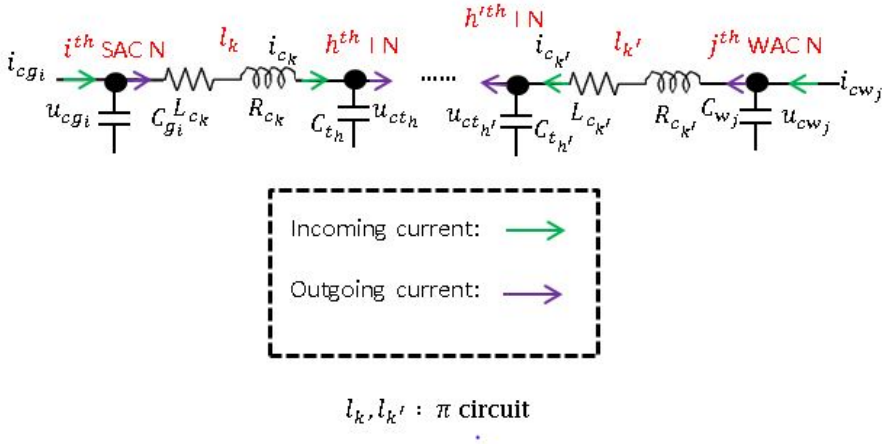

Figure 3.6: DC circuit.

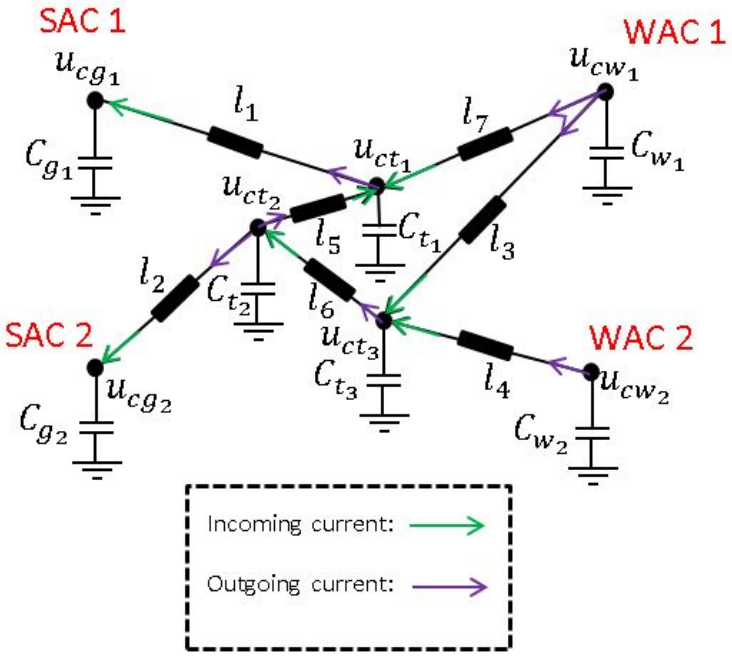

Figure 3.7: An example of the DC grid.

According to basic circuit laws, the dynamic equations for the DC network are

$$\begin{aligned} C_{g_i}\frac{du_{cg_i}}{dt} &= i_{cg_i} + I^+_{cg_i} - I^-_{cg_i} \\ C_{w_j}\frac{du_{cw_j}}{dt} &= i_{cw_j} + I^+_{cw_j} - I^-_{cw_j} \\ C_{t_h}\frac{du_{ct_h}}{dt} &= I^+_{ct_h} - I^-_{ct_h} \\ L_{c_k}\frac{di_{c_k}}{dt} &= U^+_{c_k} - U^-_{c_k} - R_{c_k} i_{c_k} \end{aligned} \tag{3.33}$$

where $I^+_{(\cdot)}$ and $I^-_{(\cdot)}$ represent the node's total incoming and outgoing transmission branch currents respectively. $U^+_{(\cdot)}$ and $U^-_{(\cdot)}$ are the DC voltages of the two nodes connected by l_k.

In order to better understand the properties of the DC network, we analyze its topology structure with the help of graph theory [Parthasarathy 1994]. In this thesis, we study a class of DC networks which can be represented by a weakly connected directed graph G without self-loops. This graph is labeled by $G = (V, E)$. $V = \{V_1,\ V_2,\ V_3\}$ is the set of the vertices where $V_1 = \{v_1,\ \cdots,\ v_N\}$, $V_2 = \{v_{N+1},\ \cdots,\ v_{N+M}\}$ and $V_3 = \{v_{N+M+1},\ \cdots,\ v_{N+M+P}\}$ correspond to the N SAC converter nodes, the M WAC converter nodes and the P intermediate nodes, respectively. $E = \{e_1,\ \cdots,\ e_L\}$ is the set of the edges mapping to the L circuit branches. The incidence matrix of $G = (V, E)$ is denoted by $H \in \mathbb{R}^{(N+M+P)\times L}$ and its element in the l^{th} row and the k^{th} column, i.e. H_{lk}, satisfies

$$H_{lk} = \begin{cases} 1 & \text{if the branch current of } e_k \text{ flows into the node } v_l, \\ -1 & \text{if the branch current of } e_k \text{ flows from the node } v_l, \\ 0 & \text{otherswise.} \end{cases} \tag{3.34}$$

Consider the example illustrated in Fig. 3.7. The corresponding incidence matrix H is of the form

$$H = \begin{array}{c} \\ u_{cg_1} \\ u_{cg_2} \\ u_{cw_1} \\ u_{cw_2} \\ u_{ct_1} \\ u_{ct_2} \\ u_{ct_3} \end{array} \begin{array}{c} \begin{array}{ccccccc} l_1 & l_2 & l_3 & l_4 & l_5 & l_6 & l_7 \end{array} \\ \begin{pmatrix} 1 & 0 & 0 & 0 & 0 & 0 & 0 \\ 0 & 1 & 0 & 0 & 0 & 0 & 0 \\ 0 & 0 & -1 & 0 & 0 & 0 & -1 \\ 0 & 0 & 0 & -1 & 0 & 0 & 0 \\ -1 & 0 & 0 & 0 & 1 & 0 & 1 \\ 0 & -1 & 0 & 0 & -1 & 1 & 0 \\ 0 & 0 & 1 & 1 & 0 & -1 & 0 \end{pmatrix} \end{array} \tag{3.35}$$

As a result, the dynamics of the DC grid (3.33) can be rewritten in matrix expression form

$$\dot{z} = Az + \vartheta \tag{3.36}$$

with the following definitions

$$\begin{aligned}
z &\triangleq \begin{bmatrix} u_c & i_c \end{bmatrix}^T \in \mathbb{R}^{N+M+P+L} \\
u_c &\triangleq \begin{bmatrix} u_{cg} & u_{cw} & u_{ct} \end{bmatrix}^T \\
u_{cg} &\triangleq \begin{bmatrix} u_{cg_1} & \cdots & u_{cg_N} \end{bmatrix}^T \\
u_{cw} &\triangleq \begin{bmatrix} u_{cw_1} & \cdots & u_{cw_M} \end{bmatrix}^T \\
u_{ct} &\triangleq \begin{bmatrix} u_{ct_1} & \cdots & u_{ct_P} \end{bmatrix}^T \\
i_c &\triangleq \begin{bmatrix} i_{c_1} & \cdots & i_{c_L} \end{bmatrix}^T \\
\vartheta &\triangleq \begin{bmatrix} \frac{i_{cg_1}}{C_{g_1}} & \cdots & \frac{i_{cg_N}}{C_{g_N}} & \frac{i_{cw_1}}{C_{w_1}} & \cdots & \frac{i_{cw_M}}{C_{w_M}} & 0_{(P+L)} \end{bmatrix}^T
\end{aligned} \tag{3.37}$$

The matrix A is of the form

$$A = \begin{bmatrix} 0_{(N+M+P)\times(N+M+P)} & C^{-1}H \\ -L^{-1}H^T & -L^{-1}R \end{bmatrix} \tag{3.38}$$

where $C \in \mathbb{R}^{(N+M+P)\times(N+M+P)}$ and $L, R \in \mathbb{R}^{L\times L}$ are the capacitor, inductance and resistance matrices, respectively, which are given by

$$\begin{aligned}
C &= \text{diag}(C_{g_1} \cdots C_{g_N}\ C_{w_1} \cdots C_{w_M}\ C_{t_1} \cdots C_{t_P}) \\
L &= \text{diag}(L_{c_1} \cdots L_{c_L}) \\
R &= \text{diag}(R_{c_1} \cdots R_{c_L})
\end{aligned}$$

In general, the incidence matrix H of the weakly connected directed graph G without self-loops has the following features

- Since the directed graph G is weakly connected, the numbers of the vertices and the edges must satisfy $L \geq (N + M + P) - 1$.
- Every edge (transmission line) can only connect two vertices (nodes) and hence, each column of H has only two non-zero elements, i.e. 1 and -1.

Based on these characteristics, we have the following results whose proofs are referred in [Parthasarathy 1994, Bondy 1976].

Lemma 3.4.1. *The vectors $H(1,:)$, $H(2,:)$, ..., $H(N+M+P,:)$[2] are linearly dependent. In addition, we have $\sum_{i=1}^{N+M+P} H(i,:) = 0_L^T$. The rank of H, i.e. rank(H), is equal to $N + M + P - 1$.*

Lemma 3.4.2. *If any one row is removed from H, for example, the l^{th} row, i.e. $H(l,:)$, we obtain a reduced incidence matrix denoted by $\mathcal{R}(H)_l$ whose rank is still equal to $N + M + P - 1$. It means that any $(N + M + P - 1)$ row vectors of H are linearly independent.*

[2] See the notations.

3.4.4 Domain of interest

It is worthwhile to keep in mind that taking into account physical considerations [Mohan 2003], the feasible region of the state variables is not boundless [Stijn 2010, Haileselassie 2012a]. Therefore, in this thesis work, we restrict the state variables to some domains of interest. All DC voltage u_{cg_i}, u_{cw_j} and u_{ct_h} are considered on the domain $\mathbb{D}_{u_c} \triangleq [u_{c,\min},\ u_{c,\max}] \in \mathbb{R}$ where $u_{c,\min}$ is positive. The current $i_{g_i,dq}$ and $i_{w_j,dq}$ are defined on $\mathbb{D}_{i_{g_i,dq}} \in \mathbb{R}$ and $\mathbb{D}_{i_{w_j,dq}} \in \mathbb{R}$, respectively. All branch currents i_{c_k} are on the domain $\mathbb{D}_{i_c}$. Consequently, the domains $\mathbb{D}_{(\cdot)}$ are defined as the domains of interest, which are bounded.

3.5 Conventional control methods

It is essential for any VSC HVDC system the ability to counteract disturbances with fast response, good transient and steady-state performances. This ability is strongly dependent on the employed control system and hence, a study of control system design for MTDC systems is necessary. Many researches have been devoted to the control design of VSC HVDC systems. In this section, we briefly introduce two conventional control methods, direct and vector control methods, which are widely used and discussed.

3.5.1 Direct control method

Direct control strategy [Ohnishi 1991, Noguchi 1998] is realized by measuring and comparing the controlled outputs to their references in such a way that the control variables, i.e. the phase angle δ and the amplitude modulation ratio m, can be directly obtained by means of PI control technique, and then sent to the pulse width modulator. Figure 3.8 gives the block diagrams of direct control method applied to the four control modes (as discussed in Section 2.4.2) of the i^{th} VSC connected strong grid [Sood 2010]. It can be seen that the errors denoted by $\tilde{(\cdot)}$ between the measured values and the references denoted by $(\cdot)^o$ are sent to PI controllers as the inputs to generate the control variables of the converter. It is interesting to remark that the choice of these PI controllers is completely arbitrary or empirical, without vigorous mathematical proofs for their design. Nevertheless, the direct control method has the following advantages:

- The design concept is quite simple and the controller is easy to be implemented. The control variables are given by

$$\begin{aligned} \delta_{g_i} &= K_{g_i,p_1}(P^o_{g_i} - P_{g_i}) + K_{g_i,i_1}\int(P^o_{g_i} - P_{g_i}) \\ m_{g_i} &= K_{g_i,p_2}(Q^o_{g_i} - Q_{g_i}) + K_{g_i,i_2}\int(Q^o_{g_i} - Q_{g_i}) \\ \delta_{g_i} &= K_{g_i,p_3}(u^o_{cg_i} - u_{cg_i}) + K_{g_i,i_3}\int(u^o_{cg_i} - u_{cg_i}) \\ m_{g_i} &= K_{g_i,p_4}(V^o_{g_i,\text{rms}} - V_{g_i,\text{rms}}) + K_{g_i,i_4}\int(V^o_{g_i,\text{rms}} - V_{g_i,\text{rms}}) \end{aligned} \tag{3.39}$$

  where the control gains of the PI controllers, $K_{g_i,p_{(\cdot)}}$ and $K_{g_i,i_{(\cdot)}}$, are positive. It is shown that the formulas of δ_{g_i} and m_{g_i} are indeed expressed in a fairly simple way.

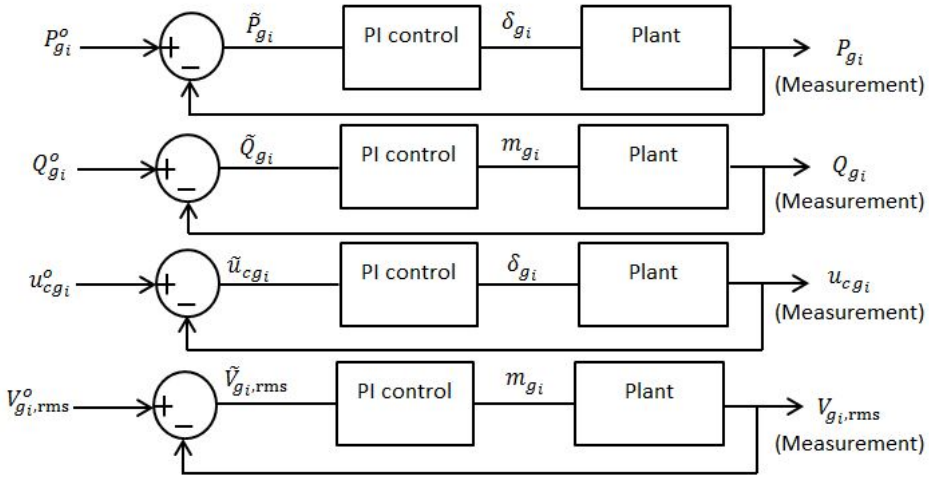

Figure 3.8: Block diagrams of direct control method.

- As seen in the control blocks, there are no other control loops. The direct control method provides a direct and effective way to control both active power (or DC voltage) and reactive power (or AC voltage) without using any other intermediate variable such as the AC current.

- Since the control variables are deduced directly by using the measurements, there is no need to use Clarke's or Park's transformation and hence, no PLL is required in the control algorithm. This avoids an unfavorable influence on the performance of the system due to the non-linearity caused by PLL.

However, the most serious problem of the direct control method is that it has no ability to limit the current flowing into the converter, which may damage the converter in case of over-current. In addition, because of cross-coupling between the control variables as seen in (2.2), the active power and the reactive power can not be controlled independently [Sood 2010]. For example, consider that the i^{th} SAC connection terminal operates in active and reactive control modes. At an instant $t = t_1$, if $P^o_{g_i}$ is subjected to a step change, the control variable δ_{g_i} varies correspondingly. Because of the coupling relation described by (2.2), the reactive power is readily influenced [Zakaria Moustafa 2008].

3.5.2 Vector control method

Vector control method [Lindberg 1994, Lindberg 1996, Blasko 1997] is the most widely used control approach in today's electric power system applications. This control system has a cascaded control structure consisting of two loops, the inner current and the outer control loops. The vector control structure involves the field-oriented vector control technique, which is developed from the representation described by (3.20) of the AC quantities in the dq synchronous reference frame. The

detailed control diagrams of the i^{th} connection terminal are presented in Figs. (3.9) and (3.10).

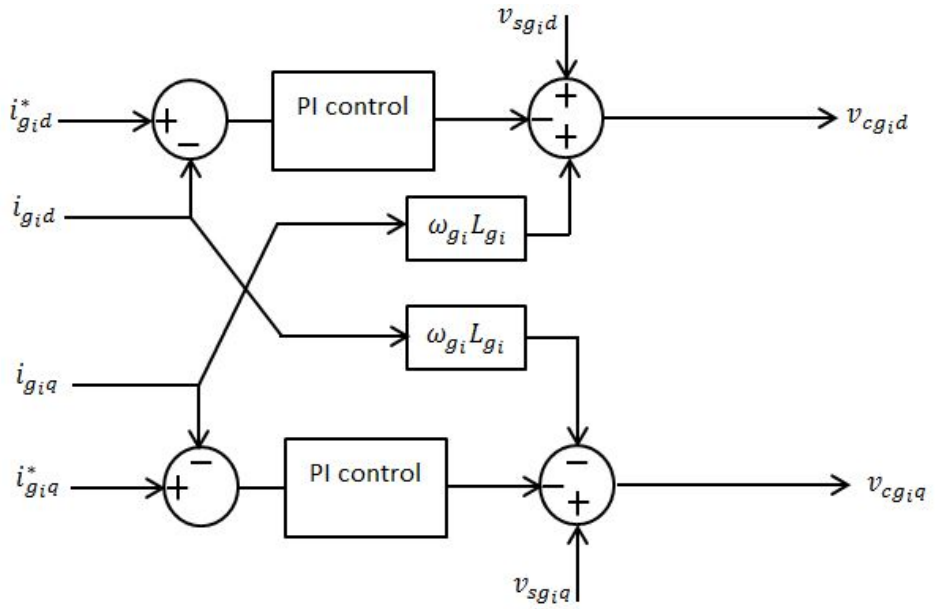

Figure 3.9: Inner current loop.

The vector control algorithm is based on the assumption that the dq currents and the DC voltage are associated to fast and slow dynamics and hence, the inner current and outer loops can be designed independently. To ensure a separation in timescales between the dq current dynamics and the DC voltage dynamics, the size of the DC capacitor should be characterized by a time constant τ defined by

$$\tau = \frac{C_{g_i} u_{\text{rate}}^2}{2S_{\text{rate}}} \tag{3.40}$$

which is the ratio of the energy stored in the capacitor at the rated DC voltage u_{rate} to the rated apparent power S_{rate} of the converter. The time constant is usually chosen no less than 5 ms by taking into account practical constraints [Du 2003].

The main objective of the inner current loop is to design v_{cg_id} and v_{cg_iq} such that i_{g_id} and i_{g_iq} follow their respective reference trajectories $i^*_{g_id}$ and $i^*_{g_iq}$. As illustrated in Fig. 3.9, two PI controllers are involved and then, $v_{cg_i,dq}$ are given by

$$\begin{aligned} v_{cg_id} &= K_{g_i,p_d}(i_{g_id} - i^*_{g_id}) + K_{g_i,i_d}\int(i_{g_id} - i^*_{g_id}) + v_{sg_id} + \omega_{g_i}L_{g_i}i_{g_iq} \\ v_{cg_iq} &= K_{g_i,p_q}(i_{g_iq} - i^*_{g_iq}) + K_{g_i,i_q}\int(i_{g_iq} - i^*_{g_iq}) + v_{sg_iq} - \omega_{g_i}L_{g_i}i_{g_id} \end{aligned} \tag{3.41}$$

Depending on the application (or control mode), the reference $i^*_{g_id}$ can be provided by a DC voltage outer loop or an active power outer loop as

$$\begin{aligned} i^*_{g_id} &= K_{g_i,p_P}(P^o_{g_i} - P_{g_i}) + K_{g_i,i_P}\int(P^o_{g_i} - P_{g_i}) \\ i^*_{g_id} &= K_{g_i,p_u}(u^o_{cg_i} - u_{cg_i}) + K_{g_i,i_u}\int(u^o_{cg_i} - u_{cg_i}) \end{aligned} \tag{3.42}$$

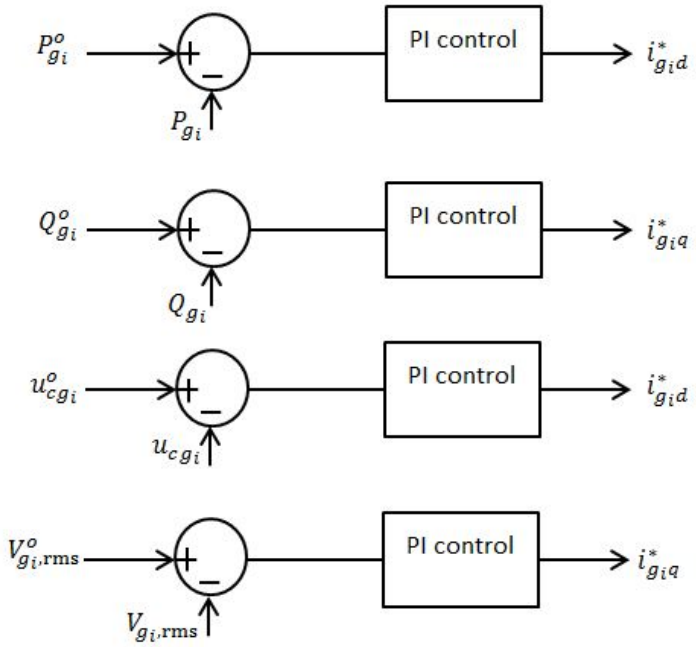

Figure 3.10: Outer current loop.

while the reference $i^*_{g_iq}$ are derived from a reactive outer loop or an AC voltage outer loop as

$$\begin{aligned} i^*_{g_iq} &= K_{g_i,p_Q}(Q^o_{g_i} - Q_{g_i}) + K_{g_i,i_Q}\int(Q^o_{g_i} - Q_{g_i}) \\ i^*_{g_iq} &= K_{g_i,p_V}(V^o_{g_i,\mathrm{rms}} - V_{g_i,\mathrm{rms}}) + K_{g_i,i_V}\int(V^o_{g_i,\mathrm{rms}} - V_{g_i,\mathrm{rms}}) \end{aligned} \tag{3.43}$$

To obtain the best possible performance of the system, modulus optimum and symmetrical optimum techniques are usually applied to tune the control gains of the PI controllers [Bajracharya 2008].

Compared to the direct control method, the vector control method has superior advantages:

- The active power and the reactive power can be controlled independently by using the inner current loop with feed-forward compensations to remove the coupling terms.
- This method inherently has the ability to protect the converter against overcurrent in case of disturbances due to the inner current control loop.
- It provides faster response and better performance than the direct control method in case of variations in references or some other disturbances.

The vector control structure is basically composed by several standard PI controllers, whose implementation and design are simple. Nevertheless, the use of such pure PI controllers results in some limitations [Dannehl 2009, Durrant 2003]. On the one hand, the performance of the vector control scheme is very sensible to the

system uncertainties. On the other hand, in order to apply Park's transformation, a PLL is needed to provide a synchronous reference frame. The dynamics of the PLL and AC filters increase the difficulty in the VSC control when the SCR of the connected AC system decreases.

3.6 Chapter conclusions

In this chapter, we choose the averaged modeling approach to develop the dynamical model for a multi-terminal VSC HVDC system. The modeling work mainly focuses on three parts, i.e. the VSC connected strong AC networks, the VSC connected wind farms and the DC network. According to the features of the VSC connected AC systems, we have different considerations:

- For the VSC connected strong AC networks, the SRF-PLL is usually required to detect the phase and frequency of the electrical circuit such that the VSC can be synchronized to its connected strong AC system whereas there is no need for the VSC connected weak AC network.
- For a strong AC system, we consider that its AC voltage at the PCC can be kept by TSO at fixed frequency and amplitude. This is contrary to the case of a weak AC system, which with high impedance is very sensible to any disturbances (for example, the change of power flow), it is necessary in that case to consider the dynamics of the weak AC system's AC voltage at the PCC.

For the sake of convenience, Park's transformation is applied to transform the system from the *abc* frame into the *dq* reference frame, which greatly simplifies the expression of the dynamic equations. For the DC network, we map it to a weakly connected directed graph and then use a incidence matrix to describe its topology. It is much easier to analyze the DC grid in matrix form since there exist quite a lot of results on matrix and graph studies.

Finally, a detailed averaged state-space model for the multi-terminal VSC HVDC system described by (3.20), (3.28), (3.29) and (3.36) is established. We summarize this model as follows

- The dimension of the full scale system is $3N + 5M + P + L$.
- The state variables are $i_{g_i,dq}$, $i_{w_j,dq}$, $v_{sw_j,dq}$, u_{cg_i}, u_{cw_j}, u_{ct_h} and i_{c_k} for $i \in \mathcal{N}$, $j \in \mathcal{M}$, $h \in \mathcal{P}$ and $k \in \mathcal{L}$[3].
- The control inputs are the modulation indices, i.e. $m_{g_i,dq}$ and $m_{w_j,dq}$ for $i \in \mathcal{N}$ and $j \in \mathcal{M}$.
- The external parameters $I_{w_j,dq}$, for $j \in \mathcal{M}$, are considered constant.

[3]Unless otherwise stated, the subscripts i, j, t and k mean $\forall i \in \mathcal{N} = \{1, \cdots, N\}$, $\forall j \in \mathcal{M} = \{1, \cdots, M\}$, $\forall h \in \mathcal{P} = \{1, \cdots, P\}$ and $\forall k \in \mathcal{L} = \{1, \cdots, L\}$.

- The values of all physical parameters, i.e. the resistances, the inductances and the the capacitors, are positive.

Moreover, in this chapter, we have also presented two most investigated conventional control strategies, direct and vector control strategies, and introduced their control principles. In addition, we have also discussed their advantages and disadvantages.

Chapter 4

Control methods based on nonlinear control design tools

Contents

Although the vector control method occupies a predominant position in the field of control design for VSC HVDC systems, the limitations of this approach also draw our attention [Dannehl 2009]. In particular, in [Dannehl 2009], it indicates that the traditional vector current control is very sensitive to system uncertainties. In [Durrant 2003], a detailed analysis of a VSC connected to a weak AC system is carried out. It is shown that the dynamics of PLL and AC filter increase the difficulty in the VSC control when the SCR of the connected AC system decreases. In order to improve the performance of VSC HVDC systems, developing new control structures has been a very popular research topic.

In this chapter, we propose new control structures by means of different nonlinear control design tools for VSC HVDC systems.

4.1 Feedback linearization control

Feedback linearization is well-known in the field of nonlinear control design. The principle of this technique is to transform the nonlinear system fully or partly to a linear one and thereafter, linear control, robust control or some other control techniques can be applied. As presented in [Lee 2000, Kim 2010], feedback linearization is applied to three-phase converters. However, only a single three-phase converter station is considered in their study case. Reference [Moharana 2010] proposes a nonlinear controller based on input-output feedback linearizaiton and sliding mode control. However, in [Moharana 2010], the stability of the zero dynamics of the system is not analyzed, which determines whether the feedback linearization is applicable for the control design.

In this section, according to the control objectives of HVDC systems, we develop different nonlinear controllers by making full use of feedback linearization where the corresponding zero dynamics are also analyzed.

Before designing the exact control structures to VSC HVDC systems, we give a brief introduction to feedback linearizaiton for multi-input and multi-output (MIMO) nonlinear systems [Khalil 1996, Isidori 1995, Slotine 1991, Hedrick 2005].

4.1.1 Theoretical results

Consider a class of MIMO systems

$$\begin{array}{l} \dot{x}= f(x)+\sum_{j=1}^{j=m} g_j(x)u_j \\ y\triangleq \begin{bmatrix} y_1 & \cdots & y_m \end{bmatrix}^T = \begin{bmatrix} h_1(x) & \cdots & h_m(x) \end{bmatrix}^T \end{array} \tag{4.1}$$

where the control input vector $u = \begin{bmatrix} u_i & \cdots & u_m \end{bmatrix} \in \mathbb{R}^m$ has the same dimension as the output vector y. The functions f, g_j and h_j, $i = 1, \cdots, m$, are sufficiently smooth in an open set $\mathbb{D} \subset \mathbb{R}^m$. The mappings $f : \mathbb{D} \to \mathbb{R}^n$ and $g_i : \mathbb{D} \to \mathbb{R}$ are the vector fields on $\mathbb{D}$. The derivative of the i^{th} output y_i is given by

$$\dot{y}_i = L_f h_i(x) + \sum_{j=1}^{j=m} L_{g_j} h_i(x) u_j \tag{4.2}$$

where

$$\begin{array}{l} L_f h_i(x) \triangleq \dfrac{\partial h_i}{\partial x} f(x) \\ L_{g_j} h_i(x) \triangleq \dfrac{\partial h_i}{\partial x} g_j(x) \end{array} \tag{4.3}$$

are the Lie derivatives of $h_i(x)$ with respect to f and g_i. If all $L_{g_j} h_i(x) = 0$, we continue to differentiate y_i until some u_j explicitly appears in the γ_i^{th} derivative of y_i as follows

$$y_i^{(\gamma_i)} = L_f^{\gamma_i} h_i(x) + \sum_{j=1}^{j=m} L_{g_j} (L_f^{\gamma_i - 1} h_i) u_j \tag{4.4}$$

where $L_{g_j} (L_f^{\gamma_i - 1} h_i) = \dfrac{\partial (L_f^{\gamma_i - 1} h_i)}{\partial x} g_j \neq 0$ for some $j \in \{1, \ , \cdots, \ m\}$. In this case, γ_i is called the relative degree (see Definition 13.2 in [Khalil 1996]) of the i^{th} output

$y_i = h_i(x)$. After performing the above procedure for each output, we obtain m equations in a similar form as (4.4), which can be expressed in matrix form

$$y^\gamma = l^\gamma + Eu \tag{4.5}$$

where the decoupling matrix $E \in \mathbb{R}^{m\times m}$ and the vectors y^γ, l^γ and u are given by

$$\begin{aligned} E(x) &= \begin{bmatrix} L_{g_1}(L_f^{\gamma_1-1}h_1) & \cdots & L_{g_m}(L_f^{\gamma_1-1}h_1) \\ \cdots & \cdots & \cdots \\ L_{g_1}(L_f^{\gamma_m-1}h_m) & \cdots & L_{g_m}(L_f^{\gamma_m-1}h_m) \end{bmatrix} \\ y^\gamma &= \begin{bmatrix} y_1^{(\gamma_1)} & \cdots & y_m^{(\gamma_m)} \end{bmatrix}^T \\ l^\gamma &= \begin{bmatrix} L_f^{\gamma_1}h_1 & \cdots & L_f^{\gamma_m}h_m \end{bmatrix}^T \\ u &= \begin{bmatrix} u_1 & \cdots & u_m \end{bmatrix}^T \end{aligned} \tag{4.6}$$

If the decoupling matrix E is non-singular in $\mathbb{D}$, then the control vector u can be designed as

$$u = E^{-1}(v - l^\gamma) \tag{4.7}$$

where $v = \begin{bmatrix} v_1 & \cdots & v_m \end{bmatrix}^T$ is the additional input vector. Substituting (4.7) into (4.5) yields

$$\begin{bmatrix} y_1^{(\gamma_1)} \\ \cdots \\ y_m^{(\gamma_m)} \end{bmatrix} = \begin{bmatrix} v_1 \\ \cdots \\ v_m \end{bmatrix} \tag{4.8}$$

which results in a decoupled set of equations. The additional input v can be designed using any linear method or other techniques. For example, if the control objective is to make y follow the reference $y_d = \begin{bmatrix} y_{d1} & \cdots & y_{dm} \end{bmatrix}^T$, then v can be designed as

$$\begin{bmatrix} v_1 \\ \cdots \\ v_m \end{bmatrix} = \begin{bmatrix} -c_{1,0}(y_1 - y_{d1}) - \cdots - c_{1,\gamma_1-1}(y_1^{(\gamma_1-1)} - y_{d1}^{(\gamma_1-1)}) \\ \cdots \\ -c_{m,0}(y_m - y_{dm}) - \cdots - c_{m,\gamma_m-1}(y_m^{(\gamma_m-1)} - y_{dm}^{(\gamma_m-1)}) \end{bmatrix} \tag{4.9}$$

where the coefficients $c_{(\cdot)}$ are chosen such that for all $j \in \{1, \cdots, m\}$

$$C_j = \begin{bmatrix} 0 & 1 & 0 & \cdots & 0 \\ 0 & 0 & 1 & \cdots & 0 \\ \cdots & \cdots & \cdots & \cdots & \cdots \\ 0 & 0 & 0 & \cdots & 1 \\ -c_{j,0} & -c_{j,1} & -c_{j,2} & \cdots & -c_{j,\gamma_j-1} \end{bmatrix} \in \mathbb{R}^{\gamma_j\times\gamma_j} \tag{4.10}$$

are Hurwitz. In addition, with the integrated tracking error $e \triangleq \begin{bmatrix} e_1 & \cdots & e_m \end{bmatrix}^T = y - y_d$, v is then designed as

$$\begin{bmatrix} v_1 \\ \cdots \\ v_m \end{bmatrix} = \begin{bmatrix} -c_{1,0}(y_1 - y_{d1}) - \cdots - c_{1,\gamma_1-1}(y_1^{(\gamma_1-1)} - y_{d1}^{(\gamma_1-1)}) - k_{I1}e_{I1} \\ \cdots \\ -c_{m,0}(y_m - y_{dm}) - \cdots - c_{m,\gamma_m-1}(y_m^{(\gamma_m-1)} - y_{dm}^{(\gamma_m-1)}) - k_{Im}e_{Im} \end{bmatrix} \tag{4.11}$$

where e_{Ij} satisfies

$$\dot{e}_{Ij} = e_j = y_j - y_{dj} \tag{4.12}$$

Again, the control gains must be chosen such that for all $j \in \{1, \cdots, m\}$

$$C'_j = \begin{bmatrix} 0 & 1 & 0 & \cdots & 0 \\ 0 & 0 & 1 & \cdots & 0 \\ \cdots & \cdots & \cdots & \cdots & \cdots \\ 0 & 0 & 0 & \cdots & 1 \\ -k_{Ij} & -c_{j,0} & -c_{j,1} & \cdots & -c_{j,\gamma_j-1} \end{bmatrix} \in \mathbb{R}^{(\gamma_j+1)\times(\gamma_j+1)} \tag{4.13}$$

are Hurwitz. The term $(-k_{Ij}e_{Ij})$ is used to eliminate the tracking error so as to improve the robustness of the system.

If the relative degree of the whole system (4.1)

$$\gamma = \textstyle\sum_{j=1}^{m} \gamma_j \tag{4.14}$$

is smaller than n, there exist internal dynamics of order $n-\gamma$ which are unobservable. We perform the change of variables

$$z = T(x) \triangleq \begin{bmatrix} & \eta & \\ - & - & - \\ & \xi & \end{bmatrix} \triangleq \begin{bmatrix} & \phi_1(x) & \\ & \cdots & \\ & \phi_{n-r}(x) & \\ - & - & - \\ & \xi & \end{bmatrix} \tag{4.15}$$

and ξ is taken as

$$\xi \triangleq \begin{bmatrix} \xi_1 \\ \cdots \\ \xi_m \end{bmatrix}, \ \xi_j \triangleq \begin{bmatrix} y_j \\ \cdots \\ y_j^{(\gamma_j-1)} \end{bmatrix} \tag{4.16}$$

where ϕ_k, $k = 1, \cdots, n-\gamma$, are chosen to ensure that the transformation T is a diffeomorphism on $\mathbb{D}$. In the new variable (η, ξ), the system (4.1) becomes

$$\begin{aligned} \dot{\eta} &= \Psi_1(\eta, \xi) + \Psi_2(\eta, \xi)u \\ \dot{\xi}_j &= A_j\xi_j + B_j v_j \end{aligned} \tag{4.17}$$

where

$$A_j = \begin{bmatrix} 0 & 1 & 0 & \cdots & 0 \\ 0 & 0 & 1 & \cdots & 0 \\ \cdots & \cdots & \cdots & \cdots & \cdots \\ 0 & 0 & 0 & \cdots & 1 \\ 0 & 0 & 0 & \cdots & 0 \end{bmatrix} \in \mathbb{R}^{\gamma_j\times\gamma_j}, \ B_j = \begin{bmatrix} 0 \\ 0 \\ \cdots \\ 0 \\ 1 \end{bmatrix} \in \mathbb{R}^{\gamma_j} \tag{4.18}$$

When the output y is identically equal to the reference y_d, the system (4.17) is degenerated into

$$\dot{\eta} = \Psi_1(\eta, \bar{\xi}) + \Psi_2(\eta, \bar{\xi})\bar{u} \tag{4.19}$$

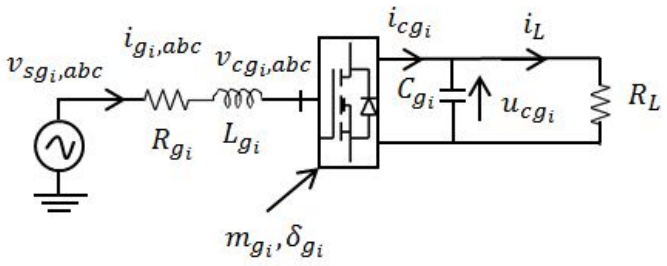

Figure 4.1: A resistive load R_L is connected to the i^{th} SAC terminal.

According to (4.7), $\bar{u}$ and $\bar{\xi}$ are given by

$$\bar{u} = -E^{-1}l^{\gamma},\ \bar{\xi} \triangleq \begin{bmatrix} \bar{\xi}_1 \\ \bar{\xi}_2 \\ \cdots \\ \bar{\xi}_m \end{bmatrix},\ \bar{\xi}_j = \begin{bmatrix} y_{dj} \\ 0 \\ \cdots \\ 0 \end{bmatrix} \tag{4.20}$$

Actually, the autonomous system (4.19) is called the zero dynamics. Since ξ can be stabilized at its equilibrium $\bar{\xi}$ by designing a suitable expression for the additional input v, the stability of the system (4.17) totally depends on the stability of the zero dynamics (4.19). The system (4.1) is said to be minimum phase if the equilibrium point of the zero dynamics is asymptotically stable. Moreover, the input-output linearization is applicable to the system (4.1) when it is minimum phase.

4.1.2 Application to a VSC HVDC link connected to a resistive load

4.1.2.1 Control design

A simple VSC HVDC link is considered as shown in Fig. 4.1 where a resistive load R_L is connected to the i^{th} SAC terminal. As presented in Section 3.4.1, the system can be modeled by

$$\begin{aligned} \frac{di_{g_id}}{dt} &= -\frac{R_{g_i}}{L_{g_i}} i_{g_id} + \omega_{g_i} i_{g_iq} + \frac{v_{sg_id}}{L_{g_i}} - \frac{u_{cg_i}}{2L_{g_i}} m_{g_id} \\ \frac{di_{g_iq}}{dt} &= -\frac{R_{g_i}}{L_{g_i}} i_{lq} - \omega_{g_i} i_{g_id} + \frac{v_{sg_iq}}{L_{g_i}} - \frac{u_{cg_i}}{2L_{g_i}} m_{g_iq} \\ \frac{du_{cg_i}}{dt} &= \frac{1}{C_{g_i}}(i_{cg_i} - i_L) \end{aligned} \tag{4.21}$$

According to (3.23), i_{cg_i} is deduced as

$$i_{cg_i} = \frac{3}{2} \frac{v_{sg_id} i_{g_id} + v_{sg_iq} i_{g_iq}}{u_{cg_i}} \tag{4.22}$$

and i_L is given by

$$i_L = \frac{u_{cg_i}}{R_L} \tag{4.23}$$

Since there are two control inputs $m_{g_i,dq}$, it is possible to control two outputs. To ensure the normal operation of the system, the DC voltage transmission level must be always kept within its acceptable range. As a results, u_{cg_i} is chosen as one output, which is required to track the reference $u^o_{cg_i}$. For the purpose of good power quality, the reactive power Q_{g_i} should be well-behaved. From (3.22), it is clear that i_{g_id} and i_{g_iq} regulate the active and reactive power, respectively. Consequently, i_{g_iq} is chosen as the other output, which is expected to follow the reference $i^o_{g_iq}$ given by

$$i^o_{g_iq} = -\frac{2}{3}\frac{Q^o_{g_i}}{v_{sg_id}} \tag{4.24}$$

where $Q^o_{g_i}$ is the desired reactive power. For example, in order to get the unitary power factor, $Q^o_{g_i}$ is usually set to zero.

By defining $\begin{bmatrix} x_1 & x_2 & x_3 \end{bmatrix} \triangleq \begin{bmatrix} i_{g_id} & i_{g_iq} & u_{cg_i} \end{bmatrix}$, the system (4.21) can be rewritten as

$$\dot{x} = f_x(x) + g_d m_{g_id} + g_q m_{g_iq} \tag{4.25}$$

where $f(x)$, g_d and g_q are given by

$$f_x = \begin{bmatrix} -\frac{R_{g_i}}{L_{g_i}} i_{g_id} + \omega_{g_i} i_{g_iq} + \frac{v_{sg_id}}{L_{g_i}} \\ -\frac{R_{g_i}}{L_{g_i}} i_{lq} - \omega_{g_i} i_{g_id} + \frac{v_{sg_iq}}{L_{g_i}} \\ \frac{1}{C_{g_i}}\left(\frac{3}{2}\frac{v_{sg_id} i_{g_id} + v_{sg_iq} i_{g_iq}}{u_{cg_i}} - \frac{u_{cg_i}}{R_L}\right) \end{bmatrix} \tag{4.26}$$

and

$$g_d = \begin{bmatrix} -\frac{u_{cg_i}}{2L_{g_i}} \\ 0 \\ 0 \end{bmatrix}, \; g_q = \begin{bmatrix} 0 \\ -\frac{u_{cg_i}}{2L_{g_i}} \\ 0 \end{bmatrix} \tag{4.27}$$

The two outputs in this case are defined as

$$y \triangleq \begin{bmatrix} y_1 & y_2 \end{bmatrix}^T = \begin{bmatrix} i_{g_iq} & u_{cg_i} \end{bmatrix}^T \tag{4.28}$$

which are needed to be regulated at $y^o \triangleq \begin{bmatrix} y^o_1 & y^o_2 \end{bmatrix}^T = \begin{bmatrix} i^o_{g_iq} & u^o_{cg_i} \end{bmatrix}^T$.

It is evident that γ_1 and γ_2, the relative degrees of u_{cg_i} and i_{g_iq}, are equal to 2 and 1, respectively. The relative degree of the whole system is 3 which is equal to the dimension of the system (4.21). This means that the system is feedback linearizable and there is no unobservable dynamics. The decoupling matrix E_1 is given by

$$E_1 = \begin{bmatrix} L_{g_d}(i_{g_iq}) & L_{g_q}(i_{g_iq}) \\ L_{g_d}L_{f_x}(u_{cg_i}) & L_{g_q}L_{f_x}(u_{cg_i}) \end{bmatrix} \tag{4.29}$$

where

$$\begin{aligned} L_{g_d}(i_{g_iq}) &= 0 \\ L_{g_q}(i_{g_iq}) &= -\frac{u_{cg_i}}{2L_{g_i}} \\ L_{g_d}L_{f_x}(u_{cg_i}) &= -\frac{1}{C_{g_i}}\frac{3}{4}\frac{v_{sg_id}}{L_{g_i}} \\ L_{g_q}L_{f_x}(u_{cg_i}) &= -\frac{1}{C_{g_i}}\frac{3}{4}\frac{v_{sg_iq}}{L_{g_i}} \end{aligned} \tag{4.30}$$

Since we only consider the case when u_{cg_i} is positive, E is invertible in the domain of interest. Therefore, a nonlinear feedback control can be developed as

$$\begin{bmatrix} m_{g_id} \\ m_{g_iq} \end{bmatrix} = E_1^{-1} \begin{bmatrix} v_1 - L_{f_x}(i_{g_iq}) \\ v_2 - L_{f_x}^2(u_{cg_i}) \end{bmatrix} \tag{4.31}$$

where

$$\begin{aligned} L_{f_x}(i_{g_iq}) = & -\tfrac{R_{g_i}}{L_{g_i}} i_{g_id} + \omega_{g_i} i_{g_iq} + \tfrac{v_{sg_id}}{L_{g_i}} \\ L_{f_x}^2(u_{cg_i}) = & \frac{1}{C_{g_i}} \{ \frac{3}{2} \frac{v_{sg_id}}{u_{cg_i}} (-\frac{R_{g_i}}{L_{g_i}} i_{g_id} + \omega_{g_i} i_{g_iq} + \frac{v_{sg_id}}{L_{g_i}}) \\ & + \frac{3}{2} \frac{v_{sg_iq}}{u_{cg_i}} (-\frac{R_{g_i}}{L_{g_i}} i_{g_iq} - \omega_{g_i} i_{g_id} + \frac{v_{sg_iq}}{L_{g_i}}) \} \\ & - [\frac{3}{2} \frac{v_{sg_id} i_{g_id} + v_{sg_iq} i_{g_iq}}{u_{cg_i}^2} + \frac{1}{R_{load}}] \frac{du_{cg_i}}{dt} \} \end{aligned} \tag{4.32}$$

The additional control inputs v_1 and v_2 are yet to be designed.

Consider the transformation

$$z \triangleq \begin{bmatrix} z_1 \\ z_2 \\ z_3 \end{bmatrix} = T_x = \begin{bmatrix} i_{g_iq} \\ u_{cg_i} \\ \dot{u}_{cg_i} \end{bmatrix} \tag{4.33}$$

which is a diffeomorphism on the domains of interest and then, the original system (4.21) can be converted into the following expression

$$\begin{aligned} \dot{z}_1 &= v_1 \\ \dot{z}_2 &= z_3 \\ \dot{z}_3 &= v_2 \end{aligned} \tag{4.34}$$

We define the tracking errors as

$$\begin{aligned} e_1 &= z_1 - i_{g_iq}^o \\ e_2 &= z_2 - u_{cg_i}^o \end{aligned} \tag{4.35}$$

To achieve zero steady-state errors, the integrated tracking errors

$$\begin{aligned} \dot{e}_{I1} &= e_1 \\ \dot{e}_{I2} &= e_2 \end{aligned} \tag{4.36}$$

are considered, which result in an augmented system described by

$$\begin{aligned} \dot{e}_{I1} &= e_1 \\ \dot{e}_1 &= v_1 \\ \dot{e}_{I2} &= e_2 \\ \dot{e}_2 &= z_3 \\ \dot{z}_3 &= v_2 \end{aligned} \tag{4.37}$$

Applying linear control technique, v_1 and v_2 are designed as

$$\begin{aligned} v_1 &= -k_{I1} e_{I1} - c_{1,0} e_1 \\ v_2 &= -k_{I2} e_{I2} - c_{2,0} e_2 - c_{2,1} \dot{z}_3 \end{aligned} \tag{4.38}$$

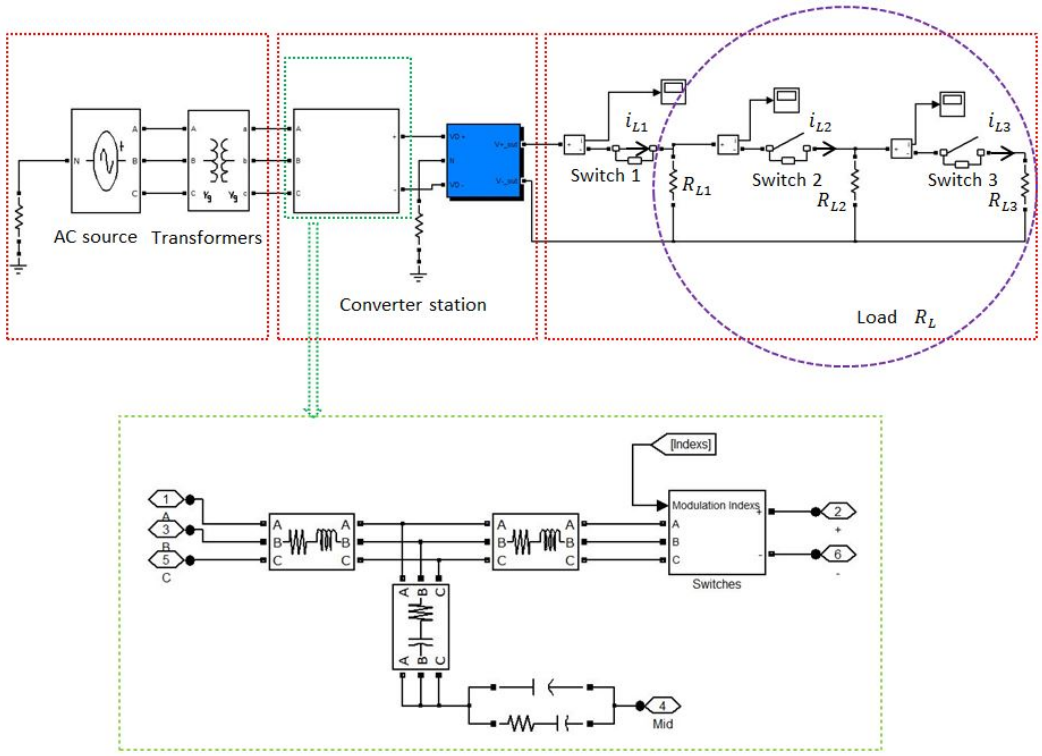

Figure 4.2: Model of VSC HVDC link connected to a resistive load using SimPowerSystems toolbox.

The control gains are chosen such that matrices C_1' and C_2' given by

$$C_1' = \begin{bmatrix} 0 & 1 \\ -k_{I1} & -c_{1,0} \end{bmatrix}, \; C_2' = \begin{bmatrix} 0 & 1 & 0 \\ 0 & 0 & 1 \\ -k_{I2} & -c_{2,0} & -c_{2,1} \end{bmatrix} \tag{4.39}$$

are Hurwitz. Now the controller composed by (4.31) and (4.38) has been developed.

4.1.2.2 Simulation studies

To evaluate the performance of the nonlinear controller, numerical simulations are carried out by using SimPowerSystems toolbox of MATLAB/Simulink as depicted in Fig. 4.2. Detailed parameters of the VSC link are provided in Table 4.1. The DC voltage reference $u_{cg_i}^o$ is set to 150 V and to get the unitary power factor, the reference of $q-$axis $i_{g_iq}^o$ is equal to 0 A. At the start of the simulation, only Switch 1 is closed and the other two switches are open and hence we have $R_L = R_{L1}$. The VSC HVDC link initially operates in a steady-state condition given by Table 4.2.

Figures 4.3-4.5 present the tracking performance of the system that responds to the step change imposed on the DC voltage reference $u_{cg_i}^o$ while $i_{g_iq}^o$ is always set to zero. At $t = 0.8$, $u_{cg_i}^o$ is changed from 150 V to 151.5 V and then, at $t = 1.8$ s, it is set back to 150 V. As depicted in Fig. 4.3, both PI and feedback nonlinear

Table 4.1: Parameters of the VSC HVDC link.

Parameters	Value
Power System Rating	4 KVA
Source Voltage Amplitude (V_{rms} phase-to-phase)	127 V
Source Voltage Frequency	50 Hz
Switching Frequency for PWM	1500 Hz
Transformer Primary Voltage	127 V
Transformer Secondary Voltage	50 V
Inductance L_{g_i}	2.1 mH
Resistance R_{g_i}	0.142 Ω
$R_{L_{1,2,3}}$	150 Ω

Table 4.2: Initial values of the system variables.

Variables	Values
R_L	150 Ω
u_{cg_i}	150 V
i_{g_iq}	0 A
i_L	1 A
i_{g_id}	2.46 A

controllers have similar performance, i.e. they make u_{cg_i} track its reference $u^o_{cg_i}$ with fast response and good transient performance. In addition, i_{g_iq} as displayed in Fig. 4.4 is always regulated at zero irrespective of the change in $u^o_{cg_i}$. As illustrated in Fig. 4.5, every time u_{cg_i} achieves a new steady state, i_{L1} also arrives at a corresponding steady state since in steady-state condition, i_{L1} and u_{cg_i} satisfy $u_{cg_i} = R_L i_{L1}$.

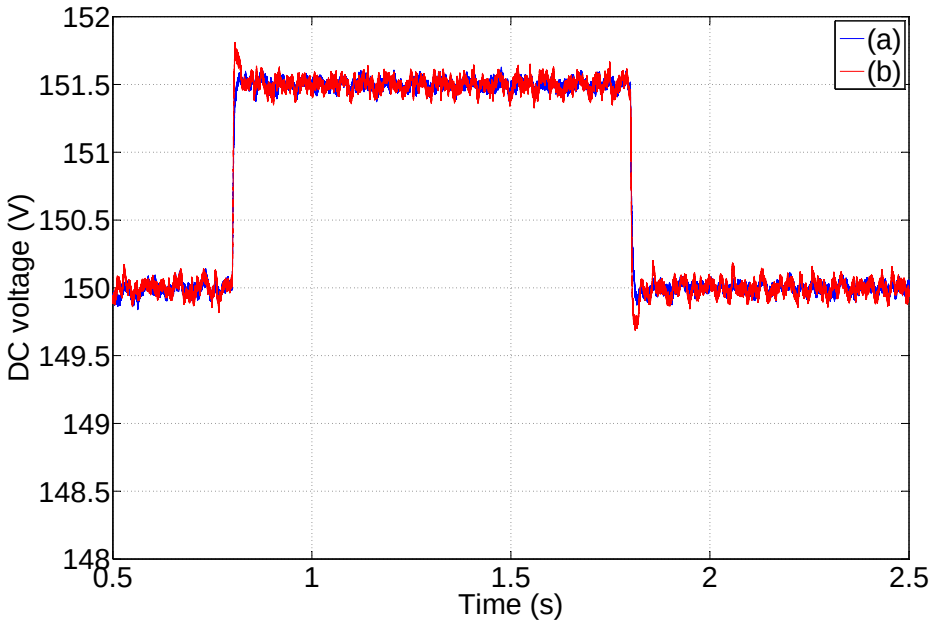

Figure 4.3: The response of DC voltage for the change of $u^o_{cg_i}$. (a) PI controller. (b) Feedback nonlinear controller.

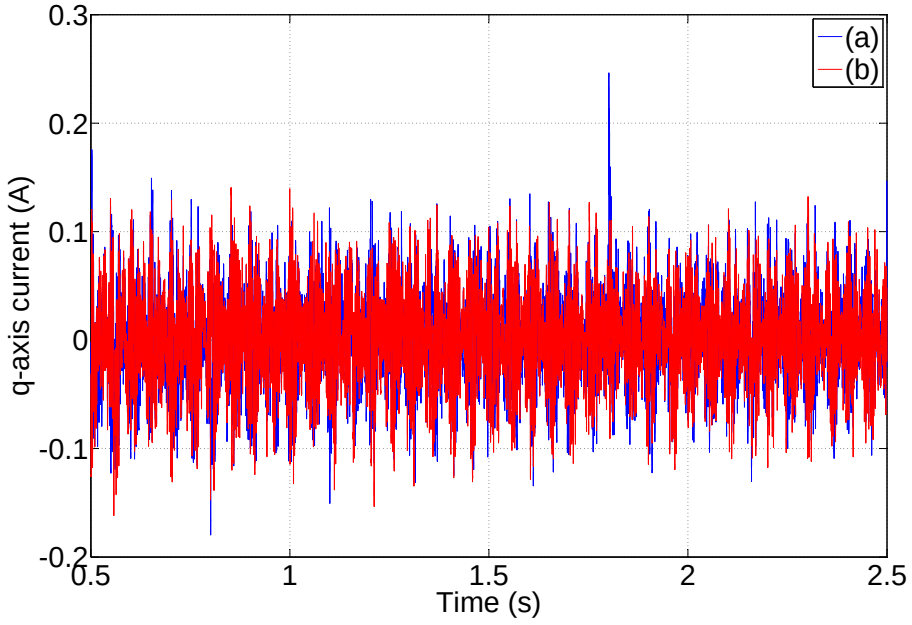

Figure 4.4: The response of i_{g_iq} for the change of $u^o_{cg_i}$. (a) PI controller. (b) Feedback nonlinear controller.

Table 4.3: Sequence of events applied to the VSC HVDC link.

	t=1 s	t=1.5 s	t=2 s
Switch 2	closed		
Switch 3		closed	
$i^o_{g_iq}$			6.53 A

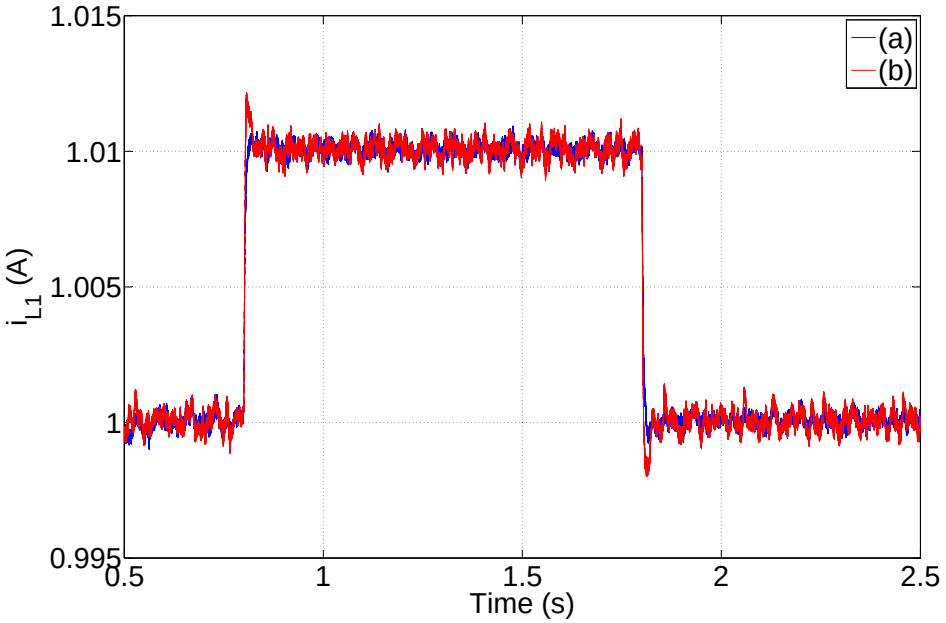

Figure 4.5: The response of i_L for the change of $u^o_{cg_i}$. (a) PI controller. (b) Feedback nonlinear controller.

To test the robustness of both controllers in case of the variations in R_L and the step change in $i^o_{g_iq}$, a sequence of events is applied to the system, as listed in Table 4.3. The simulation results are illustrated in Figs. 4.6-4.11 where the performances of the conventional PI and feedback nonlinear controller are compared. Due to the operations of Switch 2 and Switch 3, R_L is changed from 150 Ω to 75 Ω at $t = 1$ s, and then it is reduced to 50 Ω at $t = 1.5$ s.

As shown in Fig. 4.6, the trajectories of u_{cg_i} are always kept within the safe operating domain $[0.9u^o_{cg_i},\ 1.1u^o_{cg_i}]$ under both controllers, but the response of u_{cg_i} has better performance using feedback nonlinear controller. It can be seen that u_{cg_i} has a faster response and lower crest value under the feedback nonlinear controller (see the red curve). Although both approaches are able to regulate i_{g_iq} at zero before $t = 2$ s, for the PI controller, i_{g_iq} is disturbed with remarkable transient because of the unexpected change in R_L (see the blue curves in Fig. 4.7 and Figs. 4.9-4.11). At $t = 2$ s, $i^o_{g_iq}$ is set to 6.53 A. As presented in Fig. 4.7, both trajectories of i_{g_iq} start to increase and then quickly converge to the new reference. During the

q-axis current's increasing period, we find that significant overshoots appear in the trajectories of u_{cg_i}, i_{L1}, i_{L2} and i_{L3} under the PI controller (see the blue curve in Fig. 4.6) whereas there is little or negligible influence on the responses of u_{cg_i}, i_{L1}, i_{L2} and i_{L3} under the feedback nonlinear controller. This phenomenon fully shows that the PI controller can not keep the DC voltage unaffected in case of the change of i_{g_iq} while the feedback nonlinear controller provides a much better decoupling characteristics of the DC voltage and $q-$axis current control. Moreover, Figs. 4.8-4.11 illustrate that the feedback nonlinear controller gives a faster response (a faster rising time) as well as a smaller undershoot to the DC current than the conventional PI controller.

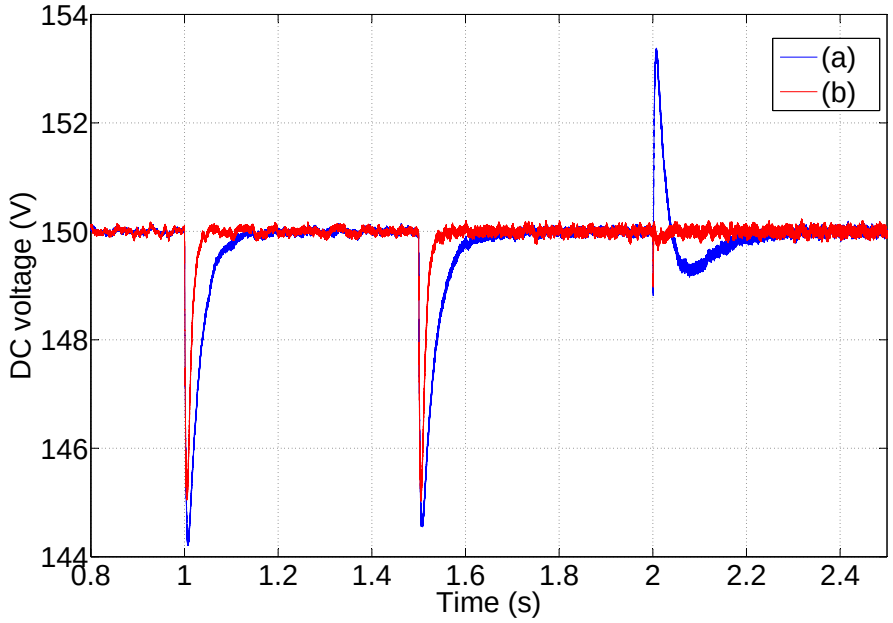

Figure 4.6: The response of DC voltage for the changes of R_L and $i^o_{g_iq}$. (a) PI controller. (b) Feedback nonlinear controller.

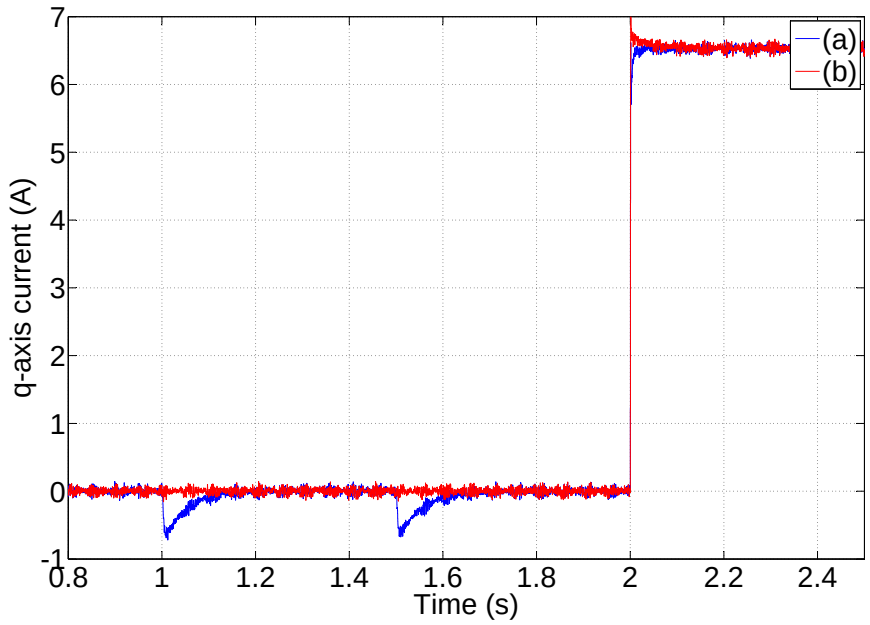

Figure 4.7: The response of i_{g_iq} for the changes of R_L and $i^o_{g_iq}$. (a) PI controller. (b) Feedback nonlinear controller.

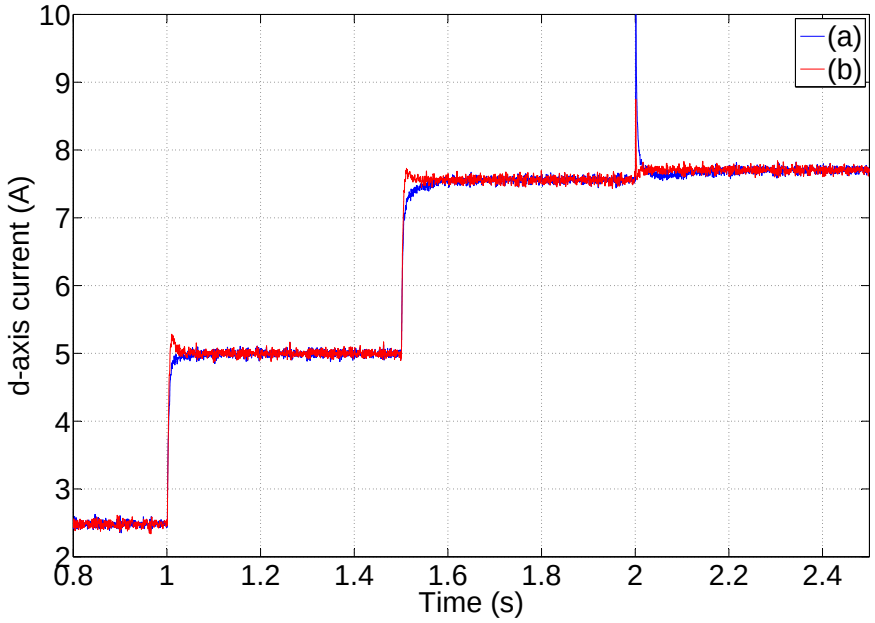

Figure 4.8: The response of i_{g_id} for the changes of R_L and $i^o_{g_iq}$. (a) PI controller. (b) Feedback nonlinear controller.

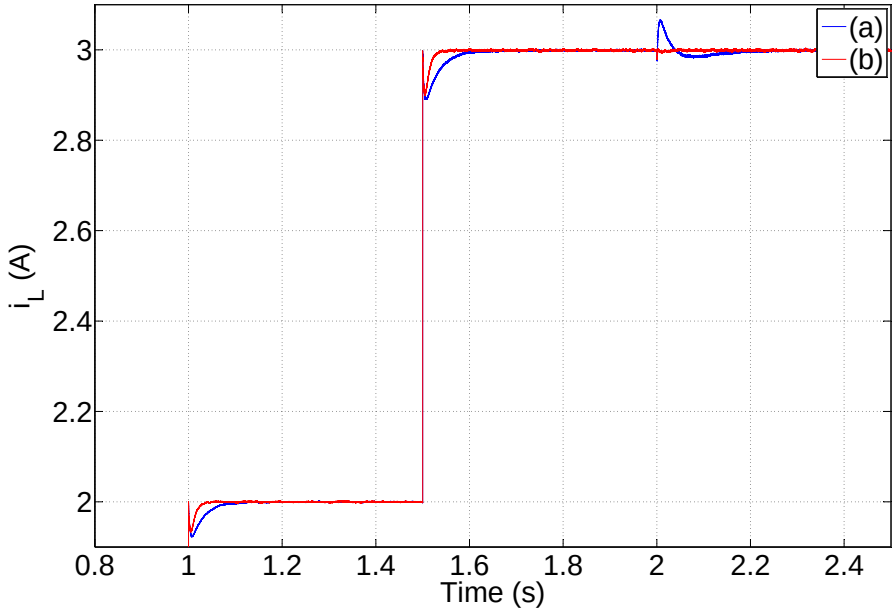

Figure 4.9: The response of i_L for the changes of R_L and i^o_{giq}. (a) PI controller. (b) Feedback nonlinear controller.

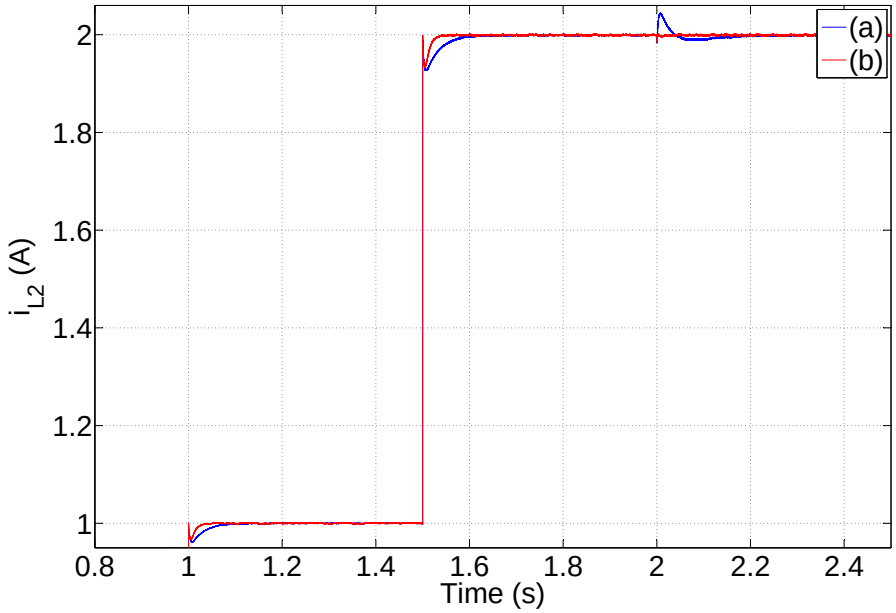

Figure 4.10: The response of i_{L2} for the changes of R_L and i^o_{giq}. (a) PI controller. (b) Feedback nonlinear controller.

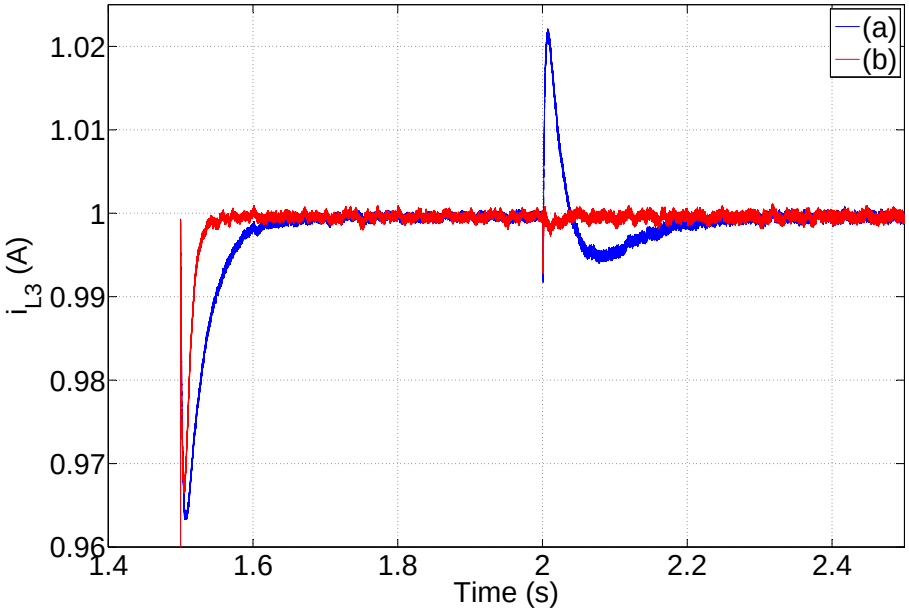

Figure 4.11: The response of i_{L3} for the changes of R_L and $i^o_{g_i q}$. (a) PI controller. (b) Feedback nonlinear controller.

4.1.3 Application to a VSC HVDC link consisting of a strong and a weak AC system

4.1.3.1 Control design

Figure 4.12 depicts the equivalent system model of a VSC HVDC link connecting two AC systems via a transmission branch.

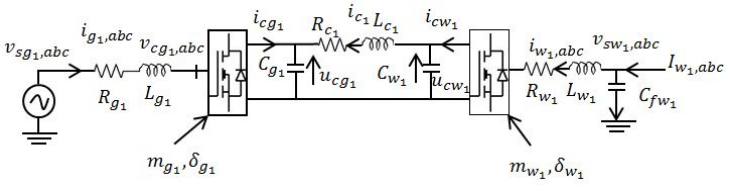

Figure 4.12: A VSC HVDC link consists of one strong and one weak AC system.

According to Section 3, the full state-space model of the system as depicted in

Fig. 4.12 is expressed as

$$\begin{aligned}
\frac{di_{g_1d}}{dt} &= -\frac{R_{g_1}}{L_{g_1}}i_{g_1d} + \omega_{g_1}i_{g_1q} + \frac{v_{sg_1d}}{L_{g_1}} - \frac{u_{cg_1}}{2L_{g_1}}m_{g_1d} \\
\frac{di_{g_1q}}{dt} &= -\frac{R_{g_1}}{L_{g_1}}i_{g_1q} - \omega_{g_1}i_{g_1d} + \frac{v_{sg_1q}}{L_{g_1}} - \frac{u_{cg_1}}{2L_{g_1}}m_{g_1q} \\
\frac{du_{cg_1}}{dt} &= \frac{1}{C_{g_1}}\left(\frac{3}{2}\frac{v_{sg_1d}i_{g_1d} + v_{sg_1q}i_{g_1q}}{u_{cg_1}} + i_{c_1}\right) \\
\frac{di_{c_1}}{dt} &= \frac{1}{L_{c_1}}\left(-R_{c_1}i_{c_1} + u_{cw_1} - u_{cg_1}\right) \\
\frac{du_{cw_1}}{dt} &= \frac{1}{C_{w_1}}\left(\frac{3}{2}\frac{v_{sw_1d}i_{w_1d} + v_{sw_1q}i_{w_1q}}{u_{cw_1}} - i_{c_1}\right) \\
\frac{dv_{sw_1d}}{dt} &= \omega_{w_1}v_{sw_1q} + \frac{1}{C_{fw_1}}\left(I_{w_1d} - i_{w_1d}\right) \\
\frac{dv_{sw_1q}}{dt} &= -\omega_{w_1}v_{sw_1d} + \frac{1}{C_{fw_1}}\left(I_{w_1q} - i_{w_1q}\right) \\
\frac{di_{w_1d}}{dt} &= -\frac{R_{w_1}}{L_{w_1}}i_{w_1d} + \omega_{w_1}i_{w_1q} + \frac{v_{sw_1d}}{L_{w_1}} - \frac{u_{cw_1}}{2L_{w_1}}m_{w_1d} \\
\frac{di_{w_1q}}{dt} &= -\frac{R_{w_1}}{L_{w_1}}i_{w_1q} - \omega_{w_1}i_{w_1d} + \frac{v_{sw_1q}}{L_{w_1}} - \frac{u_{cw_1}}{2L_{w_1}}m_{w_1q}
\end{aligned} \tag{4.40}$$

For the SAC terminal, the converter is used to maintain u_{cg_1} at a set point $u^o_{cg_1}$. In addition, i_{g_1q} should be regulated at $-\frac{2}{3}\frac{Q^o_{g_1}}{v_{sg_1d}}$ in such a way that the reactive power Q_{g_1} can be kept at its set point $Q^o_{g_1}$. Hence, the SAC converter station operates in DC voltage and reactive power control modes. For the WAC terminal, the converter is dedicated to control the AC voltage $v_{sw_1,dq}$ at the set points $v^o_{sw_1,dq}$ so that the WAC can operate at constant magnitude $V_{sw_j,\text{rms}}$ satisfying

$$V_{sw_1,\text{rms}} = \sqrt{(v^o_{sw_1d})^2 + (v^o_{sw_1q})^2} \tag{4.41}$$

Meanwhile, the power P_{w_1} generated by the wind farm can be totally transmitted to the SAC via the DC grid [Lie 2008]. Therefore, the controlled output vector is defined as $y \triangleq \begin{bmatrix} y_1 & y_2 & y_3 & y_4 \end{bmatrix}^T = \begin{bmatrix} i_{g_1q} & u_{cg_1} & v_{sw_1d} & v_{sw_1q} \end{bmatrix}^T$ and then, the control structure is designed to make the output vector y track the prescribed point $y^o = \begin{bmatrix} i^o_{g_1q} & u^o_{cg_1} & v^o_{sw_1d} & v^o_{sw_1q} \end{bmatrix}^T$.

By defining $x \triangleq \begin{bmatrix} i_{g_1d} & i_{g_1q} & u_{cg_1} & i_{c_1} & u_{cw_1} & v_{sw_1d} & v_{sw_1q} & i_{w_1d} & i_{w_1q} \end{bmatrix}^T$, the system (4.40) can be formalized as

$$\dot{x} = f(x) + g_1 m_{g_1d} + + g_2 m_{g_1q} + g_3 m_{w_1d} + g_4 m_{w_1q} \tag{4.42}$$

with the trivial expressions for f and $g_{1,2,3,4}$. Calculating the derivatives of the

output variables, we obtain

$$\begin{aligned}
y_1^{(1)} &= L_f(i_{g_1q}) \\
&\quad + L_{g_1}(i_{g_1q})m_{g_1d} + L_{g_2}(i_{g_1q})m_{g_1q} + L_{g_3}(i_{g_1q})m_{w_1d} + L_{g_3}(i_{g_1q})m_{w_1q} \\
y_2^{(2)} &= L_f^2(u_{cg_1}) + L_{g_1}L_f(u_{cg_1})m_{g_1d} + L_{g_2}L_f(u_{cg_1})m_{g_1q} \\
&\quad + L_{g_3}L_f(u_{cg_1})m_{w_1d} + L_{g_4}L_f(u_{cg_1})m_{w_1q} \\
y_3^{(2)} &= L_f^2(v_{sw_1d}) + L_{g_1}L_f(v_{sw_1d})m_{g_1d} + L_{g_2}L_f(v_{sw_1d})m_{g_1q} \\
&\quad + L_{g_3}L_f(v_{sw_1d})m_{w_1d} + L_{g_4}L_f(v_{sw_1d})m_{w_1q} \\
y_4^{(2)} &= L_f^2(v_{sw_1q}) + L_{g_1}L_f(v_{sw_1q})m_{g_1d} + L_{g_2}L_f(v_{sw_1q})m_{g_1q} \\
&\quad + L_{g_3}L_f(v_{sw_1q})m_{w_1d} + L_{g_4}L_f(v_{sw_1q})m_{w_1q}
\end{aligned} \tag{4.43}$$

where

$$\begin{aligned}
L_f(i_{g_1q}) &= -\frac{R_{g_1}}{L_{g_1}}i_{g_1q} - \omega_{g_1}i_{g_1d} + \frac{v_{sg_1q}}{L_{g_1}} \\
L_{g_2}(i_{g_1q}) &= -\frac{u_{cg_1}}{2L_{g_1}},\ L_{g_1}(i_{g_1q}) = L_{g_3}(i_{g_1q}) = L_{g_4}(i_{g_1q}) = 0 \\
L_f^2(u_{cg_1}) &= \frac{1}{C_{g_1}}\{\frac{3}{2}\frac{v_{sg_1d}}{u_{cg_1}}(-\frac{R_{g_1}}{L_{g_1}}i_{g_1d} + \omega_{g_1}i_{g_1q} + \frac{v_{sg_1d}}{L_{g_1}}) \\
&\quad + \frac{3}{2}\frac{v_{sg_1q}}{u_{cg_1}}(-\frac{R_{g_1}}{L_{g_1}}i_{g_1q} - \omega_{g_1}i_{g_1d} + \frac{v_{sg_1q}}{L_{g_1}})\} \\
&\quad - (\frac{3}{2}\frac{v_{sg_1d}i_{g_1d} + v_{sg_1q}i_{g_1q}}{u_{cg_1}^2})\frac{du_{cg_1}}{dt} + \frac{di_{c_1}}{dt}\} \\
L_{g_1}L_f(u_{cg_1}) &= -\frac{1}{C_{g_1}}\frac{3}{4}\frac{v_{sg_1d}}{L_{g_1}},\ L_{g_2}L_f(u_{cg_1}) = -\frac{1}{C_{g_1}}\frac{3}{4}\frac{v_{sg_1q}}{L_{g_1}} \\
L_{g_3}L_f(u_{cg_1}) &= L_{g_4}L_f(u_{cg_1}) = 0 \\
L_f^2(v_{sw_1d}) &= \omega_{w_1}\dot{v}_{sw_1q} + \frac{\dot{I}_{w_1d}}{C_{fw_1}} - \frac{1}{C_{fw_1}}(\omega_{w_1}i_{w_1q} - \frac{R_{w_1}}{L_{w_1}}i_{w_1d} + \frac{v_{sw_1d}}{L_{w_1}}) \\
L_{g_1}L_f(v_{sw_1d}) &= L_{g_2}L_f(v_{sw_1d}) = L_{g_4}L_f(v_{sw_1d}) = 0 \\
L_{g_3}L_f(v_{sw_1d}) &= \frac{u_{cw_1}}{2L_{w_1}C_{fw_1}} \\
L_f^2(v_{sw_1q}) &= \frac{\dot{I}_{w_1q}}{C_{fw_1}} - \omega_{w_1}\dot{v}_{sw_1d} - \frac{1}{C_{fw_1}}(\frac{v_{sw_1q}}{L_{w_1}} - \omega_{w_1}i_{w_1d} - \frac{R_{w_1}}{L_{w_1}}i_{w_1q}) \\
L_{g_1}L_f(v_{sw_1d}) &= L_{g_2}L_f(v_{sw_1d}) = L_{g_3}L_f(v_{sw_1d}) = 0 \\
L_{g_4}L_f(v_{sw_1d}) &= \frac{u_{cw_1}}{2L_{w_1}C_{fw_1}}
\end{aligned} \tag{4.44}$$

Therefore, the relative degrees of y_1, y_2, y_3 and y_4 are 1, 2, 2, 2, respectively. The system (4.40) has relative degree 7 in $\mathbb{R}^9$, which is smaller than 9, and hence, we have internal dynamics of order 2. To characterize the zero dynamics of the system, we restrict x to

$$Z^* = \{x \in \mathbb{R}^9 \mid i_{g_1q} \equiv i_{g_1q}^o,\ u_{cg_1} \equiv u_{cg_1}^o,\ v_{sw_1d} \equiv v_{sw_1d}^o,\ v_{sw_1q} \equiv v_{sw_1q}^o\} \tag{4.45}$$

This process leads to

$$\begin{aligned}
\frac{di_{c_1}}{dt} &= \frac{1}{L_{c_1}}(-R_{c_1}i_{c_1} + u_{cw_1} - u_{cg_1}^o) \\
\frac{du_{cw_1}}{dt} &= \frac{1}{C_{w_1}}(\frac{3}{2}\frac{v_{sw_1d}^o I_{w_1d} + v_{sw_1q}^o I_{w_1q}}{u_{cw_1}} - i_{c_1})
\end{aligned} \tag{4.46}$$

Linearizing (4.46) around the equilibrium denoted by $\begin{bmatrix}\bar{i}_{c_1} & \bar{u}_{cw_1}\end{bmatrix}^T$ yields the following Jacobian matrix

$$J = \begin{bmatrix} -\dfrac{R_{c_1}}{L_{c_1}} & \dfrac{1}{L_{c_1}} \\ -\dfrac{1}{C_{w_1}} & -\dfrac{3}{2}\dfrac{v^o_{sw_1d}I_{w_1d} + v^o_{sw_1q}I_{w_1q}}{C_{w_1}\bar{u}^2_{cw_1}} \end{bmatrix} \tag{4.47}$$

where $\begin{bmatrix}\bar{i}_{c_1} & \bar{u}_{cw_1}\end{bmatrix}^T$ can be obtained by solving the following equations

$$\begin{aligned} 0 &= -R_{c_1}\bar{i}_{c_1} + \bar{u}_{cw_1} - \bar{u}^o_{cg_1} \\ 0 &= \frac{3}{2}\frac{v^o_{sw_1d}I_{w_1d} + v^o_{sw_1q}I_{w_1q}}{\bar{u}_{cw_1}} - \bar{i}_{c_1} \end{aligned} \tag{4.48}$$

The characteristic polynomial $p(t)$ of the matrix J is given by

$$p(t) \triangleq \det(tI - J) = t^2 + \alpha_1 t + \alpha_0 \tag{4.49}$$

where

$$\begin{aligned} \alpha_1 &= \frac{R_{c_1}}{L_{c_1}} + \frac{3}{2}\frac{v^o_{sw_1d}I_{w_1d} + v^o_{sw_1q}I_{w_1q}}{C_{w_1}\bar{u}^2_{cw_1}} \\ \alpha_0 &= \frac{3}{2}\frac{v^o_{sw_1d}I_{w_1d} + v^o_{sw_1q}I_{w_1q}}{C_{w_1}\bar{u}^2_{cw_1}} \cdot \frac{R_{c_1}}{L_{c_1}} + \frac{1}{C_{w_1}L_{c_1}} \end{aligned} \tag{4.50}$$

Since $\dfrac{3}{2}(v^o_{sw_1d}I_{w_1d} + v^o_{sw_1q}I_{w_1q})$, the active power generated by the wind farm, is non-negative, the coefficients α_0 and α_1 are positive. Therefore, the real part of all eigenvalues of the matrix J is negative. The zero dynamics have an asymptotically stable equilibrium point at $\begin{bmatrix}\bar{i}_{c_1} & \bar{u}_{cw_1}\end{bmatrix}^T$, which shows that the system described by (4.40) is minimum phase.

Based on the above mentioned equations, the decoupling matrix E_2 is given by

$$E_2 = \begin{bmatrix} L_{g_1}(i_{g_1q}) & L_{g_2}(i_{g_1q}) & L_{g_3}(i_{g_1q}) & L_{g_4}(i_{g_1q}) \\ L_{g_1}L_f(u_{cg_1}) & L_{g_2}L_f(u_{cg_1}) & L_{g_3}L_f(u_{cg_1}) & L_{g_4}L_f(u_{cg_1}) \\ L_{g_1}L_f(v_{sw_1d}) & L_{g_2}L_f(v_{sw_1d}) & L_{g_3}L_f(v_{sw_1d}) & L_{g_4}L_f(v_{sw_1d}) \\ L_{g_1}L_f(v_{sw_1q}) & L_{g_2}L_f(v_{sw_1q}) & L_{g_3}L_f(v_{sw_1q}) & L_{g_4}L_f(v_{sw_1q}) \end{bmatrix} \tag{4.51}$$

which is non-singular for positive u_{cw_1} and u_{cg_1}. According to (4.31), the control variables are given by

$$\begin{bmatrix} m_{g_1d} \\ m_{g_1q} \\ m_{w_1d} \\ m_{w_1q} \end{bmatrix} = E_2^{-1} \begin{bmatrix} v_1 - L_f(i_{g_iq}) \\ v_2 - L^2_f(u_{cg_i}) \\ v_3 - L^2_f(v_{sw_1d}) \\ v_4 - L^2_f(v_{sw_1q}) \end{bmatrix} \tag{4.52}$$

Applying the (4.11) to the additional inputs $v_{1,2,3,4}$ leads to

$$\begin{aligned} v_1 &= -k_{I1}e_{I1} - c_{1,0}(y_1 - i^o_{g_1d}) \\ v_2 &= -k_{I2}e_{I2} - c_{2,0}(y_2 - u^o_{cg_1}) - c_{2,1}(\dot{y}_2 - \dot{u}^o_{cg_1}) \\ v_3 &= -k_{I3}e_{I3} - c_{3,0}(y_3 - v^o_{sw_1d}) - c_{3,1}(\dot{y}_3 - \dot{v}^o_{sw_1d}) \\ v_4 &= -k_{I4}e_{I4} - c_{4,0}(y_4 - v^o_{sw_1q}) - c_{4,1}(\dot{y}_4 - \dot{v}^o_{sw_1q}) \end{aligned} \tag{4.53}$$

with the integrated tracking errors

$$\begin{aligned}\dot{e}_{I1} &= y_1 - i^o_{g_1 d}\\ \dot{e}_{I2} &= y_2 - u^o_{cg_1}\\ \dot{e}_{I3} &= y_3 - v^o_{sw_1 d}\\ \dot{e}_{I4} &= y_4 - v^o_{sw_1 q}\end{aligned} \tag{4.54}$$

The control gains must be chosen such that the matrices C'_j, $j = 1,2,3,4$, are Hurwitz where

$$\begin{aligned} C'_1 &= \begin{bmatrix} 0 & 1 \\ -k_{I1} & -c_{1,0} \end{bmatrix}, \; C'_2 = \begin{bmatrix} 0 & 1 & 0 \\ 0 & 0 & 1 \\ -k_{I2} & -c_{2,0} & -c_{2,1} \end{bmatrix} \\ C'_3 &= \begin{bmatrix} 0 & 1 & 0 \\ 0 & 0 & 1 \\ -k_{I3} & -c_{3,0} & -c_{3,1} \end{bmatrix}, \; C'_4 = \begin{bmatrix} 0 & 1 & 0 \\ 0 & 0 & 1 \\ -k_{I4} & -c_{4,0} & -c_{4,1} \end{bmatrix} \end{aligned} \tag{4.55}$$

4.1.3.2 Simulation studies

Simulation studies of the VSC HVDC link depicted in Fig. 4.12 are carried out where the values of the system parameters are provided in Table 4.4. The operation of this two-terminal HVDC system is arranged as follows:

- The DC voltage of the SAC terminal is required to be maintained at $u_{cg_1} = u^o_{cg_1} = 150$ V and the reactive power Q_{g_1} is regulated at $Q_{g_1} = Q^o_{g_1} = 0$ Var.

- The frequency of the WAC's AC voltage at the PCC must be kept at 50 Hz. In addition, $V_{sw_1,\text{rms}}$ is initially set to 40.82 V. At $t = 1$ s and $t = 1.5$ s, $V_{sw_1,\text{rms}}$ is changed to 60.23 V and 63.59 V respectively. According to (4.41), this can be achieved by varying the values of $v^o_{sw_1.dq}$ as listed in Table 4.5.

In order to evaluate the performance of the nonlinear controller (4.52), two control strategies are tested by comparison as presented in Table 4.6. The HVDC system starts from a steady-state condition where $u_{cg_1} = u^o_{cg_1} = 150$ V, $i_{g_1 q} = i^o_{g_1 q} = 0$ A, $v_{sw_1 d} = v^o_{sw_1 d} = 40.82$ V and $v_{sw_1 q} = v^o_{sw_1 q} = 0$ V. Simulation results are plotted in Figs. 4.13-4.20.

As shown in Figs. 4.13 and 4.14, every time $v^o_{sw_1,dq}$ are subjected to a step change, $v_{sw_1,dq}$ can always converge to their new references under both control strategies. But for the PI controller, $v_{sw_1 q}$ is readily influenced by the change of $v^o_{sw_1 d}$ and $v_{sw_1 d}$ is also disturbed remarkably when $v^o_{sw_1 q}$ is set to another value. t reveals that the feedback nonlinear controller gives better decoupling characteristics of $d-q$ voltage control than the PI controller.

Table 4.4: Parameters of the VSC HVDC link with two terminals.

Parameters	SAC terminal	WAC terminal
Power System Rating	4 KVA	4 KVA
Source Voltage Amplitude (V_{rms} phase-to-phase)	127 V	
Source Voltage Frequency	50 Hz	50 Hz
Switching Frequency for PWM	1500 Hz	1500 Hz
Transformer Primary Voltage	127 V	
Transformer Secondary Voltage	50 V	
Inductance L_{g_i}	2.1 mH	3.3 mH
Resistance R_{g_i}	0.142 Ω	0.165 Ω

Table 4.5: Values of $v^o_{sw_1,dq}$.

	$v^o_{sw_1 d}$ (V)	$v^o_{sw_1 q}$ (V)
$t = 0$ s	40.82	0
$t = 1$ s	61.23	0
$t = 1.5$ s	61.23	20.41

Table 4.6: Two difference control strategies by comparison.

	SAC terminal	WAC terminal
(a)	Feedback linearization control ($m_{g_1,dq}$ in (4.52))	PI control
(b)	Feedback linearization control ($m_{g_1,dq}$ in (4.52))	Feedback linearization control ($m_{w_1,dq}$ in (4.52))

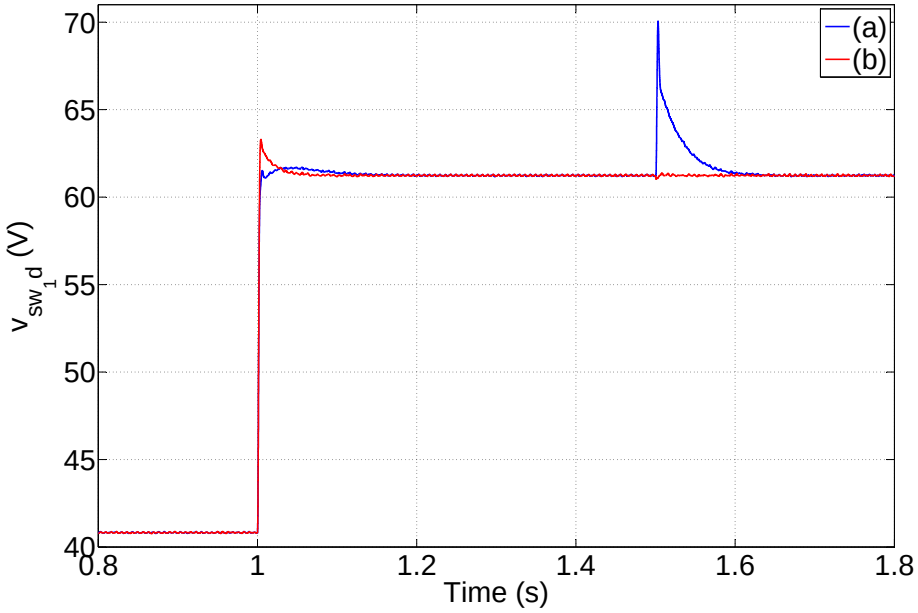

Figure 4.13: The response of v_{sw_1d} for the changes of $v^o_{sw_1d}$ and $v^o_{sw_1q}$. (a) PI controller. (b) Feedback nonlinear controller.

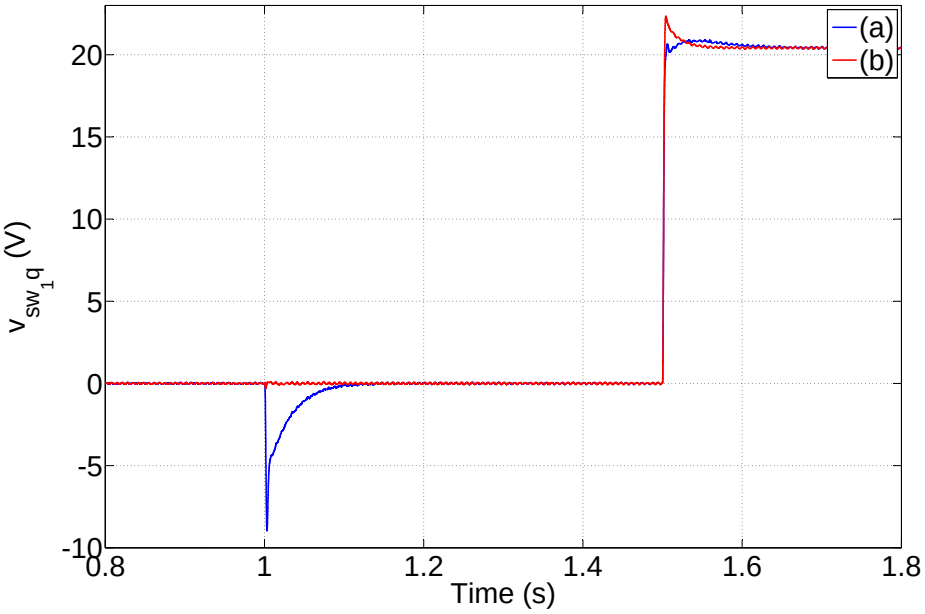

Figure 4.14: The response of v_{sw_1q} for the changes of $v^o_{sw_1d}$ and $v^o_{sw_1q}$. (a) PI controller. (b) Feedback nonlinear controller.

Figures 4.15-4.19 illustrate the responses of the AC voltage in *abc* frame. Figure 4.19 shows that the AC voltage at the PCC are always kept at $f_{w_1} = 50$ Hz. By comparing Fig. 4.16 and Fig. 4.18, the feedback nonlinear controller gives a better transient performance for $v_{sw_1,abc}$ with a smaller overshoot than the PI controller when $v^o_{sw_1q}$ is set to 4.08 V at $t = 1.5$ s.

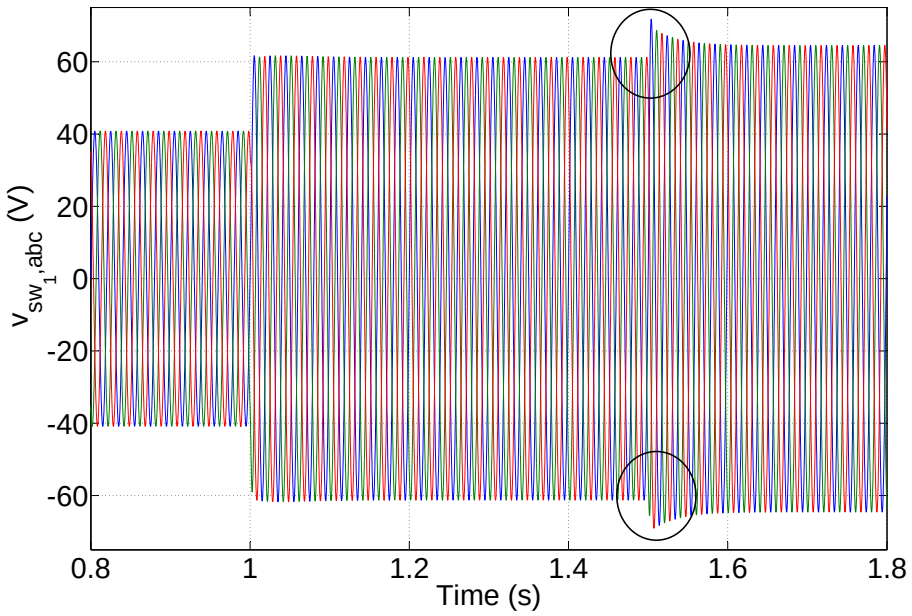

Figure 4.15: The response of $v_{sw_1,abc}$ for the changes of $v^o_{sw_1d}$ and $v^o_{sw_1q}$ using PI controller.

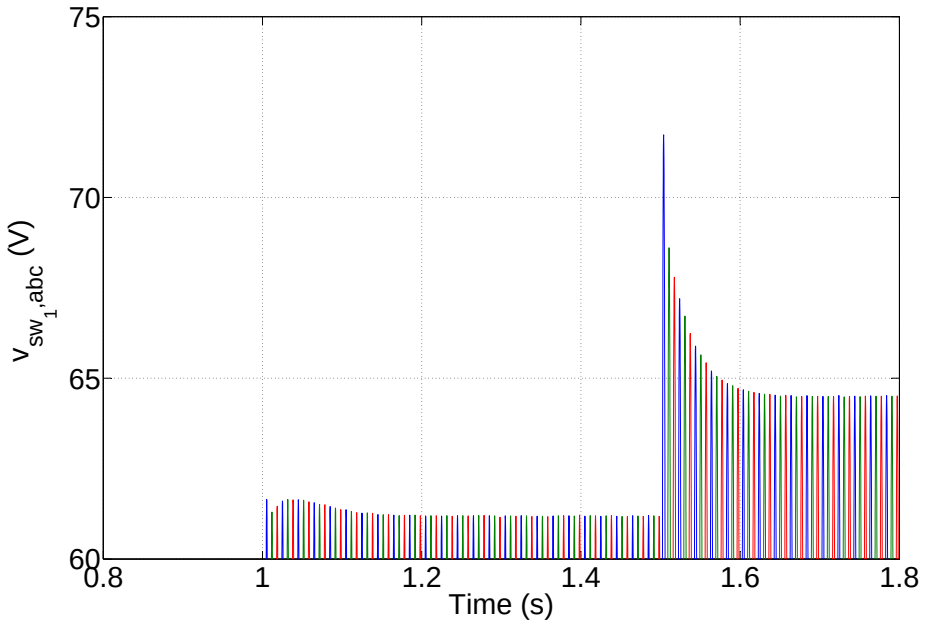

Figure 4.16: Zoom of the response of $v_{sw_1,abc}$ for the changes of $v^o_{sw_1d}$ and $v^o_{sw_1q}$ using PI controller.

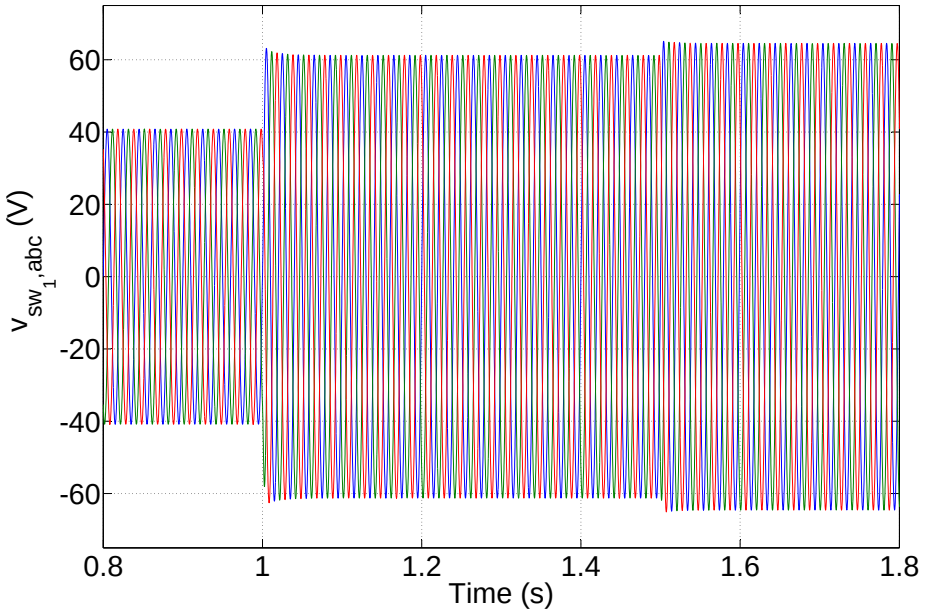

Figure 4.17: The response of $v_{sw_1,abc}$ for the changes of $v^o_{sw_1d}$ and $v^o_{sw_1q}$ using feedback linearization controller.

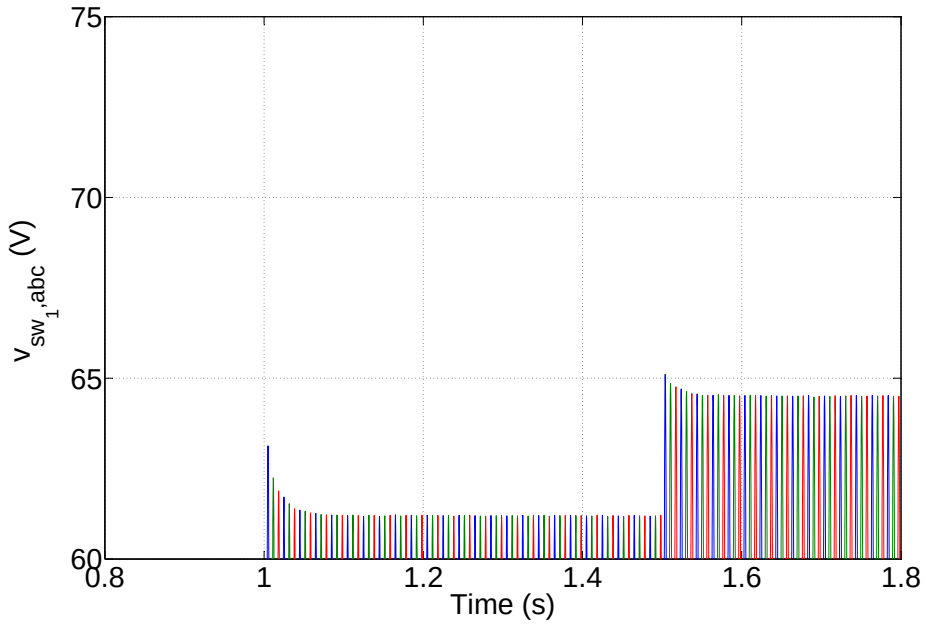

Figure 4.18: Zoom of the response of $v_{sw_1,abc}$ for the changes of $v^o_{sw_1 d}$ and $v^o_{sw_1 q}$ using feedback linearization controller.

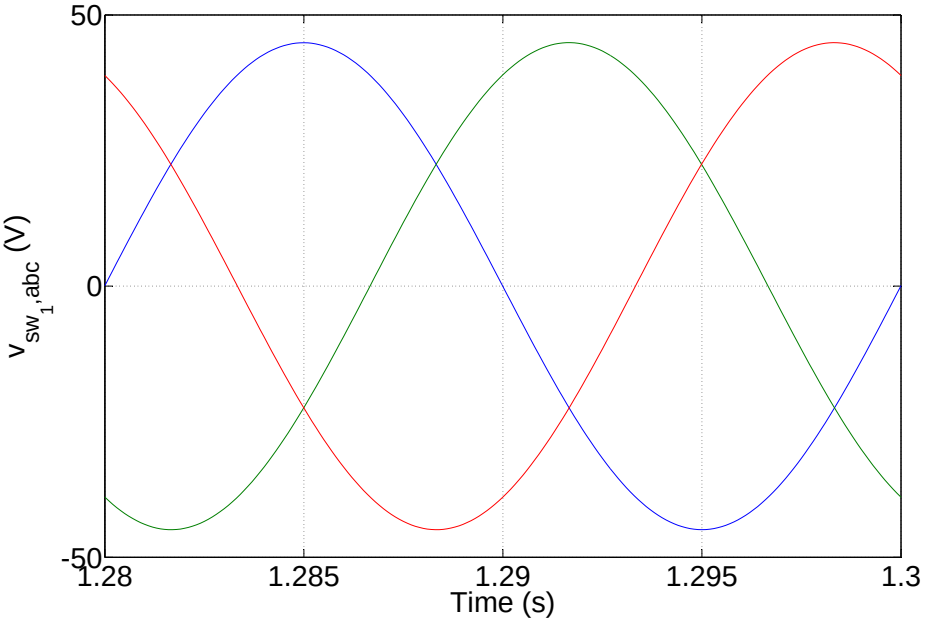

Figure 4.19: $f_{w_1} = 50$ Hz.

Since the SAC terminal uses the same control law in both control strategies, the performances of u_{cg_1} are almost identical as illustrated in Figs. 4.20.

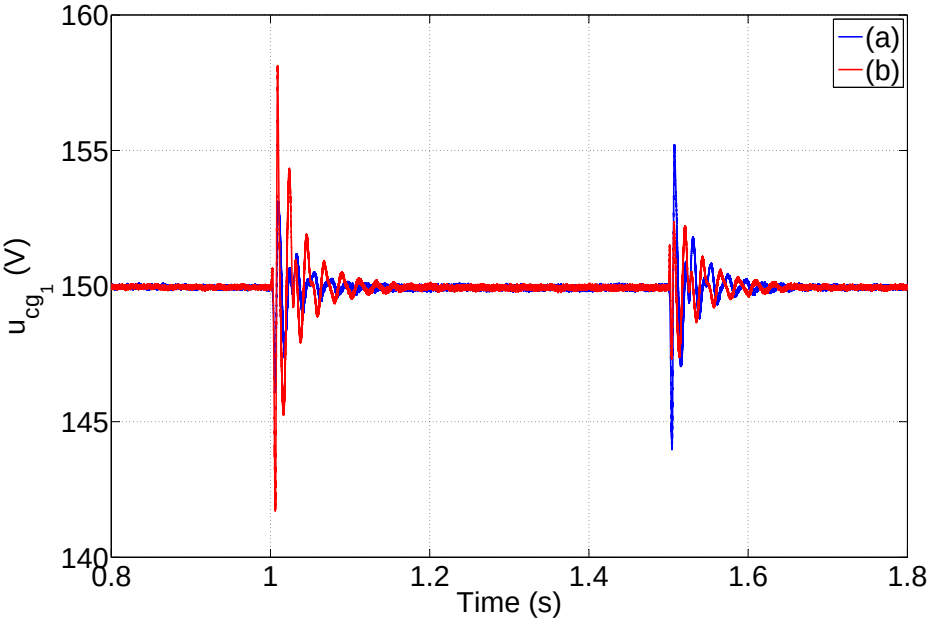

Figure 4.20: The response of u_{cg_1} for the changes of $v^o_{sw_1d}$ and $v^o_{sw_1q}$. (a) PI controller. (b) Feedback nonlinear controller.

4.1.4 Application to an MTDC system using master-slave control configuration

The use of feedback linearization for the MTDC system modeled by (3.20), (3.28), (3.29) and (3.36) in Section 3 is under consideration in this section.

4.1.4.1 Master-slave control configuration

Before applying the theoretical results in Section 4.1.1, we first discuss the control configuration for the normal operations of the MTDC system. It must be always kept in mind that the DC voltage is accepted only in a narrow region, i.e. $u_{c(\cdot)} \in \mathbb{D}_{u_c}$ as stated in Section 3.4.4. In order to keep the DC voltage within the acceptable band, at least one of the converter stations in the MTDC system must be used to regulate the DC voltage. For example, the SAC connected VSC operates in DC voltage control mode as presented in Section 4.1.3. In this study case, a single converter terminal is assigned to control the DC voltage at a constant level and the rest of the converter stations work in other control modes. This control configuration is called master-slave control. In addition, the terminal in charge of the regulation of DC voltage, is called the master terminal. It is worthwhile to note that the master

terminal takes responsibility for balancing the power flow of the DC network in case of disturbances. Consequently, this terminal usually needs a large power capacity to counteract all possible power imbalance.

The arrangement of VSC operation for the MTDC system is set as follows:

- The 1st SAC converter station chosen as the master terminal is used to maintain the DC voltage at the constant level $u_{cg_1}^o$ while the remaining SAC converter stations operate in active control mode to control P_{g_ρ} at $P_{g_\rho}^o$ [1]. Additionally, all reactive power Q_{g_i} should be kept at their respective references $Q_{g_i}^o$.

- Each WAC converter station must ensure that the magnitude and the frequency of the AC voltage at the PCC, $V_{sw,\text{rms}}$ and f_{w_j}, are kept constant. This can be fulfilled by regulating $v_{sw_j,dq}$ at their references $v_{sw_j,dq}^o$.

As mentioned in Section 4.1.3, Q_{g_i} can be kept at $Q_{g_i}^o$ by regulating i_{g_iq} at $i_{g_iq}^o = -\frac{2}{3}\frac{Q_{g_i}^o}{v_{sw_jd}}$. Likewise, we make i_{g_id} track the reference $i_{g_id}^o = \frac{2}{3}\frac{P_{g_i}^o}{v_{sw_jd}}$ for the purpose of controlling P_{g_i} at $P_{g_i}^o$. According to the above arrangement, it is natural to choose the output vector as

$$y \triangleq \begin{bmatrix} i_{g_1q} & u_{cg_1} & i_{g_\rho d} & i_{g_\rho q} & v_{sw_jd} & v_{sw_jq} \end{bmatrix}^T \in \mathbb{R}^{2N+2M} \tag{4.56}$$

Obviously, the reference vector is set to

$$y^o \triangleq \begin{bmatrix} i_{g_1q}^o & u_{cg_1}^o & i_{g_\rho d}^o & i_{g_\rho q}^o & v_{sw_jd}^o & v_{sw_jq}^o \end{bmatrix}^T \in \mathbb{R}^{2N+2M} \tag{4.57}$$

Through simple calculations, it is not difficult to get that the relative degrees of u_{cg_1}, i_{g_1q}, $i_{g_\rho d}$, $i_{g_\rho q}$, v_{sw_jd} and v_{sw_jq} are 2, 1, 1, 1, 2, 2, respectively, and hence, the order of the internal dynamics is $N-1+M+P+L$.

Before designing the exact control algorithm, we need the following feasibility assumption.

Assumption 4.1.1. *Consider the MTDC system described by (3.20), (3.28), (3.29) and (3.36). For the prescribed references $u_{cg_1}^o$, $Q_{g_1}^o$, $P_{g_\rho}^o$, $Q_{g_\rho}^o$, $v_{sw_j,dq}^o$, there exist*

[1] Unless otherwise stated, the subscript ρ mean $\forall \rho \in \mathcal{N}_{-1} = \{2, \cdots, N\}$.

constants for the state variables denoted by $\bar{(\cdot)}$ *such that*[2]

$$
\begin{aligned}
0 &= -\frac{R_{g_i}}{L_{g_i}}\bar{i}_{g_i d} + \omega_{g_i}\bar{i}_{g_i q} + \frac{v_{sg_i d}}{L_{g_i}} - \frac{\bar{u}_{cg_i}}{2L_{g_i}}\bar{m}_{g_i d} \\
0 &= -\frac{R_{g_i}}{L_{g_i}}\bar{i}_{g_i q} - \omega_{g_i}\bar{i}_{g_i d} + \frac{v_{sg_i q}}{L_{g_i}} - \frac{\bar{u}_{cg_i}}{2L_{g_i}}\bar{m}_{g_i q} \\
0 &= -\frac{R_{w_j}}{L_{w_j}}\bar{i}_{w_j d} + \omega_{w_j}\bar{i}_{w_j q} + \frac{\bar{v}_{sw_j d}}{L_{w_j}} - \frac{\bar{u}_{cw_j}}{2L_{w_j}}\bar{m}_{w_j d} \\
0 &= -\frac{R_{w_j}}{L_{w_j}}\bar{i}_{w_j q} - \omega_{w_j}\bar{i}_{w_j d} + \frac{\bar{v}_{sw_j q}}{L_{w_j}} - \frac{\bar{u}_{cw_j}}{2L_{w_j}}\bar{m}_{w_j q} \\
0 &= \omega_{w_j}\bar{v}_{sw_j q} + \frac{1}{C_{fw_j}}(I_{w_j d} - \bar{i}_{w_j d}) \\
0 &= -\omega_{w_j}\bar{v}_{sw_j d} + \frac{1}{C_{fw_j}}(I_{w_j q} - \bar{i}_{w_j q}) \\
0 &= A\bar{z} + \bar{\vartheta}
\end{aligned}
\tag{4.58}
$$

where $\bar{u}_{cg_1} = u^o_{cg_1}$, $\bar{i}_{g_1 q} = -\dfrac{2Q^o_{g_1}}{3v_{sg_1 d}}$, $\bar{i}_{g_\rho d} = \dfrac{2P^o_{g_\rho}}{3v_{sg_1 d}}$, $\bar{i}_{g_\rho q} = -\dfrac{2Q^o_{g_\rho}}{3v_{sg_1 d}}$ *and* $\bar{v}_{sw_j,dq} = v^o_{sw_j,dq}$.

By applying the theoretical results in Section 4.1.1, the following nonlinear feedback control algorithm

$$
\begin{aligned}
\begin{bmatrix} m_{g_1 d} \\ m_{g_1 q} \end{bmatrix} &= \begin{bmatrix} 0 & -\dfrac{u_{cg_1}}{2L_{g_1}} \\ -\dfrac{3v_{sg_1 d}}{4C_{g_1}L_{g_1}} & -\dfrac{3v_{sg_1 q}}{4C_{g_1}L_{g_1}} \end{bmatrix}^{-1} \begin{bmatrix} v_{g_1 q} - L_f(i_{g_1 q}) \\ v_{cg_1} - L_f^2(u_{cg_1}) \end{bmatrix} \\
\begin{bmatrix} m_{g_\rho d} \\ m_{g_\rho q} \end{bmatrix} &= \begin{bmatrix} -\dfrac{u_{cg_\rho}}{2L_{g_\rho}} & 0 \\ 0 & -\dfrac{u_{cg_\rho}}{2L_{g_\rho}} \end{bmatrix}^{-1} \begin{bmatrix} v_{g_\rho d} - L_f(i_{g_\rho d}) \\ v_{g_\rho q} - L_f(i_{g_\rho q}) \end{bmatrix} \\
\begin{bmatrix} m_{w_j d} \\ m_{w_j q} \end{bmatrix} &= \begin{bmatrix} \dfrac{u_{cw_j}}{2L_{w_j}C_{fw_j}} & 0 \\ 0 & \dfrac{u_{cw_j}}{2L_{w_j}C_{fw_j}} \end{bmatrix}^{-1} \begin{bmatrix} v_{w_j d} - L_f^2(v_{sw_j d}) \\ v_{w_j q} - L_f^2(v_{sw_j q}) \end{bmatrix}
\end{aligned}
\tag{4.59}
$$

[2]Unless otherwise stated, the notation $\bar{(\cdot)}$ represents the steady-state value (or equilibrium point) of the variable (or vector) $(\cdot)$.

with

$$\begin{aligned}
L_f(i_{g_1q}) =& -\frac{R_{g_1}}{L_{g_1}} i_{g_1q} - \omega_{g_1} i_{g_1d} + \frac{v_{sg_1q}}{L_{g_1}} \\
L_f^2(u_{cg_1}) =& \frac{1}{C_{g_1}} \{ \frac{3}{2} \frac{v_{sg_1d}}{u_{cg_1}} (-\frac{R_{g_1}}{L_{g_1}} i_{g_1d} + \omega_{g_1} i_{g_1q} + \frac{v_{sg_1d}}{L_{g_1}}) \\
&+ \frac{3}{2} \frac{v_{sg_1q}}{u_{cg_1}} (-\frac{R_{g_1}}{L_{g_1}} i_{g_1q} - \omega_{g_1} i_{g_1d} + \frac{v_{sg_1q}}{L_{g_1}}) \} \\
&- (\frac{3}{2} \frac{v_{sg_1d} i_{g_1d} + v_{sg_1q} i_{g_1q}}{u_{cg_1}^2}) \frac{du_{cg_1}}{dt} + H(1,:) \frac{di_c}{dt} \} \\
L_f(i_{g_\rho d}) =& -\frac{R_{g_\rho}}{L_{g_\rho}} i_{g_\rho d} + \omega_{g_\rho} i_{g_\rho q} + \frac{v_{sg_\rho d}}{L_{g_\rho}} \\
L_f(i_{g_\rho q}) =& -\frac{R_{g_\rho}}{L_{g_\rho}} i_{g_\rho q} - \omega_{g_\rho} i_{g_\rho d} + \frac{v_{sg_\rho q}}{L_{g_\rho}} \\
L_f^2(v_{sw_jd}) =& \omega_{w_j} \dot{v}_{sw_jq} + \frac{\dot{I}_{w_jd}}{C_{fw_j}} - \frac{1}{C_{fw_j}} (\omega_{w_j} i_{w_jq} - \frac{R_{w_j}}{L_{w_j}} i_{w_jd} + \frac{v_{sw_jd}}{L_{w_j}}) \\
L_f^2(v_{sw_jq}) =& \frac{\dot{I}_{w_jq}}{C_{fw_j}} - \omega_{w_j} \dot{v}_{sw_jd} - \frac{1}{C_{fw_j}} (\frac{v_{sw_jq}}{L_{w_j}} - \omega_{w_j} i_{w_jd} - \frac{R_{w_j}}{L_{w_j}} i_{w_jq})
\end{aligned} \tag{4.60}$$

transforms the original system described by (3.20), (3.28), (3.29) and (3.36) into the normal form (4.17). Moreover, these additional inputs $v_{(.)}$ are designed as

$$\begin{aligned}
v_{g_1q} =& -c_{g_1q,0}(i_{g_1q} - i_{g_1q}^o) - k_{Ig_1q} e_{Ig_1q} \\
v_{cg_1} =& -c_{cg_1,0}(u_{cg_1} - u_{cg_1}^o) - c_{cg_1,1}(\dot{u}_{cg_1} - \dot{u}_{cg_1}^o) - k_{Icg_1} e_{Icg_1} \\
v_{g_\rho d} =& -c_{g_\rho d,0}(i_{g_\rho d} - i_{g_\rho d}^o) - k_{Ig_\rho d} e_{Ig_\rho d} \\
v_{g_\rho q} =& -c_{g_\rho q,0}(i_{g_\rho q} - i_{g_\rho q}^o) - k_{Ig_\rho q} e_{Ig_\rho q} \\
v_{w_jd} =& -c_{w_jd,0}(v_{sw_jd} - v_{sw_jd}^o) - c_{w_jd,1}(\dot{v}_{sw_jd} - \dot{v}_{sw_jd}^o) - k_{Iw_jd} e_{Iw_jd} \\
v_{w_jq} =& -c_{w_jq,0}(v_{sw_jq} - v_{sw_jq}^o) - c_{w_jq,1}(\dot{v}_{sw_jq} - \dot{v}_{sw_jq}^o) - k_{Iw_jq} e_{Iw_jq}
\end{aligned} \tag{4.61}$$

with the integrated tracking errors

$$\begin{aligned}
\dot{e}_{Ig_1q} =& i_{g_1q} - i_{g_1q}^o, \quad \dot{e}_{Icg_1} = u_{cg_1} - u_{cg_1}^o \\
\dot{e}_{Ig_\rho d} =& i_{g_\rho d} - i_{g_\rho d}^o, \quad \dot{e}_{Ig_\rho q} = i_{g_\rho q} - i_{g_\rho q}^o \\
e_{Iw_jd} =& v_{sw_jd} - v_{sw_jd}^o, \quad e_{Iw_jd} = v_{sw_jq} - v_{sw_jq}^o
\end{aligned} \tag{4.62}$$

where the control gains $c_{(.)}$ and $k_{I(.)}$ must be chosen to satisfy (4.13).

When the output vector y is identically equal to the reference y^o, the zero dynamics of the system is deduced as

$$\dot{z}_r = A_r z_r + \vartheta_r + \vartheta_{u_{cg_1}} \triangleq f_{\text{zero}}(z_r) \tag{4.63}$$

where we introduce the new variables

$$\begin{aligned}
z_r &\triangleq \begin{bmatrix} u_{cg,r} & u_{cw} & u_{ct} & i_c \end{bmatrix}^T \in \mathbb{R}^{N+M+P+L-1} \\
u_{cg,r} &\triangleq \begin{bmatrix} u_{cg_2} & \cdots & u_{cg_N} \end{bmatrix}^T \\
\vartheta_r &\triangleq \begin{bmatrix} \frac{i'_{cg_2}}{C_{g_2}} & \cdots & \frac{i'_{cg_N}}{C_{g_N}} & \frac{i'_{cw_1}}{C_{w_1}} & \cdots & \frac{i'_{cw_M}}{C_{w_M}} & 0_{(P+L)} \end{bmatrix}^T \\
\vartheta_{u_{cg_1}} &\triangleq \begin{bmatrix} 0_{N+M+P-1} & H_{(1,1)}u^o_{cg_1} & \cdots & H_{(1,L)}u_{cg} \end{bmatrix}^T \\
i'_{cg_\rho} &\triangleq \frac{3}{2}\frac{(v_{sg_\rho d}i^o_{g_\rho d} + v_{sg_\rho q}i^o_{g_\rho q})}{u_{cg_\rho}} \\
i_{cw'_j} &\triangleq \frac{3}{2}\frac{(v^o_{sw_j d}I_{w_j d} + v^o_{sw_j q}I_{w_j q})}{u_{cw_j}}
\end{aligned} \tag{4.64}$$

The matrix A_r is the submatrix formed by deleting the $1st$ row and $1st$ column of the matrix A, which is still of the form

$$A_r = \begin{bmatrix} 0_{(N+M+P-1)\times(N+M+P-1)} & C_r^{-1}H_r \\ -L^{-1}H_r^T & -L^{-1}R \end{bmatrix} \tag{4.65}$$

where

$$C_r = \mathrm{diag}(C_{g_2}\cdots C_{g_N}\ C_{w_1}\cdots C_{w_M}\ C_{p_1}\cdots C_{p_P})$$

and the matrix H_r is the submatrix of H by removing the first row of H.

To check the stability of the equilibrium point of the zero dynamics, we linearize (4.63) around its equilibrium point $\bar{z}_r$ and then get the Jacobian matrix

$$J = \frac{\partial f_{\text{zero}}}{\partial z_r}|_{z_r=\bar{z}_r} = \begin{bmatrix} -D & C_r^{-1}H_r \\ -L^{-1}H_r^T & -L^{-1}R \end{bmatrix} \tag{4.66}$$

where $D = \mathrm{diag}(d_k)$, $k = 1, \cdots, N+M+P-1$, is a diagonal matrix given by

$$\begin{cases} d_{(\rho-1)} = \dfrac{P^o_{g_\rho}}{\bar{u}^2_{cg_\rho}}, & \rho \in \mathcal{N}_{-1} \\ d_{(j+N-1)} = \dfrac{P^o_{w_j}}{C_{w_j}\bar{u}^2_{w_j}}, & j \in \mathcal{M} \\ d_{(h+N+M-1)} = 0. & h \in \mathcal{P} \end{cases}$$
$$P^o_{w_j} = \frac{3}{2}(v^o_{sw_j d}I_{w_j d} + v^o_{sw_j q}I_{w_j q})$$

Lemma 4.1.2. *Consider the MTDC system described by (3.20), (3.28), (3.29) and (3.36). If the prescribed references $u^o_{cg_1}$, $Q^o_{g_1}$, $P^o_{g_\rho}$, $Q^o_{g_\rho}$, $v^o_{sw_j d}$ and $v^o_{sw_j q}$ and the system parameters are set such that the Jacobian matrix J is Hurwitz, the equilibrium point of the zero dynamics (4.63) is asymptotically stable and hence the MTDC system is minimum phase.*

Lemma 4.1.3. *Consider the MTDC system described by (3.20), (3.28), (3.29) and (3.36). If $P^o_{g_\rho}$, $\rho = 2, \cdots, N$ and $P^o_{w_j}$, $j = 1, \cdots, M$ are non-negative, the MTDC system is minimum phase.*

In order to prove Lemma 4.1.3, we need some properties of complex matrix as referred in [Horn 1985]. We recall the following basic facts:

Definition 4.1.4. *A matrix $\Psi \in \mathbb{C}^{n\times n}$ is said to be semi-positive definite if $Re(x^H \Psi x)$ is non-negative for every non-zero column vector $x \in \mathbb{C}^{n\times 1}$. Moreover, $\Psi \in \mathbb{C}^{n\times n}$ is said to be positive definite if $Re(x^H \Psi x)$ is positive for every non-zero column vector $x \in \mathbb{C}^{n\times 1}$. The set of the positive definite matrix Ψ is denoted as P_C^+.*

Lemma 4.1.5. *For any complex matrix $\Psi \in \mathbb{C}^{n\times n}$, it can be expressed as $\Psi = \mathcal{H}(\Psi) + \mathcal{S}(\Psi)$ where $\mathcal{H}(\Psi) \triangleq \frac{1}{2}(\Psi + \Psi^H)$ is a hermitian matrix and $\mathcal{S}(\Psi) \triangleq \frac{1}{2}(\Psi - \Psi^H)$ is an anti-hermitian matrix.*

Lemma 4.1.6. *Matrix $\Psi \in \mathbb{C}^{n\times n}$ is positive definite if and only if its hermitian part $\mathcal{H}(\Psi)$ is positive definite.*

Lemma 4.1.7. *If matrix Γ is invertible and Ψ is positive definite, then $\Gamma^H \Psi \Gamma$ is also positive definite.*

Lemma 4.1.8. *If Ψ_1 is positive definite and Ψ_2 is semi-positive definite, we have $\Psi_1 + \Psi_2 \in P_C^+$.*

Lemma 4.1.9. *If $\Psi \in P_C^+$, then Ψ is invertible and $\Psi^{-1} \in P_C^+$.*

Based on the above statements, we can now demonstrate Lemma 4.1.3 as follows.

Proof. Let us assume that there exists a particular eigenvalue of J denoted by $\lambda = \alpha + j\beta \in \mathbb{C}$, whose real part is non-negative, i.e. $\alpha \geq 0$. Then, λ satisfies

$$\det(\lambda I - J) = 0$$

Alternatively, it can be expressed as

$$\det(\begin{bmatrix} \lambda I + D & -C_r^{-1} H_r \\ L_r^{-1} H_r^T & \lambda I + L^{-1} R \end{bmatrix}) = 0 \tag{4.67}$$

We define $\Phi_1 \triangleq \lambda I + L^{-1} R = \Lambda_1 + j\Lambda_2$ where $\Lambda_{1,2}$ are expressed by

$$\Lambda_1 = \mathrm{diag}(\alpha + \frac{R_{c_1}}{L_{c_1}}, \cdots, \alpha + \frac{R_{c_L}}{L_{c_L}}) \in \mathbb{R}^{L\times L}$$
$$\Lambda_2 = \mathrm{diag}(\beta, \cdots, \beta) \in \mathbb{R}^{L\times L}$$

Since the Hermitian part of Φ_1 is equal to $\mathcal{H}(\Phi_1) = \Lambda_1$, which is positive definite, the complex matrix Φ_1 is also positive definite (Lemma 4.1.6). Consequently, Φ_1

must be invertible (Lemma 4.1.9) and $\det(\Phi_1) \neq 0$. Then, Eq. (4.67) is equal to

$$\begin{aligned}
&\det(\begin{bmatrix} \lambda I + D & -C_r^{-1} H_r \\ L_r^{-1} H_r^T & \lambda I + L^{-1} R \end{bmatrix}) \\
=&\det(\lambda I + D + C_r^{-1} H_r \Phi_1^{-1} L^{-1} H_r^T) \det(\Phi_1) \\
=&\det(\lambda C_r + C_r D + H_r (\lambda L + R)^{-1} H_r^T) \det(\Phi_1) \det(C_r^{-1})
\end{aligned}$$

Again, we define $\Phi_2 \triangleq \lambda C_r + C_r D + H_r(\lambda L + R)^{-1} H_r^T$, $\lambda C_r + C_r D = \Lambda_3 + j\Lambda_4$ and $(\lambda L + R)^{-1} = \Lambda_5 + j\Lambda_6$ with the notations

$$\begin{aligned}
&\Lambda_3 = \alpha C_r - C_r D \triangleq \operatorname{diag}(\sigma_1, \cdots, \sigma_{N+M+P-1}) \\
&\begin{cases}
\sigma_{(\rho-1)} = C_{g_\rho}(\alpha + \dfrac{P^o_{g_\rho}}{\bar{u}^2_{cg_\rho}}), & \rho \in \mathcal{N}_{-1} \\
\sigma_{(j+N-1)} = C_{w_j}(\alpha + \dfrac{P^o_{w_j}}{C_{w_j} \bar{u}^2_{w_j}}), & j \in \mathcal{M} \\
\sigma_{(h+N+M-1)} = C_{p_h} \alpha. & h \in \mathcal{P}
\end{cases} \\
&\Lambda_4 = \beta C_r \\
&\Lambda_5 = \operatorname{diag}(\frac{\alpha L_{c_k} + R_{c_k}}{(\alpha L_{c_k} + R_{c_k})^2 + (\beta L_{c_k})^2}) \in \mathbb{R}^{L \times L} \\
&\Lambda_6 = \operatorname{diag}(\frac{-\beta L_{c_k}}{(\alpha L_{c_k} + R_{c_k})^2 + (\beta L_{c_k})^2}) \in \mathbb{R}^{L \times L}
\end{aligned} \tag{4.68}$$

Now, Φ_2 can be rewritten as

$$\begin{aligned}
\Phi_2 &= \Phi_3 + j(\Lambda_4 + H_r \Lambda_6 H_r^T) \\
\Phi_3 &= \Lambda_3 + H_f H_f^T
\end{aligned} \tag{4.69}$$

where H_f are given by $H_f = H_r \Lambda_5^{\frac{1}{2}}$. Since $\Lambda_5^{\frac{1}{2}}$ is a full rank matrix, i.e. $\operatorname{rank}(\Lambda_5^{\frac{1}{2}}) = L$, then $\operatorname{rank}(H_f H_f^T) = \operatorname{rank}(H_f) = \operatorname{rank}(H_r) = N + M + P - 1$ (see Lemma 3.4.2). As a result, $H_f H_f^T$ is invertible and positive. Because $P^o_{g_\rho}$ and $P^o_{w_j}$ are non-negative, obviously, Λ_3 is semi-positive definite and furthermore, by applying Lemma 4.1.8, Φ_3 is positive definite.

As presented in (4.69), we know that $\mathcal{H}(\Phi_2) = \Phi_3$ and then, according to Lemma 4.1.6 and Lemma 4.1.9, Φ_2 is positive definite and invertible. Therefore, the following result is obtained:

$$\det(\lambda I - J) = \det(\Phi_2) \det(\Phi_1) \det(C_r^{-1}) \neq 0$$

for $\alpha \geq 0$. This leads to a contradiction to (4.67). Thus, all eigenvalues of the Jacobian matrix Φ must have negative real parts, i.e. $\alpha < 0$. Hence, J is a Hurwitz matrix. As a result, the origin of the zero dynamics (4.63) is locally asymptotically stable. Finally, the MTDC system is minimum phase. The proof is completed. □

Table 4.7: Control configuration for the four-terminal VSC HVDC system.

SAC 1 (master terminal)	SAC 2
Constant DC voltage control Reactive power control	Active power control Reactive power control
WAC 1	**WAC 2**
AC voltage control (constant frequency and magnitude)	AC voltage control (constant frequency and magnitude)

4.1.4.2 Simulation studies

To test the proposed nonlinear controller, an MTDC system with two SAC and two WAC connected VSC terminals is simulated in Fig. 4.21 where the structure of the DC grid is illustrated by Fig. 4.22. Based on the arrangement of the VSC operation as stated at the beginning of this section, the control configurations of the four terminals are listed in Table 4.7. The system parameters of the four terminals are chosen according to Table 4.4.

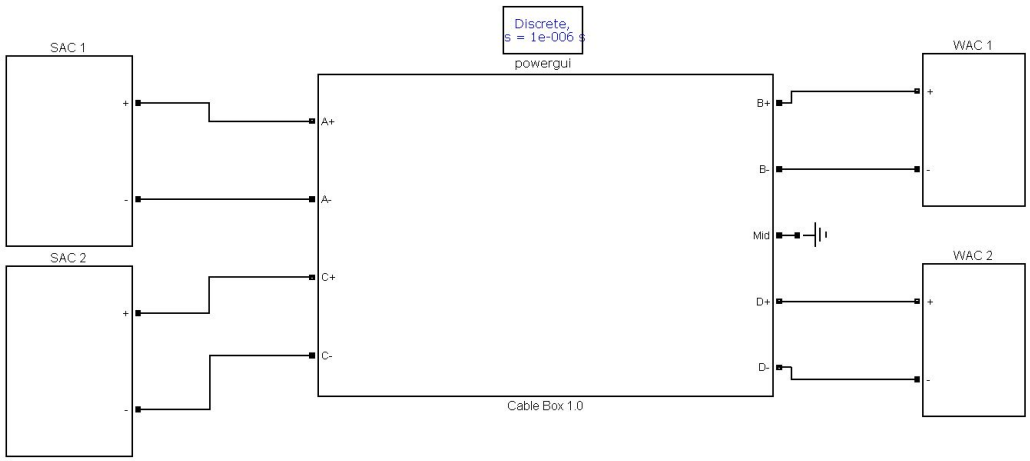

Figure 4.21: An MTDC system consists of two strong and two weak AC systems.

Table 4.8: Initial values of the system state variables.

SAC 1	SAC 2
$u_{cg_1} = u^o_{cg_1} = 150$ V	$i_{g_2d} = i^o_{g_2d} = 6.53$ A
$i_{g_1q} = i^o_{g_1q} = 0$ A	$i_{g_2q} = i^o_{g_2q} = 0$ A
WAC 1	**WAC 2**
$v_{sw_1d} = v^o_{sw_1d} = 40.82$ V	$v_{sw_2d} = v^o_{sw_2d} = 40.82$ V
$v_{sw_1q} = v^o_{sw_1q} = 0$ V	$v_{sw_2q} = v^o_{sw_2q} = 0$ V

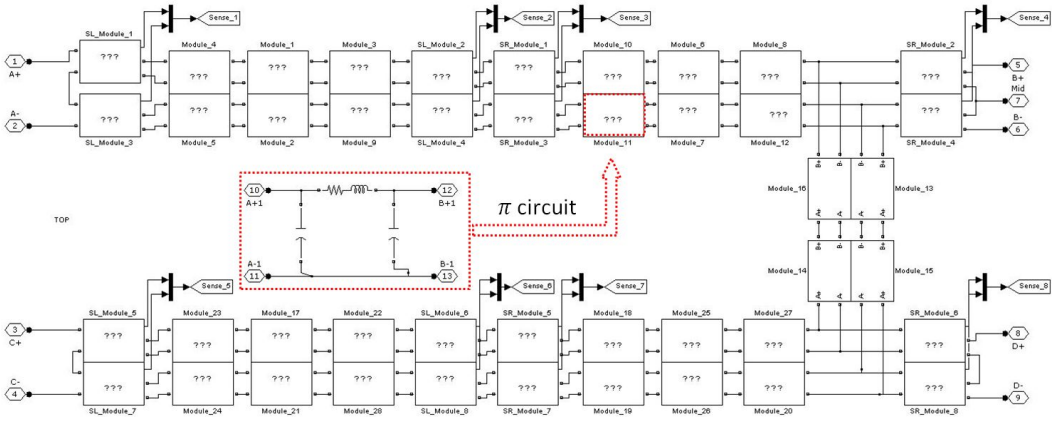

Figure 4.22: DC grid used to connect the four AC areas.

The performance of the feedback nonlinear controller is evaluated under different scenarios and also compared to the performance of the same MTDC system using PI control technique. Initially, the MTDC system operates in the steady state given by Table 4.8. At $t = 0.5$ s, $i^o_{g_2d}$ is changed to a new reference value with an increase of 50% and then, at $t = 1$ s and $t = 1.5$ s, new reference values of v_{sw_1q} and v_{sw_2q} are introduced, $v^o_{sw_1q} = v^o_{sw_1q} = 20.41$ V.

The simulation results are plotted in Figs. 4.23-4.32. Figure 4.23 demonstrates that both controllers can keep the DC voltage at $u^o_{cg_1} = 150$ V. Compared to the PI controller, the feedback nonlinear controller gives the response of u_{cg_1} a faster convergence but a larger undershoot as $v^o_{sw_1q}$ and $v^o_{sw_2q}$ are subjected to a step change at $t = 1$ s and $t = 1.5$ s respectively, since there is usually a compromise between the settling time and undershoot (or overshoot).

Figure 4.24 clearly shows that the step changes of $i^o_{g_2d}$, $v^o_{sw_1q}$ and $v^o_{sw_2q}$ greatly disturb the performance of i_{g_1q} under the PI controller while having negligible effects on i_{g_1q} under the feedback nonlinear controller. This phenomenon indicates that the feedback nonlinear controller has the benefit of providing a better decoupling characteristics of the DC voltage and $q-$axis current control.

Figures 4.25 and 4.26 (or Figures 4.29 and 4.30) depict the responses of $v_{sw_1,dq}$ (or $v_{sw_2,dq}$) and show that the feedback nonlinear controller provides faster damping and less overshoot than the PI controller. Besides, as plotted in Fig. 4.25 (or Fig.

4.25), the change of v^o_{sw1q} (or v^o_{sw2q}) has a crippling effect on the performance of v_{sw1d} (or v_{sw2d}) under the PI controller while v_{sw1d} (or v_{sw2d}) under the feedback nonlinear controller is always kept at its reference value. It reveals that the feedback nonlinear controller also gives a better decoupling characteristics of v_{sw1d} and v_{sw1q} (or v_{sw2d} and v_{sw2q}) control. As shown in Figs. 4.27 and 4.28 (or Figs. 4.31 and 4.32), the feedback nonlinear controller also improves the performance of the AC voltage of WAC1 (or WAC2) at the PCC in *abc* frame in comparison to the PI controller.

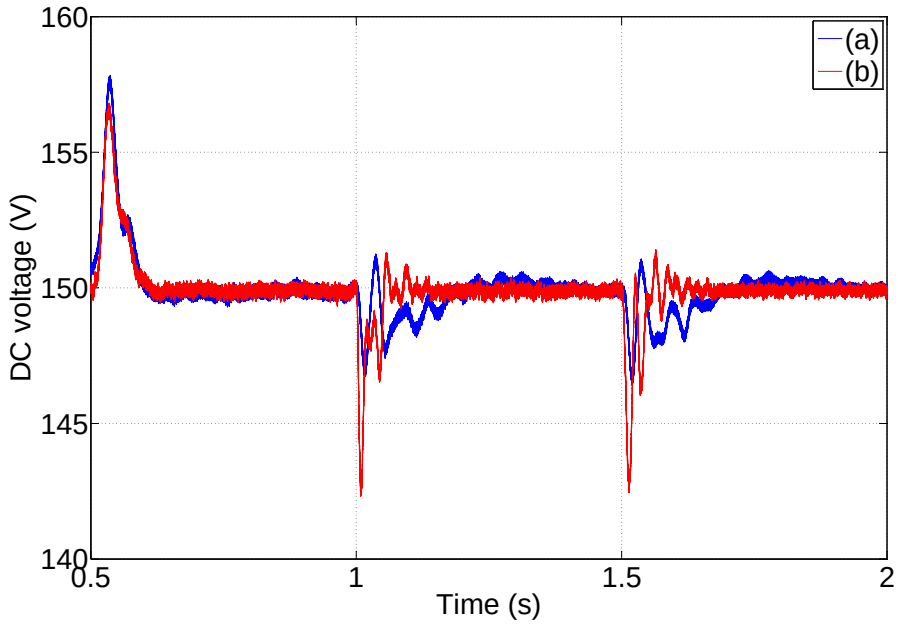

Figure 4.23: The response of u_{cg_1}. (a) PI controller. (b) Feedback nonlinear controller.

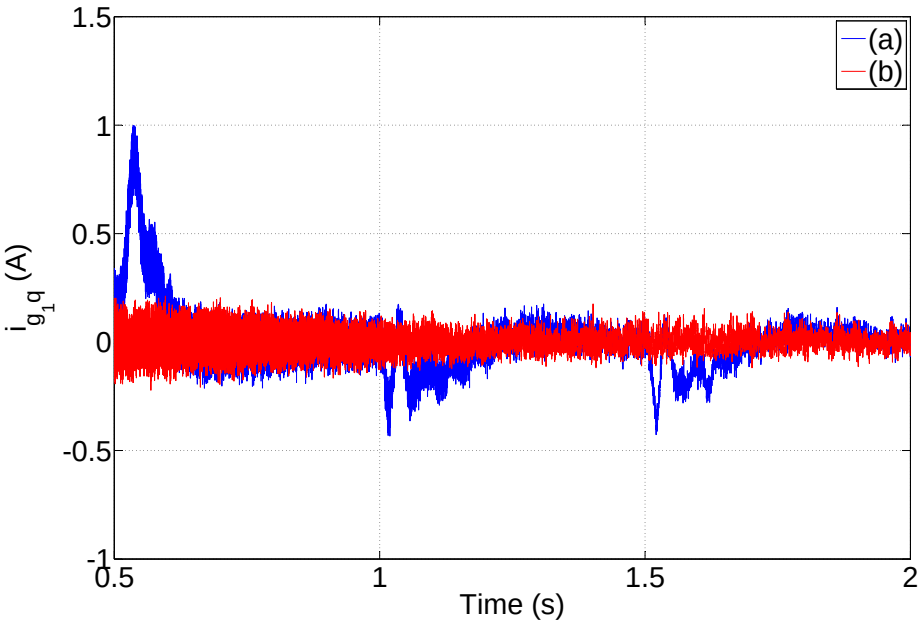

Figure 4.24: The response of i_{g_1q}. (a) PI controller. (b) Feedback nonlinear controller.

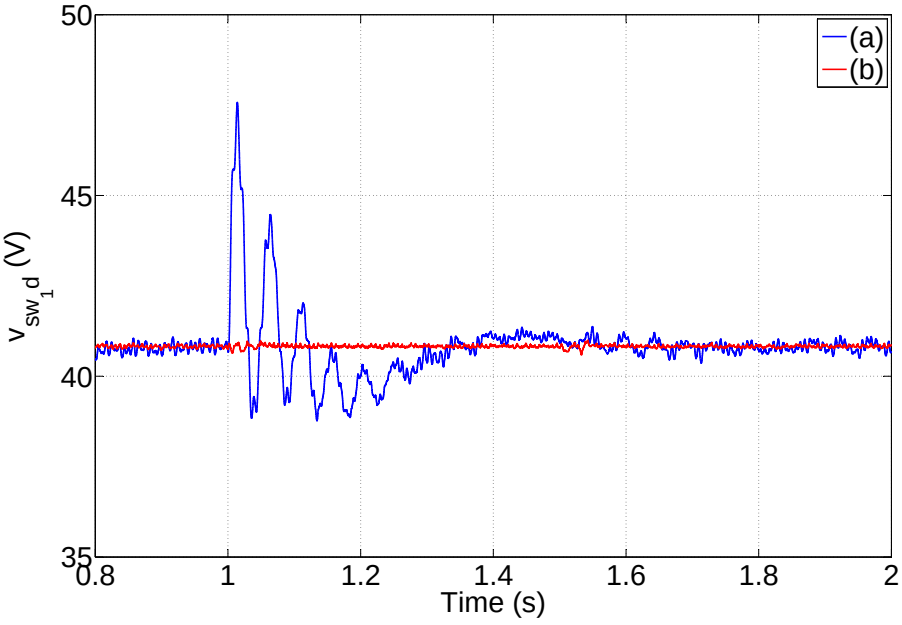

Figure 4.25: The response of v_{sw_1d}. (a) PI controller. (b) Feedback nonlinear controller.

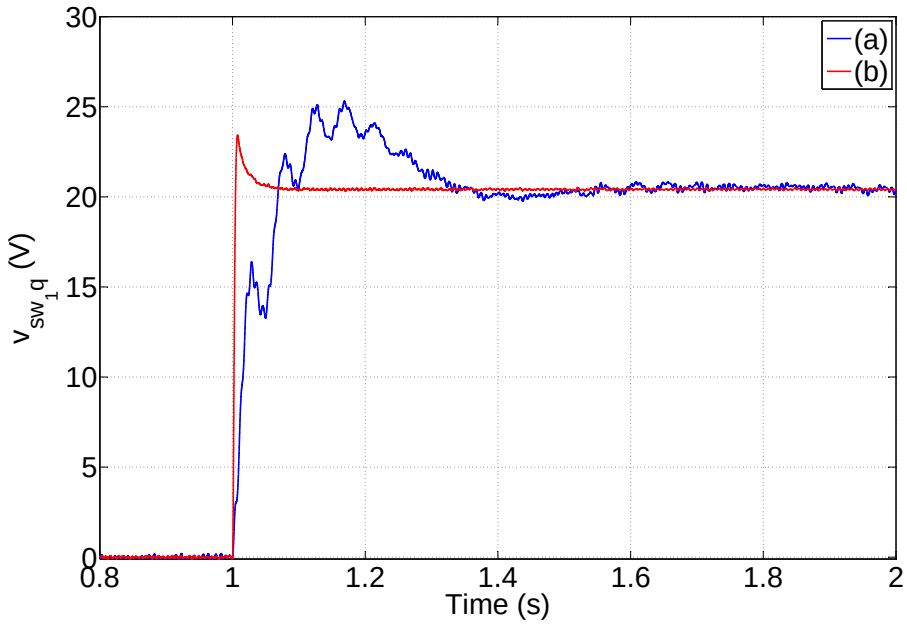

Figure 4.26: The response of v_{sw_1q}. (a) PI controller. (b) Feedback nonlinear controller.

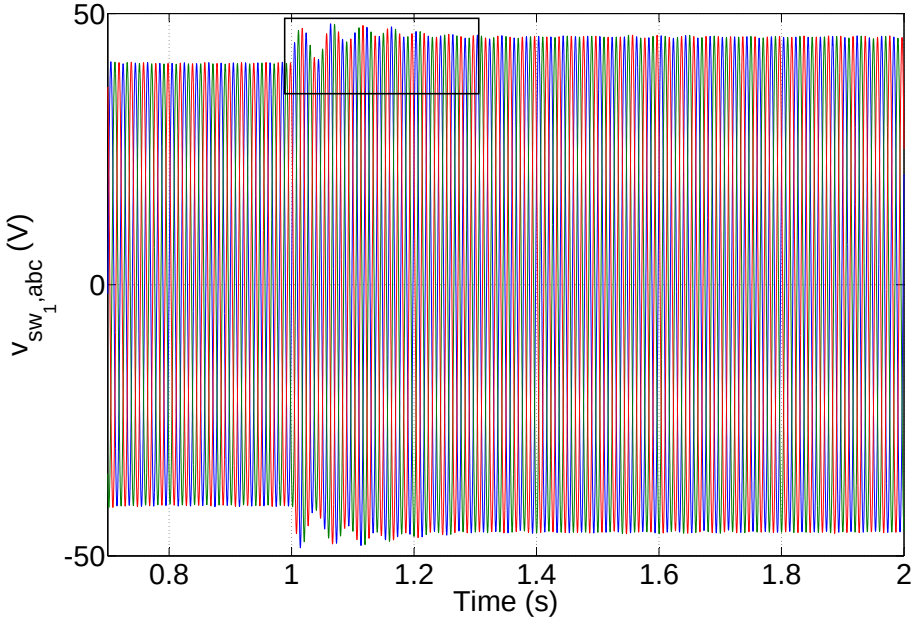

Figure 4.27: The response of $v_{sw_1,abc}$ using PI control technique.

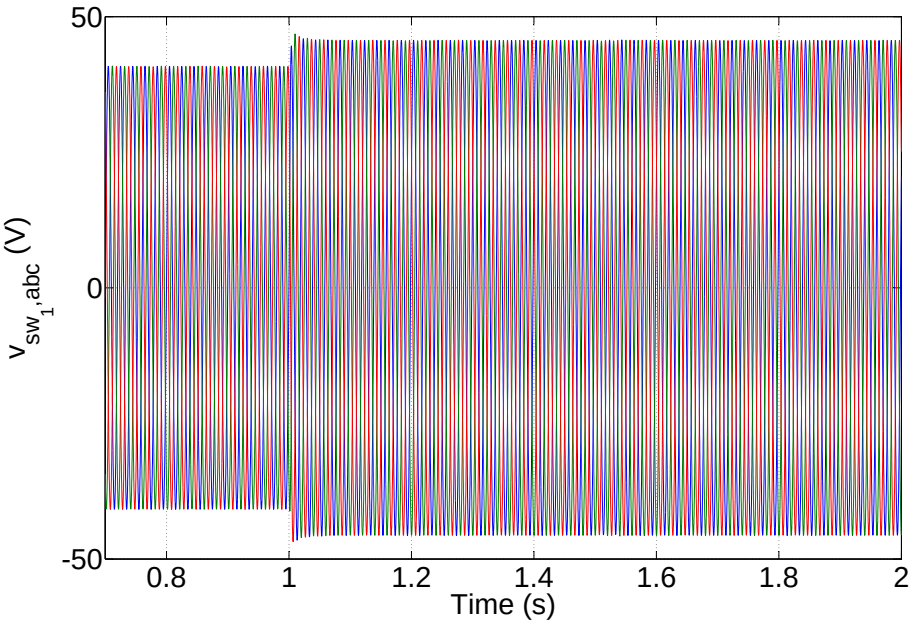

Figure 4.28: The response of $v_{sw_1,abc}$ using feedback linearization technique.

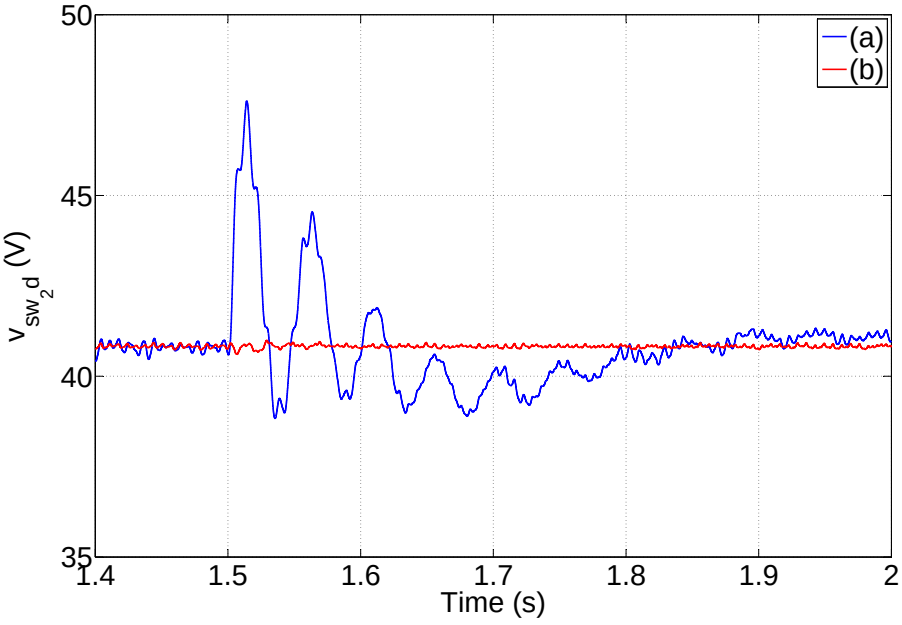

Figure 4.29: The response of v_{sw2d}. (a) PI controller. (b) Feedback nonlinear controller.

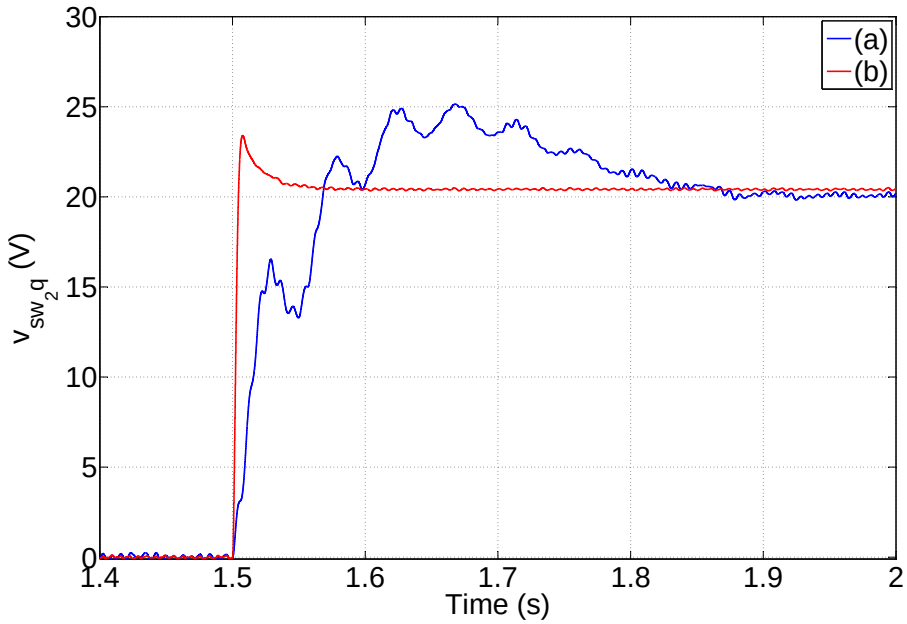

Figure 4.30: The response of v_{sw_2q}. (a) PI controller. (b) Feedback nonlinear controller.

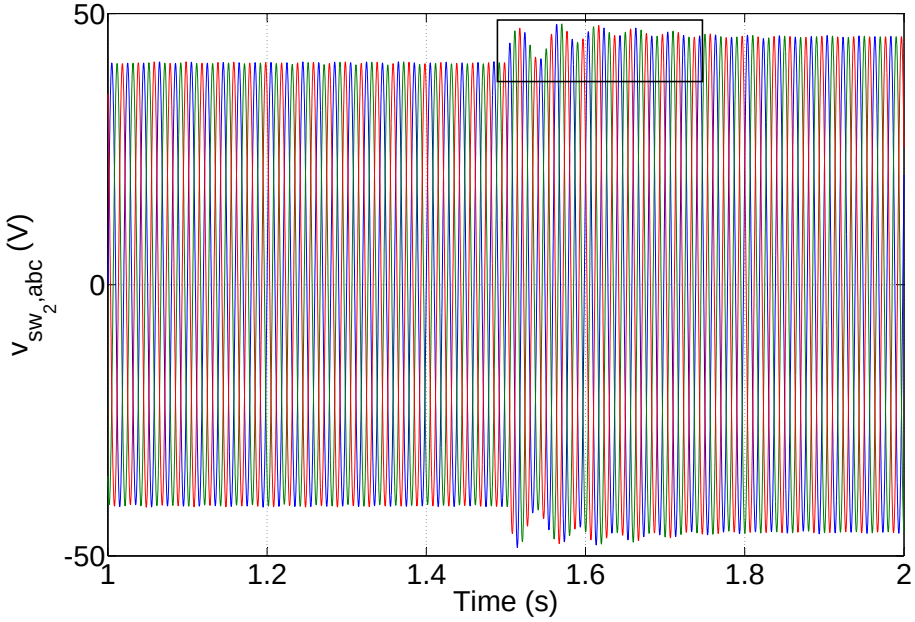

Figure 4.31: The response of $v_{sw_2,abc}$ using PI control technique.

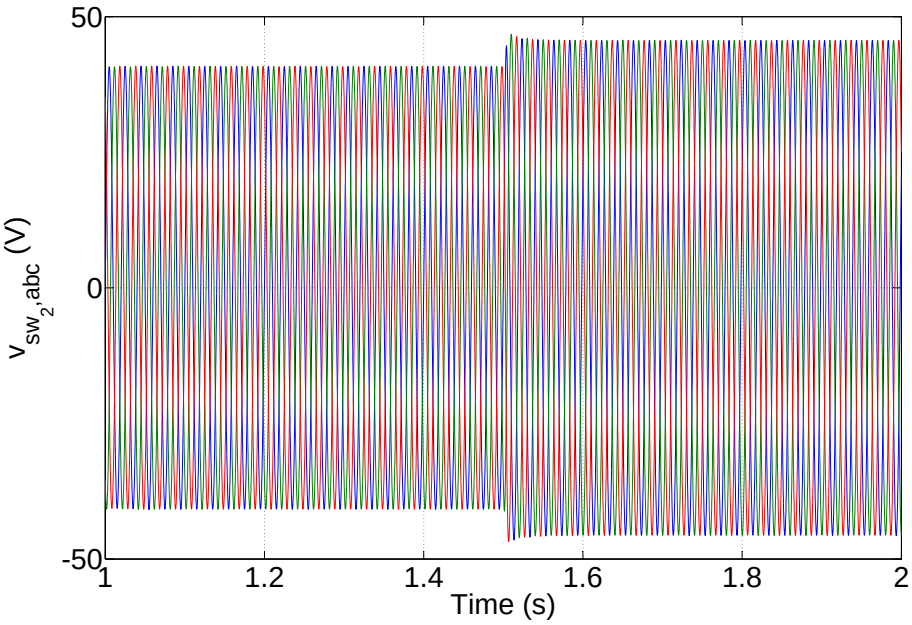

Figure 4.32: The response of $v_{sw_2,abc}$ using feedback linearization technique.

4.2 Feedback linearization with sliding mode control

4.2.1 Control design

As presented in (4.31), the developed nonlinear controller strongly depends on the system model, which requires the exact informations on the system parameters. For the purpose of good robustness, sliding mode control is used to deal with the case when the system parameters, L_{g_i}, R_{g_i}, C_{g_i} and R_L, are poorly known.

By applying the transformation T_x in (4.33) and considering the integrated tracking errors (4.36), the original system (4.21) becomes

$$\begin{aligned}
\dot{e}_{I1} &= e_1 \\
\dot{e}_1 &= L_{f_x}(i_{g_iq}) + L_{g_d}(i_{g_iq})m_{g_iq} \triangleq h_1 + \phi_1 \cdot m_{g_iq} \\
\dot{e}_{I2} &= e_2 \\
\dot{e}_2 &= z_3 \\
\dot{z}_3 &= L^2_{f_x}(u_{cg_i}) + L_{g_d}L_{f_x}(u_{cg_i})m_{g_id} + L_{g_q}L_{f_x}(u_{cg_i})m_{g_iq} \\
&\triangleq h_2 + \phi_{2d} \cdot m_{g_id} + \phi_{2q} \cdot m_{g_iq}
\end{aligned} \tag{4.70}$$

where $h_{1,2}$ and $\phi_{1,2}$ are nonlinear continuous functions on $e_{I_{1,2}}$, $e_{1,2}$ and e_3 with unknowns parameters. Let us impose two sliding surfaces as

$$\begin{aligned}
s_1 &= a_0 e_{I_1} + e_1 \\
s_2 &= b_0 e_{I_2} + b_1 e_2 + z_3
\end{aligned} \tag{4.71}$$

where a_0 is positive and $b_{0,1}$ are chosen such that the matrix

$$B_0 = \begin{bmatrix} 0 & 1 \\ -b_0 & -b_1 \end{bmatrix} \tag{4.72}$$

is Hurwitz. The derivatives of the sliding surfaces are given by

$$\begin{aligned} \dot{s}_1 &= a_0 e_1 + h_1 + \phi_1 \cdot m_{g_i q} \\ \dot{s}_2 &= b_0 e_2 + b_1 z_3 + h_2 + \phi_{2d} \cdot m_{g_i d} + \phi_{2q} \cdot m_{g_i q} \end{aligned} \tag{4.73}$$

Let us consider the Lyapunov function $V_1 = s_1^2 + s_2^2$ and then, the derivative of V_1 is deduced as

$$\begin{aligned} \dot{V}_1 &= W_1 + W_2 \\ W_1 &= s_1(a_0 e_1 + h_1 + \phi_1 \cdot m_{g_i q}) \\ W_2 &= s_2(b_0 e_2 + b_1 z_3 + h_2 + \phi_{2d} \cdot m_{g_i d} + \phi_{2q} \cdot m_{g_i q}) \end{aligned} \tag{4.74}$$

From (4.30), it is clear that ϕ_1 and ϕ_{2d} are always negative and moreover, ϕ_1 and ϕ_{2d} are continuous and invertible for positive u_{cg_i}.

Assumption 4.2.1. *In the domain of interest as described in Section 3.4.4, h_1, h_2, ϕ_1 and $\phi_{2,dq}$ satisfy the inequalities*

$$\begin{aligned} &|h_1| \leq h_{1,max},\ 0 \leq \phi_{1,min} \leq |\phi_1| \leq \phi_{1,max} \\ &|h_2| \leq h_{2,max},\ 0 \leq \phi_{2d,min} \leq |\phi_{2d}| \leq \phi_{2d,max} \\ &0 \leq \phi_{2q,min} \leq |\phi_{2q}| \leq \phi_{2q,max} \end{aligned} \tag{4.75}$$

when the system parameters are bounded.

With Assumption 4.2.1, we can then define the control law for $m_{g_i q}$ as

$$m_{g_i q} = \beta_q \frac{1}{\phi_{1,\min}} \mathrm{sgn}(s_1) \tag{4.76}$$

where β_q are designed as

$$\beta_q = a_0|e_1| + h_{1,\max} + \beta_0,\ \beta_0 > 0 \tag{4.77}$$

The control law for $m_{g_i d}$ is developed as

$$m_{g_i d} = \beta_d \frac{1}{\phi_{2d,\min}} \mathrm{sgn}(s_2) \tag{4.78}$$

where

$$\beta_d = b_0|e_2| + b_1|z_3| + h_{2,\max} + \frac{\phi_{2q,\max}}{\phi_{1,\min}}\beta_q + \beta_1,\ \beta_1 > 0 \tag{4.79}$$

Applying (4.76) to W_1, we obtain

$$W_1 = s_1(a_0 e_1 + h_1 + \beta_q \frac{\phi_1}{\phi_{1,\min}} \mathrm{sgn}(s_1)) \tag{4.80}$$

The sign of W_1 can be analyzed as follows:

- If $s_1 > 0$, then $\text{sgn}(s_1) = 1$ and recalling that ϕ_1 is negative and $\phi_{1,\min}$ is positive, we have

$$\begin{aligned}\frac{\phi_1}{\phi_{1,\min}} &\leq -1 \\ \dot{s}_1 &= a_0 e_1 + h_1 + (a_0|e_1| + h_{1,\max} + \beta_0)\frac{\phi_1}{\phi_{1,\min}} < 0\end{aligned}$$

- If $s_1 < 0$, $\text{sgn}(s_1) = -1$ leads to

$$\dot{s}_1 = a_0 e_1 + h_1 - (a_0|e_1| + h_{1,\max} + \beta_0)\frac{\phi_1}{\phi_{1,\min}} > 0$$

As a result, $W_1 = s_1\dot{s}_1$ is negative for all $s_1 \neq 0$.

Substituting (4.76) and (4.78) into (4.74) yields

$$\begin{aligned}W_2 &= s_2(b_0 e_2 + b_1 z_3 + h_2 + \phi_{2d} \cdot m_{g_i d} + \phi_{2q} \cdot m_{g_i q}) \\ &= s_2(b_0 e_2 + b_1 z_3 + h_2 + \beta_q \frac{\phi_{2q}}{\phi_{1,\min}}\text{sgn}(s_1) + \beta_d \frac{\phi_{2d}}{\phi_{2d,\min}}\text{sgn}(s_2))\end{aligned} \tag{4.81}$$

Recalling (4.75) and the design of β_d in (4.79), we have the following results:

- If $s_2 > 0$, $\text{sgn}(s_2) = 1$ and then,

$$\frac{\phi_{2d}}{\phi_{2d,\min}} \leq -1 \tag{4.82}$$

$$\dot{s}_2 = b_0 e_2 + b_1 z_3 + h_2 + \beta_q \frac{\phi_{2q}}{\phi_{1,\min}}\text{sgn}(s_1) + \beta_d \frac{\phi_{2d}}{\phi_{2d,\min}} < 0 \tag{4.83}$$

- If $s_2 < 0$, $\text{sgn}(s_2) = -1$ and then, we have

$$\dot{s}_2 = b_0 e_2 + b_1 z_3 + h_2 + \beta_q \frac{\phi_{2q}}{\phi_{1,\min}}\text{sgn}(s_1) - \beta_d \frac{\phi_{2d}}{\phi_{2d,\min}} > 0 \tag{4.84}$$

Therefore, $W_2 = s_2\dot{s}_2$ is also negative for all $s_2 \neq 0$. From the above analysis, the controller defined by (4.76) and (4.78) will lead to the manifolds $s_1 = 0$ and $s_2 = 0$. On these two manifolds, the behavior of the system is totally governed by

$$\begin{aligned}\dot{e}_{I1} &= e_1 \\ \dot{e}_1 &= -a_0 e_{I1} \\ \dot{e}_{I2} &= e_2 \\ \dot{e}_2 &= -b_0 e_{I_2} - b_1 e_2\end{aligned} \tag{4.85}$$

whose equilibrium point is asymptotically stable.

Since the use of sign function $\text{sgn}(\cdot)$ usually causes the chattering problem [Khalil 1996], in order to deal with this issue, a high-slope saturation function $\text{sat}(\cdot)$ defined as

$$\text{sat}(s/\mu) = \begin{cases} s/||s|| & \text{if } ||s|| \geq \mu \\ s/\mu & \text{if } ||s|| < \mu \end{cases} \tag{4.86}$$

is applied instead and hence the controller is modified as

$$\begin{aligned} m_{g_i d} &= -\beta_d \frac{1}{\phi_{2d,\min}} \text{sat}(\frac{s_2}{\mu_2}) \\ m_{g_i q} &= -\beta_q \frac{1}{\phi_{1,\min}} \text{sat}(\frac{s_1}{\mu_1}) \end{aligned} \tag{4.87}$$

with positive μ_1 and μ_2.

4.2.2 Simulation studies

To assess the performance of the feedback linearization controller with sliding mode control, numerical simulations are realized for a VSC HVDC link connected to a resistive load by using MATLAB/Simulink. The system parameters are the same as the case in Section 4.1.2.2.

The system starts from a steady-state condition, and then a sequence of events is applied to the resistive load R as shown in Fig. 4.33. The control objectives are to keep the DC voltage at $u^o_{cg_i} = 150$ V and to get the unitrary power factor, i.e. $i^o_{g_i q} = 0$ in spite of the variations in the resistive load. In Figs. 4.34-4.38, we show the behaviors of the state variables. As shown in the plots, both u_{cg_i} and $i_{g_i q}$ are well controlled at $u^o_{cg_i} = 150$ V and $i^o_{g_i q} = 0$ respectively no matter how the resistive load changes. Besides, as illustrated in Figs. 4.37 and 4.38, the control modulation variables $m_{g_I,dq}$ always satisfy the physical constraint $\sqrt{m^2_{g_i d} + m^2_{g_i q}} \leq 1$.

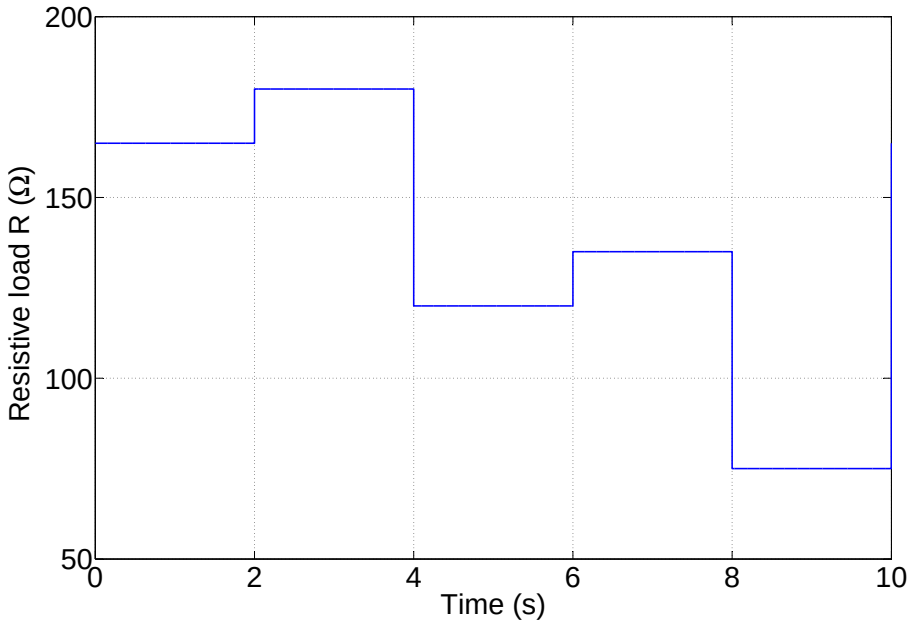

Figure 4.33: Variations in the resistive load R.

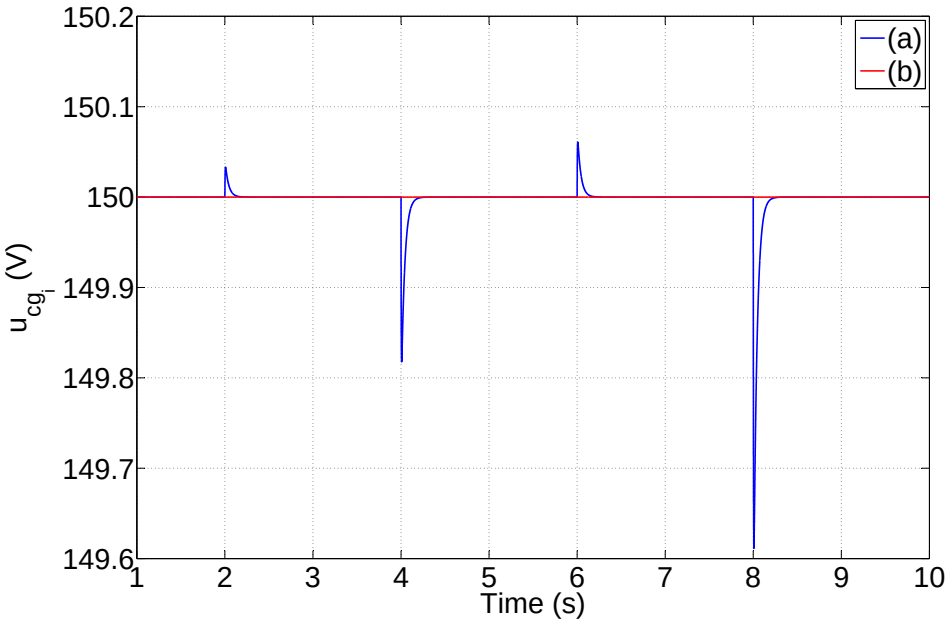

Figure 4.34: Response of u_{cg_i} (curve (a)) and its reference $u^o_{cg_i}$ (curve (b)).

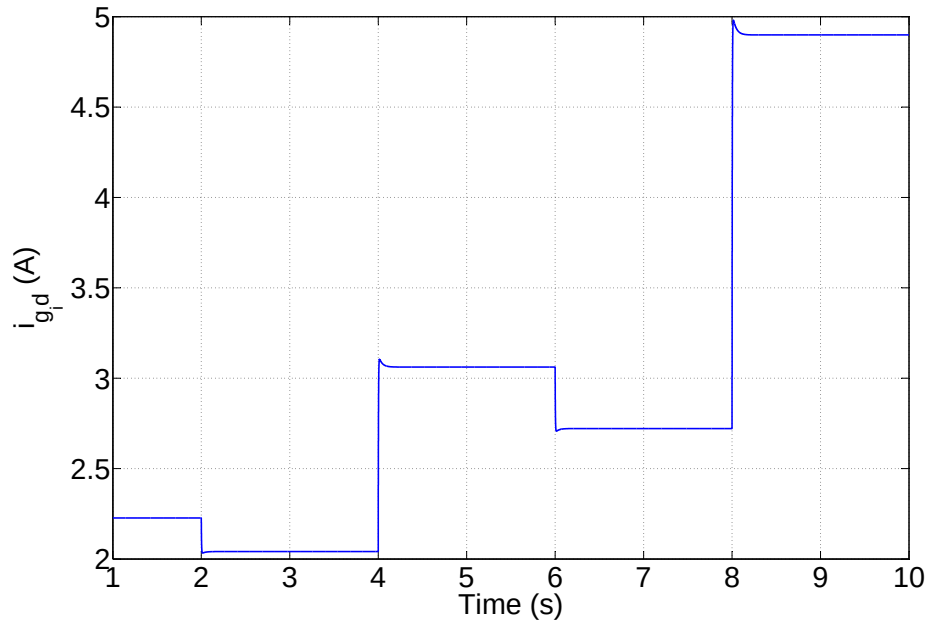

Figure 4.35: Response of $i_{g_i d}$.

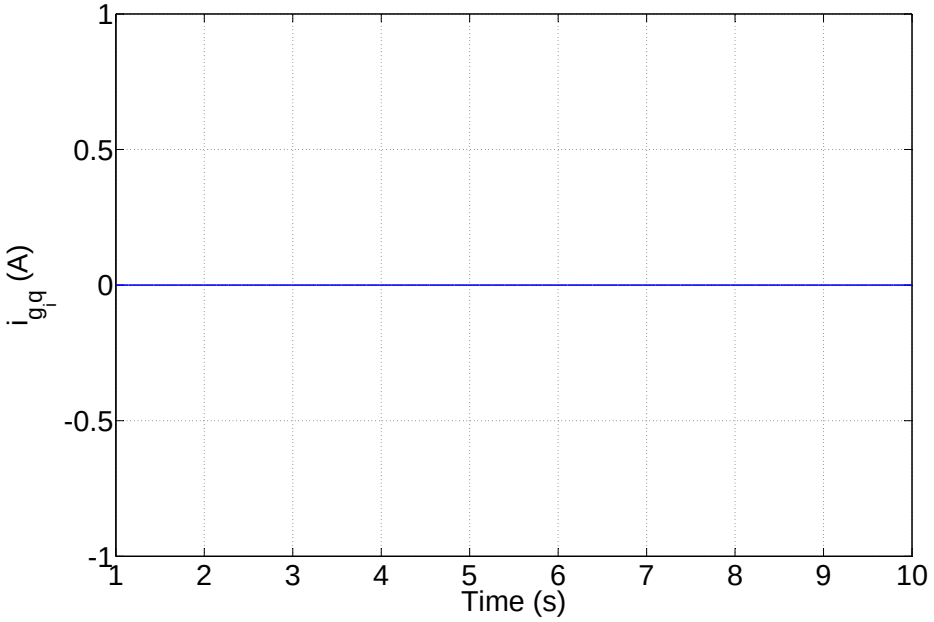

Figure 4.36: Response of $i_{g_i q}$.

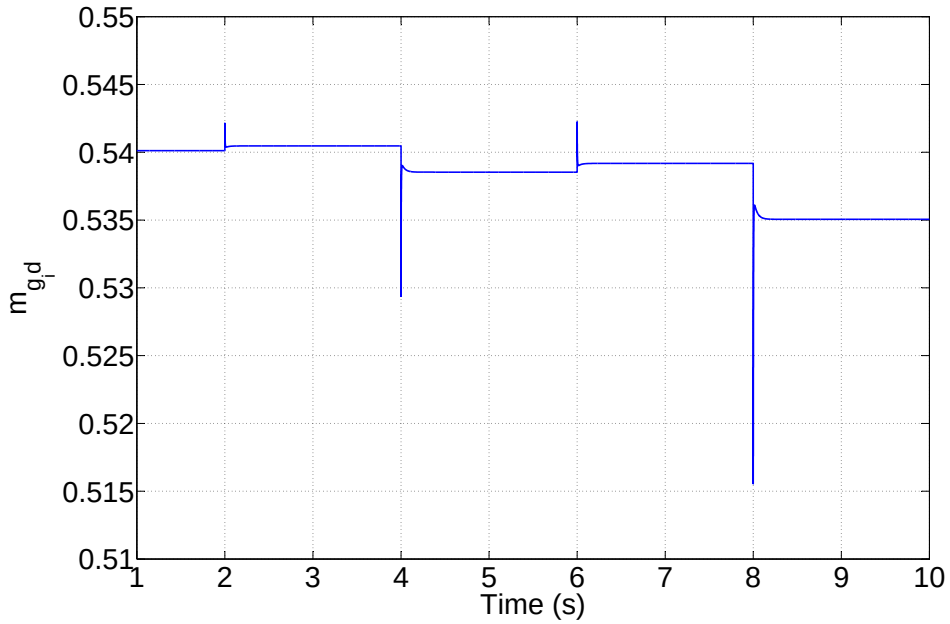

Figure 4.37: Response of $m_{g_i d}$.

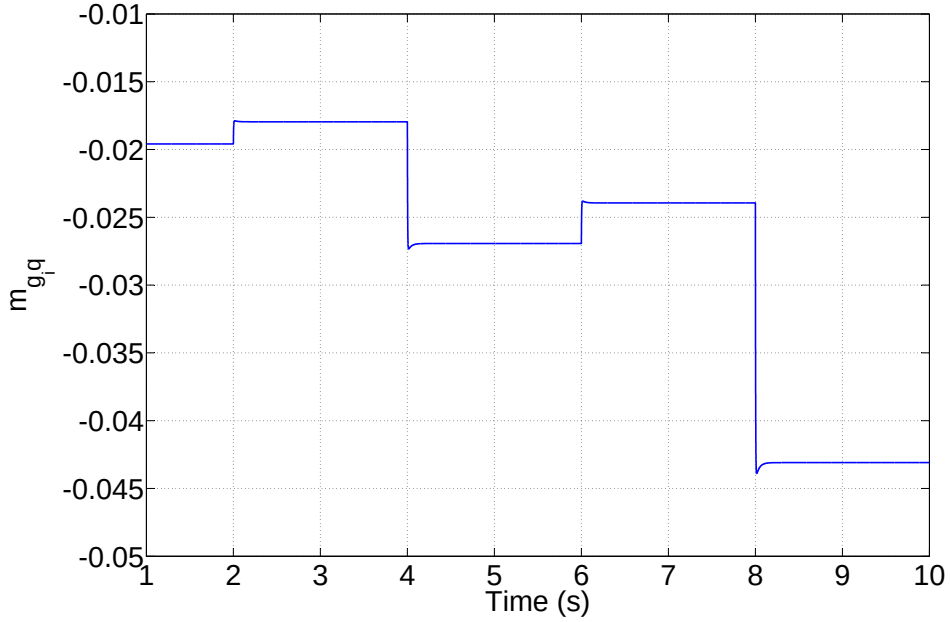

Figure 4.38: Response of $m_{g_i q}$.

4.3 Passivity-based control

As presented in Section 4.1.4, when the output is defined as (4.56), in order ensure the asymptotic stability of the equilibrium point of the zero dynamics (4.63), the prescribed references $u^o_{cg_1}$, $Q^o_{g_1}$, $P^o_{g_\rho}$, $Q^o_{g_\rho}$, $v^o_{sw_jd}$ and $v^o_{sw_jq}$ and the system parameters must be chosen such that the Jacobian matrix J in (4.66) is Hurwitz. It implies that these prescribed references can not be set arbitrarily. To overcome this shortcoming, we want to find a specific output y_s such that the stability of the equilibrium point of the zero dynamics is irrelevant to the choice of the prescribed references. In this section, we will demonstrate that this can be achieved by means of passivity theory.

In fact, there have been several studies on the passivity-based control (PBC) design for a class of switched power converters which can be described in port-Hamiltonian form [Perez 2004, Hernandez-Gomez 2010, Escobar 1999]. Apart from the prior research work, we first design a passive output derived from a storage function and then, further investigate the corresponding zero dynamics. Since some variables to be controlled belong to the state variables of the zero dynamics and the convergence rate of the zero dynamics are determined by the system inherent characteristics, additional control inputs are introduced to modify the dynamics and improve the performance of those desired controllable variables of the zero dynamics.

Recall the dynamics of the DC grid (3.33) where i_{cg_i} and i_{cw_j} are obtained from (3.23) and (3.32) by neglecting the losses of the phase reactor and the VSC. In fact, taking into account these losses and according to the power balance on both sides of the converter station, i_{cg_i} also satisfies

$$\underbrace{\frac{3}{2}(v_{cg_id}i_{g_id}+v_{cg_iq}i_{g_iq})}_{\text{Active power on the AC side of the converter}} = \underbrace{\frac{u^2_{cg_i}}{R_{\text{equi},g_i}}}_{\text{loss of the VSC}} + \underbrace{u_{cg_i}i_{cg_i}}_{\text{Active power injected to the DC grid}} \tag{4.88}$$

where the equivalent resistance $R_{\text{equi},(\cdot)}$ is used to represent the loss of the converter. According to (3.18), the converter voltages $v_{cg_i,dq}$ are expressed as

$$v_{cg_i,dq} = \frac{1}{2}u_{cg_i}m_{g_i,dq} \tag{4.89}$$

and then, substituting (4.89) into (4.88), we deduce

$$i_{cg_i} = \frac{3}{4}(m_{g_id}i_{g_id}+m_{g_iq}i_{g_iq}) - \frac{u_{cg_i}}{R_{\text{equi},g_i}} \tag{4.90}$$

A similar procedure is done to obtain a new formulation for i_{cw_j} as

$$i_{cw_j} = \frac{3}{4}(m_{w_jd}i_{w_jd}+m_{w_jq}i_{w_jq}) - \frac{u_{cw_j}}{R_{\text{equi},w_j}} \tag{4.91}$$

Now, based on (4.90) and (4.91), a new model for the DC grid is established as

$$\dot{z} = A_p z + \vartheta_p \tag{4.92}$$

where A_p and ϑ_p are given by

$$\begin{aligned}
\vartheta_p &= \begin{bmatrix} \cdots & \dfrac{3(m_{g_i d} i_{g_i d} + m_{g_i q} i_{g_i q})}{4C_{g_i}} & \cdots & \dfrac{3(m_{w_j d} i_{w_j d} + m_{w_j q} i_{w_j q})}{4C_{w_j}} & \cdots & 0_{(P+L)} \end{bmatrix}^T \\
A_p &= \begin{bmatrix} -D_p & C^{-1}H \\ -L^{-1}H^T & -L^{-1}R \end{bmatrix} \\
D_p &= C^{-1}R_{\text{equi}}^{-1} \in \mathbb{R}^{(N+M+P)\times(N+M+P)} \\
R_{\text{equi}} &= \text{diag}(\cdots, R_{\text{equi},g_i}, \cdots R_{\text{equi},w_j}, \cdots, 0, \cdots, 0)
\end{aligned} \tag{4.93}$$

Let us consider the dynamics of $v_{sw_j,dq}$ in (3.29). Similar to the modification of the dynamics of the DC grid, here we use the equivalent resistance R_{fw_j} to represent the losses of the filter and hence, $v_{sw_j,dq}$ are modeled by

$$\begin{aligned}
\frac{dv_{sw_j d}}{dt} &= \omega_{w_j} v_{sw_j q} + \frac{1}{C_{fw_j}}(I_{w_j d} - i_{w_j d} - \frac{v_{sw_j d}}{R_{fw_j}}) \\
\frac{dv_{sw_j q}}{dt} &= -\omega_{w_j} v_{sw_j d} + \frac{1}{C_{fw_j}}(I_{w_j q} - i_{w_j q} - \frac{v_{sw_j q}}{R_{fw_j}})
\end{aligned} \tag{4.94}$$

In this section, the passivity-based state feedback control design is developed based on the above new DC grid and AC voltage model.

4.3.1 Steady-state analysis

The same master-slave control configuration is used in this section as in Section 4.1.4. In addition, in order to make all SAC systems operate with unity power factor, we set

$$Q_{g_i}^o = 0 \tag{4.95}$$

Similar to Assumption 4.1.1, to ensure the operating feasibility of the MTDC system, we take the following assumption.

Assumption 4.3.1. *Consider the MTDC system described by (3.20), (3.28), (4.94) and (4.92). For the prescribed references $u_{cg_1}^o$, $Q_{g_1}^o$, $P_{g_\rho}^o$, $Q_{g_\rho}^o$, $v_{sw_j,dq}^o$, there exist equilibrium values for the state variables such that*

$$\begin{aligned}
0 &= -\frac{R_{g_i}}{L_{g_i}}\bar{i}_{g_i d} + \omega_{g_i}\bar{i}_{g_i q} + \frac{v_{sg_i d}}{L_{g_i}} - \frac{\bar{u}_{cg_i}}{2L_{g_i}}\bar{m}_{g_i d} \\
0 &= -\frac{R_{g_i}}{L_{g_i}}\bar{i}_{g_i q} - \omega_{g_i}\bar{i}_{g_i d} + \frac{v_{sg_i q}}{L_{g_i}} - \frac{\bar{u}_{cg_i}}{2L_{g_i}}\bar{m}_{g_i q} \\
0 &= -\frac{R_{w_j}}{L_{w_j}}\bar{i}_{w_j d} + \omega_{w_j}\bar{i}_{w_j q} + \frac{\bar{v}_{sw_j d}}{L_{w_j}} - \frac{\bar{u}_{cw_j}}{2L_{w_j}}\bar{m}_{w_j d} \\
0 &= -\frac{R_{w_j}}{L_{w_j}}\bar{i}_{w_j q} - \omega_{w_j}\bar{i}_{w_j d} + \frac{\bar{v}_{sw_j q}}{L_{w_j}} - \frac{\bar{u}_{cw_j}}{2L_{w_j}}\bar{m}_{w_j q} \\
0 &= \omega_{w_j}\bar{v}_{sw_j q} + \frac{1}{C_{fw_j}}(I_{w_j d} - \bar{i}_{w_j d} - \frac{\bar{v}_{sw_j d}}{R_{fw_j}}) \\
0 &= -\omega_{w_j}\bar{v}_{sw_j d} + \frac{1}{C_{fw_j}}(I_{w_j q} - \bar{i}_{w_j q} - \frac{\bar{v}_{sw_j q}}{R_{fw_j}}) \\
0 &= A_p\bar{z} + \bar{\vartheta}_p
\end{aligned} \tag{4.96}$$

where $\bar{u}_{cg_1} = u^o_{cg_1}$, $\bar{i}_{g_1q} = -\dfrac{2Q^o_{g_1}}{3v_{sg_1d}} = 0$, $\bar{i}_{g_\rho d} = \dfrac{2P^o_{g_\rho}}{3v_{sg_1d}}$, $\bar{i}_{g_\rho q} = -\dfrac{2Q^o_{g_\rho}}{3v_{sg_1d}} = 0$ *and* $\bar{v}_{sw_j,dq} = v^o_{sw_j,dq}$.

Under Assumption 4.3.1, the steady-state values of $i_{w_j,dq}$ and the control variables are deduced as

$$\begin{aligned}\bar{i}_{w_jd} &= I_{w_jd} + C_{fw_j}\omega_{w_j}v^o_{sw_jq} - \frac{v^o_{sw_jd}}{R_{fw_j}}\\ \bar{i}_{w_jq} &= I_{w_jq} - C_{fw_j}\omega_{w_j}v^o_{sw_jd} - \frac{v^o_{sw_jq}}{R_{fw_j}}\end{aligned} \tag{4.97}$$

and

$$\begin{aligned}\bar{m}_{g_id} &= \frac{2}{u_{cg_i}}(-R_{g_i}\bar{i}_{g_id} + L_{g_i}\omega_{g_i}\bar{i}_{g_iq} + v_{sg_id})\\ \bar{m}_{g_iq} &= \frac{2}{u_{cg_i}}(-R_{g_i}\bar{i}_{g_iq} - L_{g_i}\omega_{g_i}\bar{i}_{g_id} + v_{sg_iq})\\ \bar{m}_{w_jd} &= \frac{2}{u_{cw_j}}(-R_{w_j}\bar{i}_{w_jd} + L_{w_j}\omega_{w_j}\bar{i}_{w_jq} + v^o_{sw_jd})\\ \bar{m}_{w_jq} &= \frac{2}{u_{cw_j}}(-R_{w_j}\bar{i}_{w_jq} - L_{w_j}\omega_{w_j}\bar{i}_{w_jd} + v^o_{sw_jq})\end{aligned} \tag{4.98}$$

Substituting (4.97) and (4.98) into (4.96), we find that the DC grid in steady state satisfies

$$\begin{aligned}&(v_{sg_id}\bar{i}_{g_id} + v_{sg_iq}\bar{i}_{g_iq}) - R_{g_i}(\bar{i}^2_{g_id} + \bar{i}^2_{g_iq}) + \frac{2}{3}[H(i,:)\bar{i}_c\bar{u}_{cg_i} - \frac{\bar{u}^2_{cg_i}}{R_{\text{equi},g_i}}] = 0\\ &(v^o_{sw_jd}\bar{i}_{w_jd} + v^o_{sw_jq}\bar{i}_{w_jq}) - R_{w_j}(\bar{i}^2_{w_jd} + \bar{i}^2_{w_jq}) + \frac{2}{3}[H(N+j,:)\bar{i}_c\bar{u}_{cw_j} - \frac{\bar{u}^2_{cw_j}}{R_{\text{equi},w_j}}] = 0\\ &H(N+M+h,:)\bar{i}_c = 0\\ &H(:,k)^T\bar{u}_c = 0\end{aligned} \tag{4.99}$$

Note that the above expression (4.99) contains several quadratic terms. It implies that the MTDC system has more than one equilibrium point that corresponds to the prescribed references [Lee 2003, Zonetti 2014]. But, not all of these equilibrium points are achievable. As presented in [Lee 2003], there are two possible steady-state values for the $d-$axis current. However, the larger one is physically impossible, making the converter operate beyond its ability. The choice of the reasonable equilibrium point is determined by the system physical characteristics, the feasibility of the modulation technique (see (3.21) and (3.30)), etc. But this issue is beyond the scope of this thesis. Here, we make the following assumption on the equilibrium point.

Assumption 4.3.2. *Consider the MTDC system described by* (3.20), (3.28), (4.94) *and* (4.92). *For the prescribed references* $u^o_{cg_1}$, $Q^o_{g_1}$, $P^o_{g_\rho}$, $Q^o_{g_\rho}$, $v^o_{sw_j,dq}$, *for every state variable, only one steady-state value exists in their respective domain of interest defined in Section 3.4.4.*

4.3.2 Passive system

Let $\tilde{(\cdot)} = (\cdot) - \bar{(\cdot)}$ denote the error between the variable $(\cdot)$ and its steady-state value. By considering the steady-state condition (4.96), $\tilde{(\cdot)}$ satisfies the differential equations

$$\begin{aligned}
\dot{\tilde{i}}_{g_i d} &= -\frac{R_{g_i}}{L_{g_i}}\tilde{i}_{g_i d} + \omega_{g_i}\tilde{i}_{g_i q} - \frac{1}{2L_{g_i}}(\bar{m}_{g_i d}\tilde{u}_{cg_i} + \tilde{m}_{g_i d}u_{cg_i}) \\
\dot{\tilde{i}}_{g_i q} &= -\frac{R_{g_i}}{L_{g_i}}\tilde{i}_{g_i q} - \omega_{g_i}\tilde{i}_{g_i d} - \frac{1}{2L_{g_i}}(\bar{m}_{g_i q}\tilde{u}_{cg_i} + \tilde{m}_{g_i q}u_{cg_i}) \\
\dot{\tilde{i}}_{w_j d} &= -\frac{R_{w_j}}{L_{w_j}}\tilde{i}_{w_j d} + \omega_{w_j}\tilde{i}_{w_j q} + \frac{\tilde{v}_{sw_j d}}{L_{w_j}} - \frac{1}{2L_{w_j}}(\bar{m}_{w_j d}\tilde{u}_{cw_j} + \tilde{m}_{w_j d}u_{cw_j}) \\
\dot{\tilde{i}}_{w_j q} &= -\frac{R_{w_j}}{L_{w_j}}\tilde{i}_{w_j q} - \omega_{w_j}\tilde{i}_{w_j d} + \frac{\tilde{v}_{sw_j q}}{L_{w_j}} - \frac{1}{2L_{w_j}}(\bar{m}_{w_j q}\tilde{u}_{cw_j} + \tilde{m}_{w_j q}u_{cw_j}) \\
\dot{\tilde{v}}_{sw_j d} &= \omega_{w_j}\tilde{v}_{sw_j q} - \frac{1}{C_{fw_j}}(\tilde{i}_{w_j d} + \frac{\tilde{v}_{sw_j d}}{R_{fw_j}}) \\
\dot{\tilde{v}}_{sw_j q} &= -\omega_{w_j}\tilde{v}_{sw_j d} - \frac{1}{C_{fw_j}}(\tilde{i}_{w_j q} + \frac{\tilde{v}_{sw_j q}}{R_{fw_j}}) \\
\dot{\tilde{z}} &= A_p\tilde{z} + \tilde{\vartheta}_p
\end{aligned} \tag{4.100}$$

where $\tilde{\vartheta}_p$ is given by

$$\begin{cases}
\tilde{\vartheta}_p(i) = \dfrac{3}{4C_{g_i}}(\bar{m}_{g_i d}\dot{\tilde{i}}_{g_i d} + \tilde{m}_{g_i d}i_{g_i d} + \bar{m}_{g_i q}\dot{\tilde{i}}_{g_i q} + \tilde{m}_{g_i q}i_{g_i q}), & i \in \mathcal{N} \\
\tilde{\vartheta}_p(N+j) = \dfrac{3}{4C_{w_j}}(\bar{m}_{w_j d}\dot{\tilde{i}}_{w_j d} + \tilde{m}_{w_j d}i_{w_j d} + \bar{m}_{w_j q}\dot{\tilde{i}}_{w_j q} + \tilde{m}_{w_j q}i_{w_j q}), & j \in \mathcal{M} \\
\tilde{\vartheta}_p(N+M+h) = 0. & h \in \mathcal{P} \\
\tilde{\vartheta}_p(N+M+P+k) = 0. & k \in \mathcal{L}
\end{cases}$$

In addition, setting $\tilde{m}_{g_i,dq} = \tilde{m}_{w_j,dq} = 0$, we get the unforced system of (4.100) as

$$\begin{aligned}
\dot{\tilde{i}}_{g_i d} &= -\frac{R_{g_i}}{L_{g_i}}\tilde{i}_{g_i d} + \omega_{g_i}\tilde{i}_{g_i q} - \frac{1}{2L_{g_i}}\bar{m}_{g_i d}\tilde{u}_{cg_i} \\
\dot{\tilde{i}}_{g_i q} &= -\frac{R_{g_i}}{L_{g_i}}\tilde{i}_{g_i q} - \omega_{g_i}\tilde{i}_{g_i d} - \frac{1}{2L_{g_i}}\bar{m}_{g_i q}\tilde{u}_{cg_i} \\
\dot{\tilde{i}}_{w_j d} &= -\frac{R_{w_j}}{L_{w_j}}\tilde{i}_{w_j d} + \omega_{w_j}\tilde{i}_{w_j q} + \frac{\tilde{v}_{sw_j d}}{L_{w_j}} - \frac{1}{2L_{w_j}}\bar{m}_{w_j d}\tilde{u}_{cw_j} \\
\dot{\tilde{i}}_{w_j q} &= -\frac{R_{w_j}}{L_{w_j}}\tilde{i}_{w_j q} - \omega_{w_j}\tilde{i}_{w_j d} + \frac{\tilde{v}_{sw_j q}}{L_{w_j}} - \frac{1}{2L_{w_j}}\bar{m}_{w_j q}\tilde{u}_{cw_j} \\
\dot{\tilde{v}}_{sw_j d} &= \omega_{w_j}\tilde{v}_{sw_j q} - \frac{1}{C_{fw_j}}(\tilde{i}_{w_j d} + \frac{\tilde{v}_{sw_j d}}{R_{fw_j}}) \\
\dot{\tilde{v}}_{sw_j q} &= -\omega_{w_j}\tilde{v}_{sw_j d} - \frac{1}{C_{fw_j}}(\tilde{i}_{w_j q} + \frac{\tilde{v}_{sw_j q}}{R_{fw_j}}) \\
\dot{\tilde{z}} &= A_p\tilde{z} + \tilde{\vartheta}'_p
\end{aligned} \tag{4.101}$$

where $\tilde{\vartheta}'_p$ is expressed as

$$\begin{cases} \tilde{\vartheta}_p(i) = \dfrac{3}{4C_{g_i}}(\bar{m}_{g_id}\tilde{i}_{g_id} + \bar{m}_{g_iq}\tilde{i}_{g_iq}), & i \in \mathcal{N} \\ \tilde{\vartheta}_p(N+j) = \dfrac{3}{4C_{w_j}}(\bar{m}_{w_jd}\tilde{i}_{w_jd} + \bar{m}_{w_jq}\tilde{i}_{w_jq}), & j \in \mathcal{M} \\ \tilde{\vartheta}_p(N+M+h) = \tilde{\vartheta}_p(N+M+P+k) = 0. & h \in \mathcal{P},\ k \in \mathcal{L} \end{cases}$$

Take

$$\begin{aligned} V = & \frac{1}{2}\textstyle\sum_{i=1}^{N} L_{g_i}[(\tilde{i}_{g_id})^2 + (\tilde{i}_{g_iq})^2] + \frac{1}{2}\sum_{j=1}^{M} L_{w_j}[(\tilde{i}_{w_jd})^2 + (\tilde{i}_{w_jq})^2] \\ & + \frac{1}{2}\textstyle\sum_{j=1}^{M} C_{fw_j}[(\tilde{v}_{sw_jd})^2 + (\tilde{v}_{sw_jq})^2] + \frac{1}{2}\cdot\frac{2}{3}\tilde{z}^T\Lambda\tilde{z} \end{aligned} \tag{4.102}$$

as a storage function candidate with

$$\Lambda = \begin{bmatrix} C & 0_{(N+M+P)\times L} \\ 0_{L\times(N+M+P)} & L \end{bmatrix}$$

The function V is positive definite and its derivative along the trajectories of (4.100) satisfies

$$\begin{aligned} \dot{V} = & -\textstyle\sum_{i=1}^{N} R_{g_i}[(\tilde{i}_{g_id})^2 + (\tilde{i}_{g_iq})^2] - \sum_{j=1}^{M} R_{w_j}[(\tilde{i}_{w_jd})^2 + (\tilde{i}_{w_jq})^2] \\ & - \frac{2}{3}\textstyle\sum_{i=1}^{N} \dfrac{(\tilde{u}_{cg_i})^2}{R_{\text{equi},g_i}} - \frac{2}{3}\sum_{j=1}^{M} \dfrac{(\tilde{u}_{cw_j})^2}{R_{\text{equi},w_j}} \\ & - \textstyle\sum_{j=1}^{M}[\dfrac{(\tilde{v}_{sw_jd})^2 + (\tilde{v}_{sw_jq})^2}{R_{fw_j}}] - \frac{2}{3}\sum_{k=1}^{L} R_{c_k}(\tilde{i}_{c_k})^2 \\ & + \frac{1}{2}\textstyle\sum_{i=1}^{N}[\tilde{m}_{g_id}(\tilde{u}_{cg_i}i_{g_id} - u_{cg_i}\tilde{i}_{g_id}) + \tilde{m}_{g_iq}(\tilde{u}_{cg_i}i_{g_iq} - u_{cg_i}\tilde{i}_{g_iq})] \\ & + \frac{1}{2}\textstyle\sum_{j=1}^{M}[\tilde{m}_{w_jd}(\tilde{u}_{cw_j}i_{w_jd} - u_{cw_j}\tilde{i}_{w_jd}) + \tilde{m}_{w_jq}(\tilde{u}_{cw_j}i_{w_jq} - u_{cw_j}\tilde{i}_{w_jq})] \end{aligned} \tag{4.103}$$

Taking the output vector y_p as

$$\begin{aligned} y_p &= [y_{pg}\ y_{pw}]^T \in \mathbb{R}^{2N+2M} \\ y_{pg} &= [y_{pg_1d}\ y_{pg_1q}\ \cdots\ y_{pg_id}\ y_{pg_iq}\ \cdots\ y_{pg_Nd}\ y_{pg_Nq}]^T \in \mathbb{R}^{2N} \\ y_{pw} &= [y_{pw_1d}\ y_{pw_1q}\ \cdots\ y_{pw_jd}\ y_{pw_jq}\ \cdots\ y_{pw_Md}\ y_{pw_Mq}]^T \in \mathbb{R}^{2M} \\ y_{pg_id} &= \frac{1}{2}(\tilde{u}_{cg_i}i_{g_id} - u_{cg_i}\tilde{i}_{g_id});\ y_{pg_iq} = \frac{1}{2}(\tilde{u}_{cg_i}i_{g_iq} - u_{cg_i}\tilde{i}_{g_iq}) \\ y_{pw_jd} &= \frac{1}{2}(\tilde{u}_{cw_j}i_{w_jd} - u_{cw_j}\tilde{i}_{w_jd});\ y_{pw_jq} = \frac{1}{2}(\tilde{u}_{cw_j}i_{w_jq} - u_{cw_j}\tilde{i}_{w_jq}) \end{aligned} \tag{4.104}$$

$\dot{V}$ then satisfies

$$\dot{V} = L_fV + L_gVu \le y_p^Tu \tag{4.105}$$

with

$$\begin{aligned}
L_gV=&\ y_p^T\\
L_fV=&\ -\textstyle\sum_{i=1}^{N} R_{g_i}[(\tilde{i}_{g_id})^2+(\tilde{i}_{g_iq})^2]-\sum_{j=1}^{M} R_{w_j}[(\tilde{i}_{w_jd})^2+(\tilde{i}_{w_jq})^2]\\
&-\frac{2}{3}\textstyle\sum_{i=1}^{N}\frac{(\tilde{u}_{cg_i})^2}{R_{\text{equi},g_i}}-\frac{2}{3}\sum_{j=1}^{M}\frac{(\tilde{u}_{cw_j})^2}{R_{\text{equi},w_j}}\\
&-\textstyle\sum_{j=1}^{M}[\frac{(\tilde{v}_{sw_jd})^2+(\tilde{v}_{sw_jq})^2}{R_{fw_j}}]-\frac{2}{3}\sum_{k=1}^{L}R_{c_k}(\tilde{i}_{c_k})^2\\
u=&\ [u_g\ u_w]^T\in\mathbb{R}^{2N+2M}\\
u_g=&\ [m_{g_1d}\ m_{g_1q}\ \cdots\ m_{g_Nd}\ m_{g_Nq}]^T\in\mathbb{R}^{2N}\\
u_w=&\ [m_{w_1d}\ m_{w_1q}\ \cdots\ m_{w_Md}\ m_{w_Mq}]^T\in\mathbb{R}^{2M}
\end{aligned}\tag{4.106}$$

It can be seen that the MTDC system has the Kalman-Yacubovitch-Popov (KYP) property and it is passive with the passive output vector y_p.

4.3.3 Control design

Since the steady-state values of all DC voltages are positive, $\bar{u}_{c(.)}>0$, here we change the output vector to

$$\begin{aligned}
y=&\ [y_g\ y_w]^T\in\mathbb{R}^{2N+2M}\\
y_g=&\ [y_{g_1d}\ y_{g_1q}\ \cdots\ y_{g_id}\ y_{g_iq}\ \cdots\ y_{g_Nd}\ y_{g_Nq}]^T\in\mathbb{R}^{2N}\\
y_w=&\ [y_{w_1d}\ y_{w_1q}\ \cdots\ y_{w_jd}\ y_{w_jq}\ \cdots\ y_{w_Md}\ y_{w_Mq}]^T\in\mathbb{R}^{2M}\\
y_{g_id}=&\ \alpha_{g_id}u_{cg_i}-i_{g_id};\ y_{g_iq}=\alpha_{g_iq}u_{cg_i}-i_{g_iq}\\
y_{w_jd}=&\ \alpha_{w_jd}u_{cw_j}-i_{w_jd};\ y_{w_jq}=\alpha_{w_jq}u_{cw_j}-i_{w_jq}\\
\alpha_{g_i,dq}=&\ \frac{\bar{i}_{g_i,dq}}{\bar{u}_{cg_i}};\ \alpha_{w_j,dq}=\frac{\bar{i}_{w_j,dq}}{\bar{u}_{cw_j}}
\end{aligned}\tag{4.107}$$

Comparing y_p in (4.104) and y in (4.107), it is easy to find that

$$y_{g_i,dq}=\frac{2}{\bar{u}_{cg_i}}y_{pg_i,dq};\ y_{w_j,dq}=\frac{2}{\bar{u}_{cw_j}}y_{pw_j,dq}\tag{4.108}$$

Accordingly, the reference of y is $y^o=0_{(2N+2M)\times 1}$. Let us restrict $y\equiv y^o$ and then, by performing the change of variables

$$i_{g_i,dq}=\alpha_{g_i,dq}u_{cg_i}-y_{g_i,dq};\ i_{w_j,dq}=\alpha_{w_j,dq}u_{cw_j}-y_{w_j,dq}\tag{4.109}$$

we obtain the following equations

$$\begin{aligned}
0=\dot{y}_{g_id}=&\ a_{1g_i}m_{g_id}+a_{2g_i}m_{g_iq}+f_{g_id}\\
0=\dot{y}_{g_iq}=&\ a_{3g_i}m_{g_id}+a_{4g_i}m_{g_iq}+f_{g_iq}\\
0=\dot{y}_{w_jd}=&\ a_{1w_j}m_{w_jd}+a_{2w_j}m_{w_jq}+f_{w_jd}\\
0=\dot{y}_{w_jq}=&\ a_{3w_j}m_{w_jd}+a_{4w_j}m_{w_jq}+f_{w_jq}
\end{aligned}\tag{4.110}$$

where

$$
\begin{aligned}
a_{1g_i} &= \frac{3}{4}\frac{\alpha_{g_id}}{C_{g_i}}(\alpha_{g_id}u_{cg_i} - y_{g_id}) + \frac{u_{cg_i}}{2L_{g_i}} \\
a_{2g_i} &= \frac{3}{4}\frac{\alpha_{g_id}}{C_{g_i}}(\alpha_{g_iq}u_{cg_i} - y_{g_iq}) \\
a_{3g_i} &= \frac{3}{4}\frac{\alpha_{g_iq}}{C_{g_i}}(\alpha_{g_id}u_{cg_i} - y_{g_id}) \\
a_{4g_i} &= \frac{3}{4}\frac{\alpha_{g_iq}}{C_{g_i}}(\alpha_{g_iq}u_{cg_i} - y_{g_iq}) + \frac{u_{cg_i}}{2L_{g_i}} \\
a_{1w_j} &= \frac{3}{4}\frac{\alpha_{w_jd}}{C_{w_j}}(\alpha_{w_jd}u_{cw_j} - y_{w_jd}) + \frac{u_{cw_j}}{2L_{w_j}} \\
a_{2w_j} &= \frac{3}{4}\frac{\alpha_{w_jd}}{C_{w_j}}(\alpha_{w_jq}u_{cw_j} - y_{w_jq}) \\
a_{3w_j} &= \frac{3}{4}\frac{\alpha_{w_jq}}{C_{w_j}}(\alpha_{w_jd}u_{cw_j} - y_{w_jd}) \\
a_{4w_j} &= \frac{3}{4}\frac{\alpha_{w_jq}}{C_{w_j}}(\alpha_{w_jq}u_{cw_j} - y_{w_jq}) + \frac{u_{cw_j}}{2L_{w_j}} \\
f_{g_id} &= \frac{\alpha_{g_id}}{C_{g_i}}[-\frac{u_{cg_i}}{R_{\text{equi},g_i}} + H(i,:)i_c] + \frac{R_{g_i}}{L_{g_i}}(\alpha_{g_id}u_{cg_i} - y_{g_id}) \\
&\quad -\omega_{g_i}(\alpha_{g_iq}u_{cg_i} - y_{g_iq}) - \frac{v_{sg_id}}{L_{g_i}} \\
f_{g_iq} &= \frac{\alpha_{g_iq}}{C_{g_i}}[-\frac{u_{cg_i}}{R_{\text{equi},g_i}} + H(i,:)i_c] + \frac{R_{g_i}}{L_{g_i}}(\alpha_{g_iq}u_{cg_i} - y_{g_iq}) \\
&\quad +\omega_{g_i}(\alpha_{g_id}u_{cg_i} - y_{g_id}) - \frac{v_{sg_iq}}{L_{g_i}} \\
f_{w_jd} &= \frac{\alpha_{w_jd}}{C_{w_j}}[-\frac{u_{cw_j}}{R_{\text{equi},w_j}} + H(N+j,:)i_c] + \frac{R_{w_j}}{L_{w_j}}(\alpha_{w_jd}u_{cw_j} - y_{w_jd}) \\
&\quad -\omega_{w_j}(\alpha_{w_jq}u_{cw_j} - y_{w_jq}) - \frac{v_{sw_jd}}{L_{w_j}} \\
f_{w_jq} &= \frac{\alpha_{w_jq}}{C_{w_j}}[-\frac{u_{cw_j}}{R_{\text{equi},w_j}} + H(N+j,:)i_c] + \frac{R_{w_j}}{L_{w_j}}(\alpha_{w_jq}u_{cw_j} - y_{w_jq}) \\
&\quad +\omega_{w_j}(\alpha_{w_jd}u_{cw_j} - y_{w_jd}) - \frac{v_{sw_jq}}{L_{w_j}}
\end{aligned}
\tag{4.111}
$$

Let us denote

$$
E_{g_i} = \begin{bmatrix} a_{1g_i} & a_{2g_i} \\ a_{3g_i} & a_{4g_i} \end{bmatrix};\ E_{w_j} = \begin{bmatrix} a_{1w_j} & a_{2w_j} \\ a_{3w_j} & a_{4w_j} \end{bmatrix};
\tag{4.112}
$$

Lemma 4.3.3. *The decoupling matrices E_{g_i} and E_{w_j} are nonsingular at $y_{g_id} = y_{g_iq} = 0$ and $y_{w_jd} = y_{w_jq} = 0$.*

Proof. The determinants of E_{g_i} and E_{w_j} are equal to

$$
\begin{aligned}
\Delta_{g_i} &= \det(E_{g_i}) = \frac{u_{cg_i}}{2L_{g_i}}[\frac{u_{cg_i}}{2L_{g_i}} + \frac{3}{4}\frac{\alpha_{g_id}}{C_{g_i}}(\alpha_{g_id}u_{cg_i} - y_{g_id}) + \frac{3}{4}\frac{\alpha_{g_iq}}{C_{g_i}}(\alpha_{g_iq}u_{cg_i} - y_{g_iq})] \\
\Delta_{w_j} &= \det(E_{w_j}) = \frac{u_{cw_j}}{2L_{w_j}}[\frac{u_{cw_j}}{2L_{w_j}} + \frac{3}{4}\frac{\alpha_{w_jd}}{C_{w_j}}(\alpha_{w_jd}u_{cw_j} - y_{w_jd}) \\
&\quad + \frac{3}{4}\frac{\alpha_{w_jq}}{C_{w_j}}(\alpha_{w_jq}u_{cw_j} - y_{w_jq})]
\end{aligned}
$$

Setting $y_{g_id} = y_{g_iq} = 0$ and $y_{w_jd} = y_{w_jq} = 0$ yields

$$\begin{aligned}
\Delta_{g_i0} &= \Delta_{g_i}|_{y_{g_id}=y_{g_iq}=0} \\
&= \frac{u_{cg_i}}{2L_{g_i}}[\frac{u_{cg_i}}{2L_{g_i}} + \frac{3}{4}\frac{(\alpha_{g_id})^2}{C_{g_i}}u_{cg_i} + \frac{3}{4}\frac{(\alpha_{g_iq})^2}{C_{g_i}}u_{cg_i}] \\
\Delta_{w_j0} &= \Delta_{w_j}|_{y_{w_jd}=y_{w_jq}=0}] \\
&= \frac{u_{cw_j}}{2L_{w_j}}[\frac{u_{cw_j}}{2L_{w_j}} + \frac{3}{4}\frac{(\alpha_{w_jd})^2}{C_{w_j}}u_{cw_j} + \frac{3}{4}\frac{(\alpha_{w_jq})^2}{C_{w_j}}u_{cw_j}]
\end{aligned} \tag{4.113}$$

Because u_{cg_i} and u_{cw_j} are positive, $\Delta_{g_i0} \neq 0$ and $\Delta_{w_j0} \neq 0$ are always positive. □

Since Δ_{g_i} (Δ_{w_j}) are continuously differentiable for $(\alpha_{g_id},\ \alpha_{g_iq},\ y_{g_id},\ y_{g_iq}) \in \mathbb{B}_{\alpha_{g_id}} \times \mathbb{B}_{\alpha_{g_iq}} \times \mathbb{B}_{y_{g_id}} \times \mathbb{B}_{y_{g_iq}}$ ($(\alpha_{w_jd},\ \alpha_{w_jq},\ y_{w_jd},\ y_{w_jq}) \in \mathbb{B}_{\alpha_{w_jd}} \times \mathbb{B}_{\alpha_{w_jq}} \times \mathbb{B}_{y_{w_jd}} \times \mathbb{B}_{y_{w_jq}}$) where these $\mathbb{B}_{(.)} \subset \mathbb{R}$ are open connected sets, based on Lemma 4.3.3, we have the following lemma.

Lemma 4.3.4. *There exist a series of connected sets $\mathbb{S}_{(.)} \subset \mathbb{B}_{(.)}$ such that the decoupling matrices E_{g_i} and E_{w_j} are nonsigular for $(\alpha_{g_id},\ \alpha_{g_iq},\ y_{g_id},\ y_{g_iq}) \in \mathbb{S}_{\alpha_{g_id}} \times \mathbb{S}_{\alpha_{g_iq}} \times \mathbb{S}_{y_{g_id}} \times \mathbb{S}_{y_{g_iq}}$ and $(\alpha_{w_jd},\ \alpha_{w_jq},\ y_{w_jd},\ y_{w_jq}) \in \mathbb{S}_{\alpha_{w_jd}} \times \mathbb{S}_{\alpha_{w_jq}} \times \mathbb{S}_{y_{w_jd}} \times \mathbb{S}_{y_{w_jq}}$. In addition, $\mathbb{S}_{y_{g_i,dq}}$ and $\mathbb{S}_{y_{w_j,dq}}$ contain the origin. $\mathbb{S}_{\alpha_{g_id}}$, $\mathbb{S}_{\alpha_{g_iq}}$, $\mathbb{S}_{\alpha_{w_jd}}$ and $\mathbb{S}_{\alpha_{w_jq}}$ contain $\frac{\bar{i}_{g_id}}{\bar{u}_{cg_i}}$, $\frac{\bar{i}_{g_iq}}{\bar{u}_{cg_i}}$, $\frac{\bar{i}_{w_jd}}{\bar{u}_{cw_j}}$ and $\frac{\bar{i}_{w_jq}}{\bar{u}_{cw_j}}$, respectively.*

Since the solution of the state variables is restricted to (4.110) when the output vector y is identically equal to y^o, the control modulation indices must satisfy

$$\begin{aligned}
m_{g_id} &= \frac{1}{\Delta_{g_i}}(a_{4g_i}f_{g_id} - a_{2g_i}f_{g_iq})|_{y_{g_id}=y_{g_iq}=0} \\
m_{g_iq} &= \frac{1}{\Delta_{g_i}}(a_{4g_i}f_{g_id} - a_{2g_i}f_{g_iq})|_{y_{g_id}=y_{g_iq}=0} \\
m_{w_jd} &= \frac{1}{\Delta_{w_j}}(a_{4w_j}f_{w_jd} - a_{2w_j}f_{w_jq})|_{y_{w_jd}=y_{w_jq}=0} \\
m_{w_jq} &= \frac{1}{\Delta_{w_j}}(a_{4w_j}f_{w_jd} - a_{2w_j}f_{w_jq})|_{y_{w_jd}=y_{w_jq}=0}
\end{aligned} \tag{4.114}$$

Substituting (4.114) into the MTDC system, the zero dynamics are characterized

by

$$\begin{aligned}
\frac{dv_{sw_jd}}{dt} &= \omega_{w_j} v_{sw_jq} + \frac{1}{C_{fw_j}}(I_{w_jd} - \alpha_{w_jd} u_{cw_j} - \frac{v_{sw_jd}}{R_{fw_j}}) \\
\frac{dv_{sw_jq}}{dt} &= -\omega_{w_j} v_{sw_jd} + \frac{1}{C_{fw_j}}(I_{w_jq} - \alpha_{w_jq} u_{cw_j} - \frac{v_{sw_jq}}{R_{fw_j}}) \\
C_{g_i}\frac{du_{cg_i}}{dt} &= \frac{1}{\Delta_{g_i0}}\frac{1}{2L_{g_I}}[-\frac{u_{cg_i}}{R_{\text{equi},g_i}} + H(i,:)i_c] \\
&\quad -\frac{1}{\Delta_{g_i0}}\frac{3}{4}[\frac{R_{g_i}}{L_{g_i}} u_{cg_i}(\alpha_{g_id}^2 + \alpha_{g_iq}^2) - \frac{1}{L_{g_i}}(v_{sg_id}\alpha_{g_id} + v_{sg_iq}\alpha_{g_iq})] \\
C_{w_j}\frac{du_{cw_j}}{dt} &= \frac{1}{\Delta_{w_j0}}\frac{1}{2L_{w_j}}[-\frac{u_{cw_j}}{R_{\text{equi},w_j}} + H(N+j,:)i_c] \\
&\quad -\frac{1}{\Delta_{w_j0}}\frac{3}{4}[\frac{R_{w_j}}{L_{w_j}} u_{cw_j}(\alpha_{w_jd}^2 + \alpha_{w_jq}^2) - \frac{1}{L_{w_j}}(v_{sw_jd}\alpha_{w_jd} + v_{sw_jq}\alpha_{w_jq})] \\
C_{t_h}\frac{du_{ct_h}}{dt} &= H(N+M+h,:)i_c \\
L_{c_k}\frac{di_{ck}}{dt} &= -R_{c_k} i_{c_K} - H(:,k)^T u_c
\end{aligned} \tag{4.115}$$

With

$$\begin{aligned}
W = &\frac{1}{2}\textstyle\sum_{j=1}^{M} C_{fw_j}[(\tilde{v}_{sw_jd})^2 + (\tilde{v}_{sw_jq})^2] + \frac{1}{2}\sum_{j=1}^{M} C_{w_j} k_{w_j}(\tilde{u}_{cw_j})^2 \\
&+\frac{1}{2}\textstyle\sum_{h=1}^{P} C_{t_h}\frac{2}{3}(\tilde{u}_{ct_h})^2 + \frac{1}{2}\sum_{k=1}^{L}\frac{2}{3}L_{c_k}(\tilde{i}_{c_k})^2 + \frac{1}{2}\sum_{i=1}^{N} C_{g_i} k_{g_i}(\tilde{u}_{cg_i})^2
\end{aligned} \tag{4.116}$$

as a Lyapunov function candidate for the zero dynamics (4.115) where

$$\begin{aligned}
k_{w_j} &= \{\frac{1}{2L_{w_j}} + \frac{3}{4}[(\alpha_{w_jd})^2 + (\alpha_{w_jq})^2]\}\frac{4}{3}L_{w_j} \\
k_{g_i} &= \{\frac{1}{2L_{g_i}} + \frac{3}{4}[(\alpha_{g_id})^2 + (\alpha_{g_iq})^2]\}\frac{4}{3}L_{g_i}
\end{aligned} \tag{4.117}$$

The derivative of W along the trajectories of (4.115) is given by

$$\begin{aligned}
\dot{W} = &-\textstyle\sum_{j=1}^{M}[\frac{2}{3R_{\text{equi},w_j}} + R_{w_j}(\alpha_{w_jd}^2 + \alpha_{w_jq}^2)](\tilde{u}_{w_j})^2 \\
&-\textstyle\sum_{i=1}^{N}[\frac{2}{3R_{\text{equi},g_i}} + R_{g_i}(\alpha_{g_id}^2 + \alpha_{g_iq}^2)](\tilde{u}_{g_i})^2 - \frac{2}{3}R_{c_k}(\tilde{i}_{c_k})^2 \\
&-\textstyle\sum_{j=1}^{M}[\frac{(\tilde{v}_{sw_jd})^2 + (\tilde{v}_{sw_jq})^2}{R_{fw_j}}] \le 0
\end{aligned} \tag{4.118}$$

which shows that the MTDC system with the output vector y in (4.107) is weakly minimum phase. Furthermore, we have the following result.

Lemma 4.3.5. *The equilibrium point of the zero dynamics* (4.115) *is asymptotically stable.*

Proof. This lemma can be proved using Barbalat's lemma. Since $\dot{W}$ is non-positive, we then have $W(t) \le W(t=0)$, which means that all variables $\tilde{(\cdot)}$ in W are bounded.

Based on (4.118), $\ddot{W}$ can be computed, which is composed only of bounded terms. Hence, $\ddot{W}$ is also bounded. As a consequence, $\dot{W}$ is uniformly continuous in time. Applying Barbalat's lemma, we have $\dot{W} \to 0$ in (4.118) as $t \to \infty$, which implies that

$$\tilde{u}_{cw_j} \to 0;\ \tilde{u}_{cg_i} \to 0;\ \tilde{i}_{c_k} \to 0;\ \tilde{v}_{sw_jd} \to 0;\ \tilde{v}_{sw_jq} \to 0 \tag{4.119}$$

and

$$\dot{\tilde{u}}_{cw_j} \to 0;\ \dot{\tilde{u}}_{cg_i} \to 0;\ \dot{\tilde{i}}_{c_k} \to 0;\ \dot{\tilde{v}}_{sw_jd} \to 0;\ \dot{\tilde{v}}_{sw_jq} \to 0 \tag{4.120}$$

Combining (4.115), (4.119) and (4.120), we can obtain

$$H^T \tilde{u}_c \to 0 \tag{4.121}$$

with unknown $\tilde{u}_{ct_h}$. Since Lemma 3.4.1 states that $\text{rank}(H) = N + M + P - 1 \geq P$, $\tilde{u}_{ct_h} \to 0$ is the only solution of (4.121). As a result, only the trivial solution exists for $\dot{W} = 0$ and then the lemma is proved. □

Based on Lemma 4.3.5, we can also get that only the trivial solution of the unforced system (4.101) can stay in the set $\{y = y^o = 0_{(2N+2M)\times 1}\}$ where y is defined as (4.107). Finally, we can conclude that the error system (4.100) is zero-state observable.

According to Theorem 3.2 in [Byrnes 1991], the control variables $\tilde{m}_{(\cdot)}$ can be developed as

$$\begin{bmatrix}\tilde{m}_{g_id}\\ \tilde{m}_{g_iq}\end{bmatrix} = -\begin{bmatrix}\phi_{g_id}(y_{g_id})\\ \phi_{g_iq}(y_{g_iq})\end{bmatrix};\ \begin{bmatrix}\tilde{m}_{w_jd}\\ \tilde{m}_{w_jq}\end{bmatrix} = -\begin{bmatrix}\phi_{w_jd}(y_{w_jd})\\ \phi_{w_jd}(y_{w_jq})\end{bmatrix} \tag{4.122}$$

where $\phi_{(\cdot)}$ are any smooth functions such that $\phi_{(\cdot)}(0) = 0$ and

$$\begin{gathered} y_{g_id}\phi_{g_id}(y_{g_id}) > 0;\ y_{g_iq}\phi_{g_iq}(y_{g_iq}) > 0 \\ y_{w_jd}\phi_{w_jd}(y_{w_jd}) > 0;\ y_{w_jq}\phi_{w_jq}(y_{w_jq}) > 0 \end{gathered}$$

for each nonzero $y_{(\cdot)}$. Then, $m_{(\cdot)}$ can be deduced as

$$\begin{bmatrix}m_{g_id}\\ m_{g_iq}\end{bmatrix} = \begin{bmatrix}\bar{m}_{g_id}\\ \bar{m}_{g_iq}\end{bmatrix} - \begin{bmatrix}\phi_{g_id}(y_{g_id})\\ \phi_{g_iq}(y_{g_iq})\end{bmatrix};\ \begin{bmatrix}m_{w_jd}\\ m_{w_jq}\end{bmatrix} = \begin{bmatrix}\bar{m}_{w_jd}\\ \bar{m}_{w_jq}\end{bmatrix} - \begin{bmatrix}\phi_{w_jd}(y_{w_jd})\\ \phi_{w_jd}(y_{w_jq})\end{bmatrix} \tag{4.123}$$

In fact, the choice of $\phi_{(\cdot)}$ is free. In this thesis, we choose the easiest way to design the control variable as

$$\begin{aligned} m_{g_id} &= -c_{g_id,0} \cdot y_{g_id} - k_{Ig_id} \cdot e_{Iy_{g_id}} \\ m_{g_iq} &= -c_{g_iq,0} \cdot y_{g_iq} - k_{Ig_iq} \cdot e_{Iy_{g_iq}} \\ m_{w_jd} &= -c_{w_jd,0} \cdot y_{w_jd} - k_{Iw_jd} \cdot e_{Iy_{w_jd}} \\ m_{w_jq} &= -c_{w_jq,0} \cdot y_{w_jq} - k_{Iw_jq} \cdot e_{Iy_{w_jq}} \end{aligned} \tag{4.124}$$

with positive control gains $c_{(\cdot)}$ and $k_{I(\cdot)}$ and the integrated tracking errors

$$\begin{aligned} \dot{e}_{Iy_{g_id}} &= y_{g_id};\ \dot{e}_{Iy_{g_iq}} = y_{g_iq} \\ \dot{e}_{Iy_{w_jd}} &= y_{w_jd};\ \dot{e}_{Iy_{w_jq}} = y_{w_jq} \end{aligned}$$

4.3.4 Control of zero dynamics

Substituting (4.109) and the control algorithm (4.124) into (4.92) and (4.94), the dynamics of the DC grid and the AC voltages $v_{sw_j,dq}$ will be governed by the zero dynamics (4.115) if $y_{g_i,dq}$ and $y_{w_i,dq}$ exactly converge to zero (or if $\frac{i_{g_i,dq}}{u_{cg_i}}$ and $\frac{i_{w_j,dq}}{u_{cw_j}}$ perfectly follow $\alpha_{g_i,dq}$ and $\alpha_{w_j,dq}$, respectively). Therefore, by controlling the output variable at zero, we can indirectly drive u_{cg_1}, $i_{g_\rho d}$, $i_{g_i q}$ and the AC voltage $v_{sw_j,dq}$ to the prescribed references $(\cdot)^o$ given by (4.57). From Assumption 4.3.1, we get $\bar{i}_{g_i q} = 0$ and hence $\alpha_{g_i q} = \frac{\bar{i}_{g_i q}}{\bar{u}_{cg_i}} = 0$ can be directly obtained. However, there is still a need to deduce $\alpha_{g_i d}$ and $\alpha_{w_j,dq}$ by solving (4.96). Due to the uncertainties on the system parameters or unmodeled elements in the power system, it is usually difficult to get the accurate values of $\alpha_{g_i d}$ and $\alpha_{w_j,dq}$ and then steady-state errors may exist. Furthermore, the convergence rate of the uncontrolled zero dynamics totally depends on the system inherent characteristics, which would be very slow. Therefore, we expect to regulate the behaviors of the states of the zero dynamics and to achieve good tracking performance, i.e. to make u_{cg_1}, $i_{g_\rho d}$, $i_{g_i q}$ and the AC voltage $v_{sw_j,dq}$ follow their respective prescribed values $(\cdot)^o$ by designing $\alpha_{g_i d}$ and $\alpha_{w_j,dq}$. In the following part, we consider the case that $\bar{i}_{g_\rho d} \neq 0$. If $P^o_{g_\rho d}$ are set to zero for some SAC terminals, then the corresponding $\alpha_{g_\rho d} = \frac{\bar{i}_{g_i d}}{\bar{u}_{cg_i}} = \frac{2P^o_{g_\rho}}{3\bar{u}_{cg_\rho} v_{sg_\rho d}} = 0$ can be directly deduced without further design.

As mentioned in the previous section, the control goal is to make u_{cg_1}, $i_{g_\rho d}$, $i_{g_i q}$ and $v_{sw_j,dq}$ track their respective references. Thus, we substitute $\alpha_{g_i q} = 0$, the change of the variables $i_{g_\rho d} = \alpha_{g_\rho d} u_{cg_\rho}$ and $\frac{di_{g_\rho d}}{dt} = \alpha_{g_\rho d} \frac{du_{cg_\rho}}{dt}$ into the zero

dynamics (4.115) and then obtain the following transformed zero dynamics

$$
\begin{aligned}
\frac{dv_{sw_jd}}{dt} &= \omega_{w_j} v_{sw_jq} + \frac{1}{C_{fw_j}}(I_{w_jd} - \alpha^*_{w_jd} u_{cw_j} - \frac{v_{sw_jd}}{R_{fw_j}}) \\
\frac{dv_{sw_jq}}{dt} &= -\omega_{w_j} v_{sw_jd} + \frac{1}{C_{fw_j}}(I_{w_jq} - \alpha^*_{w_jq} u_{cw_j} - \frac{v_{sw_jq}}{R_{fw_j}}) \\
C_{g_1}\frac{du_{cg_1}}{dt} &= \frac{\frac{1}{2L_{g_1}}}{\frac{1}{2L_{g_1}} + \frac{3}{4}(\alpha^*_{g_1d})^2}\{[-\frac{u_{cg_1}}{R_{\text{equi},g_1}} + H(1,:)i_c] \\
&\quad -\frac{3}{2}[R_{g_1} u_{cg_1}(\alpha^*_{g_1d})^2 - v_{sg_1d}\alpha^*_{g_1d}]\} \\
C_{g_\rho}\frac{di_{g_\rho d}}{dt} &= \frac{\frac{1}{2L_{g_\rho}}}{\frac{1}{2L_{g_\rho}} + \frac{3}{4}(\alpha^*_{g_\rho d})^2}\{[-\frac{i_{g_\rho d}}{R_{\text{equi},g_\rho}} + \alpha^*_{g_\rho d} H(i,:)i_c] \\
&\quad -\frac{3}{2}[R_{g_\rho} i_{g_\rho d}(\alpha^*_{g_\rho d})^2 - \alpha^*_{g_\rho d}(v_{sg_\rho d}\alpha^*_{g_\rho d})]\} \\
C_{w_j}\frac{du_{cw_j}}{dt} &= \frac{\frac{1}{2L_{w_j}}}{\frac{1}{2L_{w_j}} + \frac{3}{4}[(\alpha^*_{w_jd})^2 + (\alpha^*_{w_jq})^2]}\{[-\frac{u_{cw_j}}{R_{\text{equi},w_j}} + H(N+j,:)i_c] \\
&\quad -\frac{3}{2}[R_{w_j} u_{cw_j}((\alpha^*_{w_jd})^2 + (\alpha^*_{w_jq})^2) - (v_{sw_jd}\alpha^*_{w_jd} + v_{sw_jq}\alpha^*_{w_jq})]\} \\
C_{t_h}\frac{du_{ct_h}}{dt} &= H(N+M+h,:)i_c \\
L_{c_k}\frac{di_{ck}}{dt} &= -R_{c_k} i_{c_K} - H(:,k)^T u_c
\end{aligned}
\tag{4.125}
$$

Now, the transformed zero dynamics (4.125) is considered as a new system where α_{g_id} and $\alpha_{w_j,dq}$ are replaced by $\alpha^*_{g_id}$ and $\alpha^*_{w_j,dq}$ to emphasize that they are considered as control inputs. It can be seen that the number of control variables ($\alpha^*_{g_id}$ and $\alpha^*_{w_j,dq}$) equals the number of controlled variables (u_{cg_1}, $i_{g_\rho d}$ and $v_{sw_j,dq}$) and moreover, $\alpha^*_{w_j,dq}$ are directly collocated with $v_{sw_j,dq}$. We can use two steps to design the control variables.

4.3.4.1 Step 1: design of $\alpha^*_{w_j,dq}$

We first design $\alpha^*_{w_j,dq}$ to regulate $v_{sw_j,dq}$ while $\alpha^*_{g_id}$ are considered equal to the steady-state values $\bar{\alpha}_{g_id} = \dfrac{\bar{i}_{g_id}}{\bar{u}_{cg_i}}$.

Feedback linearization control

Here, the input-output feedback linearzation method is applied to design $\alpha^*_{w_j,dq}$. It is natural to choose the output

$$
\begin{aligned}
y_w &= [y_{w_1} \ \cdots \ y_{w_M}]^T \\
y_{w_j} &= [v_{sw_jd} \ v_{sw_jq}]^T
\end{aligned}
\tag{4.126}
$$

Then, following the input-output feedback linearization procedure, the control law for $\alpha^*_{w_j,dq}$ is deduced as

$$\begin{aligned}\alpha^*_{w_jd}&= \frac{1}{u_{cw_j}}[I_{w_jd} - \frac{v_{sw_jd}}{R_{fw_j}} + C_{fw_j}\omega_{w_j}v_{sw_jq} - C_{fw_j}v_{\alpha_{w_jd}}]\\ \alpha^*_{w_jq}&= \frac{1}{u_{cw_j}}[I_{w_jq} - \frac{v_{sw_jq}}{R_{fw_j}} - C_{fw_j}\omega_{w_j}v_{sw_jd} - C_{fw_j}v_{\alpha_{w_jq}}]\end{aligned} \tag{4.127}$$

where

$$\begin{aligned}\dot{e}_{I\alpha_{w_jd}}&= e_{v_{sw_jd}} \triangleq v_{sw_jd} - v^o_{sw_jd}\\ v_{\alpha_{w_jd}}&= -c_{\alpha_{w_jd}} \cdot e_{v_{sw_jd}} - k_{I\alpha_{w_jd}} \cdot e_{I\alpha_{w_jd}}\\ \dot{e}_{I\alpha_{w_jq}}&= e_{v_{sw_jq}} \triangleq v_{sw_jq} - v^o_{sw_jq}\\ v_{\alpha_{w_jq}}&= -c_{\alpha_{w_jq}} \cdot e_{v_{sw_jq}} - k_{I\alpha_{w_jq}} \cdot e_{I\alpha_{w_jq}}\end{aligned}$$

with positive control gains $c_{\alpha_{w_j,dq}}$ and $k_{I\alpha_{w_j,dq}}$.

If the tracking errors $e_{\alpha_{w_j,dq}}$ approach zero, we then take $\alpha^*_{w_j,dq} = \bar{\alpha}^*_{w_j,dq}$ where

$$\begin{aligned}\bar{\alpha}^*_{w_jd}&= \frac{1}{u_{cw_j}}[I_{w_jd} - \frac{v^o_{sw_jd}}{R_{fw_j}} + C_{fw_j}\omega_{w_j}v^o_{sw_jq} + k_{I\alpha_{w_jd}}\bar{e}_{I\alpha_{w_jd}}]\\ \bar{\alpha}^*_{w_jq}&= \frac{1}{u_{cw_j}}[I_{w_jq} - \frac{v^o_{sw_jq}}{R_{fw_j}} - C_{fw_j}\omega_{w_j}v^o_{sw_jd} + k_{I\alpha_{w_jq}}\bar{e}_{I\alpha_{w_jq}}]\end{aligned} \tag{4.128}$$

which are calculated by restricting $v_{sw_j,dq} = v^o_{sw_j,dq}$ and

$$\begin{aligned}0 &= \omega_{w_j}v^o_{sw_jq} + \frac{1}{C_{fw_j}}(I_{w_jd} - \bar{\alpha}^*_{w_jd}u_{cw_j} - \frac{v^o_{sw_jd}}{R_{fw_j}})\\ 0 &= -\omega_{w_j}v^o_{sw_jd} + \frac{1}{C_{fw_j}}(I_{w_jq} - \bar{\alpha}^*_{w_jq}u_{cw_j} - \frac{v^o_{sw_jq}}{R_{fw_j}})\end{aligned}$$

Recall that the steady-state values of $\bar{\alpha}^*_{w_j,dq}$ satisfy

$$\begin{aligned}\bar{\alpha}_{w_jd} &= \frac{\bar{i}_{w_jd}}{\bar{u}_{cw_j}} = \frac{1}{\bar{u}_{cw_j}}[I_{w_jd} - \frac{\bar{v}_{sw_jd}}{R_{fw_j}} + C_{fw_j}\omega_{w_j}v^o_{sw_jq} + k_{I\alpha_{w_jd}}\bar{e}_{I\alpha_{w_jd}}]\\ \bar{\alpha}_{w_jq} &= \frac{\bar{i}_{w_jq}}{\bar{u}_{cw_j}} = \frac{1}{\bar{u}_{cw_j}}[I_{w_jq} - \frac{\bar{v}_{sw_jq}}{R_{fw_j}} - C_{fw_j}\omega_{w_j}v^o_{sw_jd} + k_{I\alpha_{w_jq}}\bar{e}_{I\alpha_{w_jq}}]\end{aligned}$$

and hence, $\bar{\alpha}^*_{w_j,dq}$ can be rewritten as

$$\begin{aligned}\bar{\alpha}^*_{w_jd}&= \frac{1}{u_{cw_j}}\bar{i}_{w_jd}\\ \bar{\alpha}^*_{w_jq}&= \frac{1}{u_{cw_j}}\bar{i}_{w_jq}\end{aligned} \tag{4.129}$$

In addition, we can also obtain

$$\begin{aligned}\frac{\partial\bar{\alpha}^*_{w_jd}}{\partial u_{cw_j}}&= -\frac{1}{(u_{cw_j})^2}\bar{i}_{w_jd}\\ \frac{\partial\bar{\alpha}^*_{w_jq}}{\partial u_{cw_j}}&= -\frac{1}{(u_{cw_j})^2}\bar{i}_{w_jq}\end{aligned} \tag{4.130}$$

Then, the zero dynamics of the system (4.125) are characterized by

$$
\begin{aligned}
C_{g_1}\frac{du_{cg_1}}{dt} &= \frac{\dfrac{1}{2L_{g_1}}}{\dfrac{1}{2L_{g_1}}+\dfrac{3}{4}(\alpha^*_{g_1d})^2}\{[-\frac{u_{cg_1}}{R_{\text{equi},g_1}}+H(1,:)i_c] \\
&\quad -\frac{3}{2}[R_{g_1}u_{cg_1}(\alpha^*_{g_1d})^2 - v_{sg_1d}\alpha^*_{g_1d}]\} \\
C_{g_\rho}\frac{di_{g_\rho d}}{dt} &= \frac{\dfrac{1}{2L_{g_\rho}}}{\dfrac{1}{2L_{g_\rho}}+\dfrac{3}{4}(\alpha^*_{g_\rho d})^2}\{[-\frac{i_{g_\rho d}}{R_{\text{equi},g_\rho}}+\alpha^*_{g_\rho d}H(\rho,:)i_c] \\
&\quad -\frac{3}{2}[R_{g_\rho}i_{g_\rho d}(\alpha^*_{g_\rho d})^2 - \alpha^*_{g_\rho d}(v_{sg_\rho d}\alpha^*_{g_\rho d})]\} \\
C_{w_j}\frac{du_{cw_j}}{dt} &= \frac{\dfrac{1}{2L_{w_j}}}{\dfrac{1}{2L_{w_j}}+\dfrac{3}{4}[(\bar{\alpha}^*_{w_jd})^2+(\bar{\alpha}^*_{w_jq})^2]}\{[-\frac{u_{cw_j}}{R_{\text{equi},w_j}}+H(N+j,:)i_c] \\
&\quad -\frac{3}{2}[R_{w_j}u_{cw_j}((\bar{\alpha}^*_{w_jd})^2+(\bar{\alpha}^*_{w_jq})^2) - (v^o_{sw_jd}\bar{\alpha}^*_{w_jd}+v^o_{sw_jq}\bar{\alpha}^*_{w_jq})]\} \\
C_{t_h}\frac{du_{ct_h}}{dt} &= H(N+M+h,:)i_c \\
L_{c_k}\frac{di_{ck}}{dt} &= -R_{c_k}i_{c_K} - H(:,k)^T u_c
\end{aligned}
\tag{4.131}
$$

The stability of the equilibrium point of the zero dynamics (4.131) is verified by linearizating (4.131) around the equilibrium point and we can obtain the following Jacobian matrix

$$
J_1 = \begin{bmatrix} -\Sigma_1 & C^{-1}\Sigma_2\Sigma_3 H \\ -L^{-1}H^T\Sigma_3^{-1} & -L^{-1}R \end{bmatrix}
$$

where $\Sigma_{1,2,3}$ are given by

$$
\begin{aligned}
\Sigma_1 &= \text{diag}(\sigma^1_1,\ \cdots,\ \sigma^1_{N+M+P}) \\
\Sigma_2 &= \text{diag}(\sigma^2_1,\ \cdots,\ \sigma^2_{N+M+P}) \\
\Sigma_3 &= \text{diag}(\sigma^3_1,\ \cdots,\ \sigma^3_L)
\end{aligned}
$$

with the elements

$$\begin{cases} \sigma_1^1 = \dfrac{\dfrac{1}{2L_{g_1}C_{g_1}}}{\dfrac{1}{2L_{g_1}}+\dfrac{3}{4}(\alpha^*_{g_1d})^2}[\dfrac{1}{R_{\text{equi},g_1}}+\dfrac{3}{2}R_{g_1}(\alpha^*_{g_id})^2], \\ \sigma_\rho^1 = \dfrac{\dfrac{1}{2L_{g_\rho}C_{g_\rho}}}{\dfrac{1}{2L_{g_\rho}}+\dfrac{3}{4}(\alpha^*_{g_\rho d})^2}[\dfrac{1}{R_{\text{equi},g_\rho}}+\dfrac{3}{2}R_{g_\rho}(\alpha^*_{g_\rho d})^2], & \rho \in \mathcal{N}_{-1} \\ \sigma_{N+j}^1 = \dfrac{\dfrac{1}{2L_{w_j}C_{w_j}}}{\dfrac{1}{2L_{w_j}}+\dfrac{3}{4}[(\bar{\alpha}_{w_jd})^2+(\bar{\alpha}_{w_jq})^2]}\{\dfrac{1}{R_{\text{equi},w_j}}+R_{w_j}((\bar{\alpha}_{w_jd})^2+(\bar{\alpha}_{w_jq})^2) \\ +\dfrac{3}{2}\dfrac{1}{(\bar{u}_{w_j})^2}[(v^o_{sw_jd}\bar{i}_{w_jd}+v^o_{sw_jq}\bar{i}_{w_jq})-2R_{w_j}((\bar{i}_{w_jd})^2+(\bar{i}_{w_jq})^2)], & j \in \mathcal{M} \\ \sigma^1_{(N+M+h)} = 0. & h \in \mathcal{P} \end{cases}$$

$$\begin{cases} \sigma_1^2 = \dfrac{\dfrac{1}{2L_{g_1}}}{\dfrac{1}{2L_{g_1}}+\dfrac{3}{4}(\alpha^*_{g_1d})^2}, \\ \sigma_\rho^2 = \dfrac{\dfrac{1}{2L_{g_\rho}}}{\dfrac{1}{2L_{g_\rho}}+\dfrac{3}{4}(\alpha^*_{g_\rho d})^2}, & \rho \in \mathcal{N}_{-1} \\ \sigma_{N+j}^2 = \dfrac{\dfrac{1}{2L_{w_j}}}{\dfrac{1}{2L_{w_j}}+\dfrac{3}{4}[(\bar{\alpha}_{w_jd})^2+(\bar{\alpha}_{w_jq})^2]}, & j \in \mathcal{M} \\ \sigma^2_{(N+M+h)} = 1. & h \in \mathcal{P} \end{cases}$$

$$\begin{cases} \sigma_1^3 = 1, \\ \sigma_\rho^3 = \alpha^*_{g_\rho d}, & \rho \in \mathcal{N}_{-1} \\ \sigma_{N+j}^3 = 1, & j \in \mathcal{M} \\ \sigma^3_{(N+M+h)} = 1. & h \in \mathcal{P} \end{cases}$$

The terms $R_{w_j}((\bar{i}_{w_jd})^2+(\bar{i}_{w_jd})^2)$ and $R_{w_j}((\bar{i}_{w_jd})+(\bar{i}_{w_jd}))$ represent the losses and the decrease of AC voltage caused by the reactor phases. An optimized HVDC transmission system should have lower losses than AC lines for the same power capacity. The losses in the converter station are only about 0.6 % of the transmitted power [ABB 2014]. As a consequence, it is reasonable to consider that

$$\begin{aligned} v^o_{sw_jd}\bar{i}_{w_jd}+v^o_{sw_jq}\bar{i}_{w_jq}-2R_{w_j}((\bar{i}_{w_jd})^2+(\bar{i}_{w_jq})^2) &> 0 \\ v^o_{sw_jd}+v^o_{sw_jq}-2R_{w_j}(\bar{i}_{w_jd}+\bar{i}_{w_jq}) &> 0 \end{aligned}$$

Lemma 4.3.6. *The system described by (4.125) with control variables $\alpha^*_{w_j,dq}$ and output y_w in (4.126) is minimum phase .*

Proof. To demonstrate this lemma, we only need to prove that the Jacobian matrix J_1 is Hurwitz. Similar to demonstrate Lemma 4.1.3, we also assume that there exists an eigenvalue of J_1 denoted by $\lambda = \alpha + \beta \in \mathbb{C}$ whose real part is non-negative, i.e. $\alpha \geq 0$. By definition of eigenvalues, we have

$$\det(\lambda I - J_1) = \det(\begin{bmatrix} \lambda I + \Sigma_1 & -C^{-1}\Sigma_2\Sigma_3 H \\ L^{-1}H^T\Sigma_3^{-1} & \lambda I + L^{-1}R \end{bmatrix}) = 0 \tag{4.132}$$

As described in the demonstration of Lemma 4.1.3 in Section 4.1.4.1, $\Phi_1 \triangleq \lambda I + L^{-1}R = \Lambda_1 + j\Lambda_2$ are positive definite where $\Lambda_{1,2}$ are given by

$$\begin{aligned} \Lambda_1 &= \mathrm{diag}(\alpha + \frac{R_{c_1}}{L_{c_1}}, \cdots, \alpha + \frac{R_{c_L}}{L_{c_L}}) \in \mathbb{R}^{L\times L} \\ \Lambda_2 &= \mathrm{diag}(\beta, \cdots, \beta) \in \mathbb{R}^{L\times L} \end{aligned}$$

Therefore, $\det(\lambda I - J_1)$ is equivalent to

$$\begin{aligned} &\det(\lambda I - J_1) \\ =&\det(\lambda I + \Sigma_1 + C^{-1}\Sigma_2\Sigma_3 H\Phi_1^{-1}L^{-1}H^T\Sigma_3^{-1})\det(\Phi_1) \\ =&\det(C^{-1}\Sigma_2\Sigma_3\Sigma_3^{-1})\det(\lambda\Sigma_3^{-1}\Sigma_2^{-1}C\Sigma_3 + \Sigma_3^{-1}\Sigma_2^{-1}C\Sigma_1\Sigma_3 + H\Phi_1^{-1}L^{-1}H^T)\det(\Phi_1) \end{aligned}$$

Since C and $\Sigma_{1,2,3}$ are diagonal, the above expression can be rewritten as

$$\begin{aligned} &\det(\lambda I - J_1) \\ =&\det(C^{-1}\Sigma_2)\det(\lambda\Sigma_2^{-1}C + \Sigma_2^{-1}C\Sigma_1 + H\Phi_1^{-1}L^{-1}H^T)\det(\Phi_1) \end{aligned}$$

We introduce

$$\begin{aligned} \Phi_2 &= \lambda C\Sigma_2^{-1} + \Sigma_1 C\Sigma_2^{-1} + H\Phi_1^{-1}L^{-1}H^T \\ \lambda C\Sigma_2^{-1} + \Sigma_1 C\Sigma_2^{-1} &= \Lambda_3 + j\Lambda_4 \\ \Phi_1^{-1}L^{-1} = (\lambda I + R)^{-1} &= \Lambda_5 + j\Lambda_6 \end{aligned}$$

Recalling the expressions of C, Σ_1 and Σ_2 (Σ_1 and Σ_2 are positive definite), it is evident that Λ_5 and Λ_3 are semi-positive definite where Λ_3 is given by

$$\Lambda_3 = \mathrm{diag}(\sigma_1, \cdots, \sigma_{N+M+P})$$

and Λ_5 is expressed in (4.68). Now, Φ_2 can be rewritten as

$$\begin{aligned} \Phi_2 &= \Phi_3 + j(\Lambda_4 + (\Sigma_3 H)\Lambda_6(\Sigma_3 H)^T) \\ \Phi_3 &= \Lambda_3^1 + \Lambda_3^{1'} + H_f H_f^T \end{aligned} \tag{4.133}$$

where Λ_3^1 is a diagonal matrix whose first element on the main diagonal is $\sigma_1 > 0$ and all other elements are zero. $\Lambda_3^{1'}$ and H_f are given by

$$\Lambda_3^{1'} = \Lambda_3 - \Lambda_3^1$$
$$H_f = H\Lambda_5^{\frac{1}{2}}$$

Let us define

$$\Phi_4 = \Lambda_3^1 + H_f H_f^T$$

which is semi-positive definite. Then the determinant of Φ_4 is calculated as

$$\det(\Phi_4) = \sigma_1 \det(\mathcal{R}(H_f)_1 \mathcal{R}(H_f)_1^T) + \det(H_f H_f^T)$$

Recall that $\mathcal{R}(H_f)_1$ is the matrix obtained by removing the first row of H_f. Since $\Lambda_5^{\frac{1}{2}}$ is a full rank matrix, i.e. $\text{rank}(\Lambda_5^{\frac{1}{2}}) = L$, then $\text{rank}(H_f H_f^T) = \text{rank}(H_f) = \text{rank}(H) = N + M + P - 1$ and as a results, $\det(H_f H_f^T) = 0$. According to Lemma 3.4.2, the rank of $\mathcal{R}(H_f)_1$ is $N + M + P - 1$. Consequently, $\mathcal{R}(H_f)_1 \mathcal{R}(H_f)_1^T$ is invertible and positive definite. Because of the positive σ_1, we then have

$$\begin{aligned}\det(\Phi_4) &= \sigma_1 \det(\mathcal{R}(H_f)_1 \mathcal{R}(H_f)_1^T) + \det(H_f H_f^T) \\ &= \sigma_1 \det(\mathcal{R}(H_f)_1 \mathcal{R}(H_f)_1^T) > 0\end{aligned}$$

and hence, the semi-definite matrix Φ_4 must be positive definite. Recalling that $\Phi_3 = \Phi_4 + \Lambda_3^{1'}$ as derived from (4.133), Φ_3 is also positive definite (see Lemma 4.1.8). Since the hermitian part of Φ_2, i.e. $\mathcal{H}(\Phi_2)$, is Φ_3 which is positive definite, we get the result that Φ_2 is also positive definite (see Lemma 4.1.7). Therefore, we deduce that

$$\begin{aligned}&\det(\lambda I - J_1) \\ =&\det(\Phi_2)\det(\Phi_1)\det(C^{-1}\Sigma_2) \neq 0\end{aligned}$$

for $\alpha \geq 0$. This leads to a contradiction to (4.132). Thus, we must have that the real part of all eigenvalues of J_1 is negative, i.e. $\alpha < 0$. Finally, we prove that J_1 is Hurwitz and as a result, the equilibrium point of the zero dynamics is asymptotically stable. The proof is completed. □

Adaptive control

Let us revisit the zero dynamics (4.125) which is a multiple-input and multiple-output (MIMO) system with the control variables $\alpha^*_{w_j,dq}$. In the previous part, by using the feedback linearization technique, $\alpha^*_{w_j,dq}$ is designed as (4.127) which strongly depend on the system parameters, R_{fw_j} C_{fw_j}, ω_j and $I_{w_j,dq}$. However, due to the ageing of the facilities, the system parameters are usually slowly varying.

In particular, R_{fw_j} used to model the losses of the filter is very hard to obtain its exact value. Several studies have been carried out to deal with the uncertainties of the system parameters [Ruan 2007, Hernandez-Gomez 2010, Durrant 2004]. In Section 4.2, the sliding mode control method is also applied to make the system more robust. In this part, the adaptive control method is proposed to adjust the system parameters for enhancing the dynamic performance of the system [Narendra 2012].

We recall the dynamics of $v_{sw_j,dq}$ given by

$$\begin{aligned}\frac{dv_{sw_jd}}{dt} &= \omega_{w_j} v_{sw_jq} + \frac{1}{C_{fw_j}} I_{w_jd} - \alpha^*_{w_jd} u_{cw_j} \frac{1}{C_{fw_j}} - \frac{v_{sw_jd}}{R_{fw_j}} \frac{1}{C_{fw_j}} \\ \frac{dv_{sw_jq}}{dt} &= -\omega_{w_j} v_{sw_jd} + \frac{1}{C_{fw_j}} I_{w_jq} - \alpha^*_{w_jq} u_{cw_j} \frac{1}{C_{fw_j}} - \frac{v_{sw_jq}}{R_{fw_j}} \frac{1}{C_{fw_j}}\end{aligned} \tag{4.134}$$

with the uncertain C_{fw_j}, ω_{w_j}, R_{fw_j} and $I_{w_j,dq}$. Our task here is to design $\alpha^*_{w_j,dq}$ to make $v_{sw_j,dq}$ track their respective references $v^o_{sw_j,dq}$. Then, the output tracking errors are given by

$$\begin{aligned}e_{v_{sw_jd}} &= v_{sw_jd} - v^o_{sw_jd} \\ e_{v_{sw_jq}} &= v_{sw_jq} - v^o_{sw_jq}\end{aligned} \tag{4.135}$$

Augmenting (4.134) with the integrated output tracking errors

$$\begin{aligned}\dot{e}_{Iv_{sw_jd}} &= e_{v_{sw_jd}} \\ \dot{e}_{Iv_{sw_jq}} &= e_{v_{sw_jq}}\end{aligned} \tag{4.136}$$

results in the following extend open-loop system

$$\begin{aligned}\begin{bmatrix}\dot{e}_{Iv_{sw_jd}} \\ \dot{v}_{sw_jd} \\ \dot{e}_{Iv_{sw_jq}} \\ \dot{v}_{sw_jq}\end{bmatrix} = \underbrace{\begin{bmatrix}0 & 1 & 0 & 0 \\ 0 & -\frac{1}{C_{fw_j}R_{fw_j}} & 0 & \omega_{w_j} \\ 0 & 0 & 0 & 1 \\ 0 & -\omega_{w_j} & 0 & -\frac{1}{C_{fw_j}R_{fw_j}}\end{bmatrix}}_{A_{P_j}} \begin{bmatrix}e_{Iv_{sw_jd}} \\ v_{sw_jd} \\ e_{Iv_{sw_jq}} \\ v_{sw_jq}\end{bmatrix} + \begin{bmatrix}0 \\ \frac{I_{w_jd}}{C_{fw_j}} \\ 0 \\ \frac{I_{w_jd}}{C_{fw_j}}\end{bmatrix} \\ + \underbrace{\begin{bmatrix}0 & 0 \\ -\frac{1}{C_{fwj}} & 0 \\ 0 & 0 \\ 0 & -\frac{1}{C_{fwj}}\end{bmatrix}}_{B_{P_j}} \begin{bmatrix}u_{cw_j}\alpha^*_{w_jd} \\ u_{cw_j}\alpha^*_{w_jq}\end{bmatrix} + \begin{bmatrix}-v^o_{sw_jd} \\ 0 \\ -v^o_{sw_jq} \\ 0\end{bmatrix}\end{aligned} \tag{4.137}$$

Let us consider the reference model

$$\begin{bmatrix} \dot{e}_{Iv_{sw_jd,\mathrm{m}}} \\ \dot{v}_{sw_jd,\mathrm{m}} \\ \dot{e}_{Iv_{sw_jq,\mathrm{m}}} \\ \dot{v}_{sw_jq,\mathrm{m}} \end{bmatrix} = \underbrace{\begin{bmatrix} 0 & 1 & 0 & 0 \\ -k_{I\alpha_{w_jd}} & -c_{\alpha_{w_jd}} & 0 & 0 \\ 0 & 0 & 0 & 1 \\ 0 & 0 & -k_{I\alpha_{w_jq}} & -c_{\alpha_{w_jq}} \end{bmatrix}}_{A_{\mathrm{m}_j}} \begin{bmatrix} e_{Iv_{sw_jd,\mathrm{m}}} \\ v_{sw_jd,\mathrm{m}} \\ e_{Iv_{sw_jq,\mathrm{m}}} \\ v_{sw_jq,\mathrm{m}} \end{bmatrix} + \begin{bmatrix} 0 \\ c_{\alpha_{w_jd}} v^o_{sw_d} \\ 0 \\ c_{\alpha_{w_jq}} v^o_{sw_q} \end{bmatrix} + \begin{bmatrix} -v^o_{sw_jd} \\ 0 \\ -v^o_{sw_jq} \\ 0 \end{bmatrix} \tag{4.138}$$

It is evident that A_{m_j} is Hurwitz. If all system parameters are known, $\alpha_{w_j,dq}$ can be developed as

$$\begin{aligned} \alpha^*_{w_jd} = & \frac{C_{fw_j}}{u_{cw_j}} [\frac{I_{w_jd}}{C_{fw_j}} - \frac{v_{sw_jd}}{C_{fw_j} R_{fw_j}} + \omega_{w_j} v_{sw_jq} \\ & + c_{\alpha_{w_jd}} \cdot e_{v_{sw_jd}} + k_{I\alpha_{w_jd}} \cdot e_{I\alpha_{w_jd}}] \\ \alpha^*_{w_jq} = & \frac{C_{fw_j}}{u_{cw_j}} [\frac{I_{w_jq}}{C_{fw_j}} - \frac{v_{sw_jq}}{C_{fw_j} R_{fw_j}} \\ & + c_{\alpha_{w_jd}} \cdot e_{v_{sw_jd}} + k_{I\alpha_{w_jd}} \cdot e_{I\alpha_{w_jd}}] \end{aligned} \tag{4.139}$$

so that the closed-loop of the system (4.137) becomes

$$\begin{bmatrix} \dot{e}_{Iv_{sw_jd}} \\ \dot{v}_{sw_jd} \\ \dot{e}_{Iv_{sw_jq}} \\ \dot{v}_{sw_jq} \end{bmatrix} = A_{\mathrm{m}_j} \begin{bmatrix} e_{Iv_{sw_jd}} \\ v_{sw_jd} \\ e_{Iv_{sw_jq}} \\ v_{sw_jq} \end{bmatrix} + \begin{bmatrix} 0 \\ c_{\alpha_{w_jd}} v^o_{sw_d} \\ 0 \\ c_{\alpha_{w_jq}} v^o_{sw_q} \end{bmatrix} + \begin{bmatrix} -v^o_{sw_jd} \\ 0 \\ -v^o_{sw_jq} \\ 0 \end{bmatrix} \tag{4.140}$$

which exhibits the same behavior as the reference model (4.138). However, in the current study case, since the system parameters are unknown, the controller is designed as

$$\begin{aligned} \alpha^*_{w_jd} = & \frac{1}{u_{cw_j}} [\hat{I}_{w_jd} - \frac{v_{sw_jd}}{\hat{R}_{fw_j}} + \hat{C}_{fw_j} \hat{\omega}_{w_j} v_{sw_jq} + \hat{C}_{fw_j} (c_{\alpha_{w_jd}} \cdot e_{v_{sw_jd}} + k_{I\alpha_{w_jd}} \cdot e_{I\alpha_{w_jd}})] \\ \alpha^*_{w_jq} = & \frac{1}{u_{cw_j}} [\hat{I}_{w_jq} - \frac{v_{sw_jq}}{\hat{R}_{fw_j}} - \hat{C}_{fw_j} \hat{\omega}_{w_j} v_{sw_jd} + \hat{C}_{fw_j} (c_{\alpha_{w_jq}} \cdot e_{v_{sw_jq}} + k_{I\alpha_{w_jq}} \cdot e_{I\alpha_{w_jq}})] \end{aligned} \tag{4.141}$$

which is based on the estimate of the parameter $(\cdot)$ denoted by $(\hat{\cdot})$. Due to the nonlinear terms $\dfrac{1}{\hat{R}_{fw_j}}$ and $\hat{C}_{fw_j}\hat{\omega}_{w_j}$, the parameter adjustment of the controller (4.141) is a nonlinear parameterized adaptive control problem. For the sake of simplicity, we perform the change of variables

$$\psi_{1_j} = I_{w_jd};\ \psi_{2_j} = I_{w_jq};\ \psi_{3_j} = \frac{1}{R_{fw_j}};\ \psi_{4_j} = C_{fw_j}\omega_{w_j}; \tag{4.142}$$

and then, rewrite the controller (4.141) in these new variables as

$$\begin{aligned}\alpha^*_{w_jd}&= \frac{1}{u_{cw_j}}[\hat{\psi}_{1_j} - \hat{\psi}_{3_j} v_{sw_jd} + \hat{\psi}_{4_j} v_{sw_jq} - \hat{C}_{fw_j} v_{\alpha_{w_jd}}]\\ \alpha^*_{w_jq}&= \frac{1}{u_{cw_j}}[\hat{\psi}_{2_j} - \hat{\psi}_{3_j} v_{sw_jq} - \hat{\psi}_{4_j} v_{sw_jd} - \hat{C}_{fw_j} v_{\alpha_{w_jq}}]\end{aligned} \tag{4.143}$$

Now, the parameter adjustment of the controller becomes a linear parameter adaptive control problem. Substituting (4.143) into the zero dynamics (4.125), we get

$$\begin{aligned}\begin{bmatrix}\dot{e}_{Iv_{sw_jd}}\\ \dot{v}_{sw_jd}\\ \dot{e}_{Iv_{sw_jq}}\\ \dot{v}_{sw_jq}\end{bmatrix} &= \begin{bmatrix}1 & 0 & 0 & 0\\ 0 & \dfrac{\hat{C}_{fw_j}}{C_{fw_j}} & 0 & 0\\ 0 & 0 & 1 & 0\\ 0 & 0 & 0 & \dfrac{\hat{C}_{fw_j}}{C_{fw_j}}\end{bmatrix} A_{\mathrm{m}_j} \begin{bmatrix}e_{Iv_{sw_jd}}\\ v_{sw_jd}\\ e_{Iv_{sw_jq}}\\ v_{sw_jq}\end{bmatrix} + \begin{bmatrix}0\\ \dfrac{\hat{C}_{fw_j}}{C_{fw_j}} c_{\alpha_{w_jd}} v^o_{sw_d}\\ 0\\ \dfrac{\hat{C}_{fw_j}}{C_{fw_j}} c_{\alpha_{w_jq}} v^o_{sw_q}\end{bmatrix}\\ &+ \begin{bmatrix}0 & 0 & 0 & 0\\ \dfrac{1}{C_{fw_j}} & 0 & -\dfrac{1}{C_{fw_j}} v_{sw_jd} & \dfrac{1}{C_{fw_j}} v_{sw_jq}\\ 0 & 0 & 0 & 0\\ 0 & \dfrac{1}{C_{fw_j}} & -\dfrac{1}{C_{fw_j}} v_{sw_jq} & -\dfrac{1}{C_{fw_j}} v_{sw_jd}\end{bmatrix} \begin{bmatrix}\tilde{\psi}_{1_j}\\ \tilde{\psi}_{2_j}\\ \tilde{\psi}_{3_j}\\ \tilde{\psi}_{4_j}\end{bmatrix} + \begin{bmatrix}-v^o_{sw_jd}\\ 0\\ -v^o_{sw_jq}\\ 0\end{bmatrix}\end{aligned} \tag{4.144}$$

which can be rewritten as

$$\begin{aligned}\begin{bmatrix}\dot{e}_{Iv_{sw_jd}}\\ \dot{e}_{v_{sw_jd}}\\ \dot{e}_{Iv_{sw_jq}}\\ \dot{e}_{v_{sw_jq}}\end{bmatrix} &= \begin{bmatrix}1 & 0 & 0 & 0\\ 0 & \dfrac{\hat{C}_{fw_j}}{C_{fw_j}} & 0 & 0\\ 0 & 0 & 1 & 0\\ 0 & 0 & 0 & \dfrac{\hat{C}_{fw_j}}{C_{fw_j}}\end{bmatrix} A_{\mathrm{m}_j} \begin{bmatrix}e_{Iv_{sw_jd}}\\ e_{v_{sw_jd}}\\ e_{Iv_{sw_jq}}\\ e_{v_{sw_jq}}\end{bmatrix}\\ &+ \begin{bmatrix}0 & 0 & 0 & 0\\ \dfrac{1}{C_{fw_j}} & 0 & -\dfrac{1}{C_{fw_j}} v_{sw_jd} & \dfrac{1}{C_{fw_j}} v_{sw_jq}\\ 0 & 0 & 0 & 0\\ 0 & \dfrac{1}{C_{fw_j}} & -\dfrac{1}{C_{fw_j}} v_{sw_jq} & -\dfrac{1}{C_{fw_j}} v_{sw_jd}\end{bmatrix} \begin{bmatrix}\tilde{\psi}_{1_j}\\ \tilde{\psi}_{2_j}\\ \tilde{\psi}_{3_j}\\ \tilde{\psi}_{4_j}\end{bmatrix}\end{aligned} \tag{4.145}$$

where $\tilde{\psi}_{(\cdot)} = \psi_{(\cdot)} - \hat{\psi}_{(\cdot)}$ denotes the error between the parameter's estimated value and its actual value. Although the exact value of C_{fw_j} is unknown, we can confirm that C_{fw_j} is positive. The classical adaptive law can be given by

$$\begin{aligned}\hat{C}_{fw_j}&= \mathrm{sgn}(C_{fw_j}) = 1\\ \dot{\tilde{\psi}}_{1_j}&= -c_{1_j} e_{v_{sw_jd}}\\ \dot{\tilde{\psi}}_{2_j}&= -c_{2_j} e_{v_{sw_jq}}\\ \dot{\tilde{\psi}}_{3_j}&= c_{3_j}(e_{v_{sw_jd}} v_{sw_jd} + e_{v_{sw_jq}} v_{sw_jq})\\ \dot{\tilde{\psi}}_{4_j}&= c_{4_j}(e_{v_{sw_jq}} v_{sw_jd} - e_{v_{sw_jd}} v_{sw_jq})\end{aligned} \tag{4.146}$$

where the adaptive gains $c_{1,2,3,4_j}$ are positive. We consider a quadratic positive definite function as

$$\begin{aligned} V= &\frac{1}{2}C_{fw_j}(e^2_{v_{sw_jd}}+e^2_{v_{sw_jd}})+\frac{1}{2}k_{I\alpha_{w_jd}}e^2_{Iv_{sw_jd}}+\frac{1}{2}k_{I\alpha_{w_jq}}e^2_{Iv_{sw_jq}} \\ &+\frac{1}{2c_{1_j}}\tilde{\psi}^2_{1_j}+\frac{1}{2c_{2_j}}\tilde{\psi}^2_{2_j}+\frac{1}{2c_{3_j}}\tilde{\psi}^2_{3_j}+\frac{1}{2c_{4_j}}\tilde{\psi}^2_{4_j} \end{aligned} \tag{4.147}$$

whose derivative is deduced as

$$\dot{V}=-c_{\alpha_{w_jd}}e^2_{v_{sw_jd}}-c_{\alpha_{w_jq}}e^2_{v_{sw_jq}}\leq 0 \tag{4.148}$$

Since $\dot{V}$ is non-positive, we have $V(t)\leq V(t=0)$ and hence $e_{v_{sw_j,dq}}$, $e_{Iv_{sw_j,dq}}$ and $\tilde{\psi}_{1,2,3,4_j}$ are bounded. Furthermore, $\ddot{V}$ can be calculated, which contains only bounded terms. Consequently, $\dot{V}$ is also bounded and then $\dot{V}$ is uniformly continuous. Based on Barbalat's lemma, we get $\dot{V}\to 0$ as $t\to\infty$. It reveals that $e_{v_{sw_j,dq}}\to 0$ as $t\to\infty$. Finally, the adaptive controller is developed, which is composed by (4.143) and (4.146).

4.3.4.2 Step 2: design of $\alpha^*_{g_id}$

From the previous section, we get that, when $v_{sw_j,dq}$ converge to $v^o_{sw_jdq}$, the system behavior is governed by the zero dynamics (4.131) whose state variables, u_{cg_1}, i_{g_ρ}, u_{cw_j}, u_{ct_h} and i_c, are uncontrolled. Again, we want to regulate these states via $\alpha^*_{g_id}$. In this part, the control algorithm for $\alpha^*_{g_id}$ is based on (4.131) where $\alpha^*_{g_id}$ are considered as control variables and $\bar{\alpha}^*_{w_j,dq}$ are considered equal to their steady-state values $\bar{\alpha}_{w_j,dq}=\dfrac{\bar{i}_{w_j,dq}}{\bar{u}_{cw_j}}$.

We first consider using the following simple proportional controllers for $\alpha^*_{g_id}$

$$\begin{aligned} \alpha^*_{g1d}&=-k_{Pu_{cg_1}}\tilde{u}_{cg_1}+\bar{\alpha}_{g1d} \\ \alpha^*_{g_\rho d}&=-k_{Pi_{g_\rho d}}\tilde{i}_{g_\rho d}+\bar{\alpha}_{g_\rho d} \end{aligned} \tag{4.149}$$

with positive control gains $k_{Pu_{cg_1}}$ and $k_{Pi_{g_\rho d}}$. From (4.149), it can be seen that when $\tilde{u}_{cg_1}$ and $\tilde{i}_{g_\rho d}$ converge to zero, $\alpha^*_{g_id}$ also converge to their steady-state values.

Substituting (4.149) into (4.131) results in the following closed-loop system

$$
\begin{aligned}
C_{g_1}\frac{du_{cg_1}}{dt} &= \frac{\dfrac{1}{2L_{g_1}}}{\dfrac{1}{2L_{g_1}}+\dfrac{3}{4}(-k_{Pu_{cg_1}}\tilde{u}_{cg_1}+\bar{\alpha}_{g_1d})^2}\{[-\frac{u_{cg_1}}{R_{\text{equi},g_1}}+H(1,:)i_c] \\
&\quad -\frac{3}{2}[R_{g_1}u_{cg_1}(-k_{Pu_{cg_1}}\tilde{u}_{cg_1}+\bar{\alpha}_{g_1d})^2 - v_{sg_1d}(-k_{Pu_{cg_1}}\tilde{u}_{cg_1}+\bar{\alpha}_{g_1d})]\} \\
C_{g_\rho}\frac{di_{g_\rho d}}{dt} &= \frac{\dfrac{1}{2L_{g_\rho}}}{\dfrac{1}{2L_{g_\rho}}+\dfrac{3}{4}(-k_{Pi_{g_\rho d}}\tilde{i}_{g_\rho d}+\bar{\alpha}_{g_\rho d})^2}\{[-\frac{i_{g_\rho d}}{R_{\text{equi},g_\rho}} \\
&\quad +(-k_{Pi_{g_\rho d}}\tilde{i}_{g_\rho d}+\bar{\alpha}_{g_\rho d})H(\rho,:)i_c] \\
&\quad +\frac{3}{2}[(v_{s_\rho d}-R_{g_\rho}i_{g_\rho d})(-k_{Pi_{g_\rho d}}\tilde{i}_{g_\rho d}+\bar{\alpha}_{g_\rho d})^2]\} \\
C_{w_j}\frac{du_{cw_j}}{dt} &= \frac{\dfrac{1}{2L_{w_j}}}{\dfrac{1}{2L_{w_j}}+\dfrac{3}{4}[(\bar{\alpha}^*_{w_jd})^2+(\bar{\alpha}^*_{w_jq})^2]}\{[-\frac{u_{cw_j}}{R_{\text{equi},w_j}}+H(N+j,:)i_c] \\
&\quad -\frac{3}{2}[R_{w_j}u_{cw_j}((\bar{\alpha}^*_{w_jd})^2+(\bar{\alpha}^*_{w_jq})^2) - (v^o_{sw_jd}\bar{\alpha}^*_{w_jd}+v^o_{sw_jq}\bar{\alpha}^*_{w_jq})] \\
C_{t_h}\frac{du_{ct_h}}{dt} &= H(N+M+h,:)i_c \\
L_{c_k}\frac{di_{ck}}{dt} &= -R_{c_k}i_{c_K}-H(:,k)^Tu_c
\end{aligned}
\tag{4.150}
$$

To check the stability of the above closed-loop system, we linearize the system (4.150) around the equilibrium point and then get the following Jacobian matrix

$$
J_2 = \begin{bmatrix} -\Theta_1 & C^{-1}\Theta_2\Theta_3 H \\ -L^{-1}H^T\Theta_3^{-1}\Theta_4 & -L^{-1}R \end{bmatrix}
$$

where $\Theta_{1,2,3,4}$ are given by

$$
\begin{aligned}
\Theta_1 &= \text{diag}(\theta_1^1,\ \cdots,\ \theta^1_{N+M+P}) \\
\Theta_2 &= \text{diag}(\sigma_1^2,\ \cdots,\ \sigma^2_{N+M+P}) \\
\Theta_3 &= \text{diag}(\sigma_1^3,\ \cdots,\ \sigma^3_{L}) \\
\Theta_4 &= \text{diag}(\sigma_1^4,\ \cdots,\ \sigma^4_{L})
\end{aligned}
\tag{4.151}
$$

Keeping in mind that the steady-state value of $i_{g_\rho d}$ equals its prescribed setpoint $i^o_{g_\rho d}$ and the relation between $\bar{\alpha}_{g_id}$, $\bar{u}_{cg_i}$ and $\bar{i}_{g_id}$ satisfy $\bar{\alpha}_{g_id} = \dfrac{\bar{i}_{g_id}}{\bar{u}_{cg_i}}$, then we can

deduced the elements of $\Theta_{1,2,3,4}$ as

$$
\begin{cases}
\theta_1^1 = \dfrac{\dfrac{1}{2L_{g_1}C_{g_1}}}{\dfrac{1}{2L_{g_1}}+\dfrac{3}{4}(\bar{\alpha}_{g_1d})^2}[\dfrac{1}{R_{\text{equi},g_1}}+\dfrac{3}{2}R_{g_1}(\bar{\alpha}_{g_1d})^2+\dfrac{3}{2}(v_{sg_1d}-2R_{g_1}\bar{i}_{g_1d})k_{Pu_{cg_1}}], \\
\theta_\rho^1 = \dfrac{\dfrac{1}{2L_{g_\rho}C_{g_\rho}}}{\dfrac{1}{2L_{g_\rho}}+\dfrac{3}{4}(\bar{\alpha}_{g_\rho d})^2}[\dfrac{1}{R_{\text{equi},g_\rho}}+\dfrac{3}{2}R_{g_\rho}(\bar{\alpha}_{g_\rho d})^2 \\
\quad +k_{Pi_{g_\rho d}}[\dfrac{3}{2}\cdot 2(v_{sg_\rho d}-R_{g_\rho}\bar{i}_{g_\rho d})\bar{\alpha}_{g_\rho d}+H(\rho,:)\bar{i}_c], & \rho\in\mathcal{N}_{-1} \\
\theta_{N+j}^1 = \dfrac{\dfrac{1}{2L_{w_j}C_{w_j}}}{\dfrac{1}{2L_{w_j}}+\dfrac{3}{4}[(\bar{\alpha}_{w_jd})^2+(\bar{\alpha}_{w_jq})^2]}\{\dfrac{1}{R_{\text{equi},w_j}}+\dfrac{3}{2}R_{w_j}((\alpha^*_{w_jd})^2+(\alpha^*_{w_jq})^2), & j\in\mathcal{M} \\
\theta_{(N+M+h)}^1 = 0. & h\in\mathcal{P}
\end{cases}
$$

$$
\begin{cases}
\theta_1^2 = \dfrac{\dfrac{1}{2L_{g_1}}}{\dfrac{1}{2L_{g_1}}+\dfrac{3}{4}(\bar{\alpha}_{g_1d})^2}, \\
\theta_\rho^2 = \dfrac{\dfrac{1}{2L_{g_\rho}}}{\dfrac{1}{2L_{g_\rho}}+\dfrac{3}{4}(\bar{\alpha}_{g_\rho d})^2}, & \rho\in\mathcal{N}_{-1} \\
\theta_{N+j}^2 = \dfrac{\dfrac{1}{2L_{w_j}}}{\dfrac{1}{2L_{w_j}}+\dfrac{3}{4}[(\alpha^*_{w_jd})^2+(\alpha^*_{w_jq})^2]}, & j\in\mathcal{M} \\
\theta_{(N+M+h)}^2 = 1. & h\in\mathcal{P}
\end{cases}
$$

$$
\begin{cases}
\theta_1^3 = 1, \\
\theta_\rho^3 = \bar{\alpha}_{g_\rho d}, & \rho\in\mathcal{N}_{-1} \\
\theta_{N+j}^3 = 1, & j\in\mathcal{M} \\
\theta_{(N+M+h)}^3 = 1. & h\in\mathcal{P}
\end{cases}
$$

$$
\begin{cases}
\theta_1^4 = 1, \\
\theta_\rho^4 = 1+k_{Pi_{g_\rho d}}\bar{u}_{cg_\rho}, & \rho\in\mathcal{N}_{-1} \\
\theta_{N+j}^4 = 1, & j\in\mathcal{M} \\
\theta_{(N+M+h)}^4 = 1. & h\in\mathcal{P}
\end{cases}
\tag{4.152}
$$

When the system is in steady state, we have

$$
-\frac{i_{g_\rho d}}{R_{\text{equi},g_\rho}}+\bar{\alpha}_{g_\rho d}H(\rho,:)i_c-\frac{3}{2}[R_{g_\rho}i_{g_\rho d}(\bar{\alpha}_{g_\rho d})^2-\bar{\alpha}_{g_\rho d}(v_{sg_\rho d}\bar{\alpha}_{g_\rho d})]=0
$$

which leads to

$$H(\rho,:)\bar{i}_c = \frac{\bar{u}_{cg_\rho}}{R_{\text{equi},g_\rho}} + \frac{3}{2}(R_{g_\rho} i_{g_\rho d} - v_{sg_\rho d})\bar{\alpha}_{g_\rho d} \tag{4.153}$$

Substituting (4.153) into θ_ρ^1 in (4.152) yields

$$\begin{aligned}\theta_\rho^1 = & \frac{\frac{1}{2L_{g_\rho}C_{g_\rho}}}{\frac{1}{2L_{g_\rho}} + \frac{3}{4}(\bar{\alpha}_{g_\rho d})^2}\{\frac{1}{R_{\text{equi},g_\rho}} + \frac{3}{2}R_{g_\rho}(\bar{\alpha}_{g_\rho d})^2 \\ & + k_{Pi_{g_\rho d}}[\frac{3}{2}(v_{sg_\rho d} - R_{g_\rho}\bar{i}_{g_\rho d})\bar{\alpha}_{g_\rho d} + \frac{\bar{u}_{cg_\rho}}{R_{\text{equi},g_\rho}}]\}\end{aligned} \tag{4.154}$$

To ensure the stability of the closed-loop system (4.150), the control gains must render the Jacobian matrix J_2 Hurwitz.

Lemma 4.3.7. *By choosing $k_{Pi_{g_\rho d}}$ such that*

$$\begin{aligned} 1 + k_{Pi_{g_\rho d}}\bar{u}_{cg_\rho} > 0 \\ \frac{1}{R_{equi,g_\rho}} + \frac{3}{2}R_{g_\rho}(\bar{\alpha}_{g_\rho d})^2 + k_{Pi_{g_\rho d}}[\frac{3}{2}(v_{sg_\rho d} - R_{g_\rho}\bar{i}_{g_\rho d})\bar{\alpha}_{g_\rho d} + \frac{\bar{u}_{cg_\rho}}{R_{equi,g_\rho}}] > 0 \end{aligned} \tag{4.155}$$

J_2 is Hurwitz.

Proof. When $k_{Pi_{g_\rho d}}$ satisfies (4.155), then Θ_4 becomes positive define. By the definition of $\Theta_{1,2}$ (see (4.151)), both of them are diagonal and positive definite. By following the similar procedure used in the proof of Lemma 4.3.6, we can prove that J_2 is Hurwitz. □

The above description clearly shows that the simple proportional controller (4.149) can stabilize the zero dynamics (4.131). To get good tracking performance, we use the PI controllers to replace the proportional controllers as

$$\begin{aligned} \dot{e}_{Iu_{cg_1}} &= \tilde{u}_{cg_1} \\ \alpha^*_{g_1 d} &= -k_{Pu_{cg_1}}\tilde{u}_{cg_1} - k_{Iu_{cg_1}}e_{Iu_{cg_1}} \\ \dot{e}_{Ii_{g_\rho d}} &= \tilde{i}_{g_\rho d} \\ \alpha^*_{g_\rho d} &= -k_{Pi_{g_\rho d}}\tilde{i}_{g_\rho d} - k_{Ii_{g_\rho d}}e_{Ii_{g_\rho d}} \end{aligned} \tag{4.156}$$

with the integrated errors and positive control gains $k_{I(\cdot)}$.

Of course, there are different approaches to choosing the PI control gains. As presented in [Lee 2003], the absolute tracking results for Lur'e plants is applied to get a criterion for tuning the control gain. It can also be used to deduce the constraints for $k_{P(\cdot)}$ and $k_{I(\cdot)}$ via linearization. In this thesis, we are not tangled on this issue. Finally, the overall control structure are built, which is composed of (4.122), (4.156) and the adaptive law (4.146).

Table 4.9: Initial values of the system state variables.

SAC 1	SAC 2
$u_{cg_1} = u^o_{cg_1} = 150$ V	$i_{g_2d} = i^o_{g_2d} = 13.1$ A
$i_{g_1q} = i^o_{g_1q} = 0$ A	$i_{g_2q} = i^o_{g_2q} = 0$ A
WAC 1	WAC 2
$v_{sw_1d} = v^o_{sw_1d} = 40.82$ V	$v_{sw_2d} = v^o_{sw_2d} = 40.82$ V
$v_{sw_1q} = v^o_{sw_1q} = 0$ V	$v_{sw_2q} = v^o_{sw_2q} = 0$ V

4.3.5 Simulation studies

In this section, we first apply the passive control scheme which is composed of (4.124), (4.127) and (4.149) to the MTDC system described by Fig. 4.21 and then apply the adaptive passive control scheme which consists of (4.124), (4.143), (4.146) and (4.149) to the same MTDC system.

4.3.5.1 Performance evaluation of the passive control strategy

The proposed passive control scheme composed of (4.124), (4.127) and (4.149) is applied to the MTDC system described by Fig. 4.21 in Section 4.1.4 where two WACs and two SACs are considered. To evaluate the performance of the proposed control scheme, several scenarios are studied in the simulations.

Scenario 1: DC voltage regulation and power reversal operation

Initially, the MTDC system works in the steady state as illustrated in Table 4.9. At $t = 0.5$ s, $i^o_{g_2d}$ is set to -6.53 A from 13.1 A. It means that the 2^{nd} SAC connected VSC is required to operate in the inversion mode as a power consumer from the rectification mode as a power supplier. Then, at $t = 1$ s, a new reference value of u_{cg_1} is given with an increase of 5%.

The simulation results are shown in Figs. 4.39- 4.44. As shown in Fig. 4.39, both controllers can make u_{cg_1} always track its reference $u^o_{cg_1}$. However, when the power reversal happens in the 2^{nd} SAC connected VSC terminal, the trajectory of u_{cg_1} under the feedback nonlinear controller drops very fast and has an unacceptable undershoot. Compared to the feedback nonlinear controller, the passivity-based controller gives a much better performance with a faster convergence and keeps u_{cg_1} within its acceptable region. As illustrated in Figs. 4.40 and 4.41, the changes of $u^o_{cg_1}$ and $i^o_{g_2d}$ have negligible effects on the performance of i_{g_1q} (and i_{g_2q}) under feedback nonlinear controller while remarkable overshoot (and undershoot) appears when the passivity-based controller is used. These phenomena imply that the feedback nonlinear controller always provides a better decoupling characteristics of the DC voltage (or the AC $d-$ axis current) and the AC $q-$ axis current control than the passivity-based controller. Figs. 4.43 and 4.44 depict the response of $v_{sw_1,abc}$ under the feedback nonlinear controller and the passivity-based controller. Both of them ensure that the WAC connected VSC terminal operates at the fixed AC voltage

magnitude and the fixed AC frequency in spite of the change of DC voltage or the power reversal of the 2nd SAC connected VSC terminal.

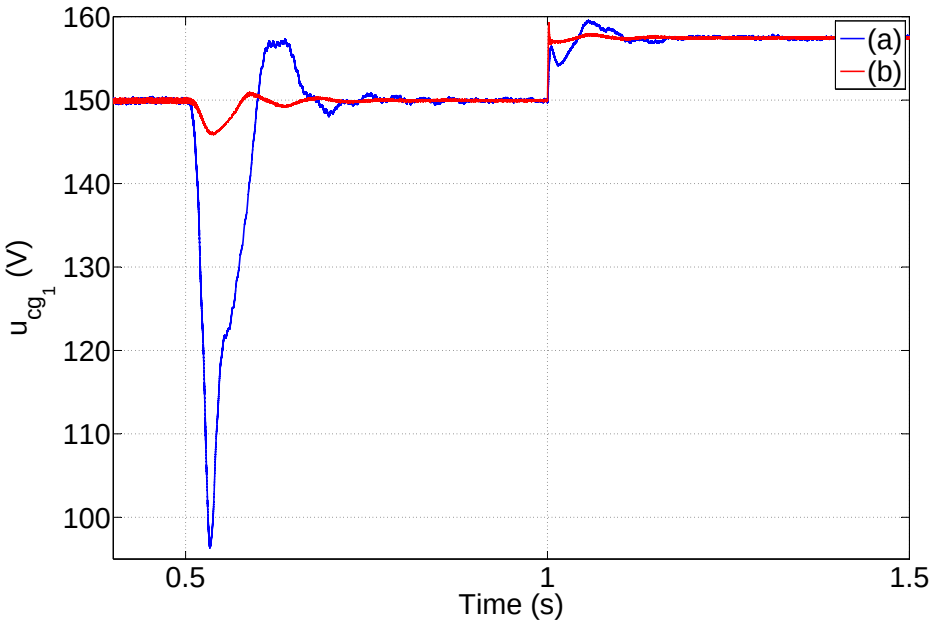

Figure 4.39: The response of u_{cg_1} (a) Feedback nonlinear controller. (b) Passivity-based controller.

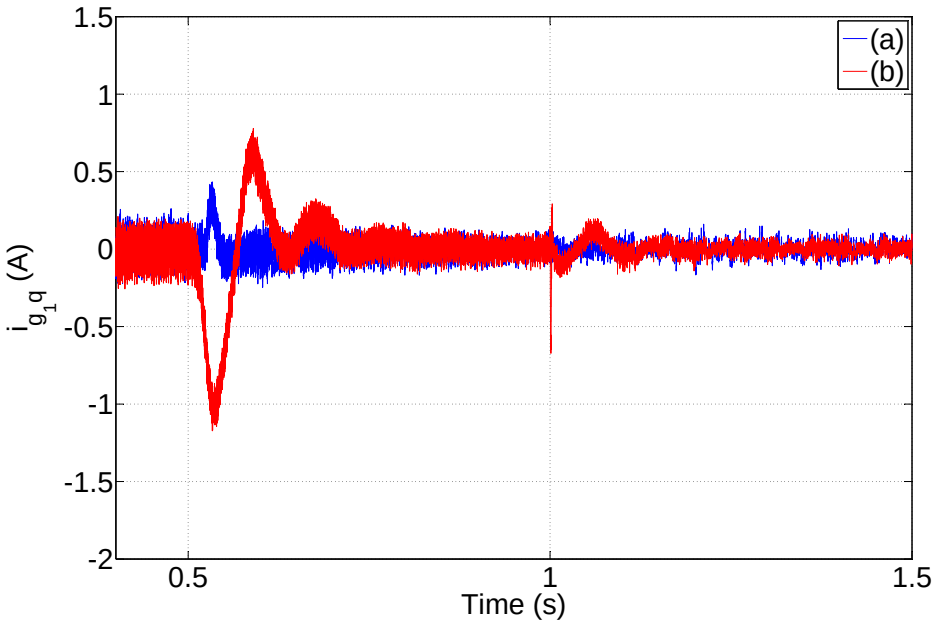

Figure 4.40: The response of i_{g_1q} (a) Feedback nonlinear controller. (b) Passivity-based controller.

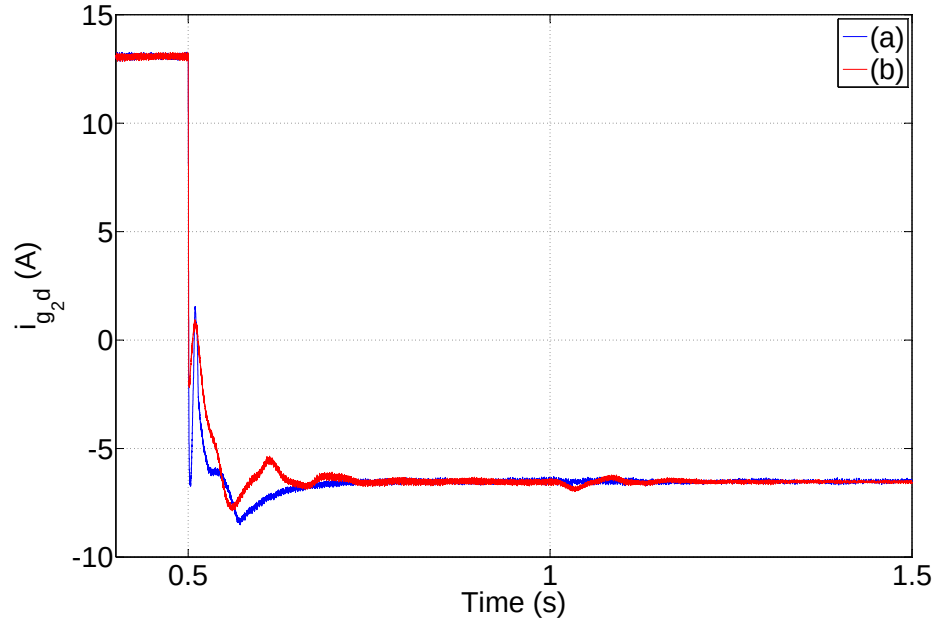

Figure 4.41: The response of i_{g_2d} (a) Feedback nonlinear controller. (b) Passivity-based controller.

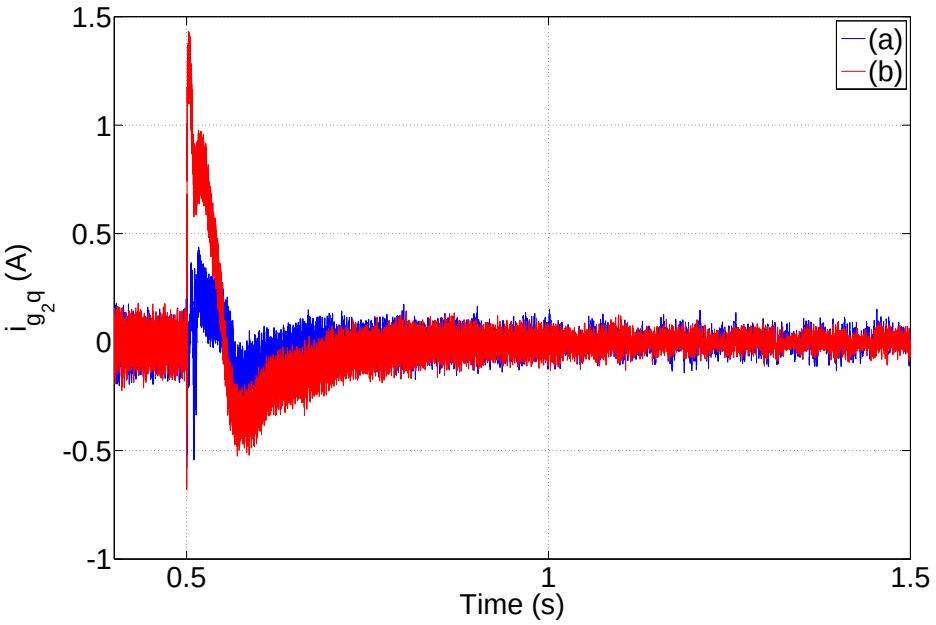

Figure 4.42: The response of i_{g2q} (a) Feedback nonlinear controller. (b) Passivity-based controller.

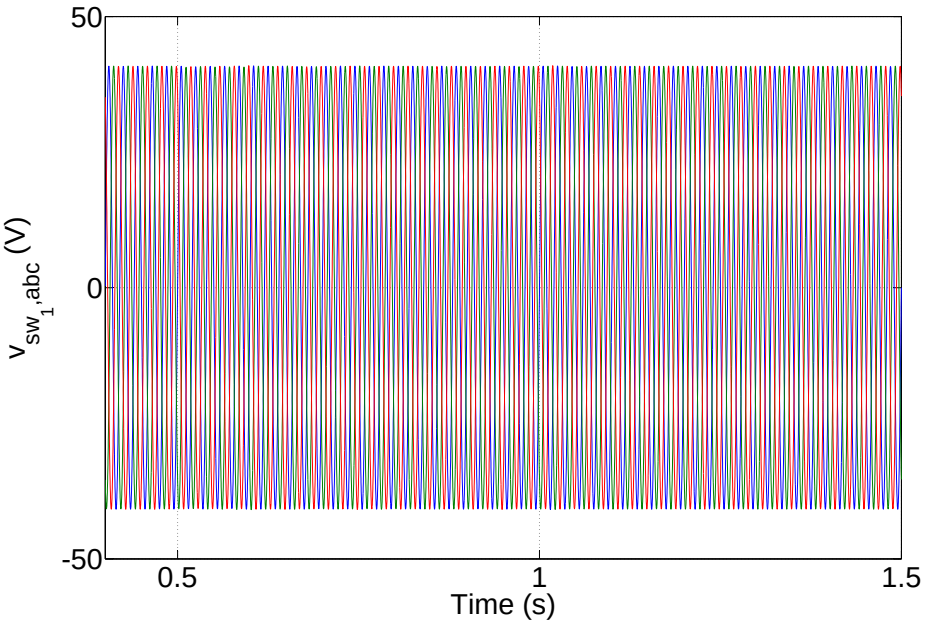

Figure 4.43: The response of $v_{sw_1,abc}$ using feedback nonlinear controller.

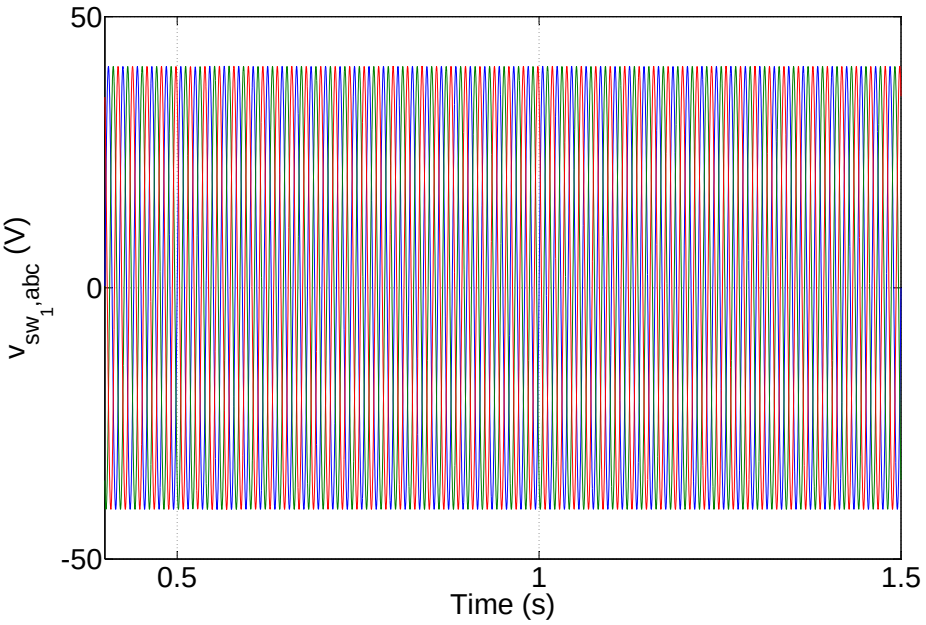

Figure 4.44: The response of $v_{sw_1,abc}$ using passivity-based controller.

Scenario 2: AC voltage regulation

To evaluate the capability of the passivity-based controller in terms of AC voltage regulation, the step changes of $v^o_{sw_1 d}$ and v^o_{sw2q} are considered in this scenario. Similar to Scenario 1, the MTDC system initially operates in the steady state provided by Table 4.9. At $t = 0.5$ s and $t = 1$ s, $v^o_{sw_1 d}$ and $v^o_{sw_2 q}$ are changed to 61.24 V and 20.41 V respectively. The simulation results are plotted in Figs. 4.45-4.49. The transient response of u_{cg_1} is illustrated in Fig. 4.45. It is evident that the performance of u_{cg_1} under the passivity-based controller is much better than the feedback nonlinear controller. Less oscillations, smaller overshoots and faster response convergence are found in the trajectory of u_{cg_1} under the passivity-based controller. Similar to the results in Scenario 1, Figs. 4.46-4.49 clearly show that the feedback nonlinear controller gives a better decoupling characteristics of the AC $d-$ axis and $q-$ axis voltage control.

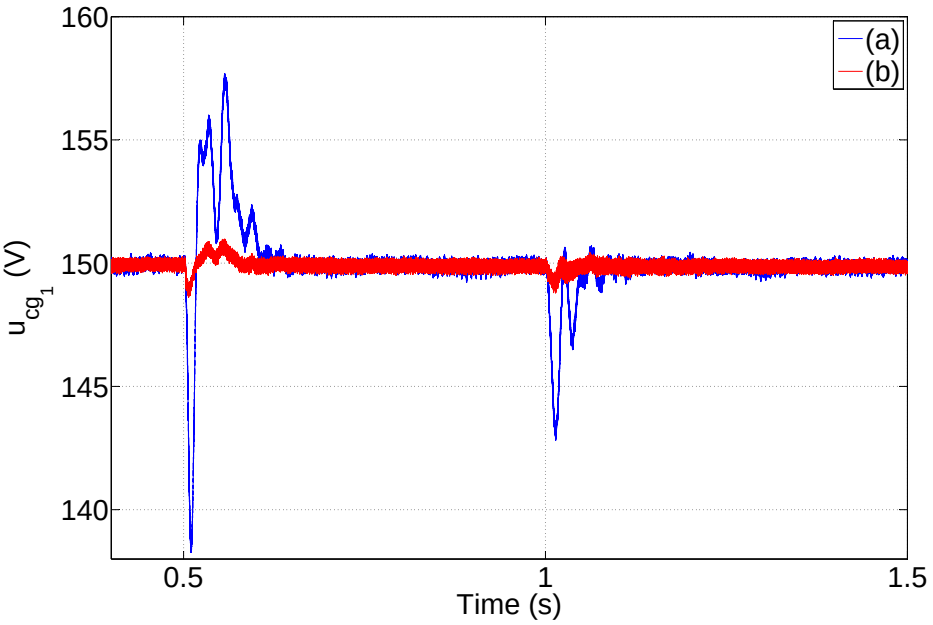

Figure 4.45: The response of u_{cg_1} (a) Feedback nonlinear controller. (b) Passivity-based controller.

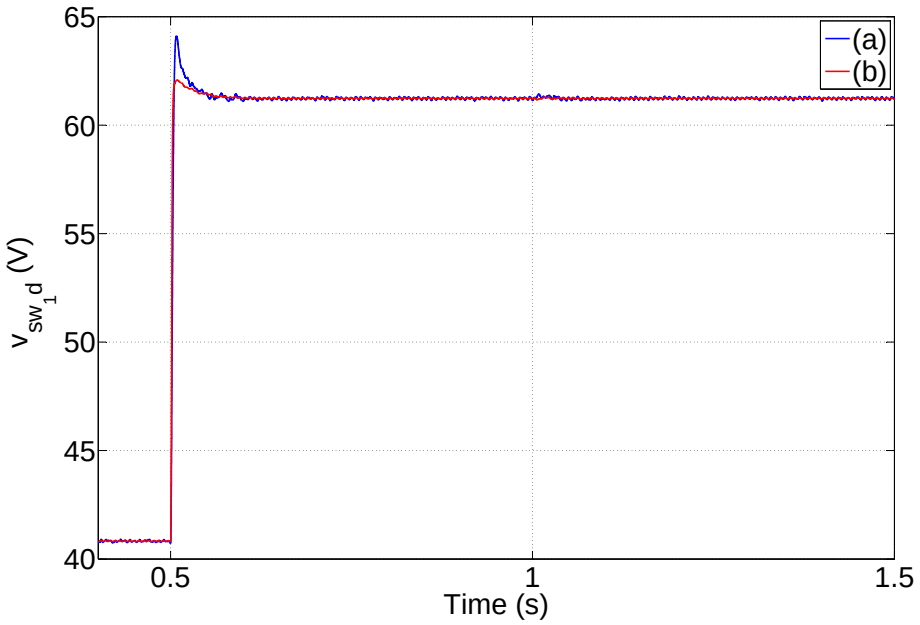

Figure 4.46: The response of $v_{sw_1 d}$ (a) Feedback nonlinear controller. (b) Passivity-based controller.

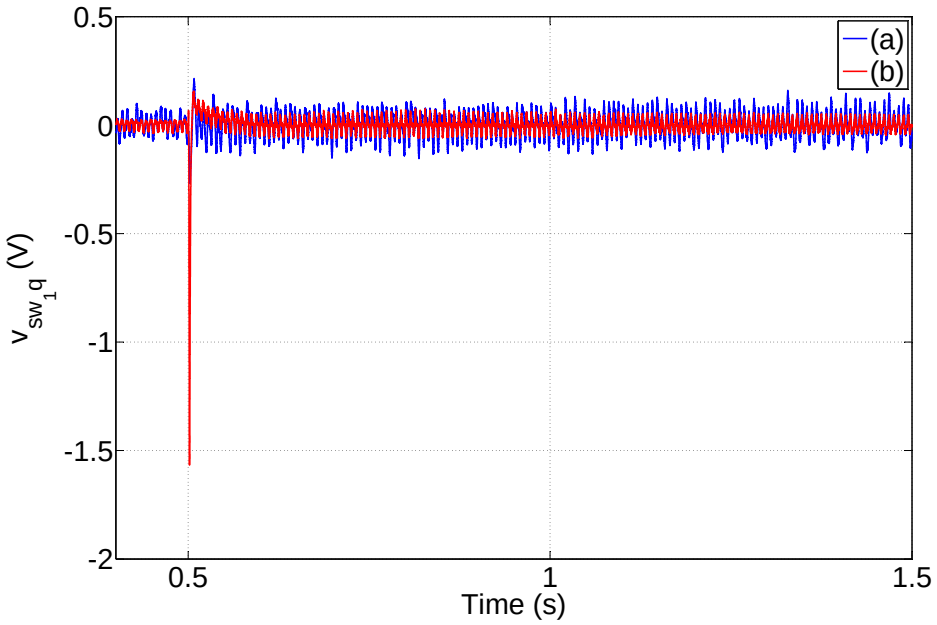

Figure 4.47: The response of v_{sw_1q} (a) Feedback nonlinear controller. (b) Passivity-based controller.

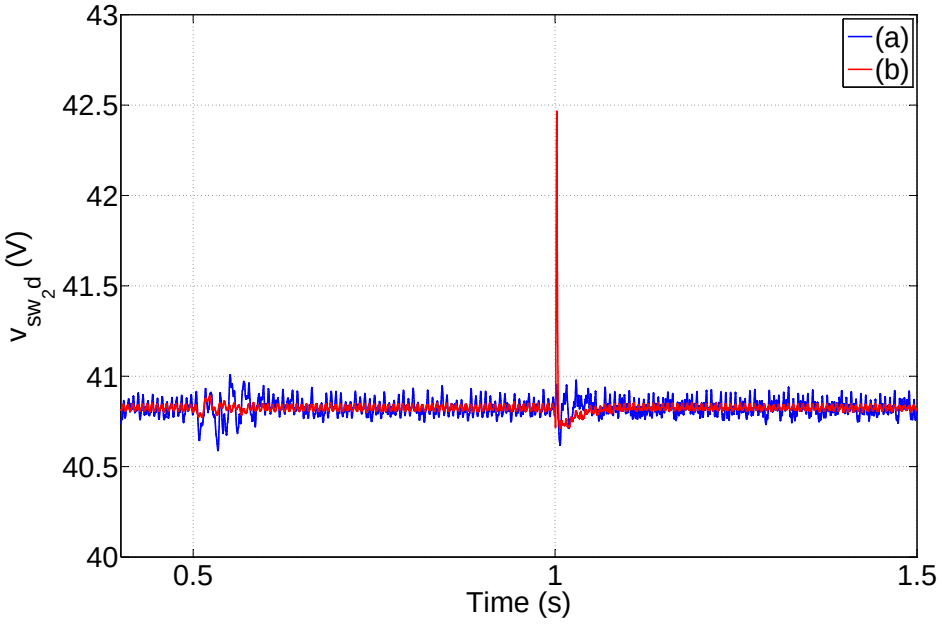

Figure 4.48: The response of v_{sw2d} (a) Feedback nonlinear controller. (b) Passivity-based controller.

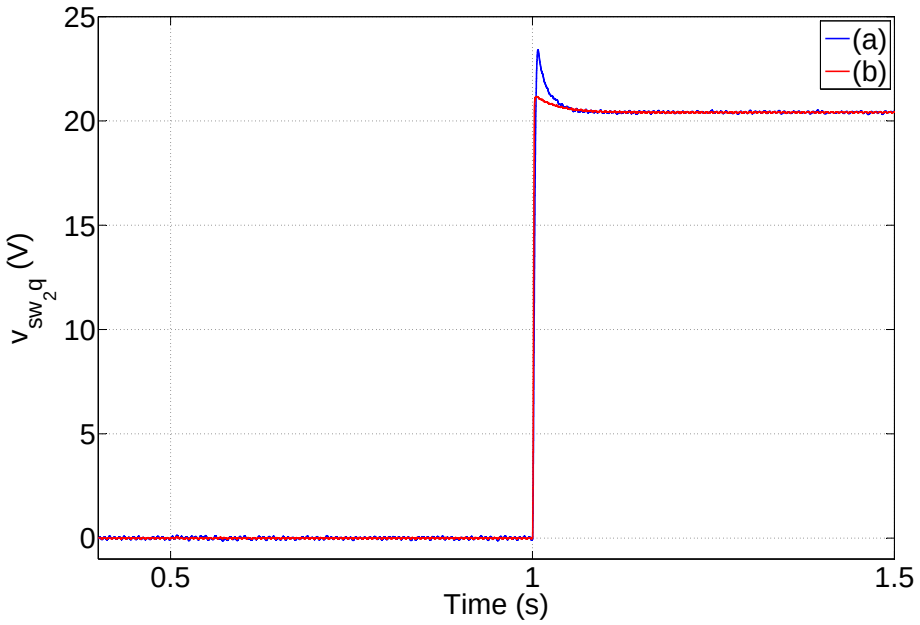

Figure 4.49: The response of v_{sw2q} (a) Feedback nonlinear controller. (b) Passivity-based controller.

4.3.5.2 Performance evaluation of the adaptive passive control strategy

Simulations are carried out to compare the performance between the adaptive controller and the nominal controller where R_{fw_1} and R_{fw_2} are unknown. For the nominal controller, R_{fw_1} and R_{fw_2} are considered equal to their nominal values $R_{fw_1,\text{nom}} = 5\ \Omega$ and $R_{fw_2,\text{nom}} = 8\ \Omega$ respectively. The MTDC system initially operates in the steady state provided by Table 4.9. Then, a sequence of events applied to R_{fw_1} and R_{fw_2} are depicted in Figs. 4.50 and 4.51.

The simulation results are shown in Figs. 4.52-4.59. As presented in Figs. 4.52 and 4.55, only when the actual values of R_{fw_1} and R_{fw_2} equal their nominal values, the nominal controller can make v_{sw_1d} and v_{sw2q} accurately track their reference trajectories $v^o_{sw_1d}$ and v^o_{sw2d}. If this is not the case, the steady-state errors exist (see the trajectories of v_{sw_1d} and v_{sw2d} during the intervals [0.5, 0.7] s and [0.9, 1.1] s in in Figs. 4.52 and 4.55.) Thanks to the adaptive law, v_{sw_1d} and v_{sw2q} can be always kept at their reference values after short transients under the adaptive passivity-based controller. Figs. 4.53 and 4.56 also clearly show that the nominal controller can not make the amplitude of WAC's AC voltage at the PCC operate at constant level while the adaptive passivity-based controller has this ability in spite of the change of R_{fw_1} and R_{fw_2}.

Figures 4.58 and 4.59 illustrate the actual system parameters and their estimated values. Interesting, we find that the estimated values ($\hat{\psi}_{3_1}$ and $\hat{\psi}_{3_2}$) are not exactly equal to their actual values (ψ_{3_1} and ψ_{3_2}). This phenomenon does not surprise us

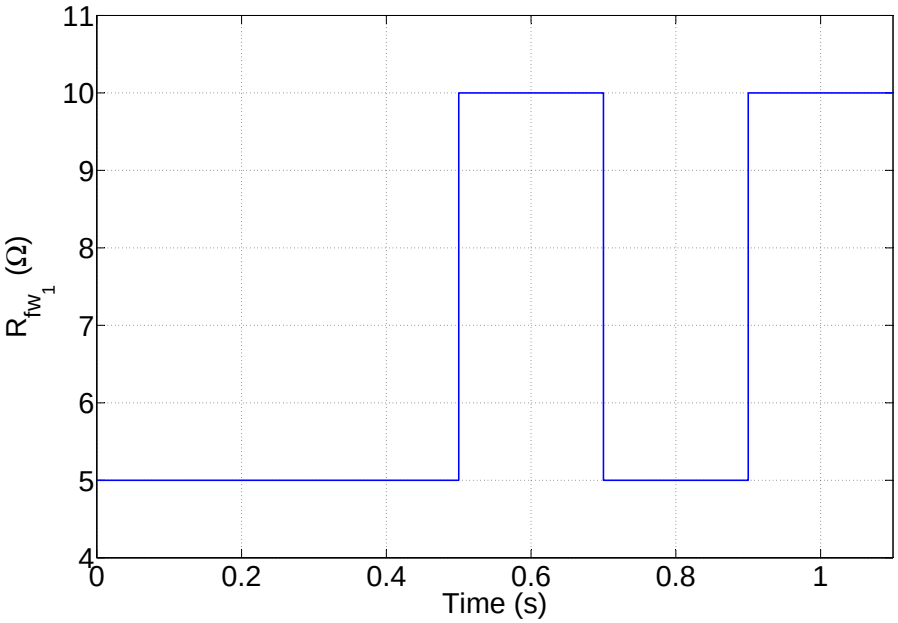

Figure 4.50: Variations in R_{fw_1}.

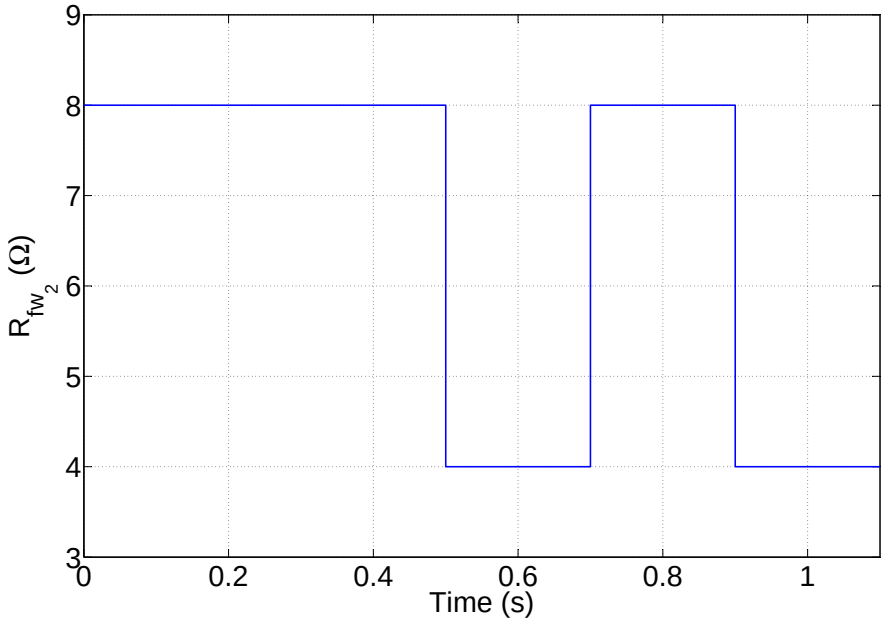

Figure 4.51: Variations in R_{fw_2}.

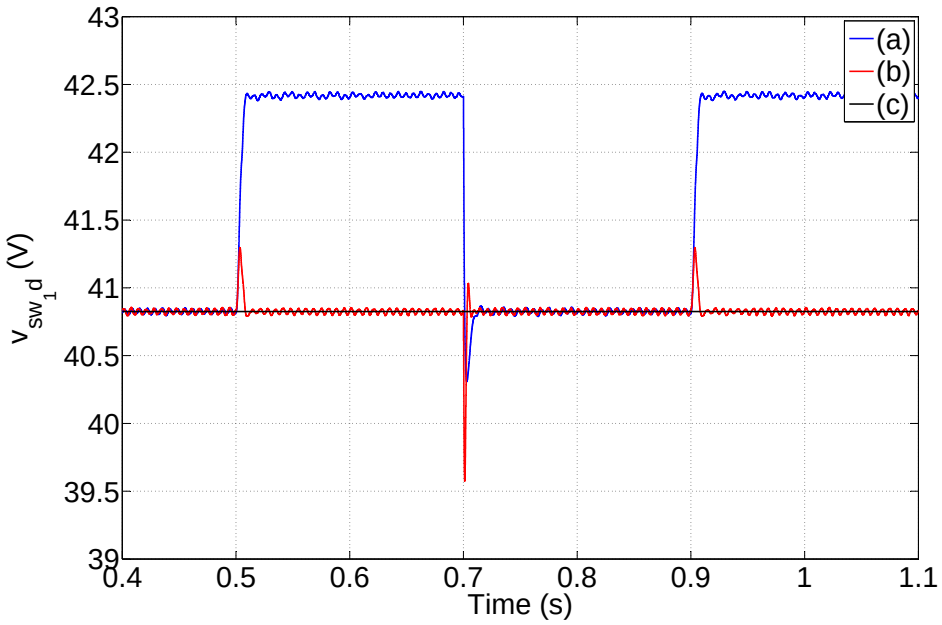

Figure 4.52: The response of $v_{sw_1 d}$ (a) Nominal passivity-based controller (b) Adaptive passivity-based controller (c) Reference values of $v^o_{sw_1 d} = 40.82$ V.

since the adaptive law (4.146) is used to provide the way to adjust the parameters of the passivity-based controller but does not ensure that the estimated parameters converge to their actual values.

4.4 Chapter conclusions

This chapter has presented different control strategies for VSC HVDC systems. The input-output feedback linearization technique is first applied to the control design. Comparing to the conventional PI controller, the feedback nonlinear controller gives a better decoupling characteristics of the system state control. Since the performance of the feedback nonlinear system is relevant to the system structure and parameters, in order to make the system be more robust, sliding mode control is used combined with feedback linearization. Due to the use of sliding mode control, the uncertainties of the system parameters and other possible exogenous inputs are taken into account. As stated in Section 4.1.4, if it is natural to choose the controlled variables as the output (see (4.56)), the input-output feedback linearization is applicable only when the system is (weakly) minimum phase (see Lemma 4.1.2). This restricts the choice of those prescribed references. To deal with this problem, we find a passive output defined by (4.107) by means of passivity theory. It turns out that the MTDC system with the passive output is munimum phase. Following the input-output feedback linearizaiton procedure, the control algorithm (4.122) is

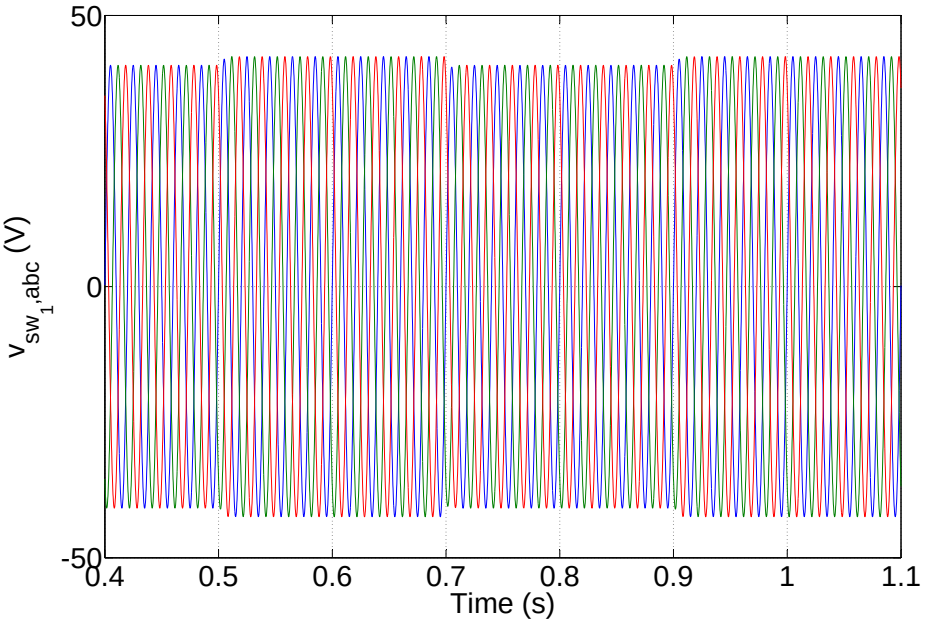

Figure 4.53: The response of $v_{sw_1,abc}$ under the nominal passivity-based controller.

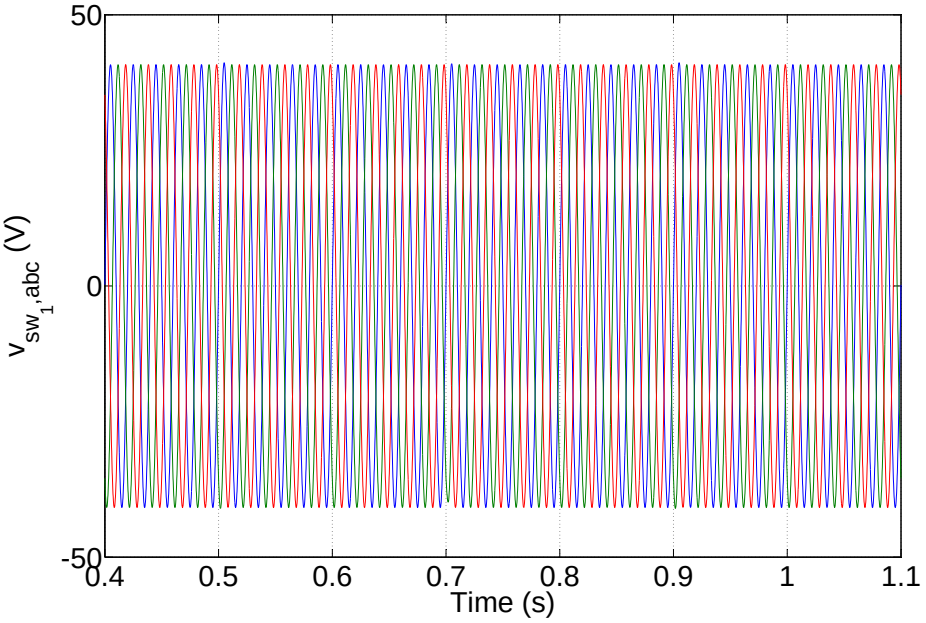

Figure 4.54: The response of $v_{sw_1,abc}$ under the adaptive passivity-based controller.

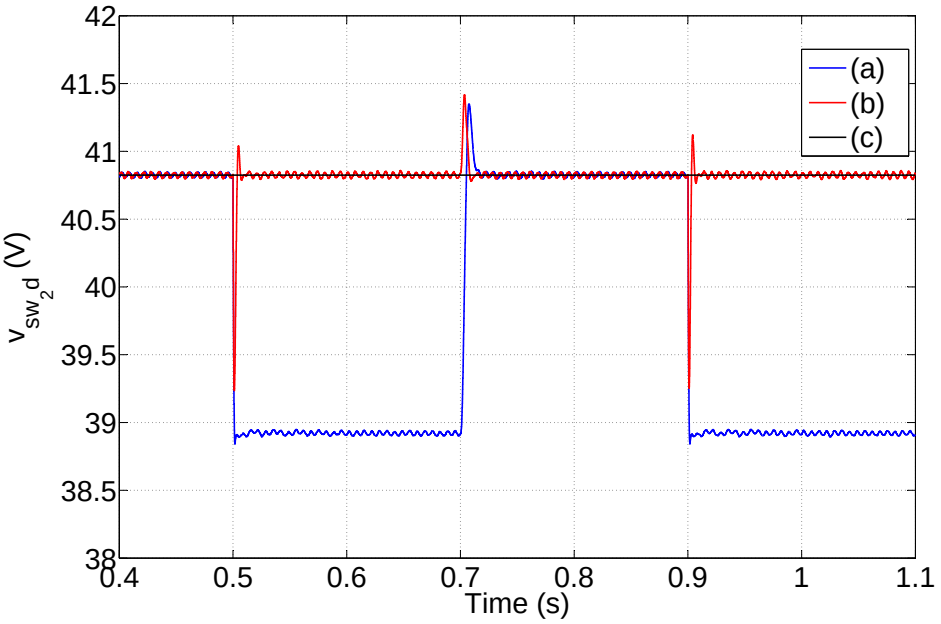

Figure 4.55: The response of v_{sw_2d} (a) Nominal passivity-based controller (b) Adaptive passivity-based controller (c) Reference values of $v^o_{sw_2d} = 40.82$ V.

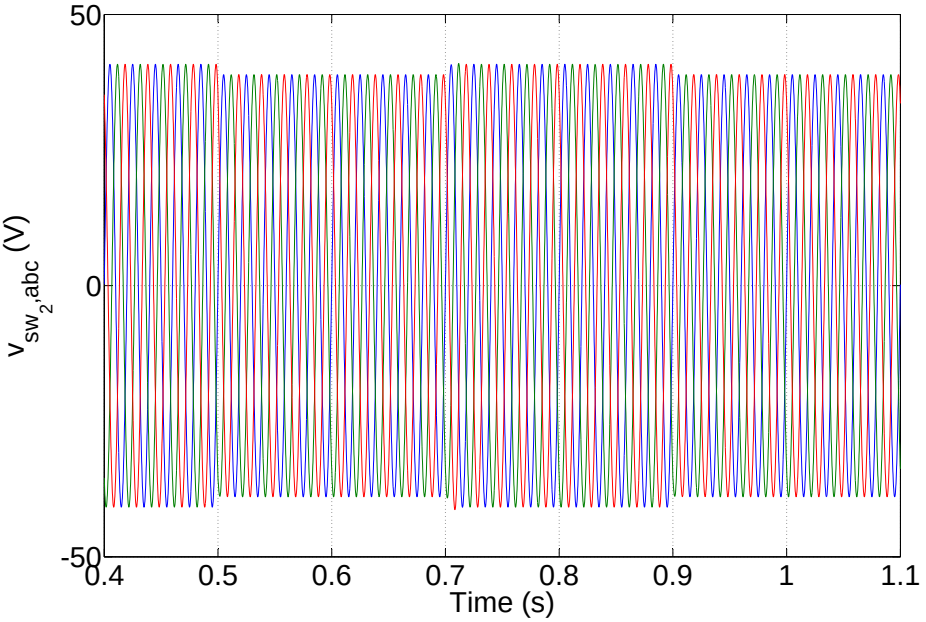

Figure 4.56: The response of $v_{sw_2,abc}$ under the nominal passivity-based controller.

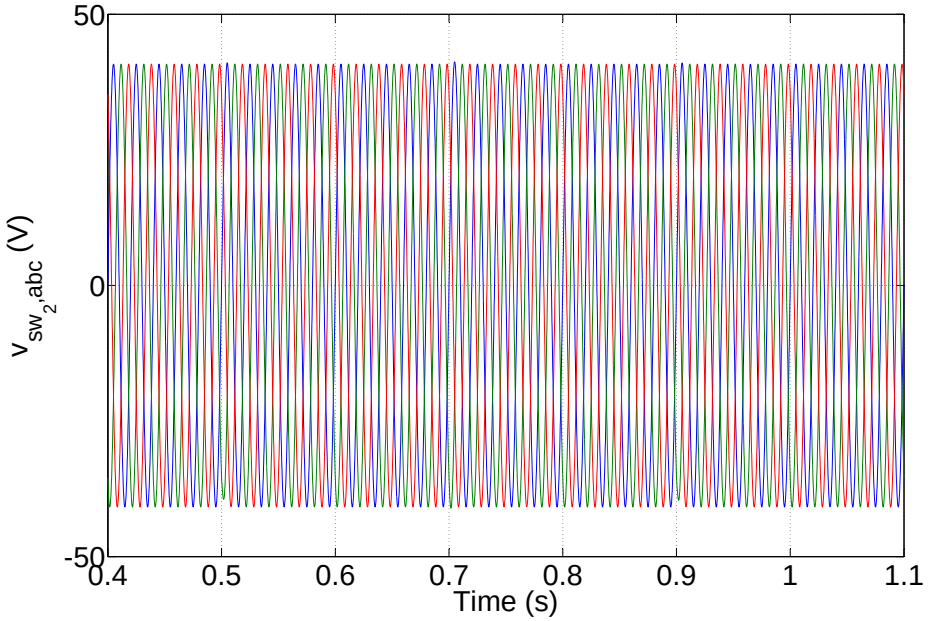

Figure 4.57: The response of $v_{sw_2,abc}$ under the adaptive passivity-based controller.

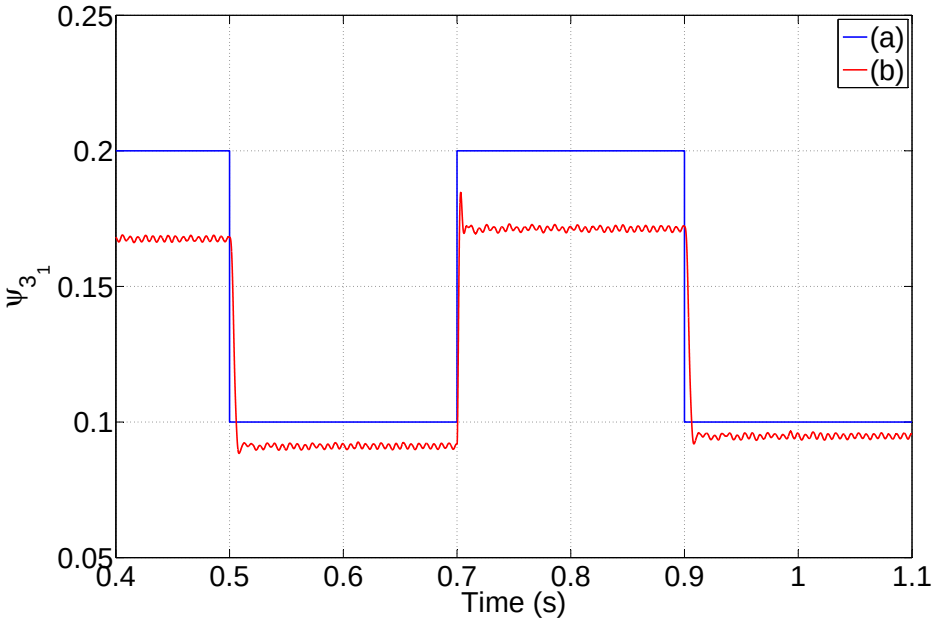

Figure 4.58: Comparison between (a) the actual parameter value $\psi_{3_1} = \dfrac{1}{R_{fw_1}}$ and (b) the parameter estimation $\hat{\psi}_{3_1} = \dfrac{1}{\hat{R}_{fw_1}}$.

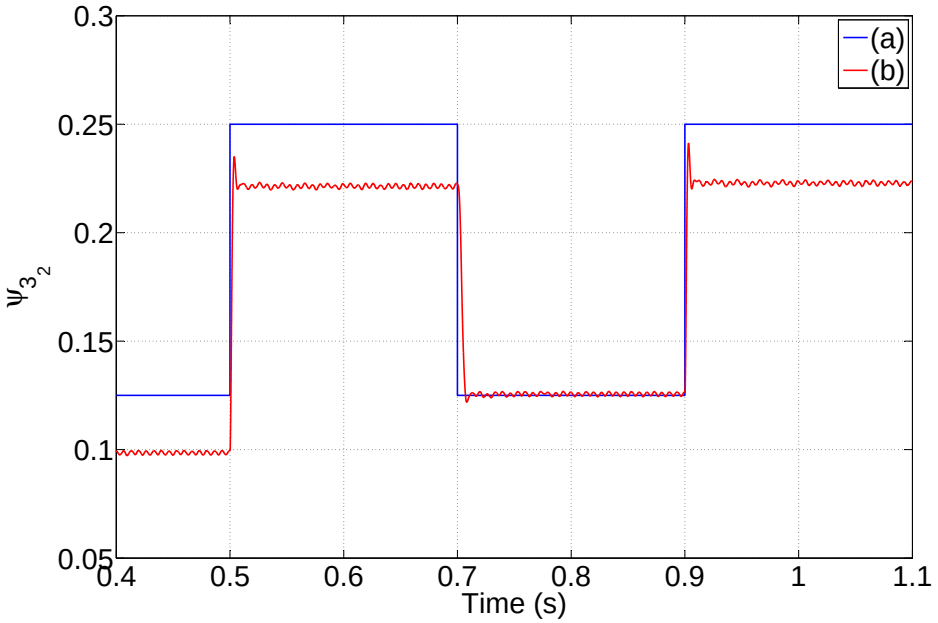

Figure 4.59: Comparison between (a) the actual parameter value $\psi_{3_2} = \dfrac{1}{R_{fw_2}}$ and (b) the parameter estimation $\hat{\psi}_{3_2} = \dfrac{1}{\hat{R}_{fw_2}}$.

developed. When the output perfectly approaches to zero, the dynamics of u_{cg_1}, $i_{g_\rho d}$ and $v_{sw_j,dq}$ are eventually governed by the zero dynamics (4.115). Regulating $\frac{i_{g_i,dq}}{u_{cg_i}}$ and $\frac{i_{g_j,dq}}{u_{cw_j}}$ to the desired $\frac{\bar{i}_{g_i,dq}}{\bar{u}_{cg_i}}$ and $\frac{\bar{i}_{g_j,dq}}{\bar{u}_{cw_j}}$, obtained from the steady-state condition (4.96), indirectly drives u_{cg_1}, $i_{g_\rho d}$ and $v_{sw_j,dq}$ to the prescribed values. However, due to the uncertainties of the system, it is usually difficult to get the accurate values of $\frac{\bar{i}_{g_i,dq}}{\bar{u}_{cg_i}}$ and $\frac{\bar{i}_{g_j,dq}}{\bar{u}_{cw_j}}$. Moreover, the convergence rate of the uncontrolled states of the zero dynamics totally depends on the system parameters. Thus, to get a better tracking performance and improve the dynamics of those uncontrolled state variables, the control law (4.156) for $\alpha^*_{g_i,dq}$ and $\alpha_{w_j,dq}$ is derived based on the zero dynamics.

Chapter 5

Control induced time-scale separation

Contents

A common assumption used in the vector current control design (see Section 3.5.2) of VSCs is that the reactor phase currents have much faster dynamics than the capacitor DC voltage. Hence, the two loops, i.e. the inner and the outer loop, can be designed independently. Interestingly, no relevant work has ever mathematically explained the validity and the implications of this hypothesis. The main idea of this chapter is to provide a detailed theoretical analysis, inspired by a long stand practice that consists of empirical design of two control loops for the VSC terminals. Furthermore, experience has shown that such loops, when heuristically tuned, often display very different dynamics. Here, we acknowledge this practice and give

explanation and fundamental analysis on why and how this empirical control practice works, and how to rigorously design the algorithms. In particular, we formalize this intuition from practitioners into a control scheme that artificially induces two different time scales to the closed-loop system. From the theoretical analysis, the time-scale separation between the system state variables are clearly illustrated by means of singular perturbation theory. In this way, the controller allows the full-scale system to be divided into a boundary-layer and a reduced model. These two models are the key point in the designing of the full control scheme, and they greatly reduce the complexity of the task. Furthermore, in this chapter, our analysis allows to determine strict attraction regions based on well determined control gains, such that there is a clear trade-off between system performance (actuators constraints and as a consequence cost) and the size of the region of attraction of the controllers.

5.1 Control induced time-scale separation for a class of nonlinear systems

5.1.1 Introduction and motivation

This section aims at providing a multi-layered control architecture for a class of underactuated nonlinear systems. The control of such systems, for example several robotic systems and even the well known pendulum-cart problem [Spong 1994, Spong 1995, Ortega 2002], is classical. Nevertheless, it is rather difficult to propose systematic control design approaches for them. One of the main reasons for this difficulty comes from the interconnection between subsystems. In fact, most analytical approaches based on rigorous mathematical techniques rely on trajectory design. However, the trajectories are usually difficult to develop due to the subsystems' interaction. Furthermore, if additional subsystems are added or control goals are required, the existing control algorithms need to be re-designed, which involves extra re-engineering efforts. This motivates the development of a more flexible and more functional control structure.

Inspired by "plug and play philosophy" [Pernebo 2002, Bendtsen 2013, Riverso 2013], we desire to build a control structure that consists of a "fundamental" control module and various "outer" control modules as shown in Fig. 5.1. In this way, when a new objective, such as Objective 1 (see Fig. 5.1), is required, we just need to connect the corresponding outer control module, i.e. Outer control module 1, to the fundamental control module without decommissioning the whole existing control structure or re-designing a new control algorithm from the full-scale model. Thus, it is recommendable to develop new control functionality based on the existing fundamental module. This control design concept is attractive since it can greatly reduce the complexity of the algorithm. However, the difficulty here is how to design the fundamental and the outer control modules since such interconnected control scheme may easily lead to a circular reasoning, and to stability issues.

For years, multi-time-scale analysis has been exploited to derive modular struc-

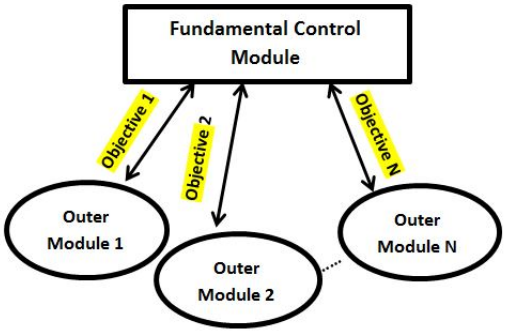

Figure 5.1: A description of the proposed control scheme.

tures [Simon 1962]. In a mathematical sense, dynamical systems that exhibit multi-time-scale behavior can be described as singularly perturbed systems. The most prominent feature of singularly perturbed systems is that the derivatives of their partial states are multiplied by a small positive parameter ε which is used to quantify the time-scale decomposition [Del Vecchio 2013, Chen 2013, Yang 2011, Petersen 2013, Teel 2003]. Based on singular perturbation theory, lower-order subsystems in different time scales can be derived to approximate the behavior of the original system. The main results of singular perturbation theory have existed for several decades [Kokotovic 1968, Kokotovic 1976, Kokotovic 1999, Khalil 1996] and they have been widely applied in the context of the dynamic modeling and analysis of power systems [Kokotovic 1980, Winkelman 1980, Xu 1998, Peponides 1982, Martinez 2007, Xin 2010, Pekarek 2002, Xu 2000]. In [Kokotovic 1980], an iterative approach for time-scale separation is proposed, which improves the accuracy of the lower-order subsystems. Furthermore, an application of this iterative separation method is presented in [Winkelman 1980] where a 20^{th} order model of a three-machine power system is analyzed as a two-time-scale and a four-time-scale systems. Reference [Xu 1998] investigates the reformulation of a full model of generators and their controllers, which demonstrates that singular perturbation method can provide an effective approach to simulating the system behavior. Recently, singular perturbation theory is also employed in analyzing some power electronics. In [Kimball 2008], singular perturbation theory is applied to analyze DC-DC converters and a rigorous demonstration of the time-scale separation is also given. In those prior works, the considered power systems or power converters can be usually modeled by a standard form of singularly perturbed system, which means that ε can be directly obtained from the system model. However, many nonlinear systems are not expressed in the standard form. It means that ε cannot be deduced directly from the system parameters. In this case, high-gain technique, which has the ability to reduce some effects of disturbances, provides a design approach such that the multi-time-scale dynamics can be created by the control gains. There are many studies devoted to the use of high-gain feedback applied to control problems [Khalil 1987, Marino 1985, Young 1977, Marino 1988, Krishnamurthy 2007, Krishnamurthy 2013]. Our inter-

est here is the linkage between the high-gain technique and the singularly perturbed system. In general, a nonlinear system with a high-gain control can be analyzed as a singular perturbed system [Marino 1985, Krishnamurthy 2013].

In this thesis, we further investigate the use of high-gain and singular perturbation techniques to develop a systematic control method for a class of nonlinear systems with multiple inputs and multiple outputs. The control system is desired to separate the original system into different time-scale subsystems, with the aim of creating a "plug and play" characteristic. Here we define a class of nonlinear systems in the form

$$\begin{aligned} \dot{x} &= f_1(x,y) + g_1(x,y)u \\ \dot{y} &= f_2(x,y) \end{aligned} \tag{5.1}$$

where $x \in D_x \subset \mathbb{R}^n$ and $y \in D_y \subset \mathbb{R}^m$ are the state variables and $u \in D_u \subset \mathbb{R}^n$ is the control input. $f_{1,2}$ and g_1 are continuously differentiable in their arguments for $(t,\ x,\ y) \in [0,\ t_f] \times D_x \times D_y$. This type of nonlinear system is similar to underactuated mechanical system [Spong 1994] where the system's degree of freedom is larger than the actuated degree of freedom. In addition, part of the state variables, i.e. x, is collocated with the input u. We first divide the full system into two subsystems, i.e. a driving subsystem and a driven subsystem represented by the dynamics of x and y in (5.1), respectively and then, we develop a subcontroller such that the driving subsystem quickly enters an arbitrary manifold x^* yet to be designed. During the design process of such subcontroller, the dynamics of x^* are neglected. The fundamental control module is then established, which is composed of the driving subsystem and its subcontroller. The interaction between the fundamental and the outer control modules is given by x^*. Different outer control modules could provide different corresponding manifolds. It is true that not all x^* from the outer modules can be accepted by the fundamental control module. Therefore, in this work, a rigorous theoretical analysis based on singular perturbation theory is carried out, from which conditions on the design of the fundamental and the outer control modules are derived to ensure the system stability. We further investigate the importance of the time-scale separation between the fundamental and the outer control modules based on Lyapunov theory.

5.1.2 Problem formulation

Considering the nonlinear system (5.1), we assume that it can be expressed as

$$\begin{aligned} \dot{x}_1 &= f_{11}(x_1,x_2,y_1,y_2) + g_{11}(x_1,x_2,y_1,y_2)u \\ \dot{x}_2 &= f_{12}(x_1,x_2,y_1,y_2) + g_{12}(x_1,x_2,y_1,y_2)u \end{aligned} \tag{5.2}$$

$$\begin{aligned} \dot{y}_1 &= f_{21}(x_1,x_2,y_1,y_2) \\ \dot{y}_2 &= f_{22}(x_1,x_2,y_1,y_2) \end{aligned} \tag{5.3}$$

where the system states x and y are partitioned into two vector parts, $x_1 \in D_{x_1} \subset \mathbb{R}^p$, $x_2 \in D_{x_2} \subset \mathbb{R}^{n-p}$, $y_1 \in D_{y_1} \subset \mathbb{R}^{m+p-n}$ and $y_2 \in D_{y_2} \subset \mathbb{R}^{n-p}$. p is a non-negative integer and satisfies $n-m \leq p \leq n$. In addition, D_x and D_y satisfy $D_x =$

$\{(x_1,\ x_2) \mid x_1 \in D_{x_1}$ and $x_2 \in D_{x_2}\}$ and $D_y = \{(y_1,\ y_2) \mid y_1 \in D_{y_1}$ and $y_2 \in D_{y_2}\}$. The functions f_{ij} and g_{1j} with $i, j = 1, 2$ are continuously differentiable in their arguments. We define the control output as

$$s \triangleq [x_1\ y_2]^T \in \mathbb{R}^n \tag{5.4}$$

Let s^o, i.e. $[x_1^o\ y_2^o]^T$, be a prescribed setpoint. The main purpose of this work is to establish a flexible control scheme that regulates s at the prescribed setpoint s^o and at the same time, ensures the system stability. Here, we first introduce the following assumptions to describe the characteristics of the system (5.2)-(5.3).

Assumption 5.1.1. *For a given $s^o = [x_1^o\ y_2^o]^T$, there exist corresponding steady values of $\bar{x}_1$, $\bar{x}_2$, $\bar{y}_1$, $\bar{y}_2$ and $\bar{u}$ such that*

$$\begin{aligned} 0 &= f_{11}(\bar{x}_1, \bar{x}_2, \bar{y}_1, \bar{y}_2) + g_{11}(\bar{x}_1, \bar{x}_2, \bar{y}_1, \bar{y}_2)\bar{u} \\ 0 &= f_{12}(\bar{x}_1, \bar{x}_2, \bar{y}_1, \bar{y}_2) + g_{12}(\bar{x}_1, \bar{x}_2, \bar{y}_1, \bar{y}_2)\bar{u} \\ 0 &= f_{21}(\bar{x}_1, \bar{x}_2, \bar{y}_1, \bar{y}_2) \\ 0 &= f_{22}(\bar{x}_1, \bar{x}_2, \bar{y}_1, \bar{y}_2) \\ x_1^o &= \bar{x}_1 \\ y_2^o &= \bar{y}_2 \end{aligned} \tag{5.5}$$

where $\bar{x}_1 \in D_{x_1}$, $\bar{x}_2 \in D_{x_2}$, $\bar{y}_1 \in D_{x_1}$ and $\bar{y}_2 \in D_{y_2}$. We denote $\bar{P}_1 = [\bar{x}_1\ \bar{x}_2\ \bar{y}_1\ \bar{y}_2]^T$ as the equilibrium point.

Under Assumption 5.1.1, the existence of the equilibrium point of the system (5.2)-(5.3) is ensured, which implies the physical feasibility of the system.

Assumption 5.1.2. *f_{ij}, g_{1j} and their partial derivatives up to the first order are continuously differentiable and bounded in $[0,\ t_f] \times D_{x_1} \times D_{x_2} \times D_{y_1} \times D_{y_2}$ where $i, j = 1, 2$.*

Assumption 5.1.3. *For $(x,\ y) \in D_x \times D_y$, $g_1 = [g_{11}\ g_{12}]^T$ is non-singular and g_1^{-1} is continuously differentiable.*

With Assumptions 5.1.2-5.1.3, the functions f_{ij}, g_{1j} and g_1^{-1} are locally Lipschitz, as continuous functions are locally bounded and hence their gradients are locally bounded as well.

Assumption 5.1.4. *Consider the following subsystem with Assumption 5.1.1*

$$\begin{aligned} \dot{y}_1 &= f_{21}(x_1^o, x_2, y_1, y_2) \\ \dot{y}_2 &= f_{22}(x_1^o, x_2, y_1, y_2) \end{aligned} \tag{5.6}$$

where x_2 can be viewed as the auxiliary control input. It is obvious that $\bar{P}_2 = [\bar{y}_1\ \bar{y}_2]^T$ is an equilibrium of the subsystem (5.6) as $x_2 = \bar{x}_2$. We suppose that information of $x_2 = h_2(y_1, y_2, x_1^o, y_2^o) \in D_{x_2}$ is available such that:

1) *The function h_2 yet to be designed has continuous first partial derivatives with respect to its arguments. In addition, when $y_2 = y_2^o$, we have*

$$h_2(\bar{y}_1, \bar{y}_2, x_1^o, y_2^o) = \bar{x}_2$$

2) $\bar{P}_2 = [\bar{y}_1\ \bar{y}_2]^T$ *is an equilibrium of the following closed-loop system*

$$\begin{aligned} \dot{y}_1 &= f_{21}(x_1^o, h_2, y_1, y_2) \\ \dot{y}_2 &= f_{22}(x_1^o, h_2, y_1, y_2) \end{aligned} \tag{5.7}$$

Moreover, $\bar{P}_2$ *is exponentially stable in a region* $(y_1,\ y_2) \in B_{y_1} \times B_{y_2}$ *where* $B_{y_1} \subset D_{y_1}$ *and* $B_{y_2} \subset D_{y_2}$.

To get a better understanding of Assumption 5.1.2-5.1.4, we consider the following example

$$\begin{aligned} \begin{bmatrix} \dot{x}_1 \\ \dot{x}_2 \end{bmatrix} &= \begin{bmatrix} x_1x_2 + x_1y_1 - 2 \\ x_1^2 + x_2y_1 - 1 \end{bmatrix} + \begin{bmatrix} x_1 & 0 \\ y_1 & x_1x_2 \end{bmatrix} \begin{bmatrix} u_1 \\ u_2 \end{bmatrix} \\ \dot{y}_1 &= x_1y_1 - x_2 \\ s &= [x_2\ y_1]^T \end{aligned} \tag{5.8}$$

where $x_{1,2} \in [0.5, 1.5]$, $y_1 \in [0.5, 2]$ and $s^o = [1\ 1]^T$.

Assumption 5.1.2 is satisfied due to the boundedness of $x_{1,2}$ and $y_{1,2}$. Since $(\bar{x}_1, \bar{x}_2, \bar{y}_1, \bar{y}_2, \bar{u}_1, \bar{u}_2) = (1, 1, 1, 1, 0, -1)$ that satisfies (5.8), Assumption 5.1.1 is also verified. The inverse matrix of g_1 can be deduced as:

$$g_1^{-1} = \begin{bmatrix} \frac{1}{x_1} & 0 \\ -\frac{y_1}{x_1^2x_2} & \frac{1}{x_1x_2} \end{bmatrix}$$

which is continuously differentiable for $x_{1,2} \in [0.5, 1.5]$ and $y_1 \in [0.5, 2]$. Thus, Assumption 5.1.3 is satisfied. When $x_2 = 1$, the subsystem of (5.8) becomes:

$$\dot{y}_1 = x_1y_1 - 1 \tag{5.9}$$

In this way, x_1 is the auxiliary control input of (5.9). Then, x_1 can be designed as:

$$x_1 = h_2 = \frac{-(y_1 - 1) + 1}{y_1}$$

such that the closed-loop system of (5.9) becomes:

$$\dot{y}_1 = -(y_1 - 1)$$

whose equilibrium $\bar{y} = 1$ is exponentially stable. Finally, Assumption 5.1.4 is verified.

5.1.3 Control design

In general, control algorithms are strongly related to the system control objectives. Once these control objectives are changed, the existing controller usually has to be decommissioned and then, new control algorithms need to be re-engineered from scratch. For example, considering the studied system (5.2)-(5.3), there exist two different outputs, i.e. $s_1 = [x_1^1\ y_2^1]^T \in \mathbb{R}^n$ and $s_2 = [x_1^2\ y_2^2]^T \in \mathbb{R}^n$ where $x_1^1 \in \mathbb{R}^{p_1}$, $x_1^2 \in \mathbb{R}^{p_2}$ and $p_1 \neq p_2$. We apply input-output feedback linearization methodology

to design the control scheme. When the system is required to track the reference from s_1 to s_2, the entire control scheme must be redesigned since the corresponding Lie derivatives are totally changed. Here, we aim at establishing a more flexible control scheme such that different control objectives can be achieved based on the existing control structure.

The described system (5.2)-(5.3) has fewer control inputs (n) than state variables ($n+m$). In addition, u has an explicit effect on x and they have the same degree of freedom. The above aspects prompt us to divide the full system into two interconnected subsystems. The state variable x collocated with the control input u is called the driving state. We denote the dynamics of $x_{1,2}$ described by (5.2) as the driving subsystem. As seen in (5.3), x_1 and x_2 can be viewed as the control inputs, which implies that u indirectly influences the behavior of y through x. Hence, y and (5.3) is called the driven state and the driven subsystem. Such solution to the division of the full system into two parts is inspired by underactuated mechanical systems [Spong 1994].

We suppose that the proposed control scheme can make the system (5.2)-(5.3) exhibit a multi-time-scale behavior where the driving subsystem has much faster dynamics than the driven subsystem. Based on this assumption, the two subsystems can be then designed independently.

5.1.3.1 Design of the driving subsystem

Step 5.1.5. *For a given $x_0 \in D_x$, let us impose the following autonomous system*

$$\dot{x} = -A_1(x - x_0) + r_1(x, x_0) \tag{5.10}$$

where $A_1 = diag(a_{1i}) \in \mathbb{R}^{n\times n}$ yet to be designed. We denote $a_1 = \min(a_{11}, \cdots, a_{1n})$. The system (5.10) is designed as

1. *$r_1(x, x_0)$ is a continuously differentiable function and $r_1(x_0, x_0) = 0$. As a consequence, for a positive γ_1, there exists $b_1 > 0$ such that, when $x \in B_{x_1} = \{x \in D_x | \ ||x - x_0|| < b_1\}$, we have*

$$||r_1(x, x_0)|| < \gamma_1 ||x - x_0|| \tag{5.11}$$

2. *a_1 is assigned to satisfy*

$$\gamma_1 + c_1 \leq a_1$$

where c_1 is a positive parameter.

Lemma 5.1.6. *The equilibrium point $x = x_0$ of (5.10) is exponentially stable in B_{x_1}.*

Proof. We choose the Lyapunov function as

$$V_1(x - x_0) = \frac{1}{2}(x - x_0)^T(x - x_0)$$

The derivative of V_1 along the trajectory of (5.10) is

$$\begin{aligned}\dot{V}_1 \leq & -||A_1||\ ||x-x_0||^2 + (x-x_0)^T r_1(x,x_0) \\ \leq & -(a_1-\gamma_1)||x-x_0||^2 = -c_1||x-x_0||^2\end{aligned} \tag{5.12}$$

Hence, Lemma (5.1.6) is proved. □

The values of γ_1, a_1 and b_1 are strongly dependent on each other. For example, considering the following system

$$\dot{x} = -ax + x^3 - x$$

we then have $x_0 = 0$, $a_1 = a$ and $r_1 = x^3 - x$. If $\gamma_1 = 3$, there exists $b_1 = 2$ such that (5.11) is satisfied. In this case, a_1 should be chosen larger than $3 + c_1$. If a larger γ_1 is given, i.e. $\gamma_1 = 8$, a new $b_1 = 3$ is then deduced. We obtain a new condition for a_1, i.e. $a_1 > 9 + c_1$. It is clear that a larger γ_1 results in a smaller feasible region for a_1.

When γ_1 is fixed, the linear term $-A_1(x - x_0)$ dominates the behavior of the autonomous system (5.10) in B_{x_1}. Consequently, the dynamics of (5.10) can be regulated by A_1.

Step 5.1.7. *Supposing that there exists a reference $x^* \in D_x$ and with the acknowledge of (5.10), we then develop a subcontroller $u = h_1(x, y, x^*)$ as*

$$u = g_1^{-1}(x,y)[-A_1(x-x^*) + r_1(x,x^*) - f_1(x,y)] \tag{5.13}$$

such that the closed-loop system of the driving subsystem becomes

$$\dot{x} = -A_1(x-x^*) + r_1(x,x^*)$$

The only information on x^* is that it has a much slower dynamic than x. As seen in (5.13), the derivative of x^* is neglected in the subcontroller.

5.1.3.2 Design of the driven subsystem

Step 5.1.8. *The main task in this step is to develop the unknown reference x^* that must be tracked by the driving subsystem. Since we suppose that x^* has a very slow dynamic, a large a_1 can then be chosen such that the state variable of the driving subsystem x quickly enters x^*. Then, the driven subsystem becomes*

$$\begin{aligned}\dot{y}_1 &= f_{21}(x_1^*, x_2^*, y_1, y_2) \\ \dot{y}_2 &= f_{22}(x_1^*, x_2^*, y_1, y_2)\end{aligned} \tag{5.14}$$

which is called the reduced model. Because x_1 is required to track its reference trajectory, x_1^* can be directly given by:

$$x_1^* = x_1^o \tag{5.15}$$

Thus, the reduced model (5.14) *becomes*

$$\begin{aligned}\dot{y}_1 &= f_{21}(x_1^o, x_2^*, y_1, y_2)\\ \dot{y}_2 &= f_{22}(x_1^o, x_2^*, y_1, y_2)\end{aligned} \tag{5.16}$$

According to Assumption 5.1.4, there exists

$$x_2^* = h_2(y_1, y_2, x_1^o, y_2^o) \tag{5.17}$$

such that the reduced model (5.14) *is exponentially stable.*

Until now, the entire control algorithm is developed, consisting of two subcontrollers, i.e. $u = h_1(x, y, x^*)$ and $x^* = [x_1^o \; h_2(y_1, y_2, x_1^o, y_2^o)]^T$, which are derived from two lower order subsystems, i.e. the driving and the driven subsystems. As mentioned in the previous section, the driving subsystem (5.2) with its subcontroller $u = h_1$ composes the fundamental control module and the reduced model of the driven subsystem (5.14) with its subcontroller x^* constitutes the outer control module. Furthermore, the proposed control structure has plug and play capabilities. When a new objective is required, we only need to design a new corresponding outer control module that provides a new x^* to the fundamental control module without abandoning the whole existing control structure. Different outer control modules share the same fundamental control module. x^* is thus considered as the tie that binds the fundamental and the outer control modules together. In addition, the new outer control module is designed based on the reduced model where the dynamics of x are neglected. This greatly simplifies the problem.

5.1.4 Theoretical study

During the design procedure in Section 5.1.3, we assume that the dynamics of the driving and the driven subsystems can be divided into different time scales with the aid of the proposed control methodology. In this section, we first verify this assumption by means of singular perturbation theory. Subsequently, we carry out a theoretical stability analysis, from which sufficient conditions for the construction of the fundamental and the outer control modules are derived.

5.1.4.1 Multi-time-scale dynamics

In this section, we present how the system (5.2)-(5.3) exhibits a multi-time-scale behavior under the proposed controller. Substituting the control algorithm (5.13), (5.15) and (5.17) into the original system (5.1), we then obtain the following closed-loop system

$$\begin{aligned}\dot{x} &= -A_1(x - x^*) + r_1(x, x^*)\\ \dot{y} &= f_2(x, y)\end{aligned} \tag{5.18}$$

Let us introduce a new variable ε which satisfies

$$\varepsilon \cdot a_1 = 1$$

The system (5.18) can be rewritten as

$$\begin{aligned} \varepsilon\dot{x} &= -A_{1\varepsilon}(x - x^*) + \varepsilon r_1(x, x^*) \\ \dot{y} &= f_2(x, y) \end{aligned} \tag{5.19}$$

where $A_{1\varepsilon} = \text{diag}(\varepsilon a_{1i})$. Denoting $a_{1i_\varepsilon} = \varepsilon a_{1i}$, we then have $a_{1i_\varepsilon} \geq 1$[1], for all $i = 1, \cdots, n$. When ε is small enough, our problem (5.19) becomes a standard singular perturbation problem. By setting $\varepsilon = 0$, the driving subsystem is degenerated into the algebraic loop, i.e. $A_{1\varepsilon}(x - x^*) = 0$, from which we can get the isolated root $x = x^*$. We call x^* the quasi-steady state of x. By recalling that $x_1^* = x_1^o$ in (5.15) and $x_2^* = h_2$ in (5.17), we substitute $x = x^*$ into the driven subsystem and then obtain

$$\dot{y} = f_2(x_1^o, h_2(y, x_1^o, y_2^o), y) \tag{5.20}$$

Due to Assumption 5.1.4, the equilibrium point $\bar{P}_2$ of the reduced model (5.20) is exponentially stable in B_{y_1}. In addition, we denote the solution of (5.20) as y^{re}.

In order to analyze the closed-loop system (5.19) more conveniently, we introduce the following new variables

$$\begin{aligned} &\tilde{x}_1 = x_1 - x_1^*;\ \tilde{x}_2 = x_2 - x_2^*;\ \tilde{x} = [\tilde{x}_1\ \tilde{x}_2]^T \\ &\tilde{y}_1 = y_1 - \bar{y}_1;\ \tilde{y}_2 = y_2 - \bar{y}_2;\ \tilde{y} = [\tilde{y}_1\ \tilde{y}_2]^T \end{aligned}$$

In these new variables, the system (5.19) is rewritten as

$$\begin{aligned} \varepsilon\dot{\tilde{x}} &= -A_{1\varepsilon}\tilde{x} + \varepsilon r_1(\tilde{x} + x^*, x^*) - \varepsilon\frac{dx^*}{dt} \\ \dot{\tilde{y}} &= f_2(\tilde{x} + x^*, \tilde{y} + \bar{y}) \end{aligned} \tag{5.21}$$

with $x^* = [x_1^o\ h_2(\tilde{y} + \bar{y})]^T$. The origin is the equilibrium point of the system (5.21). Moreover, there exist maps such that $D_x \to \tilde{D}_{\tilde{x}}$ and $D_y \to \tilde{D}_{\tilde{y}}$. The (asymptotic) stability of the origin of the error system (5.21) implies the (asymptotic) stability of the equilibrium $\bar{P}_1$ of the system (5.18).

Let us introduce a new time scale τ which satisfies

$$\varepsilon\frac{d\tilde{x}}{dt} = \frac{d\tilde{x}}{d\tau}$$

In the τ time scale, the variables t, $\tilde{y}$ and x^* are considered slowly varying. We rewrite the dynamics of $\tilde{x}$ (in (5.21)) in the τ time scale

$$\frac{d\tilde{x}}{d\tau} = -A_{1\varepsilon}\tilde{x} + \varepsilon r_1(\tilde{x} + x^*, x^*) - \varepsilon[0\ \frac{\partial h_2}{\partial \tilde{y}} f_2]^T$$

When setting $\varepsilon = 0$ and freezing t, $\tilde{y}$ and x^* at their initial values, we get the boundary-layer system

$$\frac{d\tilde{x}}{d\tau} = -A_{1\varepsilon}\tilde{x} \tag{5.22}$$

[1] See the definition of a_1 in (5.10).

whose equilibrium is exponentially stable, uniformly in $(t, \tilde{y})$. Substituting $\tilde{x} = 0$, the reduced model of (5.21) is deduced as

$$\dot{\tilde{y}} = f_2(x_1^o, h_2(\tilde{y} + \bar{y}, x_1^o, y_2^o), \tilde{y} + \bar{y}) \tag{5.23}$$

The above system has an exponentially stable equilibrium at the origin for all $\tilde{y}(t_0) \in \tilde{B}_{y_1}$ where $\tilde{B}_{y_1}$ can be deduced from B_{y_1} based on Assumption 5.1.4.

Now, we can state the following result.

Theorem 5.1.9. *Consider the nonlinear system (5.19) with Assumptions 5.1.1-5.1.4 where $x \in D_x$ and $y \in D_y$. For any given $A_{1\varepsilon}$, there exists a positive ε^* and a region $\mathcal{R}_{xy} \subset D_x \times D_y$ such that for all $0 < \varepsilon < \varepsilon^*$ and $(x(t_0), y(t_0)) \in \mathcal{R}_{xy}$, the trajectories of the state variables can be approximated by*

$$\begin{aligned} x(t) &= x^{re}(t) + \tilde{x}(t/\varepsilon) + O(\varepsilon) \\ y(t) &= y^{re}(t) + O(\varepsilon) \end{aligned}$$

where $x^{re}(t) = [x_1^o \ h_2(y^{re}(t), x_1^o, y_2^o)]$.

Proof. As presented in the previous parts:

- The reduced model (5.20) has a unique solution y^{re} that converges to $\bar{P}_2$.
- The equilibrium of the boundary-layer model (5.22) is exponentially stable, uniformly in $(t, \tilde{y})$.

Theorem 5.1.9 is then proved by direct apprehension of Theorem 11.1 in [Khalil 1996]. □

From the above description, x exhibits a multi-time-scale behavior. During the initial interval, x quickly converges to its manifold x^*, which represents a fast dynamic. After the decay of the fast transient $\tilde{x}(t/\varepsilon)$, x remains close to x^* in the future time. It is notable that the small positive parameter ε in the singularly perturbed system (5.18) is not derived from the physical system, but is created by the subcontroller $u = h_1(x, y, x^*)$. It is shown that, even though the system has no inherent multi-time-scale dynamics, we can artificially create them by the proposed control strategy.

5.1.4.2 Stability analysis

Theorem 5.1.9 guarantees the existence of the proposed time-scale separation controller. In this section, we carry out a detailed stability analysis, from which sufficient conditions on the developed controller can be derived by means of Lyapunov theory.

In order to facilitate the analysis, we rewrite the system (5.21)

$$\begin{aligned} \varepsilon\dot{\tilde{x}}_1 &= -A_{1\varepsilon}^1 \tilde{x}_1 + \varepsilon r_{11} \\ \varepsilon\dot{\tilde{x}}_2 &= -A_{1\varepsilon}^2 \tilde{x}_2 + \varepsilon r_{12} - \varepsilon \frac{d\Delta_{h_2\tilde{y}}}{dt} \\ \dot{\tilde{y}} &= \Delta_{f_2\tilde{x}} + \phi(\tilde{y}) \end{aligned} \tag{5.24}$$

where

$$\begin{aligned}
\begin{bmatrix} A^1_{1\varepsilon} & 0 \\ 0 & A^2_{1\varepsilon} \end{bmatrix} &= A_{1\varepsilon};\ [r_{11}\ r_{12}]^T = r_1 \\
\phi(\tilde{y}) &= f_2(x_1^o, h_2(\tilde{y}+\bar{y}, x_1^o, y_2^o), \tilde{y}+\bar{y}) \\
f_2(\tilde{x}+x^*, \tilde{y}+\bar{y}) &= \underbrace{f_2(\tilde{x}+x^*, \tilde{y}+\bar{y}) - f_2(x^*, \tilde{y}+\bar{y})}_{\Delta_{f_2\tilde{x}}} + \phi \\
h_2(\tilde{y}+\bar{y}, x_1^o, y_2^o) &= \underbrace{h_2(\tilde{y}+\bar{y}, x_1^o, y_2^o) - h_2(\bar{y}, x_1^o, y_2^o)}_{\Delta_{h_2\tilde{y}}} + \bar{h}_2 \\
\bar{h}_2 &= h_2(\bar{y}, x_1^o, y_2^o)
\end{aligned}$$

It can be seen that the terms $\varepsilon\dfrac{d\Delta_{h_2\tilde{y}}}{dt}$ and $\Delta_{f_2\tilde{x}}$ in (5.24) reflect the dynamic interactions between the driving and the driven subsystems. Moreover, $\Delta_{f_2\tilde{x}}$ and $\Delta_{h_2\tilde{y}}$ satisfy

$$\begin{aligned}
||\Delta_{f_2\tilde{x}}|| \to 0 \quad \text{when} \quad ||\tilde{x}|| \to 0 \\
||\Delta_{h_2\tilde{y}}|| \to 0 \quad \text{when} \quad ||\tilde{y}|| \to 0
\end{aligned}$$

Since $h_2(\tilde{y}+\bar{y}, x_1^o, y_2^o)$ and $f_2(\tilde{x}+x^*, \tilde{y}+\bar{y})$ are continuously differentiable, there exist positive $L_{1\tilde{x}}$ and $L_{1\tilde{y}}$ such that

$$\begin{aligned}
||\Delta_{f_2\tilde{x}}|| &\leq L_{1\tilde{x}}||\tilde{x}|| \\
||\Delta_{h_2\tilde{y}}|| &\leq L_{1\tilde{y}}||\tilde{y}||
\end{aligned} \tag{5.25}$$

for $\tilde{x} \in \Omega_{1\tilde{x}} \subset \tilde{D}_{\tilde{x}}$ and $\tilde{y} \in \Omega_{1\tilde{y}} \subset \tilde{D}_{\tilde{y}}$.

Since the reduced model (5.23) is exponentially stable in $\tilde{B}_{y_1} \subset \tilde{D}_{\tilde{y}}$, there exists a Lyapunov function V_0 satisfying

$$\begin{aligned}
c_1||\tilde{y}||^2 \leq V_2(\tilde{y}) &\leq c_2||\tilde{y}||^2 \\
\frac{\partial V_2}{\partial \tilde{y}}\phi(\tilde{y}) &\leq -c_3||\tilde{y}||^2 \\
||\frac{\partial V_2}{\partial \tilde{y}}|| &\leq c_4||\tilde{y}||
\end{aligned} \tag{5.26}$$

for positive constants $c_i, i = 1, \cdots, 4$.

According to Taylor's theorem, ϕ can be rewritten as

$$\phi(\tilde{y}) = A_\phi \tilde{y} + g_\phi(\tilde{y})\tilde{y} \tag{5.27}$$

which is called the Peano form of the remainder where

$$\begin{aligned}
A_\phi &= \frac{\partial \phi}{\partial \tilde{y}}|_{\tilde{y}=0} \\
\lim_{\tilde{y}\to 0} g_\phi(\tilde{y}) &= 0
\end{aligned} \tag{5.28}$$

Equation (5.28) means that, for any given $L_{1\phi} > 0$, there exists a positive b_2 such that

$$||g_\phi(\tilde{y})|| \leq L_{1\phi} \tag{5.29}$$

for all $\tilde{y} \in \tilde{B}_{y_2} = \{\tilde{y} \in \tilde{D}_{\tilde{y}} | \ ||\tilde{y}|| \leq b_2\}$. It is worth noting that the values of $L_{1\tilde{x}}$ and $L_{1\tilde{y}}$ depend on $\Omega_{1\tilde{x}}$ and $\Omega_{1\tilde{y}}$. In general, a larger $\Omega_{1\tilde{x}}(\Omega_{1\tilde{y}})$ may result in a larger $L_{1\tilde{x}}(L_{1\tilde{y}})$. The constants $c_i, i = 1, \cdots, 4$ are also strongly related to $\Omega_{2\tilde{y}}$.

We take

$$V = dV_1(\tilde{x}) + (1-d)V_2(\tilde{y})$$

as a Lyapunov function candidate for the closed-loop system (5.24) where $d \in (0,1)$. The first part of V, $V_1(\tilde{x})$, is derived from the boundary-layer model (5.22). According to Lemma 5.1.6, the origin of the system

$$\dot{\tilde{x}} = -A_1\tilde{x} + r_1(\tilde{x})$$

is exponentially stable in $\tilde{B}_{x_1}$ which corresponds to B_{x_1}. The second term V_2 is obtained from the reduced model. The composition of $V(\tilde{x}, \tilde{y})$ in this way provides us a easier way to search the feasible region of ε.

The derivative of V along the trajectories (5.24) can be then deduced as

$$\begin{aligned}\dot{V} =& d[-\tilde{x}^T A_1\tilde{x} + \tilde{x}^T r_1 - \tilde{x}_2^T \frac{\partial \Delta_{h_2\tilde{y}}}{\partial \tilde{y}}(\Delta_{f_2\tilde{x}} + \phi)] \\ &+ (1-d)\frac{\partial V_2}{\partial \tilde{y}}(\Delta_{f_2\tilde{x}} + \phi)\end{aligned} \tag{5.30}$$

Applying the inequalities (5.12) and (5.26) to (5.30), we have

$$\begin{aligned}\dot{V} \leq& -dc_1||\tilde{x}||^2 - (1-d)c_3||\tilde{y}||^2 + (1-d)\frac{\partial V_2}{\partial \tilde{y}}\Delta_{f_2\tilde{x}} \\ &- d\tilde{x}_2^T \frac{\partial \Delta_{h_2\tilde{y}}}{\partial \tilde{y}}(\Delta_{f_2\tilde{x}} + A_\phi\tilde{y} + g_\phi\tilde{y}) \\ \leq& -dc_1||\tilde{x}||^2 - (1-d)c_3||\tilde{y}||^2 + (1-d)||\frac{\partial V_2}{\partial \tilde{y}}||\ ||\Delta_{f_2\tilde{x}}|| \\ &+ d||\tilde{x}_2||\ ||\frac{\partial \Delta_{h_2\tilde{y}}}{\partial \tilde{y}}||\ [\ ||\Delta_{f_2\tilde{x}}|| \\ &+ (\ ||g_\phi|| + ||A_\phi||\ )||\tilde{y}||\ ]\end{aligned} \tag{5.31}$$

When $\tilde{x} \in \tilde{B}_{x_1} \cap \Omega_{1\tilde{x}}$, $\tilde{y} \in \tilde{B}_{y_2} \cap \tilde{B}_{y_1} \cap \Omega_{1\tilde{y}} \cap \Omega_{2\tilde{y}}$, and by using (5.25), (5.26), (5.29),

the inequality (5.31) satisfies

$$\begin{aligned}\dot{V} \leq & -dc_1||\tilde{x}||^2 - (1-d)c_3||\tilde{y}||^2 + (1-d)c_4 L_{1\tilde{x}}||\tilde{y}||\ ||\tilde{x}|| \\ & + dL_{1\tilde{y}}L_{1\phi}||\tilde{x}_2||\ ||\tilde{x}|| \\ & + dL_{1\tilde{y}}(L_{1\phi} + \sigma_{\max}(A_\phi))||\tilde{x}_2||\ ||\tilde{y}|| \\ \leq & -dc_1||\tilde{x}||^2 - (1-d)c_3||\tilde{y}||^2 + (1-d)c_4 L_{1\tilde{x}}||\tilde{y}||\ ||\tilde{x}|| \\ & + dL_{1\tilde{y}}L_{1\phi}||\tilde{x}||^2 + dL_{1\tilde{y}}(L_{1\phi} + \sigma_{\max}(A_\phi))||\tilde{x}||\ ||\tilde{y}|| \\ = & -d(a_1 - \gamma_1 - L_{1\tilde{y}}L_{1\phi})||\tilde{x}||^2 \\ & - (1-d)c_3||\tilde{y}||^2 + k_1||\tilde{x}||\ ||\tilde{y}|| \end{aligned} \tag{5.32}$$

where $k_1 = (1-d)c_4 L_{1\tilde{x}} + dL_{1\tilde{y}}(L_{1\phi} + \sigma_{\max}(A_\phi))$. Considering Young's inequality for the product

$$||\tilde{x}||\ ||\tilde{y}|| \leq \frac{1}{2m}||\tilde{x}||^2 + \frac{m}{2}||\tilde{y}||^2 \tag{5.33}$$

where m is positive, the derivative of V satisfies

$$\dot{V} \leq -k_2||\tilde{x}||^2 - k_3||\tilde{y}||^2 \tag{5.34}$$

where

$$\begin{aligned} k_2 &= d(a_1 - \gamma_1 - L_{1\tilde{y}}L_{1\phi}) - \frac{k_1}{2m} \\ k_3 &= (1-d)c_3 - \frac{mk_1}{2} \end{aligned}$$

Theorem 5.1.10. *Consider the nonlinear system (5.2)-(5.4) with Assumption 5.1.1-5.1.4. Select the control gain matrix A_1 of the subcontroller (5.13) such that k_2 and k_3 are positive. Then, the equilibrium point $(x_1^o, \bar{x}_2, \bar{y}_1, y_2^o)$ of the system (5.2)-(5.4) is asymptotically stable under the proposed time-scale separation control scheme (5.13), (5.15) and (5.17). Moreover, we can obtain an estimation of the region of attraction $\mathcal{R} = \{(\tilde{x}, \tilde{y}) \in \tilde{D}_{\tilde{x}} \times \tilde{D}_{\tilde{y}} | V(\tilde{x}, \tilde{y}) < \mathfrak{C}\}$ where $\mathfrak{C} = \min_{\tilde{x}\in\mathcal{R}_{\tilde{x}},\ \tilde{y}\in\mathcal{R}_{\tilde{y}}} V(\tilde{x}, \tilde{y})$ with $\mathcal{R}_{\tilde{x}} = \tilde{B}_{x_1} \cap \Omega_{1\tilde{x}}$ and $\mathcal{R}_{\tilde{y}} = \tilde{B}_{y_1} \cap \tilde{B}_{y_2} \cap \Omega_{1\tilde{y}} \cap \Omega_{2\tilde{y}}$.*

Proof. The proof is simple. For any fixed c_3, we can always find an m such that k_3 is positive. Once m is chosen, k_2 is positive by choosing

$$a_1 > a_1^* = \frac{k_1}{2dm}(\gamma_1 + L_{1\tilde{y}}L_{1\phi}) \tag{5.35}$$

and as a consequence, $\varepsilon < \varepsilon^* = \dfrac{1}{a_1^*}$.

For all $(\tilde{x}, \tilde{y}) \in \mathcal{R}$, it follows that for all solutions starting from $\mathcal{R}$, $\dot{V}$ is non-positive. Hence, $\mathcal{R}$ is the region of attraction [Khalil 1996] and the equilibrium point of the system (5.2)-(5.4) is stable. Since $(\tilde{x}, \tilde{y}) = (0, 0)$ is the only invariant set such that $\dot{V} = 0$ by solving (5.34), all solutions starting from $\mathcal{R}$ converge to the equilibrium point. Finally, the asymptotic stability is established and a feasible region (5.35) for a_1 (and then for ε) is also found. □

We note that the feasible region (5.35) of a_1 strongly depends on the choice of subcontroller $x_2^* = h_2(y, x_1^o, y_2^o)$. If we want to stabilize the reduced model (5.23) in a larger region, we may need a larger $L_{1\phi}$, c_3 and c_4. Alternatively, if we want to accelerate the speed of the convergence of the reduced model, it is necessary to increase $\sigma_{\max}(A_{1\phi})$. Such scenarios may result in a larger a_1^*. However, sometimes, a very large a_1 may cause a large peak value of the control input u, which is not desired. Thus, it is very important to consider associated factors when we choose a_1.

5.1.5 Study cases

In order to get a better understanding of the proposed control algorithm, two examples are studied in this section.

5.1.5.1 Example 1

Consider the following nonlinear system

$$\begin{aligned} \dot{x}_1 &= x_1 x_2 + x_3 u \\ \dot{x}_2 &= x_1 + x_3 \\ \dot{x}_3 &= x_2 + x_3 \end{aligned} \tag{5.36}$$

Two control objectives exist:

Objective 1: making $y = x_3$ track the reference x_3^o;

Objective 2: making $y = x_2$ track the reference x_2^o.

We first use the input-output feedback linearization method to design the control structure and then apply the proposed time-scale separation control scheme.

Feedback linearization control: When x_3 is the output, the system (5.36) is feedback linearizable since the relative degree of $y = x_3$ is three. Then, a controller based on input-output feedback linearization method can be developed

$$u = \frac{1}{L_g L_f^2(y)}(-L_f^3(y) + v) \tag{5.37}$$

where

$$\begin{aligned} v &= -b_0(x_3 - x_3^o) - b_1 L_f^1(y) - b_2 L_f^2(y) \\ L_f^1(y) &= x_2 + x_3 \\ L_f^2(y) &= x_1 + x_2 + 2x_3 \\ L_f^3(y) &= x_1 x_2 + x_1 + 2x_2 + 3x_3 \\ L_g L_f^2(y) &= x_3 \end{aligned}$$

The controller (5.37) is tested by numerical simulations as illustrated in Fig. 5.2. The parameter values are listed in Table 5.1. The simulation results clearly show

Table 5.1: The parameter values.

x_3^o	b_0	b_1	b_2
-3	0.125	0.75	1.5

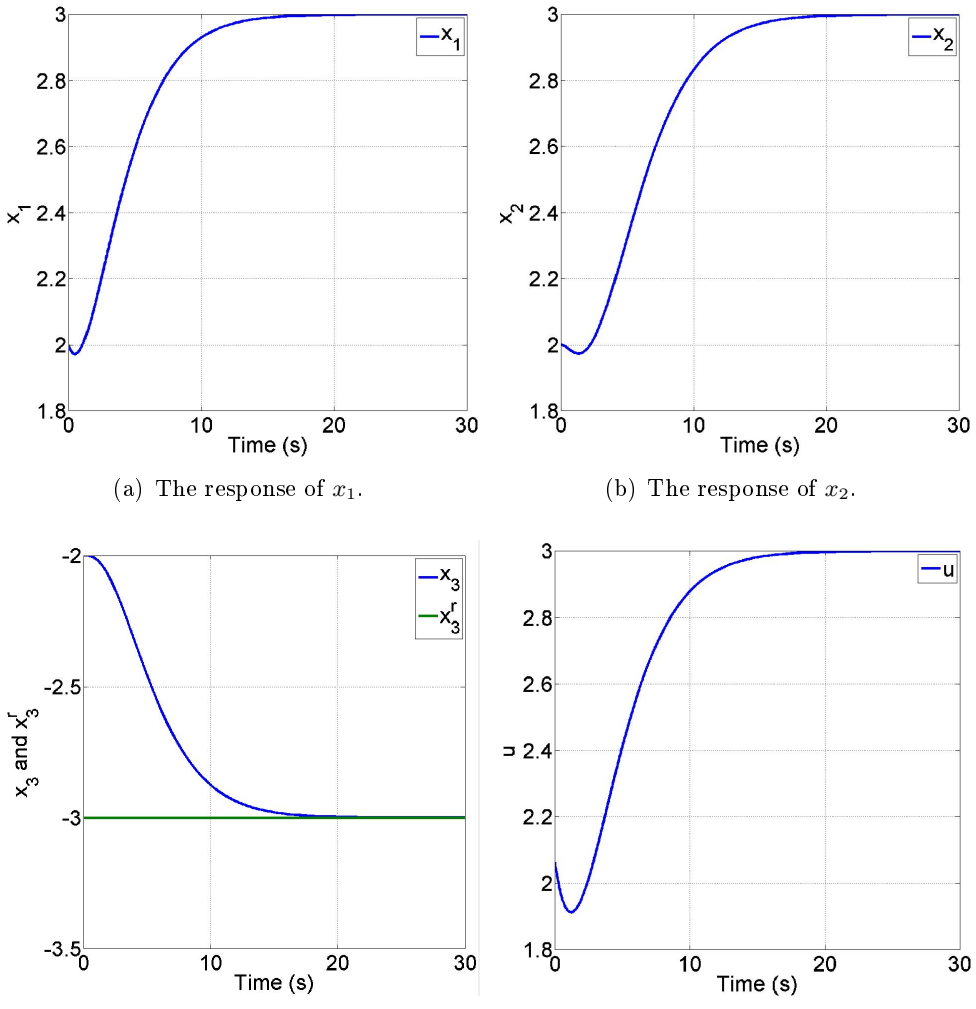

(a) The response of x_1.

(b) The response of x_2.

(c) The response of x_3 and its reference y^o.

(d) The response of u.

Figure 5.2: Simulation results by using feedback linearization.

that the controller (5.37) derived from the input-output feedback linearization method can make the system track its output trajectory.

Next, we consider that Objective 2 is to be achieved, i.e. make x_2 track its reference $y^o = 2$. In this case, the relative degree of $y = x_2$ is two, smaller than three. Thus, the zero dynamics exist and satisfy

$$\dot{x}_3 = x_3 + y^o \tag{5.38}$$

As seen in (5.38), since the zero dynamics are unstable, the system (5.36) is not feedback linearizable [Isidori 1995].

From the above description, when the control objective is changed, the input-output feedback linearization method is not practicable and we must re-design the entire control algorithm to achieve the new control objective. In the following section, we demonstrate that the proposed time-scale separation control method can realize these two objectives by just modifying the outer control modules.

Time-scale separation control: Since x_1 is directly collocated with the control input u, x_1 is considered as the driving state while x_2 and y are the driven states. The task of the fundamental control module is to make x_1 quickly enter the manifold x_1^* yet to be designed. Here, let us impose the following autonomous system

$$\begin{aligned} \dot{x}_1 &= x_1 x_2 + x_3 u \\ &= -k_1(x_1 - x_1^*) \end{aligned} \tag{5.39}$$

where $r_1 = 0$. Then u can be obtained by solving (5.39)

$$u = \frac{1}{x_3}[-k_1(x_1 - x_1^*) - x_1 x_2] \tag{5.40}$$

Note that the dynamics of x_1^* is neglected in u. When x_1 quickly enters its manifold x_1^*, we get the reduced model

$$\begin{aligned} \dot{x}_2 &= x_1^* + x_3 \\ \dot{x}_3 &= x_2 + x_3 \end{aligned} \tag{5.41}$$

where x_1^* is considered as an additional control input for the reduced model (5.41). In order to achieve Objective 1, we only need that the reduced model converges to x_3^o. Re-applying time-scale separation to (5.41), we design x_1^* such that x_2 quickly enters its manifold x_2^* yet to be designed.

$$\begin{aligned} \dot{x}_2 &= x_1^* + x_3 \\ &= -k_2(x_2 - x_2^*) \end{aligned}$$

Then, x_1^* is obtained as

$$x_1^* = -k_2(x_2 - x_2^*) - x_3 \tag{5.42}$$

At the same time, a sub-reduced model is generated as

$$\dot{x}_3 = x_2^* + x_3 \tag{5.43}$$

Table 5.2: The values of control gain (1).

	k_1	k_2	k_3
Set 1	4	2	0.125
Set 2	20	2	0.125

Table 5.3: The values of control gain (2).

	k_1	k_2	k_3
Set 1	4	2	2.25
Set 2	20	2	2.25

Finally, x_2^* can be designed as

$$x_2^* = -k_3(x_3 - x_3^o) - x_3 \tag{5.44}$$

such that the equilibrium of the sub-reduced model (5.43) is exponentially stable. In this case, the controller is composed by (5.40), (5.42) and (5.44). The system exhibits a three-time-scale behavior under the proposed controller.

Simulations are carried out with two sets of control gains as listed in Table 5.2 where k_1 in Set 2 is larger than in Set 1. Simulation results are presented in Fig. 5.3. Since both sets provide the same values of control gains to the reduced model, i.e. k_2 and k_3, the quasi-steady-states of x_1, x_2 and x_3 with $k_1 = 4$ are identical to those with $k_1 = 20$. As shown in Fig. 5.3(a)-5.3(c), a larger k_1 leads to a smaller discrepancy between the values of the state variables and their corresponding quasi-steady-state values, which exactly corresponds to our theoretical analysis.

During the design process, the time-scale separation algorithm is applied twice and x_1 and x_2 exhibit three-time-scale and two-time-scale behaviors, respectively. This example reveals that we can divide a full-scale system into multi-time-scale subsystems by re-using the proposed control approach such that these subsystems can be designed independently.

Now, when Objective 2 is to be achieved, we just need to design a new x_1^* based on the reduced model (5.41) as

$$x_1^* = -k_2(x_2 - x_2^o) - (k_3 + 1)(x_3 + x_2^o) + x_2^o$$

which can make x_2 in the reduced model converge to x_2^o.

Simulations are also carried out with two sets of control gains as listed in Table 5.3. As illustrated in Fig. 5.4, we get some similar results as in the case of Objective 1. The actual values of the state variables could be better approximated by their respective quasi-steady-state values with a larger k_1.

As mentioned in the previous section, although a larger k_1 can make the system give a fast response, it may also lead to a larger peak value of the control input during the transient. As depicted in 5.3(d)-5.4(d), the crest value of u with $k_1 = 20$ is larger than that with $k_1 = 4$.

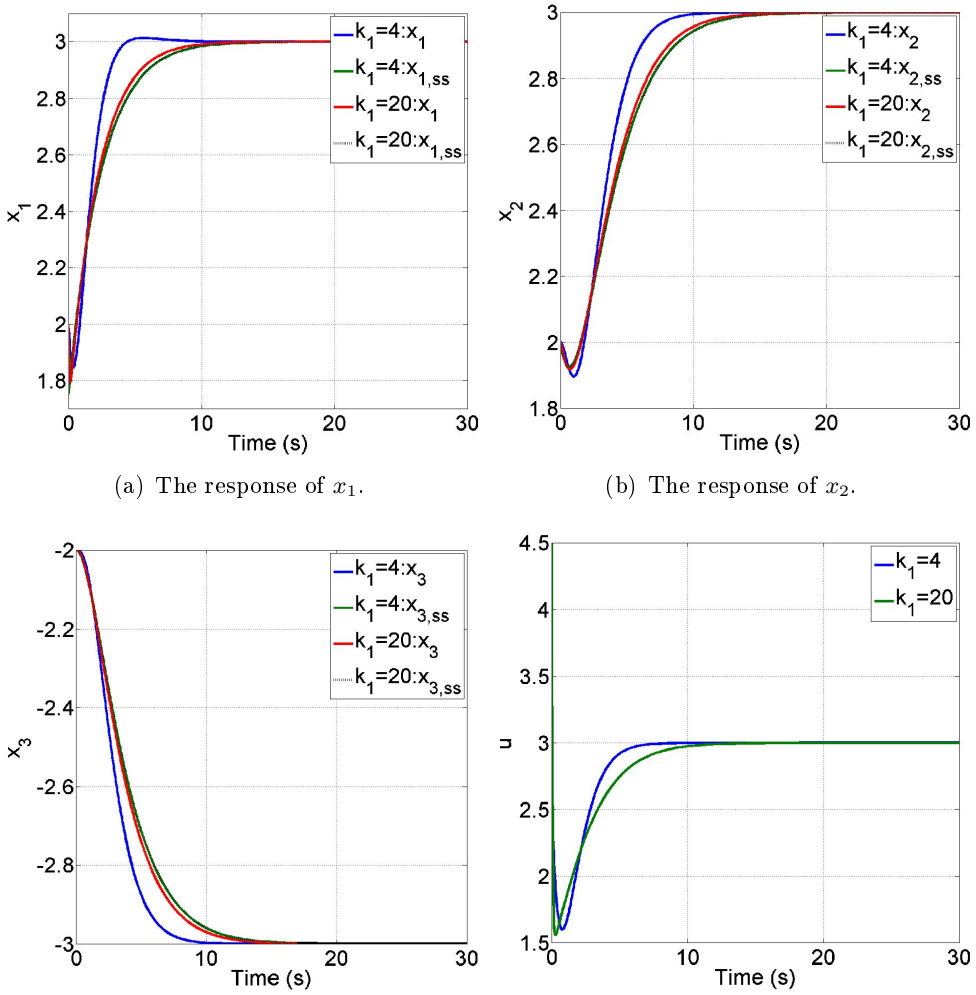

(a) The response of x_1.

(b) The response of x_2.

(c) The response of x_3 and its reference y^o.

(d) The response of u.

Figure 5.3: Simulation results by using time-scale separation control: $y = x_2$.

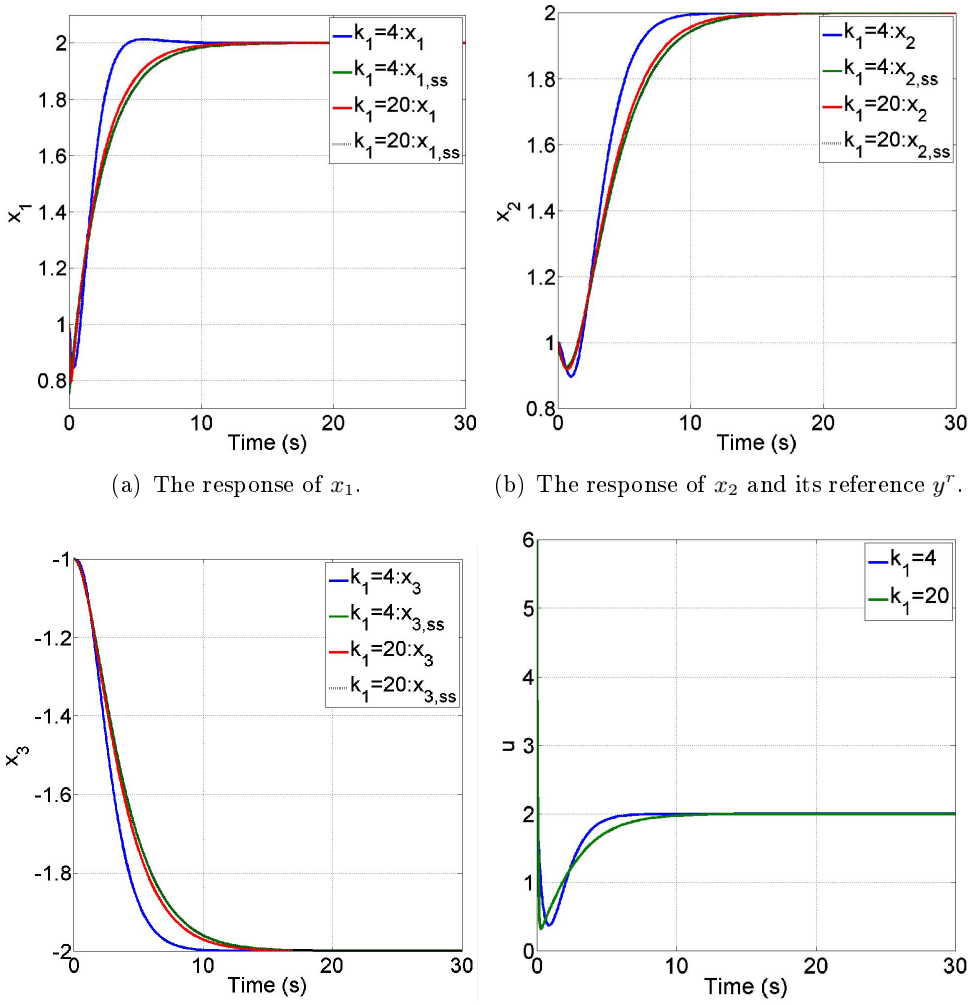

(a) The response of x_1.

(b) The response of x_2 and its reference y^r.

(c) The response of x_3.

(d) The response of u.

Figure 5.4: Simulation results by using time-scale separation control: $y = x_2$.

5.1.5.2 Example 2

The second example is expressed as

$$\begin{aligned}\dot{x}_1 &= x_1x_2 + x_3u\\ \dot{x}_2 &= x_1 + x_3\\ \dot{x}_3 &= x_2 - x_3\end{aligned} \tag{5.45}$$

which is required to achieve the same control objectives as in Example 1.

Feedback linearization control: When x_3 is defined as the output in Objective 1, (5.45) is feedback linearizable and hence, a controller by means of input/output feedback linearization is developed as

$$u = \frac{1}{L_gL_f^2(x_3)}(-L_f^3(x_3) + v) \tag{5.46}$$

where

$$\begin{aligned}v &= -b_0(x_3 - x_3^o) - b_1L_f^1(x_3) - b_2L_f^2(x_3)\\ L_f^1(x_3) &= x_2 - x_3\\ L_f^2(x_3) &= x_1x_2 + 2x_3\\ L_f^3(x_3) &= x_1x_2 - x_1 + 2x_2 - 3x_3\\ L_gL_f^2(x_3) &= x_3\end{aligned}$$

When Objective 2 is to be achieved, the relative degree of $y = x_2$ is also 2 as in Example 1. However, the zero dynamics here are expressed by

$$\dot{x}_3 = -x_3 + x_2^o \tag{5.47}$$

whose equilibrium is exponentially stable. Hence, input/output feedback linearization can be applied. The controller is developed as

$$u = \frac{1}{L_gL_f(x_2)}(-L_f^2(x_2) + v) \tag{5.48}$$

where

$$\begin{aligned}v &= -b_0(x_2 - x_2^o) - b_1L_f^1(x_2)\\ L_f^1(x_2) &= x_1 + x_3\\ L_f^2(x_2) &= x_1x_2 + x_2 - x_3\\ L_gL_f(x_2) &= x_3\end{aligned}$$

It is clear that, when the new control objective (Objective 2) is to be achieved, the existing control law (5.46) becomes invalid and should be rejected. The control design must be re-engineered to develop a new control algorithm (5.48). For a system of very high order, it is very time-consuming to re-design the control structure. However, the time-scale separation control scheme proposed in this section can effectively avoid a control re-design from scratch.

Time-scale separation control: First, we design the fundamental module as in Example 1

$$\begin{aligned} \dot{x}_1 &= x_1 x_2 + x_3 u \\ &= -k_1(x_1 - x_1^*) \end{aligned} \tag{5.49}$$

and then u can be obtained by solving (5.49)

$$u = \frac{1}{x_3}[-k_1(x_1 - x_1^*) - x_1 x_2]$$

When x_1 quickly enters its manifold x_1^*, the following reduced model is generated

$$\begin{aligned} \dot{x}_2 &= x_1^* + x_3 \\ \dot{x}_3 &= x_2 - x_3 \end{aligned}$$

In order to attain the control objective 1, the same procedure is used to design x_1^* as in Example 1

$$x_1^* = -k_2(x_2 - x_2^*) - x_3$$

where x_2^* satisfies

$$x_2^* = -k_3(x_3 - x_3^o) + x_3$$

If the control objective 2 is to be achieved, we just need to develop a new x_1^* as

$$x_1^* = -k_2(x_2 - x_2^o)$$

for the fundamental module without decommissioning the entire existing control structure.

From this example, the advantage of the proposed control structure is explicitly presented. In order to make the system achieve different control objectives, we only need redesign the subcontroller of the reduced model and provide the new manifold x^* to the fundamental control module.

In the following sections, we will apply the obtained theoretical results to explain why the vector control structure for VSC HVDC systems can consist of two control loops with different dynamics and to demonstrate how the system exhibit a multi-time-scale performance.

5.2 Control induced time-scale separation for MTDC systems using master-slave control configuration

In the present section, based on the previous theoretical results, we give a detailed description on how the MTDC system exhibits multiple time-scale dynamics using master-slave control configuration. Furthermore, a theoretical stability study is also performed where the stability limitations on this control configuration are also analyzed.

5.2.1 Control design

We consider each VSC terminal as an individual unit, which is of the form

$$\begin{aligned}\dot{x}_{1[i]} &= f_{1[i]}(x_{1[i]}) + g_{1[i]}(x_{1[i]},\ u_{cg_i})u_{1[i]} \\ \dot{x}_{2[j]} &= f_{2[j]}(x_{2[j]},\ y_{2[j]}) + g_{2[j]}(x_{2[j]},\ y_{2[j]},\ u_{cw_j})u_{2[j]}\end{aligned} \tag{5.50}$$

$$\dot{y}_{2[j]} = f_{3[j]} + I_{w_{[j]}} \tag{5.51}$$

where we use the following definitions

$$\begin{aligned}x_{1[i]} &\triangleq \begin{bmatrix} i_{g_i d} & i_{g_i q}\end{bmatrix}^T;\ x_{2[j]} \triangleq \begin{bmatrix} i_{w_j d} & i_{w_j q}\end{bmatrix}^T \\ u_{1[i]} &\triangleq \begin{bmatrix} m_{g_i d} & m_{g_i q}\end{bmatrix}^T;\ u_{2[j]} \triangleq \begin{bmatrix} m_{w_j d} & m_{w_j q}\end{bmatrix}^T \\ y_{2[j]} &\triangleq \begin{bmatrix} v_{sw_j d} & v_{sw_j q}\end{bmatrix}^T;\ I_{w_{[j]}} \triangleq \begin{bmatrix} I_{w_j d} & I_{w_j q}\end{bmatrix}^T\end{aligned} \tag{5.52}$$

The expressions of $f_{1[i]}$, $f_{2,3[j]}$, $g_{1[i]}$ and $g_{2[j]}$ are obviously obtained from the MTDC system described by (3.20), (3.28) and (3.29), which are continuous differentiable in their respective arguments for $i_{g_i,dq} \in \mathbb{D}_{i_{g_i,dq}}$, $i_{w_j,dq} \in \mathbb{D}_{i_{w_j,dq}}$, $v_{sw_j,dq} \in \mathbb{D}_{v_{sw_j,dq}}$, $u_{c(\cdot)} \in \mathbb{D}_{u_c}$ and $m_{g_i,dq},\ m_{w_j,idq} \in [-1,\ 1]$.

For convenience, we also introduce

$$\begin{aligned}x &\triangleq [x_{1[1]}\ \cdots\ x_{1[N]}\ x_{2[1]}\ \cdots\ x_{2[M]}]^T = [x_{1[i]}\ x_{2[j]}]^T \\ u &\triangleq [u_{1[1]}\ \cdots\ u_{1[N]}\ u_{2[1]}\ \cdots\ u_{2[M]}]^T = [u_{1[i]}\ u_{2[j]}]^T\end{aligned}$$

Therefore, the overall model of the MTDC system described in Chapter 3 can be expressed by a general form (5.50), (5.51) and (3.36).

Now, we are ready to develop the control algorithm by following the procedure presented in Section 5.1 as

- Step 1: We divide the full-scale system into two subsystems, i.e. the driving subsystem (5.50) and the driven subsystem (5.51) and (3.36), where the driving subsystem is directly collocated with the control inputs $u_{1[i]}$ and $u_{2[j]}$.
- Step 2: Assume that the proposed control algorithm is explicitly designed with the purpose of making the driving subsystem have much faster dynamics than the driven subsystem. Based on the dynamic separation, we then obtain a boundary-layer and a reduced model where two subcontrollers are designed to control both models, respectively.
- Step 3: Substituting the two subcontrollers into the original model, a standard singularly perturbed system can be deduced. Applying singular perturbation theory, we derive sufficient conditions on the proposed control algorithm to ensure the asymptotic stability of the MTDC system.

Note that, in Step 2, we assume that the state variables in the driving subsystem have faster dynamics than those in the driven subsystem. In fact, this assumption is only used to help us design the control system. In the section of theoretical analysis, we will demonstrate that the controller based on this assumption indeed makes the system exhibit a dynamic behavior characterized by the presence of fast and slow transients.

5.2.1.1 Design of the driving subsystem

We assume that there exists a reference trajectory for the driving subsystem as

$$x^* \triangleq [x^*_{1[1]} \ \cdots \ x^*_{1[N]} \ x^*_{2[1]} \ \cdots \ x^*_{2[M]}]^T$$

which is yet to be designed. The only information on x^* is that it is a function of the state variables of the driven subsystem with slow dynamic. We then design the subcontrollers $u_{1[i]} = h_{1[i]}$ and $u_{2[j]} = h_{2[j]}$ such that the closed-loop of the driven subsystem becomes

$$\begin{aligned} \dot{x}_{1[i]} &= v_{1[i]} \\ \dot{x}_{2[j]} &= v_{2[j]} \end{aligned} \tag{5.53}$$

where we introduce the auxiliary inputs $v_{1[i]}$ and $v_{2[j]}$. Since $g_{1[i]}$ and $g_{2[j]}$ are invertible, by combining (5.50) and (5.53), the subcontroller of the driving system is designed as

$$\begin{aligned} h_{1[i]} &= g^{-1}_{1[i]}[v_{1[i]} - f_{1[i]}] \\ h_{2[j]} &= g^{-1}_{2[j]}[v_{2[j]} - f_{2[j]}] \end{aligned} \tag{5.54}$$

The design of $v_{1[i]}, v_{2[j]} \in \mathbb{R}^2$ are free. We only need them so that the above autonomous system (5.53) at least locally exponentially converges to x^* when x^* is constant. To illustrate our control scheme more clearly, we design

$$\begin{aligned} \dot{e}_{Ix_{1[i]}} &= x_{1[i]} - x^*_{1[i]} \\ v_{1[i]} &= -K_{1[i]}(x_{1[i]} - x^*_{1[i]}) - \Gamma_{1[i]} e_{Ix_{1[i]}} \\ \dot{e}_{Ix_{2[j]}} &= x_{2[j]} - x^*_{2[j]} \\ v_{2[j]} &= -K_{2[j]}(x_{2[j]} - x^*_{2[j]}) - \Gamma_{2[j]} e_{Ix_{2[j]}} \end{aligned} \tag{5.55}$$

where the control gain matrices are of the form

$$\begin{aligned} K_{1[i]} &= \mathrm{diag}(k^{11}_{[i]}, k^{12}_{[i]}); \ K_{2[j]} = \mathrm{diag}(k^{21}_{[j]}, k^{22}_{[j]}) \\ \Gamma_{1[i]} &= \mathrm{diag}(\gamma^{11}_{[i]}, \gamma^{12}_{[i]}); \ \Gamma_{2[j]} = \mathrm{diag}(\gamma^{21}_{[j]}, \gamma^{22}_{[j]}) \end{aligned} \tag{5.56}$$

whose diagonal elements are positive.

5.2.1.2 Design of the driven system

With the aid of the subcontroller (5.54), we assume that x quickly enters the manifold x^* and then substitute $x = x^*$ into the driven subsystem (5.51) and (3.36), leading to the following reduced model

$$\begin{aligned} \dot{y}_{2[j]} &= f_{2[j]}(x^*_{2[j]}, y_{2[j]}) \\ \dot{z} &= Az + \vartheta(x^*_{1[i]}, x^*_{2[j]}) \end{aligned} \tag{5.57}$$

with $(N + 3M + P + L)^{\text{th}}$ order.

According to the master-slave control operation defined in Section 4.1.4 and the design procedure presented in Section 5.1.3.2, we then set

$$i^*_{g_\rho d} = i^o_{g_\rho d}; \ i^*_{g_i q} = i^o_{g_i q} \tag{5.58}$$

As a consequence, some components of the vector x^* are directly given by the prescribed reference values. But we still need to design $i^*_{g_1 d}$ and $i^*_{w_j,dq}$ which are considered as the control inputs of the reduced model (5.57). The control goal now is to make u_{cg_1} and $v_{sw_j,dq}$ in (5.57) track the prescribed output reference, i.e.

$$\bar{s}_o \triangleq \begin{bmatrix} u^o_{cg_1} & v^o_{sw_1,dq} & \cdots & v^o_{sw_N,dq} \end{bmatrix} \tag{5.59}$$

via $i^*_{g_1 d}$ and $i^*_{w_j,dq}$. Input-output feedback linearization is therefore applied for the reduced model as[2]

$$\begin{aligned}
\frac{du_{cg_1}}{dt} &= \frac{1}{C_{g_1}}\left(\frac{3}{2}\frac{v_{sg_1 d} i^*_{g_1 d} + v_{sg_1 q} i^o_{g_1 q}}{u_{cg_1}} - H(1,:) i_c\right) \\
&= v_{cg_1} \\
\frac{dv_{sw_j d}}{dt} &= \omega_{w_j} v_{sw_j q} + \frac{1}{C_{fw_j}}(I_{w_j d} - i^*_{w_j d}) \\
&= v_{w_j d} \\
\frac{dv_{sw_j q}}{dt} &= -\omega_{w_j} v_{sw_j d} + \frac{1}{C_{fw_j}}(I_{w_j q} - i^*_{w_j q}) \\
&= v_{w_j q}
\end{aligned}$$

Taking into account the integrated tracking error, the additional inputs $v_{(\cdot)}$ are designed as

$$\begin{aligned}
\dot{e}_{Icg_1} &= \tilde{u}_{cg_1} \triangleq u_{cg_1} - u^o_{cg_1} \\
v_{cg_1} &= -k_{g_1 d}\tilde{u}_{g_1} - k_{g_2 d} e_{Icg_1} \\
\dot{e}_{Iw_j d} &= \tilde{v}_{sw_j d} \triangleq v_{sw_j d} - v^o_{sw_j d} \\
v_{w_j d} &= -k_{w_{1j} d}\tilde{v}_{sw_j d} - k_{w_{2j} d} e_{Iw_j d} \\
\dot{e}_{Iw_j q} &= \tilde{v}_{sw_j q} \triangleq v_{sw_j q} - v^o_{sw_j q} \\
v_{w_j q} &= -k_{w_{1j} q}\tilde{v}_{sw_j q} - k_{w_{2j} q} e_{Iw_j q}
\end{aligned} \tag{5.60}$$

with positive control gains $k_{g_1 d}$, $k_{g_2 d}$, $k_{w_{1j},dq}$ and $k_{w_{2j},dq}$. Then, by solving (5.60), $i^*_{g_1 d}$ and $i^*_{g_j,dq}$ are computed as

$$\begin{aligned}
i^*_{g_1 d} &= \frac{2u_{cg_1}}{3v_{sg_1 d}}(C_{g_1} v_{cg_1} + H(1,:) i_c) - \frac{v_{sg_1 q}}{v_{sg_1 d}} i^o_{g_1 q} \\
i^*_{w_j d} &= C_{fw_j}\omega_{w_j} v_{sw_j q} - C_{fw_j} v_{w_j d} + I_{w_j d} \\
i^*_{w_j q} &= -C_{fw_j}\omega_{w_j} v_{sw_j d} - C_{fw_j} v_{w_j q} + I_{w_j q}
\end{aligned} \tag{5.61}$$

Finally, the full control scheme is established, composed by (5.54), (5.58) and (5.61).

For each VSC terminal, the controller $u_{[k]}$ just relies on local information without the knowledge of other terminals. This can prevent the possible time delay of information exchange from the collective model.

The manifold x^* is deduced from the lower-order reduced model (5.57) instead of the full-scale model (5.50), (5.51) and (3.36), and it greatly simplifies the control

[2] Recall the definition of H in Section 3.4.3.

design. Clearly, x^* is a function of the state variables of the driven system, i.e. $y_{2[j]}$ and z. It is worthwhile to note that using a reduced model will introduce errors in the system. Such errors may cause stability problems which will be studied in the next section.

5.2.2 Theoretical analysis

Before stating the main results of this section, we recall that, to ensure the physical feasibility of the MTDC system, Assumption 4.1.1 still holds and the equilibrium point is denoted as

$$\bar{P}_1 = [\cdots \ \bar{i}_{g_i d} \ \bar{i}_{g_i q} \ \cdots \ \bar{i}_{w_j d} \ \bar{i}_{w_j q} \ \cdots \ \bar{v}_{sw_j d} \ \bar{v}_{sw_j q} \cdots \ \bar{z}]^T \tag{5.62}$$

In this section, we will demonstrate how the proposed controller divides the MTDC system into different time scales and furthermore, the stability of the equilibrium point $\bar{P}_1$ will be also studied.

5.2.2.1 Two-time-scale dynamics

The aim of this section is to show how the MTDC system exhibits a multi-time-scale behavior. To establish this result, we substitute the control algorithm (5.54), (5.58) and (5.61) into the original system consisting of (5.50), (5.51) and (3.36), resulting in the following closed-loop system

$$\begin{aligned}
\dot{e}_{Ix_{1[i]}} &= x_{1[i]} - x^*_{1[i]} \\
\dot{x}_{1[i]} &= -K_{1[i]}(x_{1[i]} - x^*_{1[i]}) - \Gamma_{1[i]} e_{Ix_{1[i]}} \\
\dot{e}_{Ix_{2[j]}} &= x_{2[j]} - x^*_{2[j]} \\
\dot{x}_{2[j]} &= -K_{2[j]}(x_{2[j]} - x^*_{2[j]}) - \Gamma_{2[j]} e_{Ix_{2[j]}} \\
\dot{e}_{Iw_j d} &= v_{sw_j d} - v^o_{sw_j d} \\
\dot{e}_{Iw_j q} &= v_{sw_j q} - v^o_{sw_j q} \\
\dot{e}_{Icg_1} &= \tilde{u}_{cg_1} \\
\dot{y}_{2[j]} &= f_{3[j]} + I_{w_{[j]}} \\
\dot{z} &= Az + \vartheta
\end{aligned} \tag{5.63}$$

with $(9M + 5N + P + L)^{\text{th}}$ order. The equilibrium point of the above closed-loop system is denoted as $\bar{P}_2$.

Let us introduce a small scalar parameter ε satisfying

$$\varepsilon \cdot k_{\min} = 1$$

where $k_{\min} = \min(k^{11}_{[i]}, k^{12}_{[i]}, k^{21}_{[j]}, k^{22}_{[j]})$. We then rewrite the dynamics of $x_{1[i]}$ and $x_{2[j]}$ in (5.63) as

$$\begin{aligned}
\varepsilon \dot{x}_{1[i]} &= -\bar{K}_{1[i]}(x_{1[i]} - x^*_{1[i]}) - \varepsilon \Gamma_{1[i]} e_{Ix_{1[i]}} \\
\varepsilon \dot{x}_{2[j]} &= -\bar{K}_{2[j]}(x_{2[j]} - x^*_{2[j]}) - \varepsilon \Gamma_{2[j]} e_{Ix_{2[j]}}
\end{aligned} \tag{5.64}$$

where the new control gain matrices are defined as

$$\begin{aligned}\bar{K}_{1[i]} &= \mathrm{diag}(\bar{k}^{11}_{[i]}, \bar{k}^{12}_{[i]}) \triangleq \mathrm{diag}(\varepsilon k^{11}_{[i]}, \varepsilon k^{12}_{[i]}) \\ \bar{K}_{2[j]} &= \mathrm{diag}(\bar{k}^{21}_{[j]}, \bar{k}^{22}_{[j]}) \triangleq \mathrm{diag}(\varepsilon k^{21}_{[j]}, \varepsilon k^{22}_{[j]}) \\ \bar{k}^{11}_{[i]}, \bar{k}^{12}_{[i]}, \bar{k}^{21}_{[j]}, \bar{k}^{22}_{[j]} &\geq 1\end{aligned}$$

Now, as an alternative expression, the closed-loop system (5.63) can be rewritten as

$$\begin{aligned}\dot{e}_{Ix_{1[i]}} &= x_{1[i]} - x^*_{1[i]} \\ \varepsilon\dot{x}_{1[i]} &= -\bar{K}_{1[i]}(x_{1[i]} - x^*_{1[i]}) - \varepsilon\Gamma_{1[i]} e_{Ix_{1[i]}} \\ \dot{e}_{Ix_{2[j]}} &= x_{2[j]} - x^*_{2[j]} \\ \varepsilon\dot{x}_{2[j]} &= -\bar{K}_{2[j]}(x_{2[j]} - x^*_{2[j]}) - \varepsilon\Gamma_{2[j]} e_{Ix_{2[j]}} \\ \dot{e}_{Iw_j d} &= v_{sw_j d} - v^o_{sw_j d} \\ \dot{e}_{Iw_j q} &= v_{sw_j q} - v^o_{sw_j q} \\ \dot{e}_{Icg_1} &= \tilde{u}_{cg_1} \\ \dot{y}_{2[j]} &= f_{3[j]} + I_{w_{[j]}} \\ \dot{z} &= Az + \vartheta\end{aligned} \tag{5.65}$$

which is of a standard singularly perturbed form when ε is small enough. We call x^* as the quasi-steady state of x. It is worth noticing that, the small parameter ε, which is used to qualify the time-scale separation, is not derived from the physical system parameters but is arbitrarily created by the designed subcontroller (5.54).

For convenience, we introduce the following new variables

$$\begin{aligned}\tilde{x}_{1[i]} &= x_{1[i]} - x^*_{1[i]} \\ \tilde{x}_{2[j]} &= x_{2[j]} - x^*_{2[j]}\end{aligned}$$

that shift the quasi-steady state of x to the origin. In these new variables, the driving subsystem (5.64) becomes

$$\begin{aligned}\varepsilon\dot{\tilde{x}}_{1[i]} &= -\bar{K}_{1[i]}\tilde{x}_{1[i]} - \varepsilon\Gamma_{1[i]} e_{Ix_{1[i]}} - \varepsilon\frac{dx^*_{1[i]}}{dt} \\ \varepsilon\dot{\tilde{x}}_{2[j]} &= -\bar{K}_{2[j]}\tilde{x}_{2[j]} - \varepsilon\Gamma_{2[j]} e_{Ix_{2[j]}} - \varepsilon\frac{dx^*_{2[j]}}{dt}\end{aligned} \tag{5.66}$$

Now we define t as the time-scale variable for slow dynamics and introduce a new time variable τ for fast dynamics as

$$\varepsilon\frac{d\tilde{x}}{dt} = \frac{d\tilde{x}}{d\tau},\ \tilde{x} = [\tilde{x}_{1[1]}\ \cdots\ \tilde{x}_{1[N]}\tilde{x}_{2[1]}\ \cdots\ \tilde{x}_{2[M]}]^T \tag{5.67}$$

We then express (5.66) in the τ time scale as

$$\begin{aligned}\frac{d\tilde{x}_{1[i]}}{d\tau} &= -\bar{K}_{1[i]}\tilde{x}_{1[i]} - \varepsilon\Gamma_{1[i]} e_{Ix_{1[i]}} - \varepsilon\frac{dx^*_{1[i]}}{dt} \\ \frac{d\tilde{x}_{2[j]}}{d\tau} &= -\bar{K}_{2[j]}\tilde{x}_{2[j]} - \varepsilon\Gamma_{2[j]} e_{Ix_{2[j]}} - \varepsilon\frac{dx^*_{2[j]}}{dt}\end{aligned} \tag{5.68}$$

As $\varepsilon \to 0$,a boundary-layer system is deduced from (5.68), given by

$$\begin{aligned} \frac{d\tilde{x}_{1[i]}}{d\tau} &= -\bar{K}_{1[i]}\tilde{x}_{1[i]} \\ \frac{d\tilde{x}_{2[j]}}{d\tau} &= -\bar{K}_{2[j]}\tilde{x}_{2[j]} \end{aligned} \tag{5.69}$$

whose equilibrium point is globally exponentially stable. Meanwhile, when x enters its manifold x^*, the closed-loop system (5.65) is degenerated into a $(5M+N+P+L+1)^{\text{th}}$ order reduced model expressed by

$$\begin{aligned} \dot{e}_{Iw_jd} &= v_{sw_jd} - v^o_{sw_jd} \\ \dot{e}_{Iw_jq} &= v_{sw_jq} - v^o_{sw_jq} \\ \dot{e}_{Icg_1} &= \tilde{u}_{cg_1} \\ \dot{y}_{2[j]} &= [v_{w_jd}\ v_{w_jq}]^T \\ \dot{z} &= Az + \vartheta' \end{aligned} \tag{5.70}$$

where ϑ' is given by

$$\begin{cases} \vartheta'_i = \dfrac{3}{2}\dfrac{v_{sg_id}i^*_{g_id} + v_{sg_iq}i^*_{g_iq}}{C_{g_i}(\tilde{u}_{cg_i} + \bar{u}_{cg_i})}, & i \in \mathcal{N} \\ \vartheta'_{N+j} = \dfrac{3}{2}\dfrac{(\tilde{v}_{sw_jd} + v^o_{sw_jd})i^*_{w_jd} + (\tilde{v}_{sw_jq} + \bar{v}^o_{sw_jq})i^*_{w_jq}}{C_{w_j}(\tilde{u}_{cw_j} + \bar{u}_{cw_j})}, & j \in \mathcal{M} \\ \vartheta'_{N+M+h} = 0, & h \in \mathcal{P} \\ \vartheta'_{N+M+P+k} = 0, & k \in \mathcal{L} \end{cases} \tag{5.71}$$

Remember that $i^*_{g_i,dq}$ and $i^*_{w_j,dq}$ are given by (5.58) and (5.61). We denote the solution of the reduced model (5.70) as $(y^{re}_{2[j]}(t), z^{re}(t))$ and then, $x^{re} = x^*(y^{re}_{2[j]}(t), z^{re}(t))$ describes behavior of x^* when $(y_{2[j]}(t), z(t)) = (y^{re}_{2[j]}(t), z^{re}(t))$. As a result, according to Theorem 5.1.9 in Section 5.1.4.1, we are ready to state the following result:

Theorem 5.2.1. *Consider the system (5.63). For fixed control parameters $\bar{K}_{1[i]}$, $\bar{K}_{2[j]}$, $k_{g_{1,2}d}$, $k_{w_{1j},dq}$ and $k_{w_{2j},dq}$, there exists a region $\mathcal{R}_{xyz}$ and a positive constant ε^* (or $k^*_{\min}$) such that for all $0 < \varepsilon < \varepsilon^*$ (or $k^*_{\min} < k_{\min}$), if the system (5.63) starts from $\mathbb{R}_{xyz}$, we have*

$$\begin{aligned} y_{2[j]}(t) &= y^{re}_{2[j]}(t) + O(\varepsilon) \\ z(t) &= z^{re}(t) + O(\varepsilon) \\ x(t) &= x^{re}(t) + \tilde{x}(\tau) + O(\varepsilon) \end{aligned} \tag{5.72}$$

where $\tilde{x}(\tau)$ is the solution of the boundary-layer model (5.69).

Theorem 5.2.1 clearly indicates that the state variables of the driving system, i.e. all dq currents, exhibit a two-time-scale behavior. They start with a fast transient $\tilde{x}(\tau)$ and then remain close to $x^{re}(t)$ which presents a slow transient. If we want a remarkable time-scale separation, a smaller ε (or a lager $k_{\min}$) should be chosen. In the τ time scale, all $y_{[j]}$ and z seem slowly varying.

5.2.2.2 Stability analysis

The previous section shows that the exact solution of the original system (5.63) can be approximated by the solutions of the boundary-layer and the reduced model. In this section, we carry out a detailed stability analysis.

To simplify the analysis, we perform the change of variables

$$\begin{aligned} \tilde{y}_{2[j]} &= y_{2[j]} - \bar{y}_{2[j]} \\ \tilde{z} &= z - \bar{z} \end{aligned}$$

and then, rewrite the system (5.63) in these new variables as

$$\begin{aligned} \dot{e}_{Ix_{1[i]}} &= \tilde{x}_{1[i]} \\ \dot{\tilde{x}}_{1[i]} &= -K_{1[i]}\tilde{x}_{1[i]} - \Gamma_{1[i]}e_{Ix_{1[i]}} - \frac{dx^*_{1[i]}}{dt} \\ \dot{e}_{Ix_{2[j]}} &= \tilde{x}_{2[j]} \\ \dot{\tilde{x}}_{2[j]} &= -K_{2[j]}\tilde{x}_{2[j]} - \Gamma_{2[j]}e_{Ix_{2[j]}} - \frac{dx^*_{2[j]}}{dt} \\ \dot{e}_{Iw_jd} &= \tilde{v}_{sw_jd} \\ \dot{e}_{Iw_jq} &= \tilde{v}_{sw_jq} \\ \dot{e}_{Icg_1} &= \tilde{u}_{cg_1} \\ \dot{\tilde{y}}_{2[j]} &= v_{w[j]} + B_{[j]}\tilde{x}_{2[j]} \\ \dot{\tilde{z}} &= A\tilde{z} + \vartheta^* + A\bar{z} + \tilde{\vartheta} \end{aligned} \tag{5.73}$$

where

$$\begin{aligned} B_{[j]} &= -\frac{1}{C_{fw_j}} I_{2\times 2};\ v_{w[j]} \triangleq [v_{w_jd}\ v_{w_jq}]^T \\ \tilde{\vartheta} &\triangleq [\tilde{\vartheta}_1\ \cdots\ \tilde{\vartheta}_{M+N}\ 0_{P+L}]^T \\ \vartheta^* &\triangleq [\vartheta^*_1\ \cdots\ \vartheta^*_{M+N}\ 0_{P+L}]^T \end{aligned} \tag{5.74}$$

with the elements

$$\begin{cases} \tilde{\vartheta}_i = \dfrac{3}{2}\dfrac{v_{sg_id}\tilde{i}_{g_id} + v_{gs_iq}\tilde{i}_{g_iq}}{C_{g_i}(\tilde{u}_{cg_i} + \bar{u}_{cg_i})}, & i \in \mathcal{N} \\ \tilde{\vartheta}_{N+j} = \dfrac{3}{2}\dfrac{(\tilde{v}_{sw_jd} + \bar{v}_{sw_jd})\tilde{i}_{w_jd} + (\tilde{v}_{sw_jq} + \bar{v}_{sw_jq})\tilde{i}_{w_jq}}{C_{cw_j}(\tilde{u}_{cw_j} + \bar{u}_{cw_j})}. & j \in \mathcal{M} \\ \vartheta^*_i = \dfrac{3}{2}\dfrac{v_{sg_id}i^*_{g_id} + v_{gs_iq}i^*_{g_iq}}{C_{g_i}(\tilde{u}_{cg_i} + \bar{u}_{cg_i})}, & i \in \mathcal{N} \\ \vartheta^*_{N+j} = \dfrac{3}{2}\dfrac{(\tilde{v}_{sw_jd} + \bar{v}_{sw_jd})i^*_{w_jd} + (\tilde{v}_{sw_jq} + \bar{v}_{sw_jq})i^*_{w_jq}}{C_{w_j}(\tilde{u}_{cw_j} + \bar{u}_{cw_j})}. & j \in \mathcal{M} \end{cases} \tag{5.75}$$

It is important to remark that since x^* is the control signal of the slow subsystem, its derivative would be very small compared to the derivative of x.

We rewrite the first four equations of (5.73) in a novel matrix form

$$\dot{\varkappa} = A_\varkappa \varkappa + \theta_\varkappa \tag{5.76}$$

where

$$\begin{aligned}
\varkappa &= [\cdots\ e_{Ix_{1[i]}}\ \tilde{x}_{1[i]}\ \cdots\ e_{Ix_{2[j]}}\ \tilde{x}_{2[j]}\cdots]^T \\
\theta_\varkappa &= [\cdots\ 0_{2\times 1}\ \frac{dx^*_{1[i]}}{dt}\ \cdots\ 0_{2\times 1}\ \frac{dx^*_{2[j]}}{dt}\cdots]^T \\
A_\varkappa &= \mathrm{diag}(\cdots\ A_{x_1[i]}\cdots\ A_{x_2[j]}) \\
A_{x_1[i]} &= \begin{bmatrix} 0_{2\times 2} & I_{2\times 2} \\ -\Gamma_{1[i]} & -K_{1[i]} \end{bmatrix};\ A_{x_2[j]} = \begin{bmatrix} 0_{2\times 2} & I_{2\times 2} \\ -\Gamma_{2[j]} & -K_{2[j]} \end{bmatrix}
\end{aligned}$$

The last five equations of (5.73) can be expressed in the following form

$$\begin{aligned}
\dot{\zeta} &= A_\zeta \zeta + \tilde{\vartheta}_\zeta \\
\dot{\tilde{z}}_r &= A_r \tilde{z}_r + \vartheta^*_r + A_r \bar{z}_r + \tilde{\vartheta}_r + \bar{\vartheta}_{i_c} + \tilde{\vartheta}_{i_c}
\end{aligned} \tag{5.77}$$

where

$$\begin{aligned}
\zeta &= [e_{Icg_1}\ \tilde{u}_{cg_1}\ \cdots\ e_{Iw_jd}\ \tilde{v}_{sw_jd}\ \cdots\ e_{Iw_jq}\ \tilde{v}_{sw_jq}\ \cdots]^T \\
\tilde{\vartheta}_\zeta &= [0\ \tilde{\vartheta}_1\ \cdots\ 0\ -\frac{1}{C_{fw_j}}\tilde{i}_{w_jd}\ \cdots\ 0\ -\frac{1}{C_{fw_j}}\tilde{i}_{w_jq}\ \cdots]^T \\
\bar{\vartheta}_{i_c} &= [0_{N+M+P-1}\ \frac{H(1,1)}{L_{c_1}}\bar{u}_{cg_1}\cdots\ \frac{H(1,L)}{L_{c_L}}\bar{u}_{cg_1}]^T \\
\tilde{\vartheta}_{i_c} &= [0_{N+M+P-1}\ \frac{H(1,1)}{L_{c_1}}\tilde{u}_{cg_1}\cdots\ \frac{H(1,L)}{L_{c_L}}\tilde{u}_{cg_1}]^T \\
A_\zeta &= \mathrm{diag}(A_{g_1}\ A_{w_1d}\ \cdots\ A_{w_Md}\ A_{w_1q}\ \cdots\ A_{w_Mq}) \\
A_{g_1} &= \begin{bmatrix} 0 & 1 \\ -k_{g_1d} & -k_{g_2d} \end{bmatrix};\ A_{w_j,dq} = \begin{bmatrix} 0 & 1 \\ -k_{w_{1j},dq} & -k_{w_{2j},dq} \end{bmatrix}
\end{aligned} \tag{5.78}$$

The vectors $\tilde{\vartheta}_r$, ϑ^*_r and $\tilde{z}_r$ are the sub-vectors formed by deleting the first component of $\tilde{\vartheta}$, ϑ^* and $\tilde{z}$ (see (5.75)), respectively. The matrix A_r is given by (4.65) in Section 4.1.4 as

$$A_r = \begin{bmatrix} 0_{(N+M+P-1)\times(N+M+P-1)} & C_r^{-1}H_r \\ -L^{-1}H_r^T & -L^{-1}R \end{bmatrix} \tag{5.79}$$

Now, the original closed-loop system (5.63) is transformed into the new form composed of (5.76) and (5.77). Note that the above error system (5.76) and (5.77) has an equilibrium at the origin, the asymptotic stability of which would imply the asymptotic stability of $\bar{P}_2$ of the original system (5.63). If $\tilde{x}_{1[i]}$ and $\tilde{x}_{2[j]}$ quickly converge to zero, the error system (5.76) and (5.77) is degenerated into the following reduced model

$$\begin{aligned}
\dot{\zeta} &= A_\zeta \zeta \\
\dot{\tilde{z}}_r &= A_r \tilde{z}_r + \vartheta^*_r + A_r \bar{z}_r + \bar{\vartheta}_{i_c} + \tilde{\vartheta}_{i_c}
\end{aligned} \tag{5.80}$$

which consists the external and internal dynamics represented by ζ and $\tilde{z}_r$, respectively. As ζ converges to zero, the dynamics of the reduced model (5.80) is governed by the internal dynamics

$$\dot{\tilde{z}}_r = A_r \tilde{z}_r + \vartheta^*_r|_{\zeta=0} + A_r \bar{z}_r + \bar{\vartheta}_{i_c} \tag{5.81}$$

Similar to Lemma 4.1.2 in Section 4.1.4, we have the following result:

Lemma 5.2.2. *Consider the system (5.73). If the prescribed references $u^o_{cg_1}$, $Q^o_{g_1}$, $P^o_{g_\rho}$, $Q^o_{g_\rho}$, $v^o_{sw_jd}$ and $v^o_{sw_jq}$ and the system parameters are set such that the Jacobian matrix of the internal dynamics (5.81) at the origin*

$$J = \begin{bmatrix} -D & C_r^{-1}H_r \\ -L^{-1}H_r^T & -L^{-1}R \end{bmatrix} \tag{5.82}$$

is Hurwitz, where $D = diag(d_k)$, $k = 1, \cdots, N+M+P-1$, is a diagonal matrix given by

$$\begin{cases} d_{(\rho-1)} = \dfrac{P^o_{g_\rho}}{\bar{u}^2_{cg_\rho}}, & \rho \in \mathcal{N}_{-1} \\ d_{(j+N-1)} = \dfrac{P^o_{w_j}}{C_{w_j}\bar{u}^2_{w_j}}, & j \in \mathcal{M} \\ d_{(h+N+M)} = 0. & h \in \mathcal{P} \end{cases}$$

$$P^o_{w_j} = \frac{3}{2}(v^o_{sw_jd}I_{w_jd} + v^o_{sw_jq}I_{w_jq})$$

then, there exist control matrices $K_{1[i]}$, $K_{2[j]}$, $\Gamma_{1[i]}$ and $\Gamma_{2[j]}$ such that the origin of the system (5.73) is locally exponentially stable. As a consequence, the equilibrium point $\bar{P}_1$ of the MTDC system (5.50), (5.51) and (3.36) is locally asymptotically stable under the control algorithm (5.54), (5.58) and (5.61).

Proof. According to Taylor's theorem, the reduced model (5.77) can be expressed in the Peano form of the remainder as

$$\begin{bmatrix} \dot{\zeta} \\ \dot{\tilde{z}}_r \end{bmatrix} = \begin{bmatrix} A_\zeta & 0 \\ A_* & J \end{bmatrix} \begin{bmatrix} \zeta \\ \tilde{z}_r \end{bmatrix} + \phi_1(\zeta, \tilde{z}_r) \begin{bmatrix} \zeta \\ \tilde{z}_r \end{bmatrix} + \begin{bmatrix} 0 \\ \bar{\vartheta}^* + A_r\bar{z}_r + \bar{\vartheta}_{i_c} \end{bmatrix} \triangleq f_p \tag{5.83}$$

where $\bar{\vartheta}^*$ and $\phi(\tilde{z}_r, \zeta)$ satisfy

$$\begin{aligned} \bar{\vartheta}^* &= [\frac{\bar{i}_{g_2}}{C_{g_2}} \cdots \frac{\bar{i}_{g_N}}{C_{g_N}} \ \frac{\bar{i}_{w_1}}{C_{w_1}} \cdots \frac{\bar{i}_{w_M}}{C_{w_M}} \ 0^T_{(P+L)}]^T \\ \bar{\vartheta}^* &+ A_r\bar{z}_r + \bar{\vartheta}_{i_c} = 0 \\ \lim_{||[\zeta \ \tilde{z}_r]^T|| \to 0} &||\phi_1(\zeta, \tilde{z}_r)|| = 0 \end{aligned}$$

For any positive L_{ϕ_1}, there exists a positive b_{ϕ_1} such that:

$$||\phi_1|| \leq L_{\phi_1}, \ \forall \ [\zeta \ \tilde{z}_r]^T \in \mathfrak{B}_{\phi_1}$$

where

$$\mathfrak{B}_{\phi_1} = \{ \ [\zeta \ \tilde{z}_r]^T | \ || \ [\zeta \ \tilde{z}_r]^T || < b_{\phi_1} \}.$$

We denote $H \triangleq \begin{bmatrix} A_\zeta & 0 \\ A_* & J \end{bmatrix}$ and hence, H is Hurwitz since A_ζ and J are Hurwitz. For any symmetric matrix $Q_r > 0$, there exists $P_r > 0$ satisfying the Lyapunov equation $P_rH + H^TP_r = -Q_r$. Let

$$V_r = [\zeta \ \tilde{z}_r]P_r[\zeta \ \tilde{z}_r]^T$$

be a Lyapunov function candidate for the reduced model (5.83) and then, we have

$$\begin{aligned}\frac{dV_r}{d[\zeta\ \tilde{z}_r]^T} f_p &= -[\zeta\ \tilde{z}_r]Q_r[\zeta\ \tilde{z}_r]^T + [\zeta\ \tilde{z}_r](P_r\phi_1 + \phi_1^T P_r)[\zeta\ \tilde{z}_r]^T \\ &\leq -(\lambda_{\min}(Q_r) - 2L_{\phi_1}||P_r||)||[\zeta\ \tilde{z}_r]^T||^2\end{aligned}$$

for all $||[\zeta\ \tilde{z}_r]^T|| < b_{\phi_1}$, where L_{ϕ_1} is chosen such that

$$\beta_1 \triangleq (\lambda_{\min}(Q_r) - 2L_{\phi_1}||P_r||) > 0$$

For the subsystem (5.76), we choose

$$V_b = \varkappa^T P_\varkappa \varkappa$$

as a Lyapunov function candidate where

$$\begin{aligned}P_\varkappa &= \text{diag}(\cdots\ P_{\varkappa_{1[i]}}\ \cdots\ P_{\varkappa_{2[j]}}\ \cdots) \\ P_{\varkappa_{1[i]}} &= \text{diag}(\Gamma_{1[i]},\ I_{2\times 2})\quad P_{\varkappa_{2[j]}} = \text{diag}(\Gamma_{2[j]},\ I_{2\times 2})\end{aligned}$$

Then, the derivative of V_b is deduced as[3]

$$\begin{aligned}\frac{dV_b}{d\varkappa}\dot{\varkappa} &= -2\tilde{x}^T \text{diag}(K_{1[i]}, K_{2[j]})\tilde{x} + 2\tilde{x}^T \frac{dx^*}{dt} \\ &\leq -2k_{\min}||\tilde{x}||^2 + 2||\tilde{x}||\ ||\frac{dx^*}{dt}||\end{aligned}$$

Now, we propose a Lyapunov function V based on V_r and V_b for (5.73)

$$V = (1-d)V_r + dV_b,\ 0 < d < 1 \tag{5.84}$$

where d is yet to be designed. The derivative of V along (5.76) and (5.77) becomes

$$\begin{aligned}\dot{V} &= (1-d)\frac{dV_r}{d[\zeta\ \tilde{z}_r]^T}(f_p + [\tilde{\vartheta}_\zeta\ \tilde{\vartheta}_r]^T) + d\frac{dV_b}{d\varkappa}\dot{\varkappa} \\ &\leq -(1-d)\beta_1||[\zeta\ \tilde{z}_r]^T||^2 - 2dk_{\min}||\tilde{x}||^2 + 2d||\tilde{x}|| \cdot ||\frac{dx^*}{dt}|| \\ &+ 2(1-d)[\zeta\ \tilde{z}_r]^T P_r[\tilde{\vartheta}_\zeta\ \tilde{\vartheta}_r]^T \end{aligned} \tag{5.85}$$

We have that $[\tilde{\vartheta}_\zeta\ \tilde{\vartheta}_r]^T$ vanishes at $||\tilde{x}|| = 0$ and moreover, $\tilde{\vartheta}_\zeta$ and $\tilde{\vartheta}_r$ are continuously differentiable functions. Hence, there exists a Lipschitz parameter L_2 such that:

$$||[\tilde{\vartheta}_\zeta\ \tilde{\vartheta}_r]^T|| < L_2||\tilde{x}||,\ \forall\ \tilde{x} \in \mathcal{B}_{\tilde{x}_1}.$$

where

$$\mathcal{B}_{\tilde{x}_1} = \{\tilde{x}|\ ||\tilde{x}|| < b_{\tilde{x}_1}\}$$

[3]Recall the definition of $\tilde{x}$ in (5.67).

Since x^* is a function of $(\zeta\ z_r)$, we then have:

$$\begin{aligned}\frac{dx^*}{dt} &= \frac{\partial x^*}{\partial[\zeta\ z_r]^T}[\dot{\zeta}\ \dot{z}_r]^T \\ &= \frac{\partial x^*}{\partial[\zeta\ z_r]^T}(H+\phi)[\zeta\ z_r]^T\end{aligned}$$

Concerning the term $\dfrac{\partial x^*}{\partial[\zeta\ z_r]^T}$, there exists a positive b_{ϕ_2} such that

$$||\frac{\partial x^*}{\partial[\zeta\ z_r]^T}|| \leq L_3,\ \forall\ ||\ [\zeta\ \tilde{z}_r]^T|| < b_{\phi_2}$$

Taking the above mentioned inequalities into consideration, $\dot{V}$ in (5.85) becomes

$$\begin{aligned}\dot{V} \leq & -(1-d)\beta_1|||[\zeta\ \tilde{z}_r]^T||^2 - 2dk_{\min}||\tilde{x}||^2 \\ & +2dL_3(||H|| + L_{\phi_1})||\tilde{x}|| \cdot |||[\zeta\ \tilde{z}_r]^T|| + 2(1-d)L_2||P_r|| \cdot ||\tilde{x}|| \cdot |||[\zeta\ \tilde{z}_r]^T|| \\ & = -[\ |||[\zeta\ \tilde{z}_r]^T||\ ||\tilde{x}||] \begin{bmatrix}(1-d)\beta_1 & -\beta_2 \\ -\beta_2 & 2dk_{\min}\end{bmatrix} \begin{bmatrix}||\ [\zeta\ \tilde{z}_r]^T|| \\ ||\tilde{x}||\end{bmatrix}\end{aligned} \tag{5.86}$$

where β_2 is a positive constant given by

$$\beta_2 = dL_3(||H|| + L_{\phi_1}) + (1-d)L_2||P_r|| > 0$$

The quadratic expression (5.86) is negative definite as

$$k_{\min} \geq k^*_{\min} \triangleq \frac{\beta_2^2}{2d(1-d)\beta_1} \tag{5.87}$$

for all $||\tilde{x}|| < b_{\tilde{x}_1}$ and $|||[\zeta\ z_r]^T|| < \min(b_{\phi_1},\ b_{\phi_2})$. In addition, we can obtain an estimation of the region of attraction

$$\mathcal{R} = \{(\varkappa,\ \zeta,\ z_r) \in \mathcal{D}_\varkappa \times \mathcal{D}_\zeta \times \mathcal{D}_{z_r} | V < \mathfrak{C}\} \tag{5.88}$$

where the sets $\mathcal{D}_{(\cdot)} \in \mathbb{R}^{(\cdot)}$ are bounded and connected containing the origin and $\mathfrak{C}$ is given by

$$\mathfrak{C} = \min_{\tilde{x}\in\mathfrak{B}_2, [\zeta\ z_r]^T \in \mathfrak{B}_{\phi_1}} V(\varkappa,\ \zeta,\ z_r)$$

For all initial points starting from the attraction region $\mathcal{R}$, when the inequality (5.87) is satisfied, the solution of the problem (5.73) converges to the origin. Consequently, when the control gains of the control algorithm (5.54), (5.58) and (5.61) are chosen such that (5.87) is satisfied, the equilibrium point $\bar{P}_1$ of the MTDC system (5.50), (5.51) and (3.36) is locally asymptotically stable. □

Theorem 5.2.3. *Consider the MTDC system (5.50), (5.51) and (3.36). If $P^o_{g_\rho}$, $\rho = 2, \cdots, N$ and $P^o_{w_j}$, $j = 1, \cdots, M$ are non-negative, then, the control algorithm (5.54), (5.58) and (5.61) exists such that the equilibrium point $\bar{P}_1$ of the MTDC system (5.50), (5.51) and (3.36) is locally asymptotically stable, with a region of attraction given by (5.88).*

Proof. We have proved that, when $P^o_{g_\rho}$, $\rho = 2, \cdots, N$ and $P^o_{w_j}$, $j = 1, \cdots, M$ are non-negative, the Jacobian matrix J is Hurwitz (see the demonstration of Lemma 4.1.3 in Section 4.1.4) □

5.2.3 Plug-and-play operations

Consider that the MTDC system (5.50), (5.51) and (3.36) with the proposed control algorithm (5.54), (5.58) and (5.61) initially operates in a steady-state condition. If it is required to add or remove a VSC terminal, we propose a plug-and-play operation.

5.2.3.1 Adding one terminal

we first consider plugging in a WAC connected VSC terminal at t_1, whose AC side is characterized by $x_{2[M+1]}$, $y_{2[M+1]}$ and $u_{2_{[M+1]}}$, i.e. $i_{w_{M+1},dq}$, $v_{sw_{M+1},dq}$ and $m_{w_{M+1},dq}$. On the *DC* side, a WAC converter node is associated to the plugged WAC connected VSC terminal, characterized by $u_{cw_{M+1}}$ and $C_{w_{M+1}}$. In particular, the $(M+1)^{\text{th}}$ WAC converter node is physically coupled to the *DC* network by a branch, which is used to connect the plugged node to other existing nodes. The extra branch is characterized by $i_{c_{L+1}}$, $R_{c_{L+1}}$ and $L_{c_{L+1}}$. The new WAC connected VSC terminal is equipped with local controller $u_{2[M+1]}$ with the control gain matrices $K_{2[M+1]}$, $\Gamma_{2[M+1]}$, $A_{w_{M+1},dq}$. Here we need to check whether this new terminal could be added to the existing MTDC system without affecting the existing stability of the system. The procedure is summarized as follows:

> **Step 1:** Modify the *DC* network model (3.36) and then compute the new equilibrium and the new Jacobian matrix J. If J is Hurwitz, go to the next step. Otherwise, we stop here and declare that the new WAC connected VSC terminal can not be added.
>
> **Step 2:** When the new Jacobian matrix J is still Hurwitz, we define a desired region of attraction $\mathcal{R}'$ for the new system with $N+M+1$ terminals and then the feasible region for $k_{\min}$ could be estimated from Condition (5.87). Therefore, it is possible to extend the MTDC system by adding the new terminal.

5.2.3.2 Removing one terminal

We consider removing a WAC connected VSC terminal. For example, the k^{th} one is expected to be disconnected at t_2. Meanwhile, the branches used to connect this terminal node to other nodes are removed as well. Then, a new modified MTDC system is generated. We first check if the corresponding Jacobian matrix J of the new MTDC system is Hurwitz. If this is not the case, we can not remove the k^{th} terminal. When the new J is Hurwitz, we then estimate the new region of attraction R'. If the state of the MTDC system at t_1 is still in R', the unplugging of the terminal is allowable. Otherwise, the operation of removal may trigger the instability of the system.

Table 5.4: The VSC terminal parameters.

	SAC 1	SAC2	WAC 1
$R_{g,w}$	9.9 mΩ	9.4 mΩ	8.4 mΩ
$L_{g,w}$	3.2 mH	3.1 mH	2.7 mH
$f_{g,w}$	50 Hz	50 Hz	60 Hz
$C_{g,w}$	20.4 μF	20.4 μF	27.2 μF

Table 5.5: The transmission branch parameters.

	Branch 1	Branch 2
R_c	0.27 Ω	0.33 Ω
L_c	0.045 H	0.055 H

5.2.4 Simulation studies

In this section, we apply the proposed control scheme to an MTDC system composed of a WAC connected VSC terminal, two SAC connected VSC terminals and two transmission branches as shown in Fig. 5.5. System parameters are listed in Tables

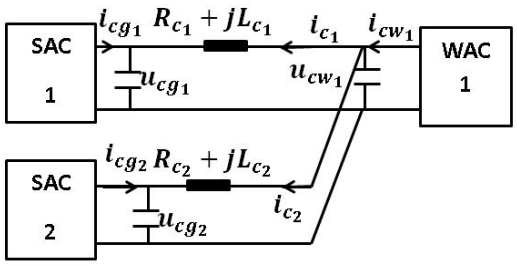

Figure 5.5: An MTDC system with a WAC and two SAC terminals.

5.4-5.5. The base quantities used in the per-unit system are given by Table 5.6.

The 1st SAC connected VSC terminal is used to control the DC-bus voltage at $u^o_{cg_1} = 1$ p.u.. The 2nd SAC connected terminal guarantees a constant power output $P^o_{g_2} = 0.2$ p.u. injected to the DC grid. Both SAC terminals are required to have the unitary power factor, i.e. $i^0_{g_{1,2}q} = 0$ p.u. The WAC terminal is used to control its AC voltage at the prescribed values of $v^o_{sw_1d} = 1$ p.u. and $v^o_{sw_1q} = 0$ p.u.. To clarify the theoretical analysis, several scenarios are considered in this section. In addition, all simulations are carried out with the same control gains where[4] $K_{1[1]} = K_{1[2]} = K_{2[1]} = 1972 \cdot I_{2\times 2}$, $\Gamma_{1[1]} = \Gamma_{1[2]} = \Gamma_{2[1]} = 1.86 \times 10^4 \cdot I_{2\times 2}$, $k_{g_1d} = k_{w_{11}d} = k_{w_{11}q} = 40$, $k_{g_2d} = k_{w_{21}d} = k_{w_{22}q} = 400$ and hence $\varepsilon = 5.071 \times 10^{-4}$.

[4]Recall the definitions of the control gains in (5.60).

Table 5.6: Base quantities in the per-unit system.

AC side	$S_b = 3000$ VA	$V_b = 338.84$ V	$I_b \approx 5.90$ A
DC side	$S_{dc,b} = 3000$ VA	$V_{dc,b} = 700$ V	$I_{dc,b} \approx 4.29$ A

5.2.4.1 Scenario 1: Verification of time-scale separation

Simulation results are shown in Figs. 5.6 and 5.7. Let us first focus on the responses of $i_{w_1 d}$ and $i_{w_1 q}$ whose trajectories display two-time-scale behaviors. In contrast to the two states $i_{w_1 d}$ and $i_{w_1 q}$, whose initial conditions are their prescribed initial values, i.e. $i_{w_1 d_0} = 0.3$ p.u. and $i_{w_1 q_0} = 0.02$ p.u., their quasi-steady states $i^{re}_{w_1 d}$ and $i^{re}_{w_1 q}$ do not start from the same initial conditions but from $i^{re}_{w_1 d_0} = 0.4638$ p.u. and $i^{re}_{w_1 q_0} = -0.202$ p.u. since the initial values of $i^{re}_{w_1,dq}$ are determined by the initial values of $v^{re}_{sw_1,dq}$ as mentioned in Section 5.2.2.1. As a consequence, large discrepancies may exist between $i_{w_1,dq}$ and $i^{re}_{w_1,dq}$ at the initial instant.

As illustrated in Fig. 5.8, the trajectories of $i_{w_1,dq}$ start with very fast transients from the initial values $i_{w_1,dq}(t_0)$ to $i^{re}_{w_1,dq}$ during the boundary-layer interval. After the decay of the transients, $i_{w_1,dq}$ remain close to $i^{re}_{w_1,dq}$ and subsequently, both $i_{w_1,dq}$ and $i^{re}_{w_1,dq}$ converge to their steady values, i.e. $\bar{i}_{w_1 d} = 0.4667$ p.u. and $\bar{i}_{w_1 q} = -0.2528$ p.u. as shown in Figs. 5.7(c)-5.7(d). A similar two-time-scale behavior can be found in the response of $i_{g_1 d}$. Unlike the dq currents, $v_{w_1,dq}$, $u_{g_{1,2}}$ and u_{w_1} start from the same initial values as $v^{re}_{sw_1,dq}$, $u^{re}_{g_{1,2}}$ and $u^{re}_{w_1}$. In addition, they uniformly converge to $v^{re}_{sw_1,dq}$, $u^{re}_{g_{1,2}}$ and $u^{re}_{w_1}$, respectively. Simulation results (not presented here) show that while keeping $k_{g_1 d}$, $k_{w_{11} d}$, $k_{w_{11} q}$, $k_{g_2 d}$, $k_{w_{21} d}$ and $k_{w_{22} q}$ unchanged, we can reduce the errors between the dq currents and their quasi-steady states by increasing the control gain matrices $K_{1[1]}$, $K_{2[1]}$ and $K_{2[1]}$.

5.2.4.2 Scenario 2: Variations of the controlled current source

Variations in the controlled current source are considered in this scenario. Simulation results are illustrated in Fig. 5.9-5.10. This scenario reflects the unpredictable variation of power produced by a wind farm. P_{I_w} in Fig. 5.10(c) represents the generated power from the controlled current source, which is equivalent to P_{w_1}, i.e. the active power of the WAC terminal at the PCC. The DC-bus voltage is always controlled to the set value of 1 p.u. by the 1$^{\text{st}}$ SAC terminal irrespective of variations of P_{I_w} as depicted in Fig. 5.9(a). In this study case, the 1$^{\text{st}}$ SAC terminal operates as the slack bus to tolerate the power imbalance caused by P_{I_w} and in addition, this terminal is responsible to keep the voltage of the DC network constant, in spite of the uncontrollable variations of the wind power generation. Therefore, P_{g_1} varies with P_{I_w} while the active power of the 2$^{\text{nd}}$ SAC terminal (P_{g_2}) remains around its setpoint (0.2 p.u.). Moreover, the DC voltages of other nodes are also kept around 1 p.u. as plotted in Figs. 5.9(c) and 5.9(d). As seen in Figs. 5.7(a) and 5.7(b), $v_{sw_1,dq}$ at the PCC are always regulated at their setpoints, which means that both the amplitude and the frequency of the AC voltage at the PCC are controlled at the desired values. However, as illustrated in Fig. 5.10(d), extra reactive power Q_{w_1} is

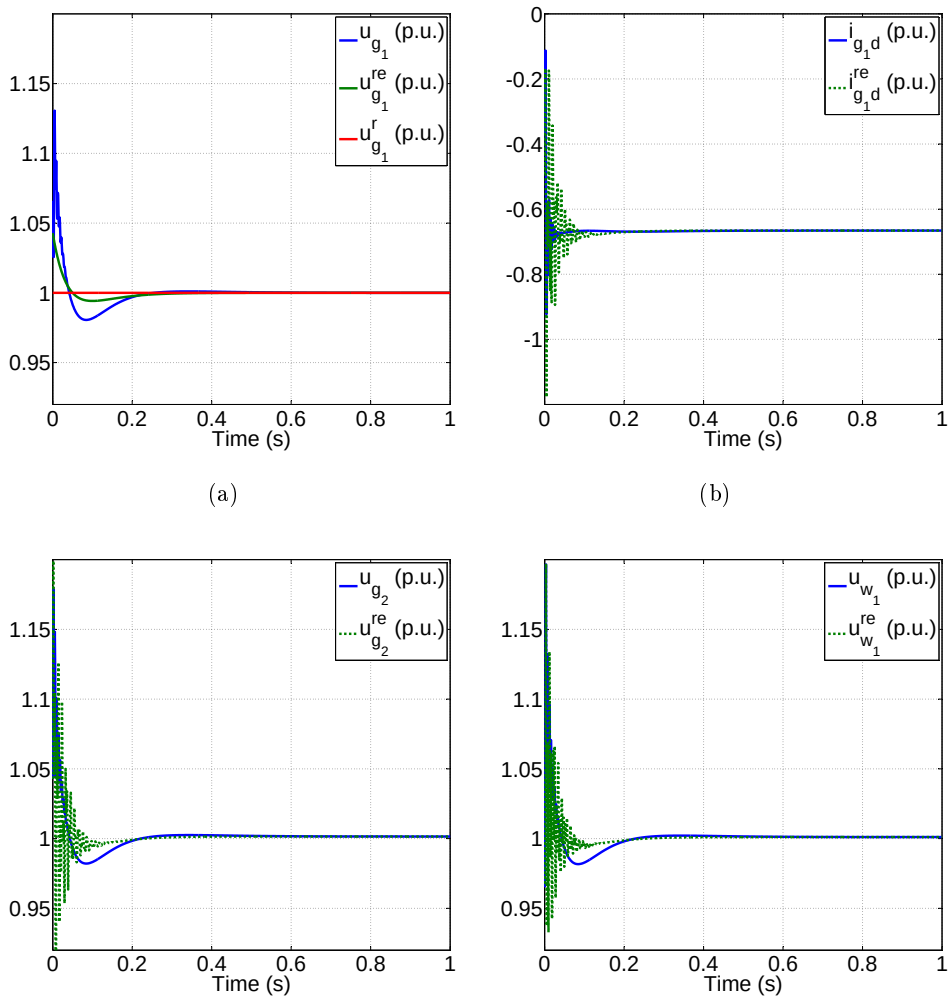

Figure 5.6: Simulation results with constant $I_{w_1,dq}$ (1).

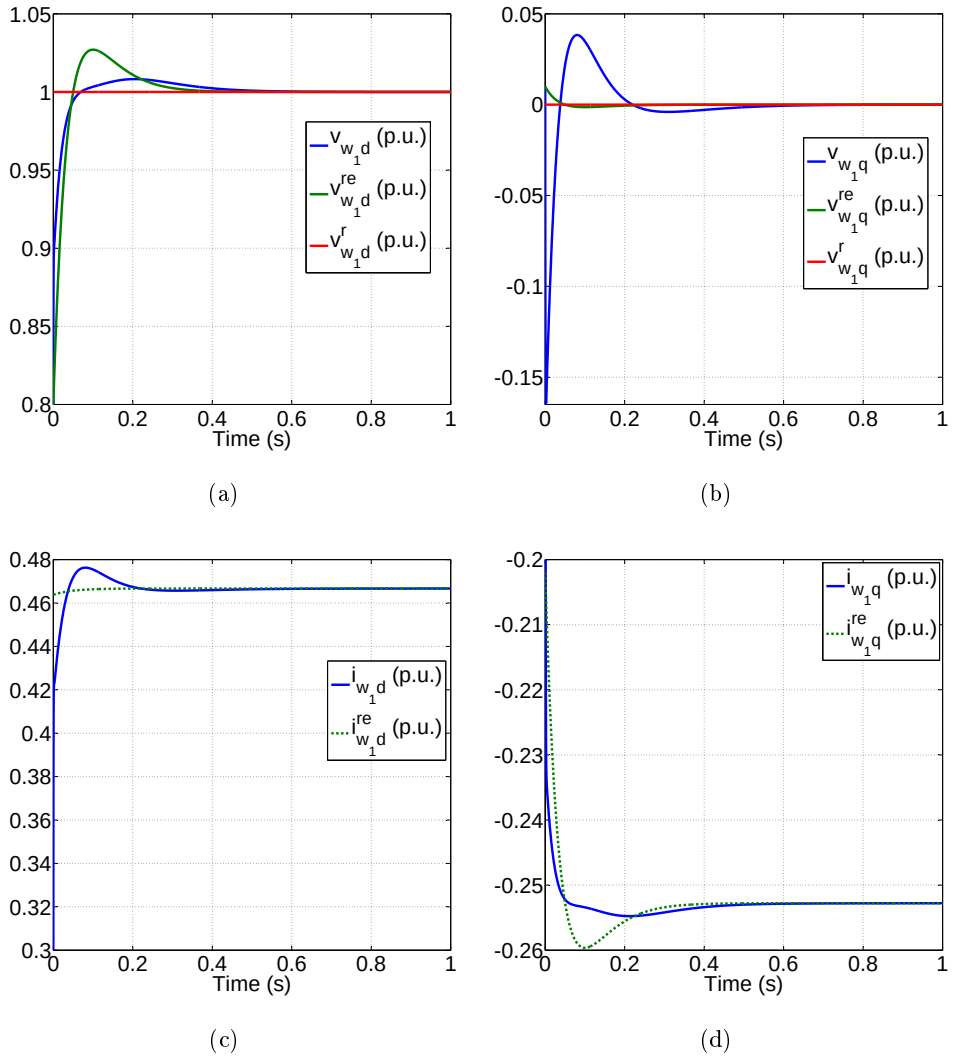

Figure 5.7: Simulation results with constant $I_{w_1,dq}$ (2).

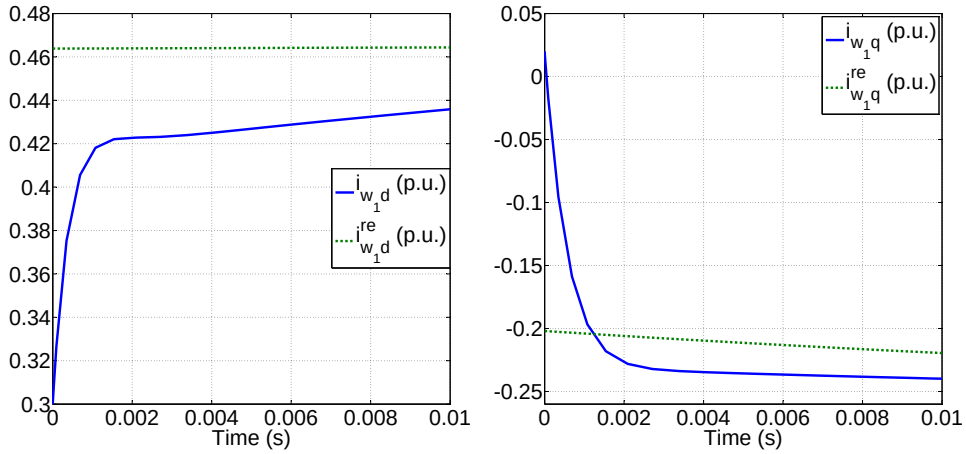

(a) (b)

Figure 5.8: Zooms of responses of $i_{w_1,dq}$ and $i^{re}_{w_1,dq}$ during the initial interval.

needed to maintain the AC voltage. Finally, a similar conclusion can be drawn as in Scenario 1, that is, the behaviors of the state variables can be well approximated by the solutions of their reduced model.

5.2.4.3 Scenario 3: Unplugging and plugging a terminal

In this study case, we evaluate the performance of the control scheme when considering the unplugging of the 2$^{\text{nd}}$ SAC connected VSC terminal and then plugging it back. Such unplugging and plugging operations can be highlighted as depicted in Fig. 5.12(d). At $t = 2$ s, the 2$^{\text{nd}}$ SAC terminal is disconnected and at the same time, the branch 2 is also removed from the MTDC system. Consequently, the WAC terminal now is the only power supplier for the 1$^{\text{st}}$ SAC terminal. As seen in Fig. 5.12(d), during $t \in [2,\ 4]$ s, P_{g_1} is almost equal to P_{w_1}. At $t = 4$ s, we re-use the branch 2 to connect the 2$^{\text{nd}}$ SAC terminal to the DC network. Now, the 2$^{\text{nd}}$ SAC terminal and the WAC terminal feed the power to the 1$^{\text{st}}$ SAC terminal together. In Figs. 5.11(a) and 5.11(c), the DC voltages are well regulated around 1 p.u. during the whole simulation with some short transients. As shown in Figs. 5.11(d) and 5.12(a), the dq components of the AC voltage at the PCC are also well controlled at their setpoints. The simulation results present that, with the aid of the proposed control strategy, the unplugging and plugging operations of the 2$^{\text{nd}}$ SAC terminal have negligible effects on the normal operations of the MTDC system.

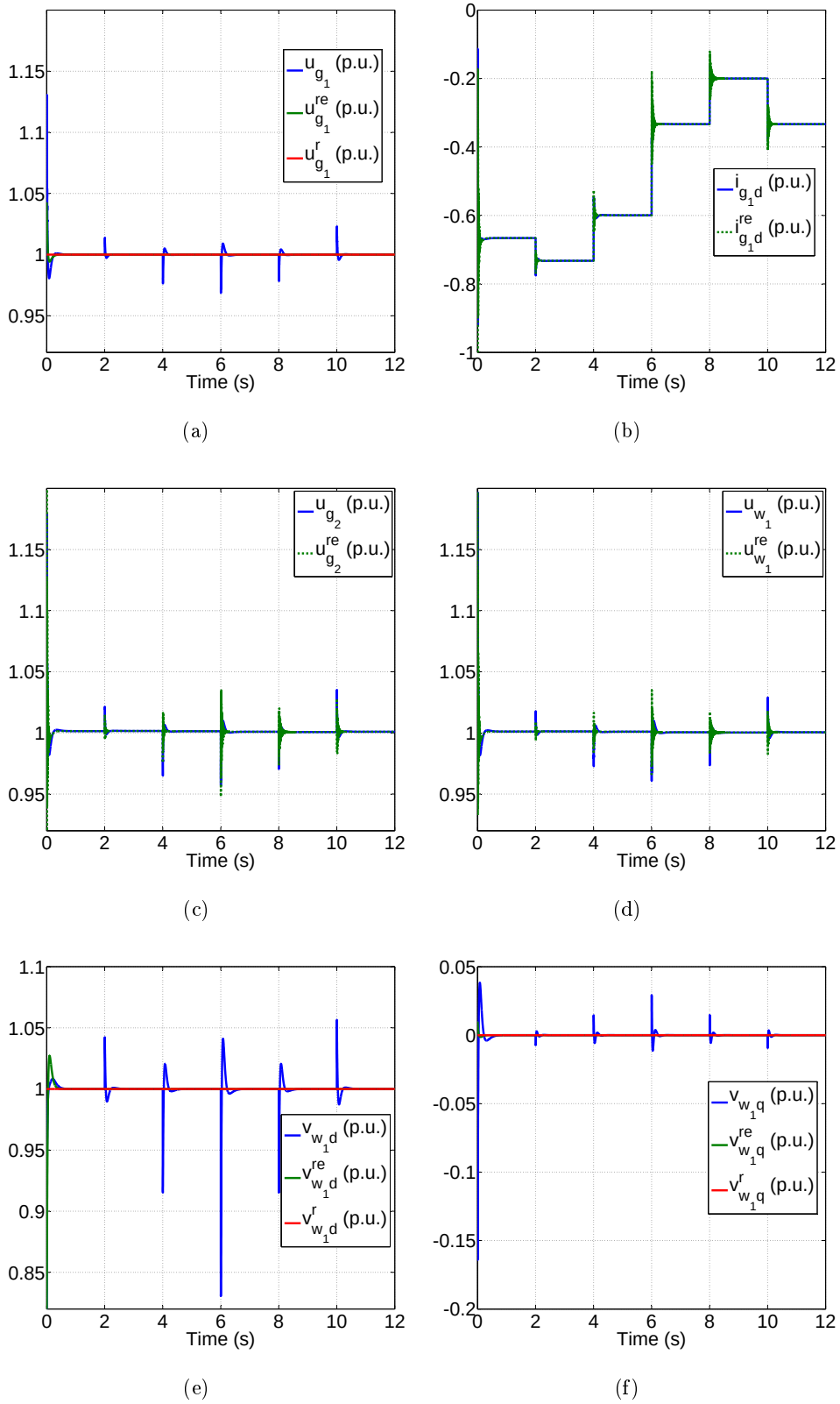

Figure 5.9: Simulation results with variations in the wind power production (1).

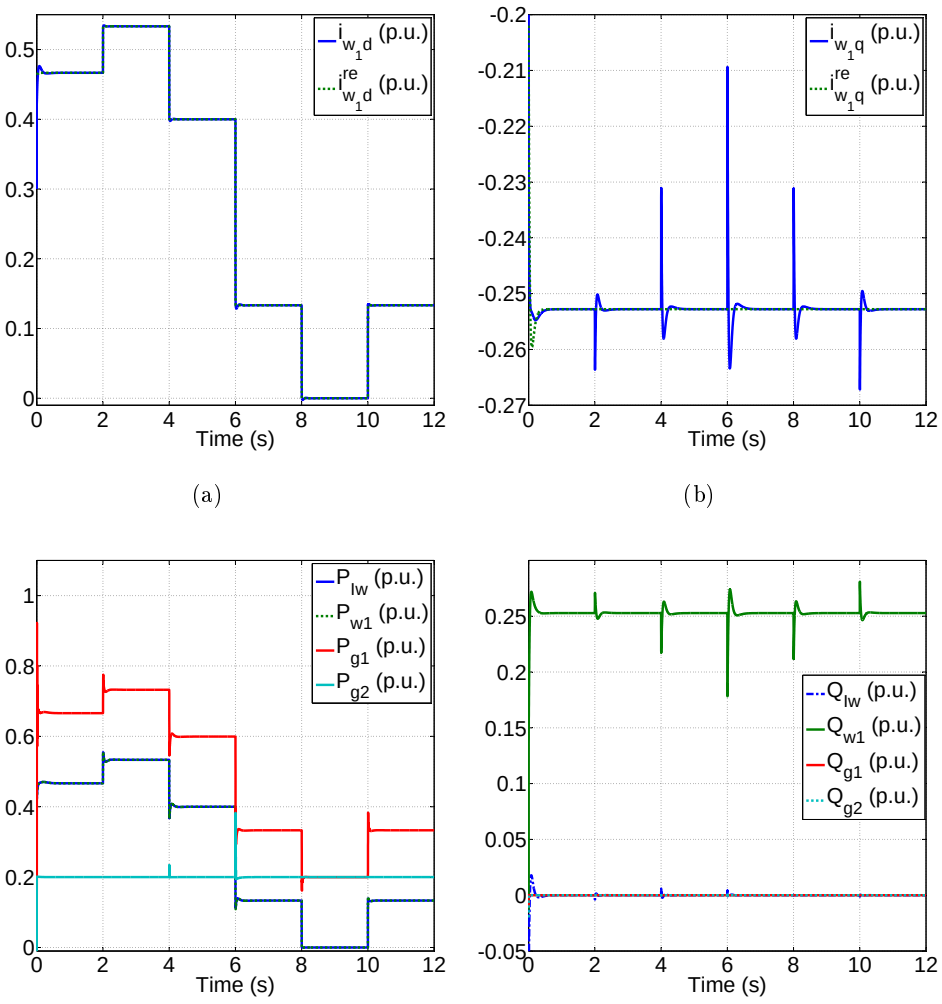

Figure 5.10: Simulation results with variations in the wind power production (2).

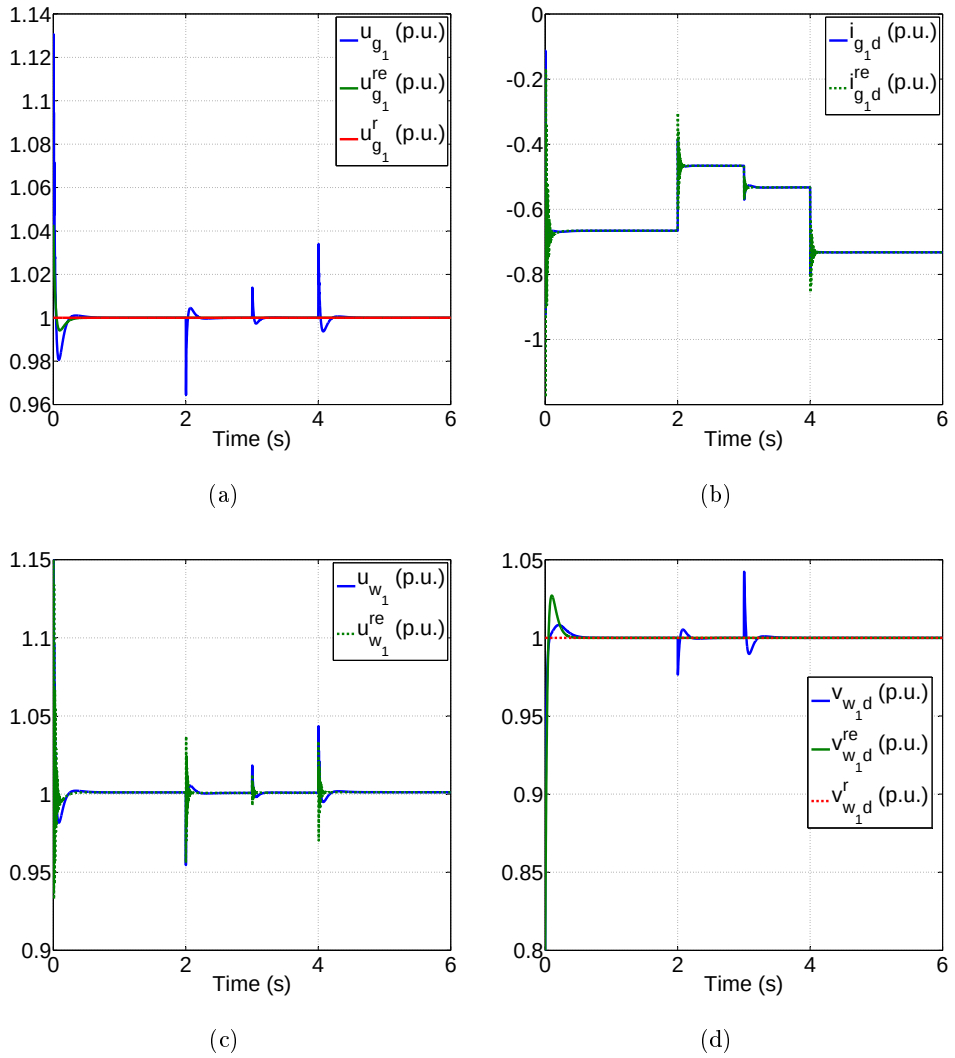

Figure 5.11: Simulation results with unplugging and plugging the 2$^{\text{nd}}$ SAC connected VSC terminal (1).

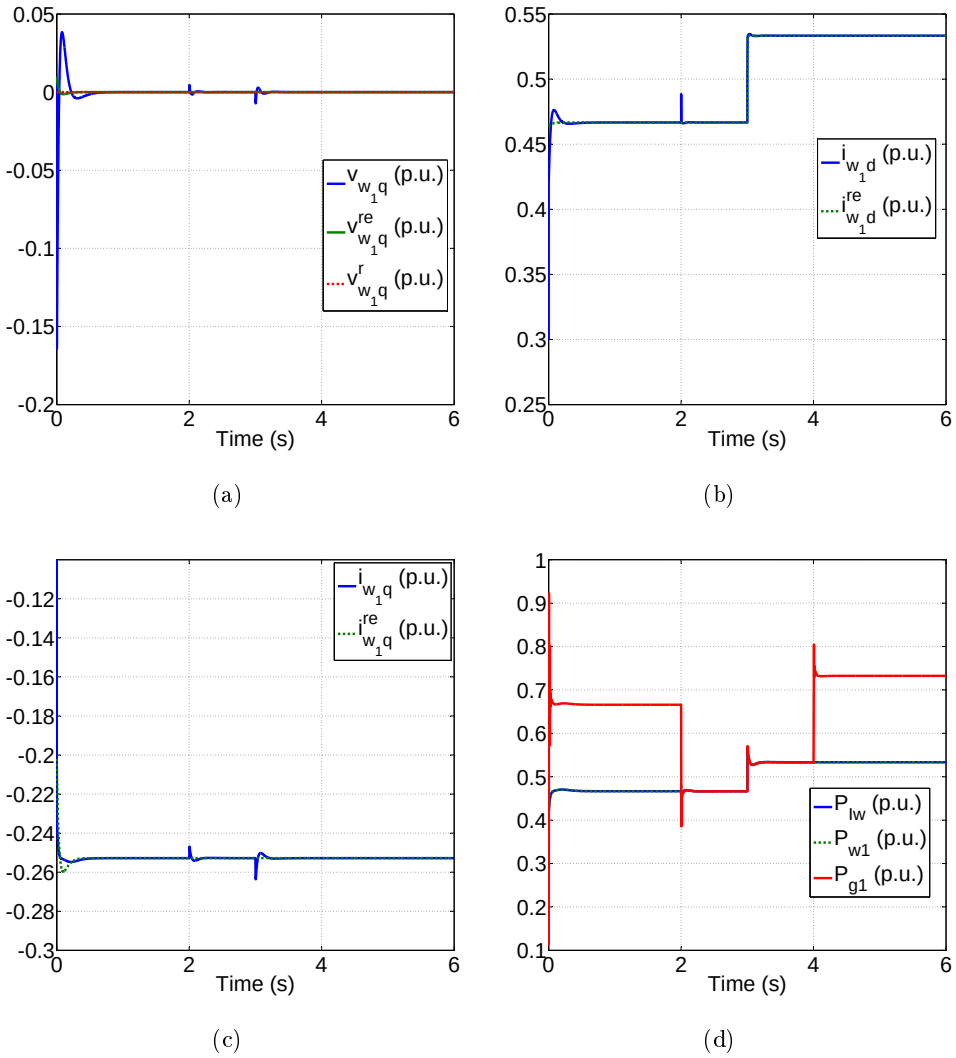

Figure 5.12: Simulation results with unplugging and plugging the 2nd SAC connected VSC terminal (2).

5.3 Control induced time-scale separation for MTDC systems using droop control configuration

As described in the previous sections, for an MTDC system, the control of DC voltage is indispensable. In Sections 4.1.4, 4.3 and 5.2, we have discussed the master-slave configuration. In this control configuration, only one VSC terminal (the master terminal) is used to regulate the DC voltage at a constant level while the other terminals operate in other control mode. The responsibility for maintaining power flow balance obviously falls on the master terminal. However, the disconnection of the master terminal leads the DC voltage beyond the safe domain of operation and thereby, damages the components of MTDC systems. In order to overcome this drawback, DC voltage droop control configuration [Wang 2014a, Prieto-Araujo 2011, Chaudhuri 2013, Bianchi 2011, Egea-Alvarez 2013, Chen 2014], usually characterized by power vs DC voltage (P vs U) or current vs DC voltage (I vs U) curves, becomes an alternative method, in particular for a large network.

In a DC voltage droop control scheme, more than one terminal is in charge of regulating the DC voltage and hence, the burden caused by power imbalance could be shared between several terminals. Additionally, this control method takes actions only based on local information without relying on remote communication. In droop control, the droop gains specify the system operation in steady-state condition and also have a great effect on the system transient performance. Different methodologies of choosing droop gains have been investigated. In [Prieto-Araujo 2011], a criterion for tuning the droop gains based on the performance specifications is proposed. In [Bianchi 2011], the droop gains are obtained by solving a constraint convex optimization problem. Reference [Chaudhuri 2013] develops an adaptive droop control scheme according to each terminal's available spare capacity. However, prior studies are usually under the unproven assertion that the dynamics of the inductor currents are much faster than the dynamics of the DC network. Therefore, the currents through the converters are assumed to equal their references and then, the dynamic interaction between AC and DC sides of the converters can be neglected.

Similar to the study on master-slave control configuration in Section 5.2, in this section, we acknowledge this assertion, then explore and explain the droop control induced time-scale separation. To achieve this aim, we will carry out a full theoretical analysis of the time-scale separation between the system state variables, mainly based on the theoretical results in Section 5.1. Furthermore, we will also demonstrate that the control gains have different effects on the system performance. For example, the droop gains play a major role in regulating the DC grid dynamics. Another objective of this section is to study the effects of the control gains, especially the droop gains, on the system stability.

5.3.1 VSC operation

The greatest difference between master-slave and droop control configuration is that the latter involves more terminals in the regulation of the DC voltage. This difference

leads to different VSC operation in droop control configuration, which is summarized as follows:

- Same to master-slave control configuration, to ensure that the power generated by the wind farms can be totally delivered via the DC grid, all WAC connected VSC terminals are still used to maintain their AC voltage magnitudes and frequencies constant at the PCCs, achieved by regulating $v_{sw_j,dq}$ at the prescribed values $v^o_{sw_j,dq}$.

- Every SAC terminal is equipped with the DC droop controller such that the duty of eliminating the power imbalance of the DC grid is shared between the SAC terminals. Moreover, the reactive powers of all the SAC terminals at the PCCs, i.e. Q_{g_i}, are required to track the reference values $Q^o_{g_i}$.

5.3.2 Droop control structure

The control design of droop control configuration is similar to that of master-slave control configuration in Section 5.2.1, which consists of two control loops, a fast inner current and a slow outer control loop, where the dynamics of state variables in the fast control loop are much faster than those in the slow control loop. But, in droop control structure, a droop law is implemented in the slow outer control loop of all SAC terminals, which generates the reference to the fast inner control loop.

5.3.2.1 Design of the fast control loop

As mentioned in Section 5.2.1.1, the control inputs $m_{(\cdot),dq}$ are directly collocated with the dq currents $i_{(\cdot),dq}$. Hence, a sub-controller can be developed such that $i_{(\cdot),dq}$ quickly converge to their reference trajectories $i^*_{(\cdot),dq}$ yet to be designed.

We first define the dq current tracking errors by

$$e_{i_{g_i,dq}} = i_{g_i,dq} - i^*_{g_i,dq}$$
$$e_{i_{w_j,dq}} = i_{w_j,dq} - i^*_{w_j,dq}$$

With the introduction of the integrated tracking errors $e_{Ii_{g_i,dq}}$ and $e_{Ii_{w_j,dq}}$, an aug-

mented dq current subsystem is then generated by

$$\begin{aligned}
\frac{de_{Ii_{g_id}}}{dt} &= e_{i_{g_id}} \\
\frac{de_{i_{g_id}}}{dt} &= -\frac{R_{g_i}}{L_{g_i}} i_{g_id} + \omega_{g_i} i_{g_iq} + \frac{v_{sg_id}}{L_{g_i}} - \frac{m_{g_id} u_{cg_i}}{2L_{g_i}} - \frac{di^*_{g_id}}{dt} \\
\frac{de_{Ii_{g_iq}}}{dt} &= e_{i_{g_iq}} \\
\frac{de_{i_{g_iq}}}{dt} &= -\frac{R_{g_i}}{L_{g_i}} i_{g_iq} - \omega_{g_i} i_{g_id} + \frac{v_{sg_iq}}{L_{g_i}} - \frac{m_{g_iq} u_{cg_i}}{2L_{g_i}} - \frac{di^*_{g_iq}}{dt} \\
\frac{de_{Ii_{w_id}}}{dt} &= e_{i_{w_id}} \\
\frac{de_{i_{w_jd}}}{dt} &= -\frac{R_{w_j}}{L_{w_j}} i_{w_jd} + \omega_{w_j} i_{w_jq} + \frac{v_{sw_jd}}{L_{w_j}} - \frac{m_{w_jd} u_{cw_j}}{2L_{w_j}} - \frac{di^*_{w_jd}}{dt} \\
\frac{de_{Ii_{w_iq}}}{dt} &= e_{i_{w_iq}} \\
\frac{de_{i_{w_jq}}}{dt} &= -\frac{R_{w_j}}{L_{w_j}} i_{w_jq} - \omega_{w_j} i_{w_jd} + \frac{v_{sw_jq}}{L_{w_j}} - \frac{m_{w_jq} u_{cw_j}}{2L_{w_j}} - \frac{di^*_{w_jq}}{dt}
\end{aligned} \tag{5.89}$$

In practice, the dynamics of $i^*_{g_i,dq}$ and $i^*_{w_j,dq}$ are usually neglected and considered as slow compared to $i_{g_i,dq}$ and $i_{w_j,dq}$. As a result, the modulation indices can then be designed as

$$\begin{aligned}
m_{g_id} =& \frac{2L_{g_i}}{u_{cg_i}}\left(-\frac{R_{g_i}}{L_{g_i}} i_{g_id} + \omega_{g_i} i_{g_iq} + \frac{v_{sg_id}}{L_{g_i}} + k_{1g_id} e_{i_{g_id}} + k_{2g_id} e_{Ii_{g_id}}\right) \\
m_{g_iq} =& \frac{2L_{g_i}}{u_{cg_i}}\left(-\frac{R_{g_i}}{L_{g_i}} i_{g_iq} - \omega_{g_i} i_{g_id} + \frac{v_{sg_iq}}{L_{g_i}} + k_{1g_iq} e_{i_{g_iq}} + k_{2g_iq} e_{Ii_{g_iq}}\right) \\
m_{w_jd} =& \frac{2L_{w_j}}{u_{cw_j}}\left(-\frac{R_{w_j}}{L_{w_j}} i_{w_jd} + \omega_{w_j} i_{w_jq} + \frac{v_{sw_jd}}{L_{w_j}} + k_{1w_id} e_{i_{w_id}} + k_{2w_id} e_{Ii_{w_id}}\right) \\
m_{w_jq} =& \frac{2L_{w_j}}{u_{cw_j}}\left(-\frac{R_{w_j}}{L_{w_j}} i_{w_jq} - \omega_{w_j} i_{w_jd} + \frac{v_{sw_jq}}{L_{w_j}} + k_{1w_iq} e_{i_{w_iq}} + k_{2w_iq} e_{Ii_{w_iq}}\right)
\end{aligned} \tag{5.90}$$

with positive control gains $k_{1g_i,dq}$, $k_{2g_i,dq}$, $k_{1w_j,dq}$ and $k_{2w_j,dq}$.

5.3.2.2 Design of the slow control loop

The main task of the slow control loop is to provide the slowly varying dq current references to the fast control loop. Most importantly, the dq current references need to be designed such that all control objectives are achieved. Since the operations of SAC terminals and WAC terminals are different, the design principles of $i^*_{g_i,dq}$ and $i^*_{w_j,dq}$ are also different.

Design of $i^*_{w_j,dq}$

We assume that $i_{w_j,dq}$ can quickly converge to their reference trajectories $i^*_{w_jdq}$ under the sub-controller (5.90). From there on, the AC voltage dynamics (3.29) of the wind

farm at the PCC become

$$\begin{aligned}\frac{dv_{sw_jd}}{dt}&= \omega_{w_j} v_{sw_jq} + \frac{1}{C_{fw_j}}(I_{w_jd} - i^*_{w_jd})\\ \frac{dv_{sw_jq}}{dt}&= -\omega_{w_j} v_{sw_jd} + \frac{1}{C_{fw_j}}(I_{w_jq} - i^*_{w_jq})\end{aligned} \tag{5.91}$$

where $i^*_{w_jdq}$ can be viewed as the control inputs. We call (5.91) the reduced model of (3.29) since the dynamics of $i_{w_j,dq}$ are neglected and $i_{w_j,dq}$ are replaced by $i^*_{w_j,dq}$. The control objective of WAC terminals is to keep $v_{sw_j,dq}$ at their reference values $v^o_{sw_j,dq}$ in spite of variations in the power productions of the wind farms. We then want to develop $i^*_{w_j,dq}$ in such a way that $v_{sw_j,dq}$ in (5.91) can be controlled at $v^o_{sw_j,dq}$. Similar to the design procedure of the fast control loop, we define the output tracking errors of voltage at the PCC as

$$e_{v_{sw_j,dq}} = v_{sw_j,dq} - v^o_{sw_j,dq} \tag{5.92}$$

We then augment (5.91) by taking the integrated tracking errors into account

$$\begin{aligned}\frac{de_{Iv_{sw_jd}}}{dt}&= e_{v_{sw_jd}}\\ \frac{de_{v_{sw_jd}}}{dt}&= \frac{1}{C_{fw_j}}(I_{w_jd} + C_{fw_j}\omega_{w_j} v_{sw_jq} - i^*_{w_jd}) - \frac{dv^o_{sw_jd}}{dt}\\ \frac{de_{Iv_{sw_jq}}}{dt}&= e_{v_{sw_jq}}\\ \frac{de_{v_{sw_jdq}}}{dt}&= \frac{1}{C_{fw_j}}(I_{w_jq} - C_{fw_j}\omega_{w_j} v_{sw_jd} - i^*_{w_jq}) - \frac{dv^o_{sw_jq}}{dt}\end{aligned} \tag{5.93}$$

Since the prescribed values $v^o_{sw_j,dq}$ are constant, we have $\frac{dv^o_{sw_j,dq}}{dt} = 0$. Finally, $i^*_{w_j,dq}$ can be designed as

$$\begin{aligned}i^*_{w_jd}&= I_{w_jd} + C_{fw_j}(k_{1d_j} e_{v_{sw_jd}} + k_{2d_j} e_{Iv_{sw_jd}} + \omega_{w_j} v_{sw_jq})\\ i^*_{w_jq}&= I_{w_jq} + C_{fw_j}(k_{1q_j} e_{v_{sw_jq}} + k_{2q_j} e_{Iv_{sw_jq}} - \omega_{w_j} v_{sw_jd})\end{aligned} \tag{5.94}$$

with positive k_{1,dq_j} and k_{2,dq_j} such that the equilibrium of the augmented model (5.93) is exponentially stable.

Design of $i^*_{g_i,dq}$

As mentioned before, a droop law is implemented in the slow outer control loop of all SAC terminal so that all SAC terminals participate in the regulation of the DC voltage in case of power imbalance. The droop control is usually expressed by DC voltage versus active power characteristic [Haileselassie 2012b].

$$P_{g_i} = P^o_{g_i} + K_{d_i}(u^o_{cg_i} - u_{cg_i}) \tag{5.95}$$

where $u^o_{cg_i}$ and $P^o_{g_i}$ refer to the reference values of DC voltage and active power respectively. The droop gain K_{d_i} is the ratio of the change in DC voltage to the

change in active power. According to (5.95), the varying reference for i_{g_id} can be expressed by

$$i^*_{g_id} = i^o_{g_id} - k_{d_i}(u_{cg_i} - u^o_{cg_i}) \tag{5.96}$$

where $i^o_{g_id}$ is obtained from (3.22) and expressed as

$$i^o_{g_id} = \frac{2P^o_{g_i}}{3v_{sg_id}}$$

In addition, the relation between K_{d_i} and k_{d_i} is given by

$$k_{d_i} = \frac{2}{3}\frac{1}{v_{sg_id}}K_{d_i}$$

The reference of i_{g_iq} is directly provided by the prescribed reference value

$$\begin{aligned} i^*_{g_iq} &= i^o_{g_iq} \\ &= -\frac{2}{3}\frac{Q^o_{g_i}}{v_{sg_id}} \end{aligned} \tag{5.97}$$

5.3.3 Theoretical analysis

As the master-slave control structure in Section 5.2.1, the developed droop control design concept is also mainly based on the assumption that a dynamic separation in time scales is imposed between the fast and slow control loops. As a consequence, z and $v_{sw_j,dq}$ can be considered as constant in the fast control loop, while the dq currents can be replaced by their references in the slow control loop.

In this section, we give a detailed theoretical analysis to demonstrate the validity of the time-scale separation assumption in droop control configuration and furthermore, to investigate the possible limitations on the droop gains.

5.3.3.1 Equilibrium analysis

Before going further, we give a brief analysis of the equilibruim point. Substituting the controller composed by (5.90), (5.94) ,(5.96) and (5.97) into the plant model described by (3.20), (3.28), (3.29) and (3.36) leads to the following augmented closed-

loop system

$$\begin{aligned}
\frac{de_{Ii_{g_id}}}{dt} &= e_{i_{g_id}} \\
\frac{di_{g_id}}{dt} &= -k_{1g_id}e_{i_{g_id}} - k_{2g_id}e_{Ii_{g_id}} \\
\frac{de_{Ii_{g_iq}}}{dt} &= e_{i_{g_iq}} \\
\frac{di_{g_iq}}{dt} &= -k_{1g_iq}e_{i_{g_iq}} - k_{2g_iq}e_{Ii_{g_iq}} \\
\frac{de_{Ii_{w_jd}}}{dt} &= e_{i_{w_jd}} \\
\frac{di_{w_jd}}{dt} &= -k_{1w_jd}e_{i_{w_jd}} - k_{2w_jd}e_{Ii_{w_jd}} \\
\frac{de_{Ii_{w_jq}}}{dt} &= e_{i_{w_jq}} \\
\frac{di_{w_jq}}{dt} &= -k_{1w_jq}e_{i_{w_jq}} - k_{2w_jq}e_{Ii_{w_jq}} \\
\frac{de_{Iv_{sw_jd}}}{dt} &= e_{v_{sw_jd}} \\
\frac{dv_{sw_jd}}{dt} &= -k_{1d_j}e_{v_{sw_jd}} - k_{2d_j}e_{Iv_{sw_jd}} - \frac{e_{i_{w_jd}}}{C_{fw_j}} \\
\frac{de_{Iv_{sw_jq}}}{dt} &= e_{v_{sw_jq}} \\
\frac{dv_{sw_jq}}{dt} &= -k_{1q_j}e_{v_{sw_jq}} - k_{2q_j}e_{Iv_{sw_jq}} - \frac{e_{i_{w_jq}}}{C_{fw_j}} \\
\dot{z} &= Az + \vartheta
\end{aligned} \tag{5.98}$$

It will be more convenient in the following analysis to divide ϑ into two parts as

$$\vartheta = \vartheta_g + \vartheta_w$$

Recalling i_{cg_i} in (3.23), i_{cw_i} in (3.32), $i^*_{w_j,dq}$ in (5.94) and $i^*_{g_i,dq}$ in (5.96) and (5.97), the new variables ϑ_g and ϑ_w are given by

$$\vartheta_g = \vartheta_{g_1} + \vartheta_{g_2} + \vartheta_{g_3},\ \vartheta_w = \vartheta_{w_1} + \vartheta_{w_2} + \vartheta_{w_3} + \vartheta_{w_4}$$

with

$$\vartheta_{g_1}(i) = \begin{cases} \dfrac{3}{2C_{g_i}} \dfrac{v_{sg_id}i^o_{g_id} + v_{sg_iq}i^o_{g_iq}}{u_{cg_i}}, & i \in \mathcal{N} \\ 0. & \text{otherwise} \end{cases}$$

$$\vartheta_{g_2}(i) = \begin{cases} -\dfrac{3}{2C_{g_i}} v_{sg_id}k_{d_i} \dfrac{u_{cg_i} - u^o_{cg_i}}{u_{cg_i}}, & i \in \mathcal{N} \\ 0. & \text{otherwise} \end{cases}$$

$$\vartheta_{g_3}(i) = \begin{cases} \dfrac{3}{2C_{g_i}} \dfrac{v_{sg_id}e_{i_{g_id}} + v_{sg_iq}e_{i_{g_iq}}}{u_{cg_i}}, & i \in \mathcal{N} \\ 0. & \text{otherwise} \end{cases}$$

and

$$\vartheta_{w_1}(j+N)=\begin{cases}\dfrac{3}{2C_{w_j}}\dfrac{v^o_{sw_jd}I_{w_jd}+v^o_{sw_jq}I_{w_jq}}{u_{cw_j}}, & j\in\mathcal{M}\\ 0. & \text{otherwise}\end{cases}$$

$$\vartheta_{w_2}(j+N)=\begin{cases}\dfrac{3}{2C_{w_j}}\left[\dfrac{v^o_{sw_jd}C_{fw_j}\omega_{w_j}e_{v_{sw_jq}}+e_{v_{sw_jd}}I_{w_jd}}{u_{cw_j}}\right.\\ \left.+\dfrac{e_{v_{sw_jq}}I_{w_jq}-v^o_{sw_jq}C_{fw_j}\omega_{w_j}e_{v_{sw_jd}}}{u_{cw_j}}\right], & j\in\mathcal{M}\\ 0. & \text{otherwise}\end{cases}$$

$$\vartheta_{w_3}(j+N)=\begin{cases}\dfrac{3}{2C_{w_j}}\left[\dfrac{v_{sw_jd}(k_{1d_j}e_{v_{sw_jd}}+k_{2d_j}e_{Iv_{sw_jd}})}{u_{cw_j}}\right.\\ \left.+\dfrac{v_{sw_jq}(k_{1q_j}e_{v_{sw_jq}}+k_{2q_j}e_{Iv_{sw_jq}})}{u_{cw_j}}\right], & j\in\mathcal{M}\\ 0. & \text{otherwise}\end{cases}$$

$$\vartheta_{w_4}(j+N)=\begin{cases}\dfrac{3}{2C_{w_j}}\dfrac{v_{sw_jd}e_{i_{w_jd}}+v_{sw_jq}e_{i_{w_jq}}}{u_{cw_j}}, & j\in\mathcal{M}\\ 0. & \text{otherwise}\end{cases}$$

It is obvious that, if the dq currents quickly enter their respective manifolds, i.e. $e_{i_{g_i,dq}}\to 0$ and $e_{i_{w_j,dq}}\to 0$, ϑ_{g_3} and ϑ_{w_4} converge to zero. Moreover, ϑ_{w_2} and ϑ_{w_3} also go to zero as $e_{v_{sw_j,dq}}\to 0$. These results are helpful for the theoretical analysis in the next part.

When the closed-loop system (5.98) is in the steady-state condition, the following algebraic equations

$$A\bar{z}+\bar{\vartheta}_g+\bar{\vartheta}_w=0 \tag{5.99}$$

must hold[5]. Since $P^o_{g_i}=3/2(v_{sg_id}i^o_{g_id}+v_{sg_iq}i^o_{g_iq})$, $\bar{\vartheta}_g$ and $\bar{\vartheta}_w$ can be then expressed as

$$\begin{aligned}\bar{\vartheta}_g(i)&=\begin{cases}\dfrac{P^0_{g_i}+\dfrac{3}{2}k_{d_i}v_{sg_id}u^o_{cg_i}}{C_{g_i}\bar{u}_{g_i}}-\dfrac{3v_{sg_id}}{2C_{g_i}}k_{d_i}, i\in\mathcal{N}\\ 0. \ \text{otherwise}\end{cases}\\ \bar{\vartheta}_w(j+N)&=\begin{cases}\dfrac{P^o_{w_j}}{C_{w_j}u_{cw_j}}, & j\in\mathcal{M}\\ 0. & \text{otherwise}\end{cases}\end{aligned} \tag{5.100}$$

where we introduced the new variable

$$P^o_{w_j}=3/2(v^o_{sw_jd}I_{w_jd}+v^o_{sw_jq}I_{w_jq})$$

[5]Recall that the notation $\bar{(\cdot)}$ denotes the steady-state value of the variable $(\cdot)$.

From the algebraic equation (5.99), it is shown that the prescribed values $(\cdot)^o$, the DC grid topology and the droop gains k_{d_i} determine the steady-state values of the system variables and the distribution of power sharing together in case of power imbalance. The control gains $k_{1g_i,dq}$, $k_{2g_i,dq}$, $k_{1w_j,dq}$, $k_{2w_j,dq}$, k_{1,dq_j} and k_{2,dq_j} have no effect on the steady state of the system. However, as (4.58) in Section 4.1.4 and (4.96) in Section 4.3.2, solving equation (5.99) to get the exact steady-state value is not easy and is not considered in this section. More details about this issue can be referred in [Wang 2014a, Haileselassie 2012b].

To ensure the operating feasibility of the MTDC system, we assume that $\bar{i}_{g_i dq}$, $\bar{i}_{w_j dq}$, $\bar{u}_{cg_i}$, $\bar{u}_{cw_j}$, $\bar{u}_{ct_h}$ and $\bar{i}_{c_k}$ exist and belong to their respective safe operating domains. The equilibrium of the closed-loop system is denoted by $\bar{S}$.

In stead-state condition, From the droop law (5.95), we have

$$\bar{P}_{g_i} = P^o_{g_i} + K_{d_i}(u^o_{cg_i} - \bar{u}_{cg_i}) \tag{5.101}$$

Consider that the MTDC system initially ($t = t_0$) operates in a steady-state condition, if the production of the wind farms increases at the instant t_1, this makes the SAC terminals absorb more power from the DC grid. When the MTDC system achieves a new steady state at t_2, we have $\bar{P}_{g_i}(t_2) < \bar{P}_{g_i}(t_0)$ (for example, $\bar{P}_{g_i}(t_0) = -100$ MW and $\bar{P}_{g_i}(t_2) = -200$ MW). According to (5.101), we can deduce that the DC voltage also rises to a new level and that $\bar{u}_{g_i}(t_2) > \bar{u}_{g_i}(t_0)$. It can be summarized that u_{cg_i} will rise if more power is injected into the DC grid, and vice versa. This statement will be illustrated by numerical simulations in Section 5.3.4.

5.3.3.2 Multi-time-scale dynamics

In this section, a theoretical analysis to describe the dynamic separation in time-scales is carried out. We present that two different dynamics are created by the designed control algorithm in Section 5.3.2. In particular, the two time-scales are quantified by the fast control gains $k_{1g_i,dq}$, $k_{2g_i,dq}$, $k_{1w_j,dq}$ and $k_{2w_j,dq}$.

In order to make the analysis convenient, we perform a change of variables.

Then, the first eight equations of the closed-loop system (5.98) can be rewritten as

$$\begin{aligned}
\frac{de_{Ii_{g_id}}}{dt} &= e_{i_{g_id}} \\
\frac{de_{i_{g_id}}}{dt} &= -k_{1g_id}e_{i_{g_id}} - k_{2g_id}e_{Ii_{g_id}} - \frac{di^*_{g_id}}{dt} \\
\frac{de_{Ii_{g_iq}}}{dt} &= e_{i_{g_iq}} \\
\frac{de_{i_{g_iq}}}{dt} &= -k_{1g_iq}e_{i_{g_iq}} - k_{2g_iq}e_{Ii_{g_iq}} - \frac{di^*_{g_iq}}{dt} \\
\frac{de_{Ii_{w_jd}}}{dt} &= e_{i_{w_jd}} \\
\frac{de_{i_{w_jd}}}{dt} &= -k_{1w_jd}e_{i_{w_jd}} - k_{2w_jd}e_{Ii_{w_jd}} - \frac{di^*_{w_jd}}{dt} \\
\frac{de_{Ii_{w_jq}}}{dt} &= e_{i_{w_jq}} \\
\frac{de_{i_{w_jq}}}{dt} &= -k_{1w_jq}e_{i_{w_jq}} - k_{2w_jq}e_{Ii_{w_jq}} - \frac{di^*_{w_jq}}{dt}
\end{aligned} \tag{5.102}$$

This shifts the quasi-steady states of the dq currents to the origin. Denote $k_1 = \min(k_{1g_id}, k_{2g_iq}, k_{1w_id}, k_{2w_iq})$ and then introduce a new variable ε satisfying $\varepsilon k_1 = 1$. The subsystem (5.102) is given by

$$\begin{aligned}
\frac{de_{Ii_{g_id}}}{dt} &= e_{i_{g_id}} \\
\varepsilon\frac{de_{i_{g_id}}}{dt} &= -\bar{k}_{1g_id}e_{i_{g_id}} - \varepsilon k_{2g_id}e_{Ii_{g_id}} - \varepsilon\frac{di^*_{g_id}}{dt} \\
\frac{de_{Ii_{g_iq}}}{dt} &= e_{i_{g_iq}} \\
\varepsilon\frac{de_{i_{g_iq}}}{dt} &= -\bar{k}_{1g_iq}e_{i_{g_iq}} - \varepsilon k_{2g_iq}e_{Ii_{g_iq}} - \varepsilon\frac{di^*_{g_iq}}{dt} \\
\frac{de_{Ii_{w_jd}}}{dt} &= e_{i_{w_jd}} \\
\varepsilon\frac{de_{i_{w_jd}}}{dt} &= -\bar{k}_{1w_jd}e_{i_{w_jd}} - \varepsilon k_{2w_jd}e_{Ii_{w_jd}} - \varepsilon\frac{di^*_{w_jd}}{dt} \\
\frac{de_{Ii_{w_jq}}}{dt} &= e_{i_{w_jq}} \\
\varepsilon\frac{de_{i_{w_jq}}}{dt} &= -\bar{k}_{1w_jq}e_{i_{w_jq}} - \varepsilon k_{2w_jq}e_{Ii_{w_jq}} - \varepsilon\frac{di^*_{w_jq}}{dt}
\end{aligned} \tag{5.103}$$

where

$$\begin{aligned}
\bar{k}_{1g_id} = \varepsilon k_{1g_id} \geq 1;\ \bar{k}_{1g_iq} = \varepsilon k_{1g_iq} \geq 1 \\
\bar{k}_{1w_jd} = \varepsilon k_{1w_jd} \geq 1;\ \bar{k}_{1w_jq} = \varepsilon k_{1w_jq} \geq 1
\end{aligned}$$

We define a new time variable τ as

$$\varepsilon\frac{dy}{dt} = \frac{dy}{d\tau} \tag{5.104}$$

Substituting (5.104) into (5.103) and then setting $\varepsilon = 0$, we obtain the following autonomous system

$$\begin{aligned}
\frac{de_{i_{g_i d}}}{d\tau} &= -\bar{k}_{1g_i d} e_{i_{g_i d}} \\
\frac{de_{i_{g_i q}}}{d\tau} &= -\bar{k}_{1g_i q} e_{i_{g_i q}} \\
\frac{de_{i_{w_j d}}}{d\tau} &= -\bar{k}_{1w_j d} e_{i_{w_j d}} \\
\frac{de_{i_{w_j q}}}{d\tau} &= -\bar{k}_{1w_j q} e_{i_{w_j q}}
\end{aligned} \tag{5.105}$$

which is called the boundary-layer model of the system (5.98). When $\varepsilon \to 0$, it seems that the time variable t and the slow state variables are frozen at their initial values. By using Lyapunov analysis, the origin of the boundary system (5.105) is exponentially stable. When the dq currents quickly converge to their reference trajectories during the initial interval, the full-scale system (5.98) is degenerated into the following reduced model

$$\begin{aligned}
\frac{de_{Iv_{sw_j d}}}{dt} &= e_{v_{sw_j d}} \\
\frac{dv_{sw_j d}}{dt} &= -k_{1d_j} e_{v_{sw_j d}} - k_{2d_j} e_{Iv_{sw_j d}} \\
\frac{de_{Iv_{sw_j q}}}{dt} &= e_{v_{sw_j q}} \\
\frac{dv_{sw_j q}}{dt} &= -k_{1q_j} e_{v_{sw_j q}} - k_{2q_j} e_{Iv_{sw_j q}} \\
\frac{dz}{dt} &= Az + \vartheta'_g + \vartheta'_w
\end{aligned} \tag{5.106}$$

where $\vartheta'_g = \vartheta_{g_1} + \vartheta_{g_2}$ and $\vartheta'_w = \vartheta_{w_1} + \vartheta_{w_2} + \vartheta_{w_3}$. In addition, the solution of the reduced model (5.106) is denoted by $(\cdot)^{re}$. Now, we can state the first result of this section.

Theorem 5.3.1. *Consider the system (5.98) where all state variables are restrict to their respective safe operating domains for $t \in [t_0,\ t_1]$. There exists a positive constant ε^* such that for all $0 < \varepsilon = 1/k_1 < \varepsilon^*$, the system (5.98) has a unique solution on $[t_0,\ t_1]$, and the trajectories of the state variables can be approximated by*

$$\begin{aligned}
i_{g_i,dq} - i^*_{g_i,dq}(z^{re}) - \widehat{e}_{i_{g_i,dq}} &= O(\varepsilon) \\
i_{w_j,dq} - i^*_{w_j,dq}(z^{re},\ v^{re}_{sw_j,dq}) - \widehat{e}_{i_{w_j,dq}} &= O(\varepsilon) \\
v_{sw_j,dq} - v^{re}_{sw_j,dq} &= O(\varepsilon) \\
z - z^{re} &= O(\varepsilon)
\end{aligned} \tag{5.107}$$

held uniformly for $t \in [t_0,\ t_1]$ where $\hat{e}_{i_{g_i,dq}}$ and $\hat{e}_{i_{w_j,dq}}$ are the solution of the boundary-layer model (5.105)

$$\begin{aligned}
\widehat{e}_{i_{g_i,dq}} &= e_{i_{g_i,dq}}(t_0)\exp(-\bar{k}_{1g_i,dq}\tau) \\
\widehat{e}_{i_{w_j,dq}} &= e_{i_{w_j,dq}}(t_0)\exp(-\bar{k}_{1w_j,dq}\tau)
\end{aligned} \tag{5.108}$$

Proof. It is obvious that the origin of the boundary-layer model (5.105) is globally exponentially stable. Besides, the reduced model (5.106) has a unique solution. Therefore, the approximations (5.107) can be deduced from the theoretical results in Section 5.2.2.1. □

In terms of (5.107), the dq currents exhibit a two-time-scale behavior by presenting a slow and a fast transients. It is the dq current tracking errors, $\widehat{e}_{i_{g_i,dq}}$ and $\widehat{e}_{i_{w_j,dq}}$, that characterize the part of fast dynamics. It is shown that $i_{(\cdot),dq}$ start with a fast transient which exactly corresponds to the solution of boundary-layer model (5.105) during the initial interval. After the exponential decay of the fast transients $\widehat{e}_{i_{g_i,dq}}$ ($\widehat{e}_{j_{w_i,dq}}$), $i_{(\cdot),dq}$ remain close to their respective manifolds $i^*_{(\cdot),dq}$ in the future time.

As expressed in (5.108), the control gains $k_{1g_i,dq}$, $k_{2g_i,dq}$, $k_{1w_j,dq}$ and $k_{2w_j,dq}$ play a major role in regulating the fast transient performance and hence we call them the fast control gains. The control gains k_{1,dq_j}, k_{2,dq_j} and k_{d_i}, dominate the slow transient performance, and they are consequently called the slow control gains.

5.3.3.3 Stability analysis

For the sake of simplicity, we introduce a new variable

$$e_z = z - \bar{z} \tag{5.109}$$

Now, the closed-loop system (5.98) becomes

$$\begin{aligned}
\frac{de_{Ii_{g_id}}}{dt} &= e_{i_{g_id}} \\
\frac{de_{i_{g_id}}}{dt} &= -k_{1g_id}e_{i_{g_id}} - k_{2g_id}e_{Ii_{g_id}} - \frac{di^*_{g_id}}{dt} \\
\frac{de_{Ii_{g_iq}}}{dt} &= e_{i_{g_iq}} \\
\frac{de_{i_{g_iq}}}{dt} &= -k_{1g_iq}e_{i_{g_iq}} - k_{2g_iq}e_{Ii_{g_iq}} - \frac{di^*_{g_iq}}{dt} \\
\frac{de_{Ii_{w_jd}}}{dt} &= e_{i_{w_jd}} \\
\frac{de_{i_{w_jd}}}{dt} &= -k_{1w_jd}e_{i_{w_jd}} - k_{2w_jd}e_{Ii_{w_jd}} - \frac{di^*_{w_jd}}{dt} \\
\frac{de_{Ii_{w_jq}}}{dt} &= e_{i_{w_jq}} \\
\frac{de_{i_{w_jq}}}{dt} &= -k_{1w_jq}e_{i_{w_jq}} - k_{2w_jq}e_{Ii_{w_jq}} - \frac{di^*_{w_jq}}{dt} \\
\frac{de_{Iv_{sw_jd}}}{dt} &= e_{v_{sw_jd}} \\
\frac{de_{v_{sw_jd}}}{dt} &= -k_{1d_j}e_{v_{sw_jd}} - k_{2d_j}e_{Iv_{sw_jd}} - \frac{e_{i_{w_jd}}}{C_{fw_j}} \\
\frac{de_{Iv_{sw_jq}}}{dt} &= e_{v_{sw_jq}} \\
\frac{de_{v_{sw_jq}}}{dt} &= -k_{1q_j}e_{v_{sw_jq}} - k_{2q_j}e_{Iv_{sw_jq}} - \frac{e_{i_{w_jq}}}{C_{fw_j}} \\
\frac{de_z}{dt} &= Ae_z + A\bar{z} + \vartheta_g + \vartheta_w
\end{aligned} \tag{5.110}$$

where the equilibrium of the original closed-loop system, $\bar{S}$, is shifted to the origin. We call (5.110) the error system of the closed-loop system. In terms of those tracking errors, the varying reference trajectories (5.94) can be expressed by

$$\begin{aligned}
i^*_{w_jd} =& C_{fw_j}\omega_{w_j}(v^o_{sw_jq} + e_{v_{sw_jq}}) + I_{w_jd} \\
&+ k_{1d_j}e_{v_{sw_jd}} + k_{2d_j}e_{Iv_{sw_jd}} \\
i^*_{w_jq} =& -C_{fw_j}\omega_{w_j}(v^o_{sw_jd} + e_{v_{sw_jd}}) + I_{w_jq} \\
&+ k_{1q_j}e_{v_{sw_jq}} + k_{2q_j}e_{Iv_{sw_jq}}
\end{aligned} \tag{5.111}$$

Since $I_{w_j,dq}$ are considered constant or slowly varying and then $\frac{dI_{w_j,dq}}{dt} = 0$, the derivatives of the dq references are given by

$$\begin{aligned}
\frac{di^*_{g_id}}{dt} &= -k_{d_i}\frac{de_{u_{g_i}}}{dt} \\
\frac{di^*_{g_iq}}{dt} &= 0 \\
\frac{di^*_{w_jd}}{dt} &= C_{fw_j}\omega_{w_j}\frac{de_{v_{sw_jq}}}{dt} + k_{1d_j}\frac{de_{v_{sw_jd}}}{dt} + k_{2d_j}e_{v_{sw_jd}} \\
\frac{di^*_{w_jq}}{dt} &= -C_{fw_j}\omega_{w_j}\frac{de_{v_{sw_jd}}}{dt} + k_{1q_j}\frac{de_{v_{sw_jq}}}{dt} + k_{2q_j}e_{v_{sw_jq}}
\end{aligned} \tag{5.112}$$

Note that the asymptotic stability of the origin of the error system (5.110) would imply the asymptotic stability of the equilibrium $\bar{S}$ of the original closed-loop system (5.98). Hence, we investigate the stability of the error system (5.110) instead of the original closed-loop system (5.98).

If $e_{i_{g_i dq}}$ and $e_{i_{w_j dq}}$ converge to zero, a new reduced model is deduced from the error system as

$$\begin{aligned}
\frac{de_{Iv_{sw_j d}}}{dt} &= e_{v_{sw_j d}} \\
\frac{de_{v_{sw_j d}}}{dt} &= -k_{1d_j} e_{v_{sw_j d}} - k_{2d_j} e_{Iv_{sw_j d}} \\
\frac{de_{Iv_{sw_j q}}}{dt} &= e_{v_{sw_j q}} \\
\frac{de_{v_{sw_j q}}}{dt} &= -k_{1q_j} e_{v_{sw_j q}} - k_{2q_j} e_{Iv_{sw_j q}} \\
\frac{de_z}{dt} &= Ae_z + A\bar{z} + \vartheta'_g + \vartheta'_w
\end{aligned} \tag{5.113}$$

where $\vartheta'_g = \vartheta_{g_1} + \vartheta_{g_2}$ and $\vartheta'_w = \vartheta_{w_1} + \vartheta_{w_2}$. The reduced model (5.113) can be divided into two parts, the external dynamics represented by $e_{v_{sw_j,dq}}$ and $e_{Iv_{sw_j,dq}}$ and the internal dynamics represented by e_z. As the external variables converge to zero, i.e. $e_{v_{sw_j,dq}} \to 0$ and $e_{Iv_{sw_j,dq}} \to 0$, the behavior of the reduced model (5.113) is governed by the internal subsystem

$$\frac{de_z}{dt} = Ae_z + A\bar{z} + \vartheta''_g + \vartheta''_w \triangleq f_{zero} \tag{5.114}$$

where $\vartheta''_g = \vartheta'_g$ and $\vartheta''_w = \vartheta_{w_1}$. We call (5.114) the zero dynamics of the reduced model (5.113).

In the reduced model (5.113), we remark that the dynamics of the external variables are controlled by k_{1,dq_j} and k_{2,dq_j} while k_{d_i} have a great effect on the dynamics of the internal variables (or the dynamics of the DC grid). It can be summarized that the control gains have different impacts on the system performance.

Lemma 5.3.2. *Consider the reduced model (5.113). Fix positive control gains $k_{1,2d_j}$ and $k_{1,2q_j}$, $\forall j \in \mathcal{M}$. Select the droop gains k_{d_i} that satisfy the following conditions:*

- *$\forall i \in \mathcal{N}$, k_{d_i} is chosen such that*

$$k_{d_i} \geq k_{d_i \min} \tag{5.115}$$

where

$$P^o_{g_i} + \frac{3}{2} v_{sg_i d} k_{d_i \min} u^o_{cg_i} = 0$$

- *There exists at least one SAC terminal whose droop gain satisfies*

$$k_{d_q} > k_{d_q \min} \tag{5.116}$$

where $q \in \mathcal{N}$.

Then, the origin of the reduced model (5.113) *is locally asymptotically stable.*

Proof. A similar approach used in the proof of Lemma 4.1.3 is applied here. For the system described by (5.113), if the zero dynamics (5.114) is locally asymptotically stable, then the origin of the system (5.113) is locally asymptotically stable. Therefore, to establish the claim, we first study the stability of the zero dynamics (5.114). This is done by linearizing the zero dynamics (5.114) around the origin. The Jacobian matrix $[\frac{\partial f_{zero}}{\partial e_z}]|_{e_z=0}$ is expressed by

$$\Phi \triangleq [\frac{\partial f_{zero}}{\partial e_z}]|_{e_z=0} = \begin{bmatrix} D & C^{-1}H \\ -L^{-1}H^T & -L^{-1}R \end{bmatrix} \tag{5.117}$$

where $D = \text{diag}(d_k)$, $k = 1, \cdots, N+M+P$, is a diagonal matrix given by

$$\begin{cases} d_i = -\dfrac{P^o_{g_i} + \dfrac{3}{2} v_{sg_i d} k_{d_i} u^o_{g_i}}{C_{g_i} \bar{u}^2_{g_i}}, & i \in \mathcal{N} \\ d_{(j+N)} = -\dfrac{P^o_{w_j}}{C_{w_j} \bar{u}^2_{w_j}}, & j \in \mathcal{M} \\ d_{(h+N+M)} = 0. & h \in \mathcal{P} \end{cases}$$

Let us assume that there exists a particular eigenvalue of Φ denoted by $\lambda = \alpha + j\beta \in \mathbb{C}$, whose real part is non-negative, i.e. $\alpha \geq 0$. Then, λ satisfies

$$\det(\lambda I - \Phi) = 0$$

Alternatively, it can be expressed as

$$\det(\begin{bmatrix} \lambda I - D & -C^{-1}H \\ L^{-1}H^T & \lambda I + L^{-1}R \end{bmatrix}) = 0 \tag{5.118}$$

We define $\Phi_1 \triangleq \lambda I + L^{-1}R = \Lambda_1 + j\Lambda_2$ where $\Lambda_{1,2}$ are expressed by

$$\Lambda_1 = \text{diag}(\alpha + \frac{R_{c_1}}{L_{c_1}}, \cdots, \alpha + \frac{R_{c_L}}{L_{c_L}}) \in \mathbb{R}^{L \times L}$$
$$\Lambda_2 = \text{diag}(\beta, \cdots, \beta) \in \mathbb{R}^{L \times L}$$

Since the Hermitian part of Φ_1 is equal to $\mathcal{H}(\Phi_1) = \Lambda_1$, which is positive definite, the complex matrix Φ_1 is also positive definite (Lemma 4.1.6). Consequently, Φ_1 must be invertible (Lemma 4.1.9) and then, Eq. (5.118) becomes

$$\begin{aligned} &\det(\begin{bmatrix} \lambda I - D & -C^{-1}H \\ L^{-1}H^T & \lambda I + L^{-1}R \end{bmatrix}) \\ =&\det(\lambda I - D + C^{-1}H\Phi_1^{-1}L^{-1}H^T)\det(\Phi_1) \\ =&\det(\lambda C - CD + H(\lambda L + R)^{-1}H^T)\det(\Phi_1)\det(C^{-1}) \end{aligned}$$

Again, we define

$$\begin{aligned} \Phi_2 &= \lambda C - CD + H(\lambda L + R)^{-1} H^T \\ \lambda C - CD &= \Lambda_3 + j\Lambda_4 \\ (\lambda L + R)^{-1} &= \Lambda_5 + j\Lambda_6 \end{aligned} \tag{5.119}$$

with the notations

$$\begin{aligned} &\Lambda_3 = \alpha C - CD \triangleq \operatorname{diag}(\sigma_1, \cdots, \sigma_{N+M+P}) \\ &\begin{cases} \sigma_i = C_{g_i}(\alpha + \dfrac{P^o_{g_i} + \dfrac{3}{2} v_{sg_i d} k_{d_i} u^o_{g_i}}{C_{g_i} \bar{u}^2_{g_i}}), & i \in \mathcal{N} \\ \sigma_{(j+N)} = C_{w_j}(\alpha + \dfrac{P^o_{w_j}}{C_{w_j} \bar{u}^2_{w_j}}), & j \in \mathcal{M} \\ \sigma_{(h+N+M)} = C_{p_h}\alpha. & h \in \mathcal{P} \end{cases} \\ &\Lambda_4 = \beta C \\ &\Lambda_5 = \operatorname{diag}(\frac{\alpha L_{c_k} + R_{c_k}}{(\alpha L_{c_k} + R_{c_k})^2 + (\beta L_{c_k})^2}) \in \mathbb{R}^{L \times L} \\ &\Lambda_6 = \operatorname{diag}(\frac{-\beta L_{c_k}}{(\alpha L_{c_k} + R_{c_k})^2 + (\beta L_{c_k})^2}) \in \mathbb{R}^{L \times L} \end{aligned} \tag{5.120}$$

Due to (5.116), we assume that $k_{d_q} > k_{d_q,\min}$, $q \in \mathcal{N}$, where

$$P^o_{g_q} + \frac{3}{2} v_{sg_q d} k_{d_q.\min} u^o_{g_q} = 0 \tag{5.121}$$

Now, Φ_2 can be rewritten as

$$\begin{aligned} \Phi_2 &= \Phi_3 + j(\Lambda_4 + H\Lambda_6 H^T) \\ \Phi_3 &= \Lambda_3^q + \Lambda_3^{q'} + H_f H_f^T \end{aligned} \tag{5.122}$$

where Λ_3^q is a diagonal matrix whose q^{th} element on the main diagonal is σ_q and other elements are zero. $\Lambda_3^{q'}$ and H_f are given by $\Lambda_3^{q'} = \Lambda_3 - \Lambda_3^q$ and $H_f = H\Lambda_5^{\frac{1}{2}}$.

Let us define $\Phi_4 \triangleq \Lambda_3^q + H_f H_f^T$ and then the determinant of Φ_4 can be calculated as

$$\det(\Phi_4) = \sigma_q \det(\mathcal{R}(H_f)_q \mathcal{R}(H_f)_q^T) + \det(H_f H_f^T)$$

Since $\Lambda_5^{\frac{1}{2}}$ is a full rank matrix, i.e. $\operatorname{rank}(\Lambda_5^{\frac{1}{2}}) = L$, then $\operatorname{rank}(H_f H_f^T) = \operatorname{rank}(H_f) = \operatorname{rank}(H) = N + M + P - 1$ and as a result, $\det(H_f H_f^T) = 0$. Similar to Lemma 3.4.2, by removing any one row from H_f, such as $H_f(j,:)$, $j \in \mathcal{T}$, the rank of the reduced matrix $\mathcal{R}(H_f)_j$ is $N + M + P - 1$. Consequently, $\mathcal{R}(H_f)_q \mathcal{R}(H_f)_q^T$ is invertible and positive definite. Since k_{d_q} satisfies (5.121), we get $\sigma_q > 0$ and then, $\det(\Phi_4) = \sigma_q \det(\mathcal{R}(H_f)_q \mathcal{R}(H_f)_q^T) > 0$. On the other hand, Φ_4 and Λ_3^q are semi-positive definite because of (5.115) and (5.116) and hence, Φ_4 is positive definite. Recalling that $\Phi_3 = \Phi_4 + \Lambda_3^{q'}$, it turns out that, Φ_3 is also positive definite. As presented in (5.122), we know that $\mathcal{H}(\Phi_2) = \Phi_3$ and then, according to Lemma 4.1.6

and Lemma 4.1.9, Φ_2 is positive definite and invertible. Therefore, the following result is obtained:

$$\det(\lambda I - \Phi) = \det(\Phi_2)\det(\Phi_1)\det(C^{-1}) \neq 0$$

for $\alpha \geq 0$. This leads to a contradiction to (5.118). Thus, all eigenvalues of the Jacobian matrix Φ must have negative real part, i.e. $\alpha < 0$. Hence, Φ is a Hurwitz matrix. As a result, the origin of the zero dynamics (5.114) is locally asymptotically stable. Thus, the reduced model (5.113) is also locally asymptotically stable. The proof is completed. □

Now, we can introduce another result of this section.

Theorem 5.3.3. *Consider the MTDC system modeled by (3.20), (3.28), (3.29) and (3.36) with the control strategy (5.90), (5.94), (5.96) and (5.97). Select the droop gains that satisfy the conditions (5.115) and (5.116) in Lemma 5.3.2. Then, there exist the control gains k_{1g_id}, k_{2g_iq}, k_{1w_id}, k_{2w_iq}, $k_{1,2d_j}$ and $k_{1,2q_j}$ such that the equilibrium $\bar{S}$ of the closed loop system (5.98) is locally asymptotically stable. Thereby, the proposed control strategy can stabilize the MTDC system.*

Proof. As previously mentioned, to study the stability of the origin of the error system (5.110) is equivalent to investigating the stability of the equilibrium $\bar{S}$ of the closed-loop system (5.98). So we still focus on the stability property of the error system (5.110).

We rewrite the last equation in (5.110) in the following special form

$$\frac{de_z}{dt} = f_{zero} + \vartheta_{g_3} + \vartheta_{w_2} + \vartheta_{w_3} + \vartheta_{w_4} \tag{5.123}$$

According to Taylor's theorem, f_{zero} can be expressed by

$$f_{zero} = \Phi \cdot e_z + \tilde{f}_{zero} \cdot e_z$$

where $\tilde{f}_{zero}$ satisfies

$$\lim_{||e_z|| \to 0} ||\tilde{f}_{zero}|| = 0$$

It means that, for any given α_0, there exists a region $\mathbb{B}_{e_z}$ such that

$$||\tilde{f}_{zero}|| \leq \alpha_0 \tag{5.124}$$

for all $e_z \in \mathbb{B}_{e_z}$. In addition, since Φ is a Hurwitz matrix, for any positive definite matrix G_{e_z}, there exists a positive definite matrix F_{e_z} such that

$$F_{e_z}\Phi + \Phi^T F_{e_z} = -G_{e_z} \tag{5.125}$$

To simplify the notations, we introduce the following variables

$$
\begin{aligned}
e_{i_{g,dq}} &\triangleq \begin{bmatrix} e_{i_{g_1,dq}} & e_{Ii_{g_1,dq}} & \cdots & e_{i_{g_N,dq}} & e_{Ii_{g_N,dq}} \end{bmatrix}^T \\
e_{i_{w,dq}} &\triangleq \begin{bmatrix} e_{i_{w_1,dq}} & e_{Ii_{w_1,dq}} & \cdots & e_{i_{w_M,dq}} & e_{Ii_{w_M,dq}} \end{bmatrix}^T \\
e_{v_{w,dq}} &\triangleq \begin{bmatrix} e_{v_{sw_1,dq}} & e_{Iv_{sw_1,dq}} & \cdots & e_{v_{sw_M,dq}} & e_{Iv_{sw_M,dq}} \end{bmatrix}^T
\end{aligned}
$$

Consider a Lyapunov function $W = dW_1 + (1-d)W_2$ where $d \in (0,\ 1)$. W_1 and W_2 are designed as

$$
\begin{aligned}
W_1 =& \frac{1}{2}(e_{i_{gd}}^T F_{i_{gd}} e_{i_{gd}} + e_{i_{gq}}^T F_{i_{gq}} e_{i_{gq}} \\
&+ e_{i_{wd}}^T F_{i_{wd}} e_{i_{wd}} + e_{i_{wq}}^T F_{i_{wq}} e_{i_{wq}})
\end{aligned}
$$

and

$$
W_2 = \frac{1}{2}(e_{v_{wd}}^T F_{v_{wd}} e_{v_{wd}} + e_{v_{wq}}^T F_{v_{wq}} e_{v_{wq}} + e_z^T F_{e_z} e_z)
$$

where

$$
\begin{aligned}
F_{i_{g,dq}} &= \mathrm{diag}(F^i_{i_{g,dq}});\ F^i_{i_{g,dq}} = \begin{bmatrix} 1 & 0 \\ 0 & k_{2g_i,dq} \end{bmatrix} \\
F_{i_{w,dq}} &= \mathrm{diag}(F^j_{i_{w,dq}});\ F^j_{i_{w,dq}} = \begin{bmatrix} 1 & 0 \\ 0 & k_{2w_j,dq} \end{bmatrix} \\
F_{v_{w,dq}} &= \mathrm{diag}(F^j_{v_{w,dq}}) \\
F^j_{v_{w,dq}} &= \begin{bmatrix} 1 + \dfrac{1}{k_{1,dq_j}} & 1 \\ 1 & k_{1,dq_j} + k_{2,dq_j} + \dfrac{k_{2,dq_j}}{k_{1,dq_j}} \end{bmatrix}
\end{aligned}
$$

It is clear that $F_{i_{g,dq}}$, $F_{i_{w,dq}}$ and $F_{v_{w,dq}}$ are positive definite. Then, the derivative of W along the trajectories (5.110) can be calculated by $\dfrac{dW}{dt} = D_1 + D_2$ where

$$
\begin{aligned}
D_1 &= \Gamma_1 + \Gamma_2 \\
D_2 &= e_{i_{gd}}^T F_{i_{gd}} \frac{d\eta_{i_{gd}}}{dt} + e_{i_{gq}}^T F_{i_{gq}} \frac{d\eta_{i_{gq}}}{dt} + e_{i_{wd}}^T F_{i_{wd}} \frac{d\eta_{i_{wd}}}{dt} \\
&+ e_{i_{wq}}^T F_{i_{wq}} \frac{d\eta_{i_{wq}}}{dt} + e_{v_{wq}}^T F_{v_{wq}} \eta_{v_{wq}} + e_{v_{wd}}^T F_{v_{wd}} \eta_{v_{wd}} \\
&+ e_z^T F_{e_z} (\tilde{f}_{zero} \cdot e_z + \vartheta_{g3} + \vartheta_{w2} + \vartheta_{w3} + \vartheta_{w4})
\end{aligned}
$$

with

$$
\begin{aligned}
\eta_{i_{g,dq}} &\triangleq \begin{bmatrix} i^*_{g1,dq} & 0 & \cdots & i^*_{gN,dq} & 0 \end{bmatrix}^T \\
\eta_{i_{w,dq}} &\triangleq \begin{bmatrix} i^*_{w1,dq} & 0 & \cdots & i^*_{wM,dq} & 0 \end{bmatrix}^T \\
\eta_{v_{w,dq}} &\triangleq \begin{bmatrix} \frac{e_{i_{w_1,dq}}}{C_{fw_1}} & 0 & \cdots & \frac{e_{i_{w_N,dq}}}{C_{fw_N}} & 0 \end{bmatrix}^T
\end{aligned}
$$

and the other expressions are given by

$$\begin{aligned}
\Gamma_1 =& -\sum_{j=1}^{M}(k_{1d_j}e_{v_{sw_jd}}^2 + k_{2d_j}e_{Iv_{w_jd}}^2 + k_{1q_j}e_{v_{sw_jq}}^2 \\
&+k_{2q_j}e_{Iv_{w_jq}}^2) - e_z^T G_{e_z} e_z \\
\Gamma_2 =& -\sum_{i=1}^{N}(k_{1g_id}e_{i_{g_id}}^2 + k_{1g_iq}e_{i_{g_iq}}^2) \\
&-\sum_{j=1}^{M}(k_{1w_jd}e_{i_{w_jd}}^2 + k_{1w_iq}e_{i_{w_iq}}^2) \\
G_{i_{g,dq}} =& \ \mathrm{diag}(Gi_{g,dq}^i),\ G_{i_{g,dq}}^i = \begin{bmatrix} k_{1g_i,dq} & 0 \\ 0 & 0 \end{bmatrix} \\
G_{i_{w,dq}} =& \ \mathrm{diag}(G_{i_{w,dq}}^j),\ G_{i_{w,dq}}^j = \begin{bmatrix} k_{1w_j,dq} & 0 \\ 0 & 0 \end{bmatrix} \\
G_{v_{w,dq}} =& \ \mathrm{diag}(G_{v_{w,dq}}^j),\ G_{v_{w,dq}}^j = \begin{bmatrix} k_{1,dq_j} & 0 \\ 0 & k_{2,dq_j} \end{bmatrix}
\end{aligned}$$

Since the dq current reference trajectories only depend on the state variables with slow dynamics, we then have

$$\begin{aligned}
\frac{d\eta_{i_{gd}}}{dt} =& \frac{d\eta_{i_{gd}}}{de_z}\frac{de_z}{dt},\ \frac{d\eta_{i_{gq}}}{dt} = \frac{d\eta_{i_{gq}}}{de_z}\frac{de_z}{dt} \\
\frac{d\eta_{i_{wd}}}{dt} =& \frac{d\eta_{i_{wd}}}{de_{v_{wd}}}\frac{de_{v_{wd}}}{dt} + \frac{d\eta_{i_{wd}}}{de_{v_{wq}}}\frac{de_{v_{wq}}}{dt} + \frac{d\eta_{i_{wd}}}{de_z}\frac{de_z}{dt} \\
\frac{d\eta_{i_{wq}}}{dt} =& \frac{d\eta_{i_{wq}}}{de_{v_{wd}}}\frac{de_{v_{wd}}}{dt} + \frac{d\eta_{i_{wq}}}{de_{v_{wq}}}\frac{de_{v_{wq}}}{dt} + \frac{d\eta_{i_{wq}}}{de_z}\frac{de_z}{dt}
\end{aligned} \tag{5.126}$$

From the aforementioned sections, we know that

$$\begin{aligned}
||\vartheta_{g_3}|| \to 0 \text{ as } ||e_{i_{gd}}|| \to 0 \text{ and } ||e_{i_{gq}}|| \to 0 \\
||\vartheta_{w_4}|| \to 0 \text{ as } ||e_{i_{wd}}|| \to 0 \text{ and } ||e_{i_{wq}}|| \to 0 \\
||\vartheta_{w_2}|| \to 0,\ ||\vartheta_{w_3}|| \to 0 \text{ as } ||e_{v_{wd}}|| \to 0 \text{ and } ||e_{v_{wq}}|| \to 0
\end{aligned}$$

and then there exist positive β_k, $k = 1, \cdots, 8$ and convex regions $\mathbb{B}_{e_{i_{g,dq}}}$, $\mathbb{B}_{e_{i_{w,dq}}}$, $\mathbb{B}_{e_{v_{w,dq}}}$ such that

$$\begin{aligned}
||\vartheta_{g_3}|| \le \beta_1||e_{i_{gd}}|| + \beta_2||e_{i_{gq}}|| \\
||\vartheta_{w_4}|| \le \beta_3||e_{i_{wd}}|| + \beta_4||e_{i_{wq}}|| \\
||\vartheta_{w_2}|| \le \beta_5||e_{v_{wd}}|| + \beta_6||e_{v_{wq}}|| \\
||\vartheta_{w_3}|| \le \beta_7||e_{v_{wd}}|| + \beta_8||e_{v_{wq}}||
\end{aligned}$$

for all $e_{i_{g,dq}} \in \mathbb{B}_{e_{i_{g,dq}}}$, $e_{i_{w,dq}} \in \mathbb{B}_{e_{i_{w,dq}}}$ and $e_{v_{w,dq}} \in \mathbb{B}_{e_{v_{w,dq}}}$. Note that, in general, a larger size of $\mathbb{B}_{(\cdot)}$ leads to larger values of β_k.

Applying the above inequalities and (5.124) to (5.123), we then get that

$$\begin{aligned}
||\frac{de_z}{dt}|| \le& ||\Phi|| \cdot ||e_z|| + \alpha_0||e_z|| + \beta_1||e_{i_{gd}}|| + \beta_2||e_{i_{gq}}|| \\
&+\beta_3||e_{i_{wd}}|| + \beta_4||e_{i_{wq}}|| + \beta_5||e_{v_{wd}}|| + \beta_6||e_{v_{wq}}|| \\
&+\beta_7||e_{v_{wd}}|| + \beta_8||e_{v_{wq}}||
\end{aligned} \tag{5.127}$$

holds for all $e_z \in \mathbb{B}_{e_z}$, $e_{i_{g,dq}} \in \mathbb{B}_{e_{i_{g,dq}}}$, $e_{i_{w,dq}} \in \mathbb{B}_{e_{i_{w,dq}}}$ and $e_{v_{w,dq}} \in \mathbb{B}_{e_{v_{w,dq}}}$.

Taking (5.112), (5.126) and (5.127) into account, it can be verified that there exist positive parameters b_k^i, for $k = 1, \cdots, L+3$, $i \in \mathcal{N}$, and c_l^j, for $l = 1, \cdots, 8$, $j \in \mathcal{M}$ such that D_2 satisfies the inequality

$$\begin{aligned} D_2 \leq & \sum_{i=1}^{N} \Bigg[|e_{i_{g_i d}}| (b_1^i |e_{i_{g_i d}}| + b_2^i |e_{i_{g_i q}}| + b_3^i |e_{u_{cg_i}}| \\ & + \sum_{t=1}^{L} b_{t+3}^i |e_{i_{c_t}}|) \Bigg] + \sum_{j=1}^{M} \Bigg[(c_1^j |e_{i_{w_j d}}| + c_2^j |e_{i_{w_j q}}|) \\ & \cdot (c_3^j |e_{v_{sw_j d}}| + c_4^j |e_{Iv_{sw_j d}}| + c_5^j |e_{v_{sw_j q}}| + c_6^j |e_{Iv_{sw_j q}}| \\ & + c_7^j |e_{i_{w_j d}}| + c_8^j |e_{i_{w_j q}}|) \Bigg] \end{aligned} \tag{5.128}$$

for all $e_z \in \mathcal{B}_{e_z} \subset \mathbb{B}_{e_z}$, $e_{i_{g,dq}} \in \mathcal{B}_{e_{i_{g,dq}}} \subset \mathbb{B}_{e_{i_{g,dq}}}$, $e_{i_{w,dq}} \in \mathcal{B}_{e_{i_{w,dq}}} \subset \mathbb{B}_{e_{i_{w,dq}}}$ and $e_{v_{w,dq}} \in \mathcal{B}_{e_{v_{w,dq}}} \subset \mathbb{B}_{e_{v_{w,dq}}}$. These positive coefficients (b_k^i and c_l^j) are determined by the size of the domains $\mathcal{B}_{(\cdot)}$, the droop gains k_{d_i}, $k_{1,2d_j}$, $k_{1,2q_j}$, the system parameters and the prescribed setpoints while they are independent of $k_{1g_i,dq}$, $k_{2g_i,dq}$, $k_{1w_j,dq}$ and $k_{2w_j,dq}$.

Using Young's inequality

$$||x|| \cdot ||y|| \leq \frac{1}{2\mu} ||x||^2 + \frac{\mu}{2} ||y||^2$$

for the cross terms in (5.128) where μ is a positive constant which can be chosen arbitrarily, we obtain

$$D_2 \leq \Gamma_3 + \Gamma_4 \tag{5.129}$$

with

$$\begin{aligned} \Gamma_3 = & \sum_{i=1}^{N} \left[\frac{b_1^i}{2} \nu_1^i |e_{i_{g_i d}}|^2 + \frac{b_2^i}{2\nu_2^i} |e_{i_{g_i q}}|^2 \right] \\ & + \sum_{j=1}^{M} \left[\frac{d_1^j}{2} \kappa_1^j |e_{i_{w_j d}}|^2 + \frac{d_2^j}{2} \kappa_2^j |e_{i_{w_j q}}|^2 \right] \end{aligned} \tag{5.130}$$

and

$$\begin{aligned} \Gamma_4 = & \sum_{i=1}^{N} \left[\frac{b_3^i}{2\nu_3^i} |e_{u_{cg_i}}|^2 + \sum_{t=1}^{L} \frac{b_{t+3}^i}{2\nu_{t+3}^i} |e_{i_{c_t}}|^2 \right] \\ & + \sum_{j=1}^{M} \left[\frac{d_3^j}{2\kappa_3^j} |e_{v_{sw_j d}}|^2 + \frac{d_4^j}{2\kappa_4^j} |e_{Iv_{sw_j d}}|^2 \right. \\ & \left. + \frac{d_5^j}{2\kappa_5^j} |e_{v_{sw_j q}}|^2 + \frac{d_6^j}{2\kappa_6^j} |e_{Iv_{sw_j q}}|^2 \right] \end{aligned} \tag{5.131}$$

where $\nu_{(\cdot)}$ and $\kappa_{(\cdot)}$ have the same role as μ, and can be chosen arbitrarily.

In order to make the derivative of W negative except at the origin, we first determine the values of droop gains k_{d_i}, $k_{1,2d_j}$, $k_{1,2q_j}$ and the size of region of attraction

$$\mathcal{R}_{att} = \mathcal{B}_{e_{i_{g,dq}}} \times \mathcal{B}_{e_{i_{w,dq}}} \times \mathcal{B}_{e_{v_{w,dq}}} \times \mathcal{B}_{e_z}$$

Then, the values of b_k^i and c_l^j can be estimated. Subsequently, we choose large $\nu_{(.)}$ and $\kappa_{(.)}$ such that $\Gamma_1 + \Gamma_4 < 0$. Once k_{d_i}, $k_{1,2d_j}$, $k_{1,2q_j}$, the size of region of attraction $\mathcal{R}_{att}$, $\nu_{(.)}$ and $\kappa_{(.)}$ are determined, no matter what values of $\frac{b_1^i}{2}\nu_1^i$, $\frac{b_2^i}{2}\nu_2^i$, $\frac{d_1^j}{2}\kappa_1^j$ and $\frac{d_2^j}{2}\kappa_d^j$ are, we can always find $\frac{b_1^i}{2}\nu_1^i < k_{1g_id}$, $\frac{b_2^i}{2}\nu_2^i < k_{1g_iq}$, $\frac{d_1^j}{2}\kappa_1^j < k_{1w_jd}$ and $\frac{d_2^j}{2}\kappa_d^j < k_{1w_jq}$ and hence, $\Gamma_2 + \Gamma_3 < 0$. Consequently, there exist k_{1g_id}, k_{2g_iq}, k_{1w_id}, k_{2w_iq}, $k_{1,2d_j}$ and $k_{1,2q_j}$ such that the derivative of W is non-negative. In addition, $\dot{W} = 0$ contains no trajectory of the system except the trivial trajectory. All solutions starting from $\mathcal{R}_{att}$ will converge to the origin. According to LaSalle theorem, the origin of the error system described by (5.110) is locally asymptotically stable. Thereby, the equilibruim $\bar{S}$ of the original closed-loop system (5.102) is also locally asymptotically stable. Finally, we can say that the control strategy can ensure the asymptotic stability of the MTDC system. □

There is a trade-off between the size of $\mathcal{R}_{att}$ and the performance of system. If we want to get a large region of attraction, then we will have large values of $k_{1g_i,dq}$ and $k_{1w_j,dq}$. As seen in (5.90), large $k_{1g_i,dq}$ and $k_{1w_j,dq}$ maybe lead to large peak values of the control variables.

5.3.4 Simulation studies

In this section, the MTDC system as depicted in Fig. 5.13 consisting of two WAC and two SAC connected VSC terminals is simulated.

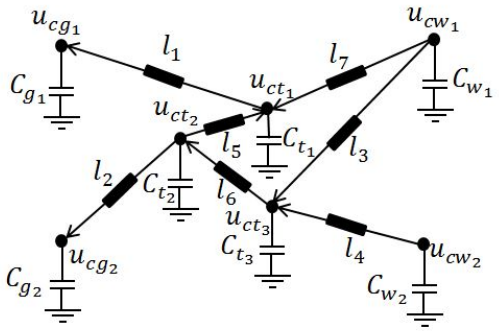

Figure 5.13: An MTDC system with two WAC and two SAC terminals.

The values of the parameters are listed in Table 5.7 and Table 5.8.

The AC line-line voltage of both SAC terminals is 415 V. The base quantities of the per-unit system applied to the simulations are presented in Table 5.9. The base quantities of the AC and DC currents are calculated as $I_{\text{ac,base}} = S_{\text{ac,base}}/V_{\text{ac,base}}$ and $I_{\text{dc,base}} = S_{\text{dc,base}}/V_{\text{dc,base}}$.

Table 5.7: Parameters of the DC network.

	Resistance R_c	Inductance L_c
l_1	0.01 Ω	6 mH
l_2	0.02 Ω	12 mH
l_3	0.15 Ω	9 mH
l_4	0.14 Ω	8.4 mH
l_5	0.16 Ω	9.6 mH
l_6	0.18 Ω	10.8 mH
l_7	0.19 Ω	11.4 mH

Table 5.8: Parameters of the VSC terminal.

	R_g (R_w)	L_g (L_w)	C_g (C_w)
SAC 1	9.9 mΩ	6 mH	68 μF
SAC 2	9.4 mΩ	12 mH	20 μF
WAC 1	8.4 mΩ	9 mH	27 μF
WAC 2	8.9 mΩ	8.4 mH	20 μF

As described in the previous section, the wind farm is modeled as a controlled current source and hence, $I_{w_1,dq}$ and $I_{w_2,dq}$ represent the power productions of the wind farms. The setpoints and the initial values of $I_{w_{1,2}d}$ are given by Table 5.10. I_{w_1q} and I_{w_2q} are set to zero. Furthermore, some system variables' initial values are provided by Table 5.11. For all the simulations in this section, the integral parts of the fast control gains are set to zero, i.e. $k_{2g_i,dq} = k_{2w_j,dq} = 0$. Three different sets of control gains as presented in Table 5.12 are chosen to verify the theoretical analysis.

5.3.4.1 Verification of two-time-scale behavior

The control gains in Set 1 are considered for the converters in this part. The simulation results are displayed in Figs. 5.14-5.15. The trajectory of i_{g_1d} in Fig. 5.14(a) clearly exhibits a two-time-scale behavior. It starts with a fast transient during the initial interval as shown in Fig. 5.14(b). After the decay of this fast dynamic, i_{g_1d} is on or close to its manifold $i^*_{g_1d}$ in all future time. Figure 5.14(c) illustrates the error between i_{g_1d} and $i^*_{g_1d}$. At the initial instant, $|i_{g_1d} - i^*_{g_1d}|$ is nearly 0.29 p.u.. After $t = 0.06$ s, the discrepancy between the two trajectories is less than 0.015 p.u.. It turns out that during the initial interval [0, 0.06] s, the trajectory of i_{g_1d} approaches that of $i^*_{g_1d}$. It is seen that the exponential decay

Table 5.9: Base quantities used in the per-unit system.

AC side	$S_{\text{ac,base}} = 4.5$ kVA	$V_{\text{ac,base}} = 415\sqrt{2/3}$ V
DC side	$S_{\text{dc,base}} = 3$ kVA	$V_{\text{dc,base}} = 700$ V

Table 5.10: Setpoints and initial values of the current source.

	$P^o_{g_i}$	$Q^o_{g_i}$	$u^o_{g_1}$
SA 1	$-0.4S_{\text{ac,base}}$	0	$V_{\text{dc,base}}$
SAC 2	$-0.5S_{\text{ac,base}}$	0	$V_{\text{dc,base}}$
	$v^0_{sw_jd}$	$v^0_{sw_jq}$	I_{w_jd}
WAC 1	$V_{\text{ac,base}}$	0	$0.4I_{\text{ac,base}}$
WAC 2	$V_{\text{ac,base}}$	0	$0.5I_{\text{ac,base}}$

Table 5.11: Initial states of the MTDC system.

i_{g_1d}	i_{g_2d}	i_{w_1d}	i_{w_2d}
-0.2 p.u.	-0.1 p.u.	0.3 p.u.	0.3 p.u.
v_{sw_1d}	v_{sw_1q}	v_{sw_2d}	v_{sw_2q}
0.7 p.u.	0.01 p.u.	0.7 p.u.	0.01 p.u.
u_{cg_1}	u_{cg_2}	u_{cw_1}	u_{cw_2}
1.043 p.u.	1.043 p.u.	1.043 p.u.	1.043 p.u.

Table 5.12: Control gains applied to the MTDC system.

	k_{d_1}	k_{d_2}	$k_{1g_i,dq}$ $(k_{1w_j,dq})$
Set 1	$10{\cdot}k_{d_{1\,\min}}$	$10{\cdot}k_{d_{2\,\min}}$	1000
Set 2	$10{\cdot}k_{d_{1\,\min}}$	$10{\cdot}k_{d_{2\,\min}}$	300
Set 3	$1{\cdot}k_{d_{1\,\min}}$	$2{\cdot}k_{d_{2\,\min}}$	1000

of the fast transient during the initial interval corresponds to the solution of the boundary-layer model. However, such two-time-scale behavior is not significant in the DC voltage and the AC voltage, which are considered to have slow dynamics. As depicted in Figs. 5.15(a)-5.15(c), there is no apparent fast transient that can be found between the trajectories of u_{cg_1} and $u^{re}_{cg_1}$ (v_{sw_1d} and $v^{re}_{sw_1d}$). It can be observed that u_{cg_1} and v_{sw_1d} are well approximated by the solution of the reduced model, i.e. $u^{re}_{cg_1}$ and $v^{re}_{sw_1d}$. Moreover, v_{sw_1d} asymptotically converges to its setpoint $v^{o}_{sw_1d}$ together with $v^{re}_{sw_1d}$.

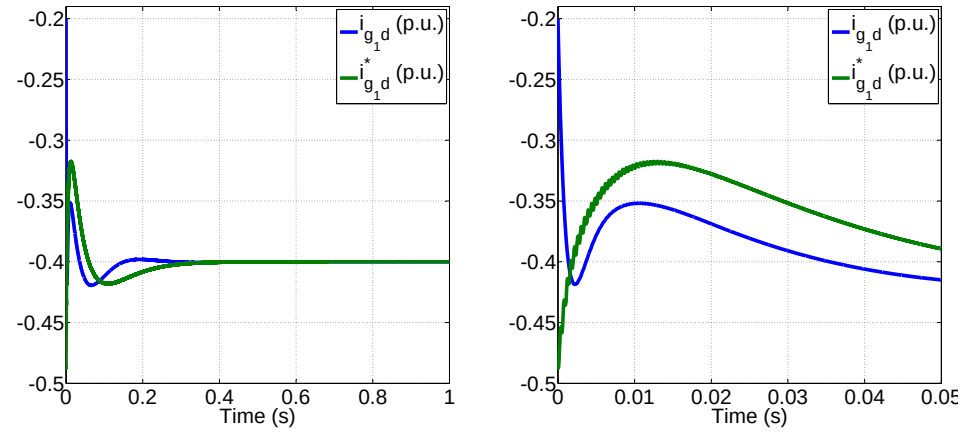

(a) Responses of i_{g_1d} and $i^*_{g_1d}$.

(b) Zoom of i_{g_1d} and $i^*_{g_1d}$.

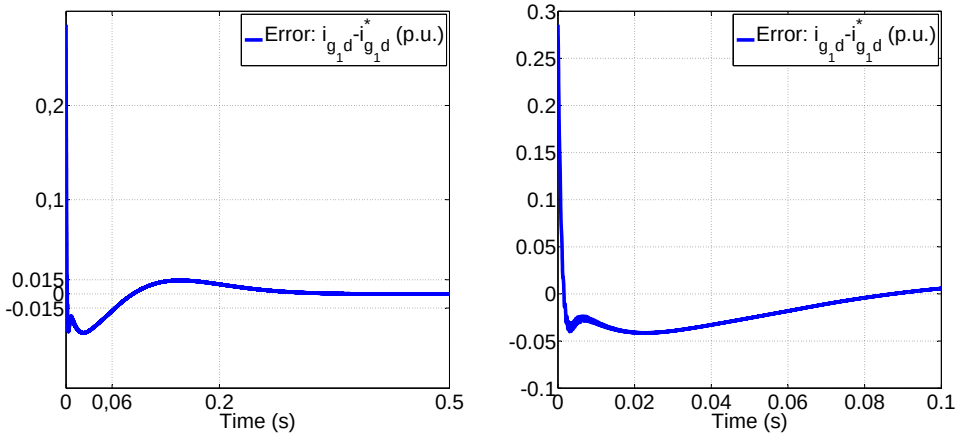

(c) Error between i_{g_1d} and $i^*_{g_1d}$.

(d) Zoom of the error between i_{g_1d} and $i^*_{g_1d}$.

Figure 5.14: Simulation results with the control gains in Set 1 (1).

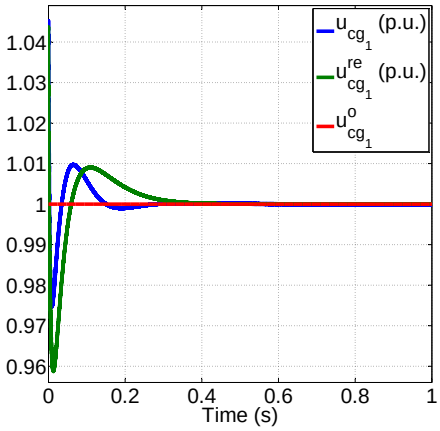

(a) Responses of u_{cg_1} and $u^{re}_{cg_1}$.

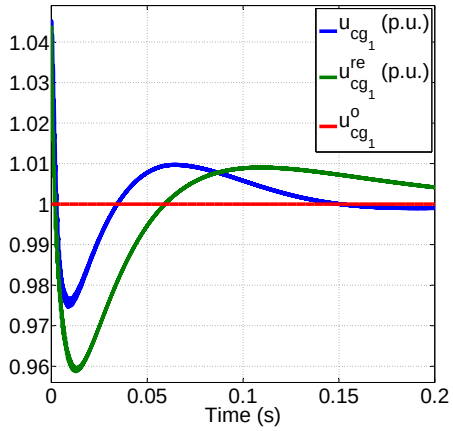

(b) Zoom of u_{cg_1} and $u^{re}_{cg_1}$.

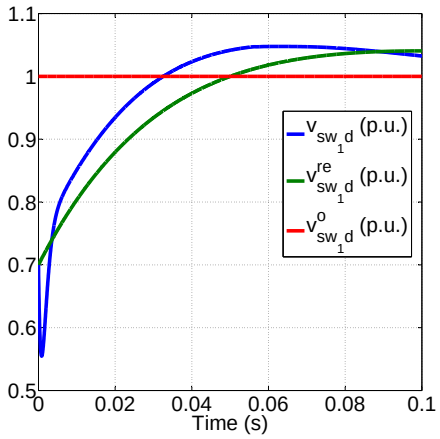

(c) Responses of v_{sw_1d} and $v^{re}_{sw_1d}$.

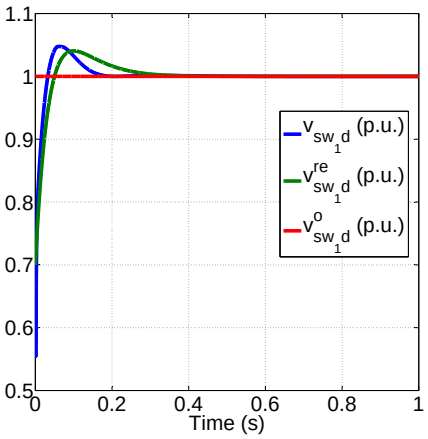

(d) Zoom of v_{sw_1d} and $v^{re}_{sw_1d}$.

Figure 5.15: Simulation results with the control gains in Set 1 (2).

5.3.4.2 Evaluation of the system performance in case of disturbance

At $t = 2$ s, I_{w_1d} is changed to 0.6 p.u. because of the increase in the active power generated by the wind farms. Consequently, both SAC connected VSC terminals should share the duty of eliminating the power unbalance caused by this increase of the power production. The simulation results are presented in Figs. 5.16-5.17. Since more power needs to be transmitted via the DC grid, in order to make the MTDC system operate normally, the two SAC terminals should absorb more power from the DC grid. As shown in Figs. 5.16(a) and 5.16(b), i_{g_1d} attains a new steady value around -0.5 p.u. from -0.4 p.u. and $\bar{i}_{g_2d}$ is also changed from -0.5 p.u. to -0.6 p.u.. According to (5.101), if more power is absorbed by the SAC terminals, this forces the DC voltages to rise and reach new steady levels. This phenomenon is clearly presented in Figs. 5.17(a) - 5.17(c). The new DC voltage transmission level is now about 1.05 p.u. which deviates from the setpoints $u^o_{cg_1,2} = 1.0$ p.u.. As seen in Fig. 5.16(c), i_{w_1d} arrives around 0.6 p.u. to response to the change of I_{w_1d}. On the other hand, v_{sw_1d} is always well controlled around its setpoint $v^o_{sw_1d} = 1.0$ p.u. irrespective of the variation in I_{w_1d} after a short transient as depicted in Fig. 5.17(d).

By contrast to the increase in I_{w_1d}, at $t = 4$ s, I_{w_2d} drops from 0.5 p.u. to 0.3 p.u.. The simulation results are summarized in Fig. 5.18. Since the generated power from the wind farm 2 decreases, i_{w_2d} starts to decrease and then converges to a new steady state of about 0.3 p.u. as shown in Fig. 5.18(c). From Figs. 5.18(a) - 5.18(b), i_{g_1d} is changed from -0.5 p.u. to -0.4 p.u. and i_{g_2d} varies from -0.6 p.u. to -0.5 p.u. This means less power is received by the two SAC terminals because less power is injected into the DC grid. Additionally, in order to comply with the droop law (5.95), the DC voltages also drop and then get to a new steady state (~ 1.0 p.u.) as displayed in Figs. 5.18(d) - 5.18(f).

To evaluate the capability in terms of AC voltage regulation, at $t = 6$ s, a new setpoint $v^o_{sw_1d} = 0.9$ p.u. is sent to the 1st WAC terminal. Now v_{sw_1d} is required to be stabilized around this new reference point. The transient response of v_{sw_1d} is illustrated in Fig. 5.19(a). It is found that v_{sw_1d} and $v^{re}_{sw_1d}$ quickly converge to the new setpoint with an acceptable undershoot. Since I_{w_1d} is unchanged during the interval [6, 7] s as depicted in Fig. 5.19(b), the change of $v^o_{sw_1d}$ has no effect on the steady state of i_{w_1d}. According to (3.31), less power flows through the 1st WAC terminal due to the decrease of the AC voltage at the PCC, which implies that the total transmitted power reduces. Therefore, both SAC terminals get less power than before and then, i_{g_1d} and i_{g_2d} start to decrease until converging to new steady states as seen in Figs. 5.19(c) and 5.19(d). Similar to the results in Figs. 5.18(d) - 5.18(f), the DC voltages start to drop and remain around 0.985 p.u. as shown in Figs. 5.19(e) and 5.19(f).

The responses of each terminal's active power at the PCC are plotted in Fig. 5.20. It is clear that the two SAC terminals participate in balancing the active power of the DC grid. When the power injection grows, both SAC terminals share the incremental power and then absorb more power from the grid. Conversely, if

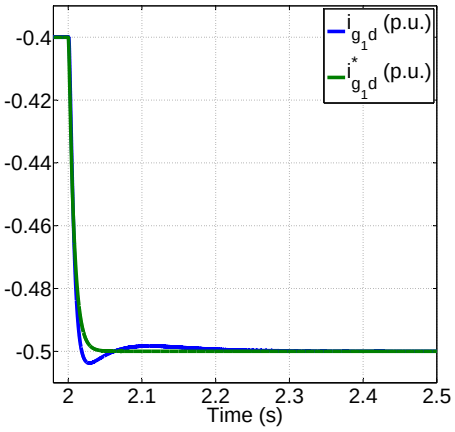

(a) Responses of $i_{g_1 d}$ and $i^*_{g_1 d}$.

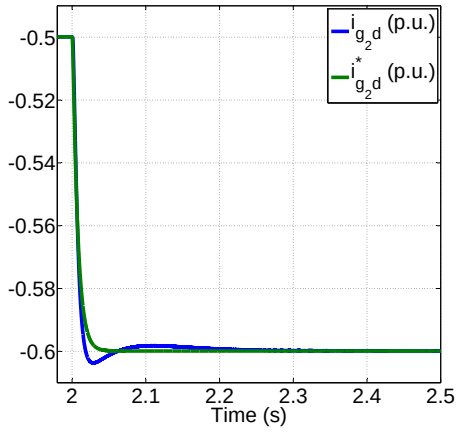

(b) Responses of $i_{g_2 d}$ and $i^*_{g_2 d}$.

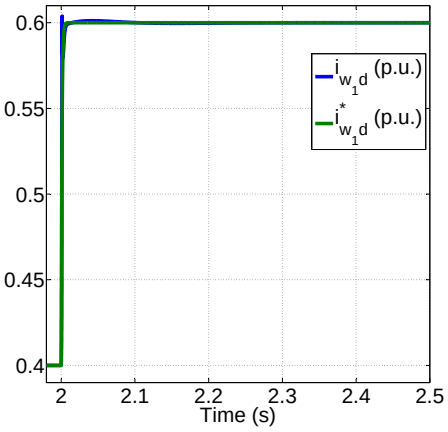

(c) Responses of $i_{w_1 d}$ and $i^*_{w_1 d}$.

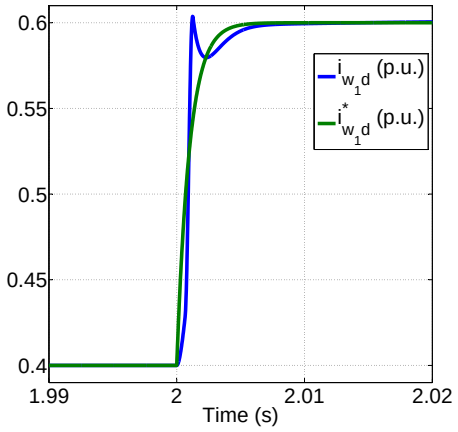

(d) Zoom of $i_{w_1 d}$ and $i^*_{w_1 d}$.

Figure 5.16: Simulation results with the variation in $I_{w_1 d}$.

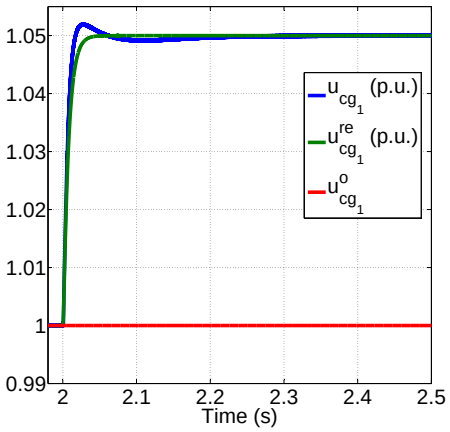

(a) Responses of u_{cg_1} and $u^{re}_{cg_1}$.

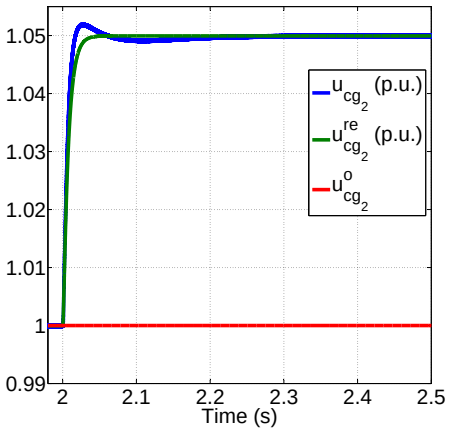

(b) Responses of u_{cg_2} and $u^{re}_{cg_2}$.

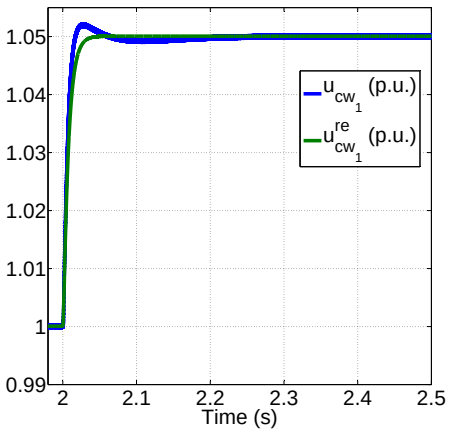

(c) Responses of u_{cw_1} and $u^{re}_{cw_1}$.

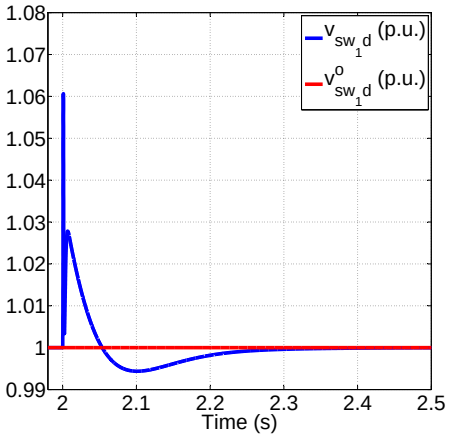

(d) Responses of v_{sw_1d}.

Figure 5.17: Simulation results with the variation in I_{w_1d}.

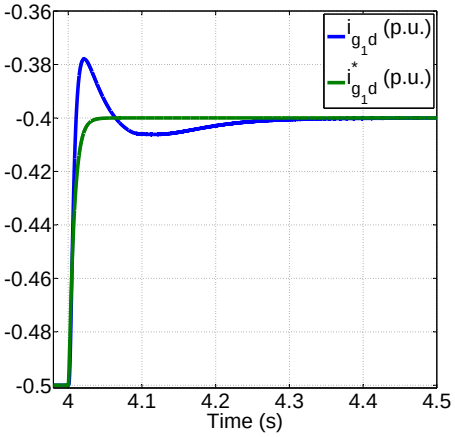

(a) Responses of $i_{g_1 d}$ and $i^*_{g_1 d}$.

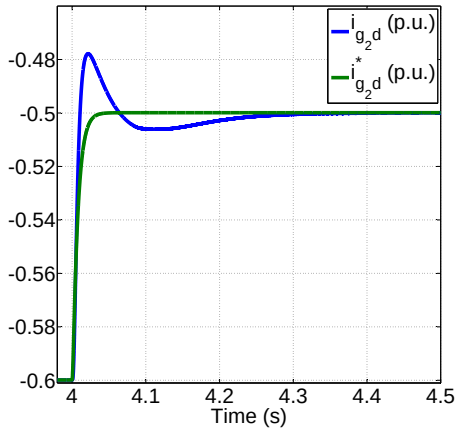

(b) Responses of $i_{g_2 d}$ and $i^*_{g_2 d}$.

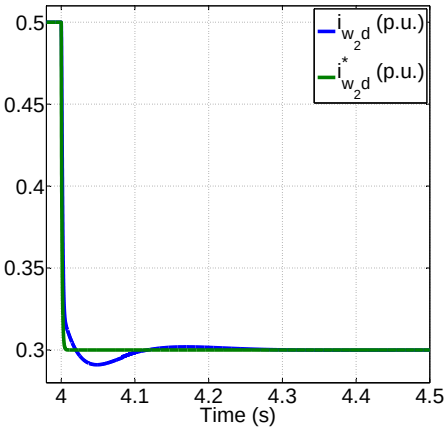

(c) Responses of $i_{w_2 d}$ and $i^*_{w_2 d}$.

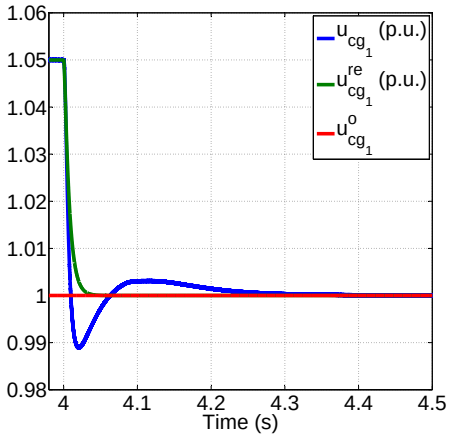

(d) Responses of u_{cg_1} and $u^{re}_{cg_1}$.

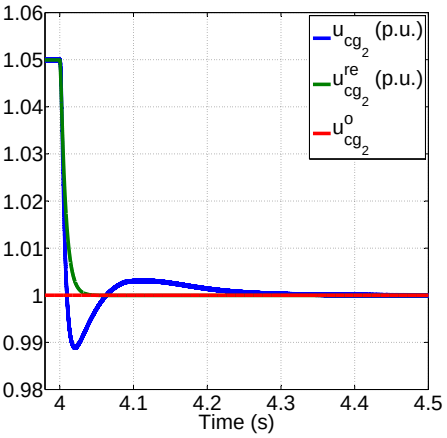

(e) Responses of u_{cg_2} and $u^{re}_{cg_2}$.

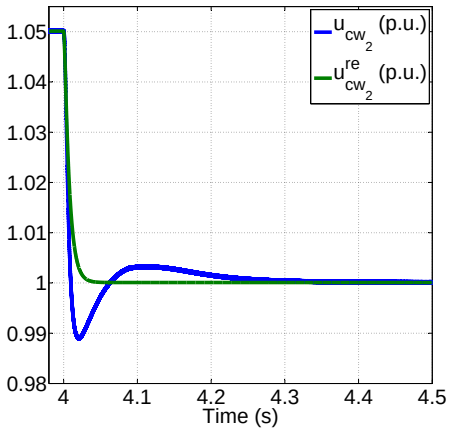

(f) Responses of u_{cw_2} and $u^{re}_{cw_2}$.

Figure 5.18: Simulation results with the variation in $I_{w_2 d}$.

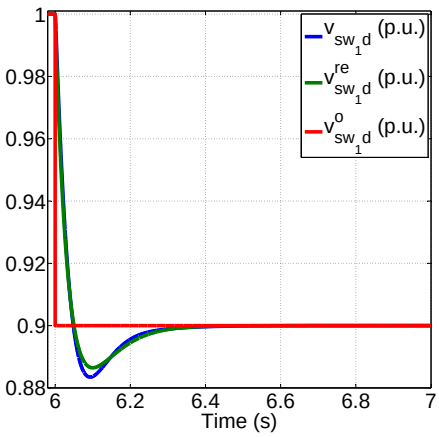

(a) Responses of v_{sw_1d} and $v^{re}_{sw_1d}$.

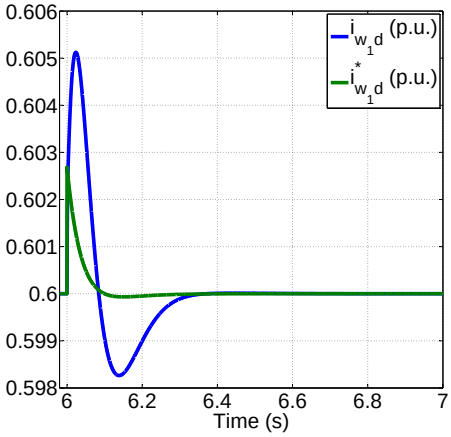

(b) Responses of i_{w_1d} and $i^*_{w_1d}$.

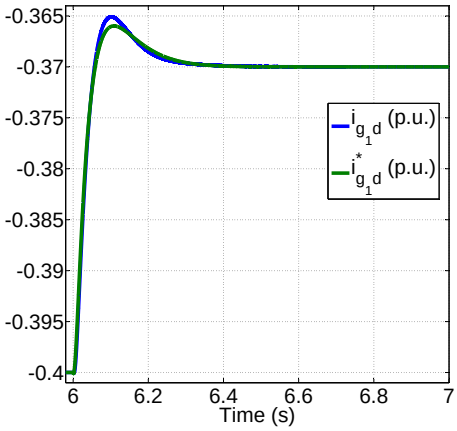

(c) Responses of i_{g_1d} and $i^*_{g_1d}$.

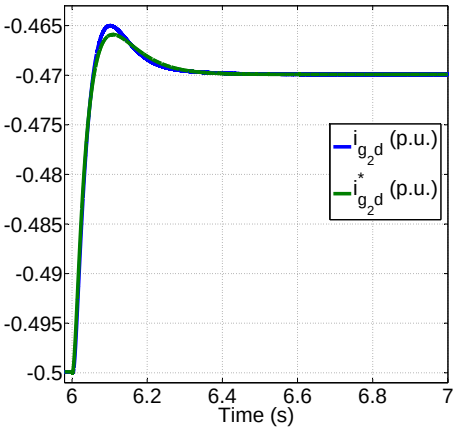

(d) Responses of i_{g_2d} and $i^*_{g_2d}$.

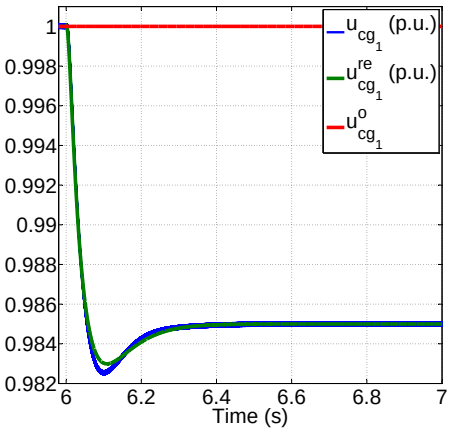

(e) Responses of u_{cg_1} and $u^{re}_{cg_1}$.

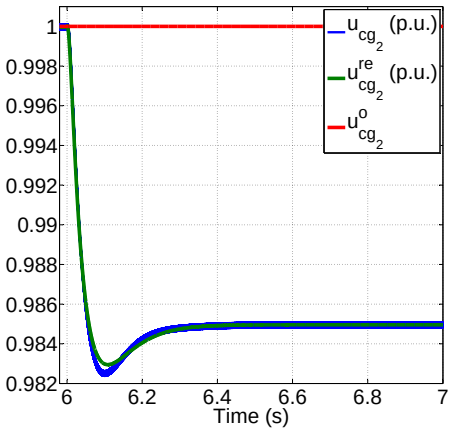

(f) Responses of u_{cg_2} and $u^{re}_{cg_2}$.

Figure 5.19: Simulation results with AC voltage regulation.

the power injection reduces, both SAC terminals decrease their power absorption accordingly.

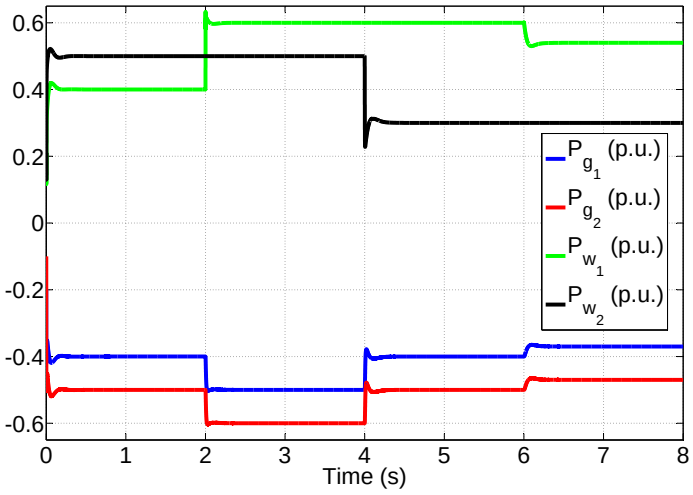

Figure 5.20: Responses of active power during the interval [0, 8] s.

5.3.4.3 Dynamics regulation

As stated in Section 5.3.3, we indicate that the control gains play different roles in regulating the system dynamics. This will be verified by the comparisons between different sets of the control gains.

We point out that the fast transient of the dq currents corresponds to the solution of the boundary-layer model and then the fast dynamics can be regulated by the fast control gains. To clarify this issue, the comparison between Set 1 and Set 2 is carried out where $k_{1g_i,dq}$ and $k_{1w_j,dq}$ in Set 1 are larger than in Set 2. The simulation results are displayed in Fig. 5.21. During the initial interval, the two trajectories in Fig. 5.21(a) start from the same initial point around 0.285 p.u.. It is evident that the blue one has a faster rate of decay than the red one because of larger k_{1g_1d} in Set 1 than in Set 2. As seen in Fig .5.21(b), the blue curve enters the error band $[-0.005,\ 0.005]$ p.u. at around $t = 0.25$ s and then remains in this band in the future time, but in contrast, the red curve reaches this error band only after $t = 0.41$ s. A similar phenomenon can be observed in the response of the error between i_{w_1d} and $i^*_{w_1d}$ as plotted in Figs. 5.21(c) and 5.21(d). Both curves in Fig. 5.21(c) have the same initial value of 0.385 p.u.. Since k_{1w_1d} in Set 1 is larger than in Set 2, the response of the error represented by the blue curve drops faster than that described by the red one. Additionally, as seen in Fig. 5.21(d), after $t = 0.2$ s, the blue curve stays in the error band $[-0.005,\ 0.005]$ p.u.. The red one needs 0.41 s to get into this error band and then remains in it. The simulation results clearly show that the fast control gains play a critical role in the regulation of the fast transient of the dq

currents.

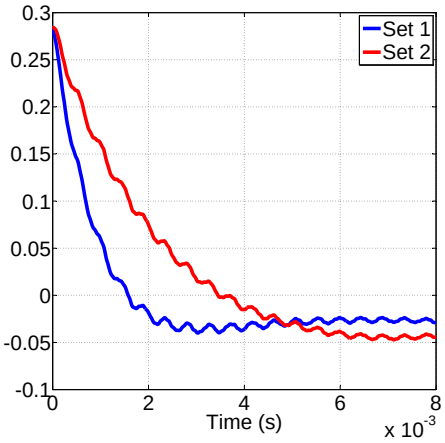

(a) Error between $i_{g_1 d}$ and $i^*_{g_1 d}$ during the initial interval.

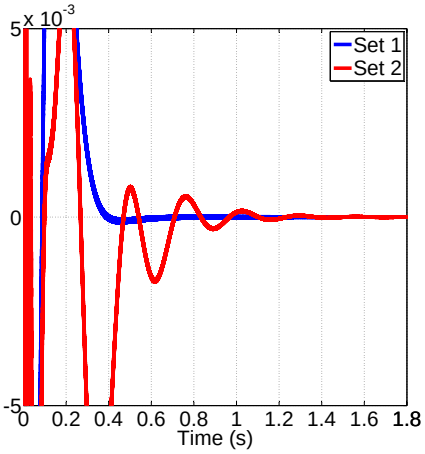

(b) Error between $i_{g_1 d}$ and $i^*_{g_1 d}$.

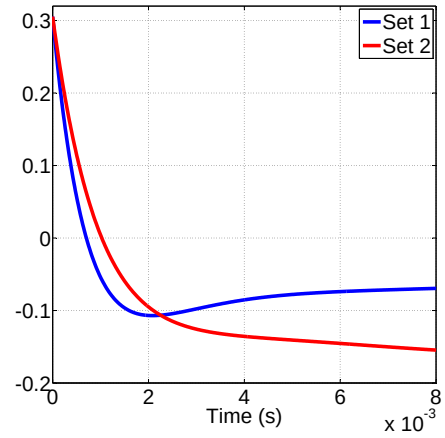

(c) Error between $i_{w_1 d}$ and $i^*_{w_1 d}$ during the initial interval.

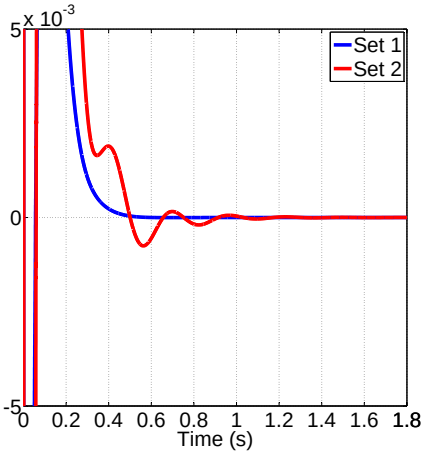

(d) Zoom of error between $i_{w_1 d}$ and $i^*_{w_1 d}$.

Figure 5.21: Comparison between Set 1 and Set 2.

As expressed in (5.113), the behavior of the reduced model is regulated by the droop gains k_{d_i}, k_{1,dq_j} and k_{2,dq_j}. Furthermore, the dynamics of $v_{sw_j,dq}$ in (5.113) heavily depend on k_{1,dq_j} and k_{2,dq_j}, while the zero dynamics (or the dynamics of the DC network) strongly rely on the choice of the droop gains k_{d_i}. To demonstrate the above points, two sets of control gains, i.e. Set 1 and Set 3, are chosen for comparison. The only difference between them is that k_{d_i} in Set 1 is larger than in Set 3.

The simulation results in Figs. 5.22-5.23 show the effect of the droop gains on the

system performance. From Figs. 5.22(a) and 5.22(c), both u_{cg_1} and u_{cw_1} with Set 1 and Set 3 are asymptotically stabilized around 1.0 p.u.. However, it can be observed that the blue trajectories remain in the domain [0.99, 1.01] p.u. after $t = 0.05$ s, whereas the red ones need nearly 1.9 s to stay in the same region. Moreover, as seen in Figs. 5.22(b) and 5.22(d), the response of u_{cg_1} (u_{cw_1}) with Set 1 is much steeper than that with Set 2 during the initial interval. The above description indicates that the performance of the state variables related to the zero dynamics can be improved by increasing the values of k_{d_i} appropriately.

Let us now focus on the responses of the AC voltage as depicted in Figs. 5.23(c) - 5.23(f). Interestingly, as seen in Fig. 5.23(c), the response of v_{sw_1d} with Set 1 is very close to that with Set 3. In particular, as seen in Fig. 5.23(d), the two curves, the blue one and the red one, almost coincide with each other. A similar result can also be obtained for v_{sw_2d} from Figs. 5.23(e) and 5.23(f). This implies that the droop gains have little effect on controlling the AC voltage. It is k_{1,dq_j} and k_{2,dq_j} that are predominant in the regulation of the AC voltage.

5.4 Conclusions

Vector current control has been widely applied in the context of VSC control, whose principle is based on the assumption (or empirical practice) of time-scale separation between the system state variables. However, this hypothesis (or experience) has been rarely theoretically studied. This chapter has bridged the gap between the theory and the practice.

First, in Section 5.1, a general control design problem was studied where a time-scale separation based control structure consisting of two loops, the fast inner and the slow outer loop, was established for a class of nonlinear systems. Further theoretical studies have been carried out, showing that the proposed control algorithm can divide the dynamics of the system's state variables into different time scales and the original closed-loop system can be divided into two models, the boundary-layer and the reduced model. Interestingly, by analyzing the two models, we find that the control gains in both control loops have different effects on the system behavior. The state variables with fast dynamics exhibit a significant two time-scale dynamical behavior by presenting a fast and a slow transient. Moreover, the fast transient exactly corresponds to the solution of the boundary-layer model, whose dynamics are dominated by the control gains of the fast inner loop.

Then, we have applied the theoretical results to the control of MTDC system where two mostly used control configurations, master-slave and droop control configuration, have been investigated in this chapter. According to the different VSC operations of the two control configurations, two different time-scale separation based controllers are presented. As stated in Lemma 5.2.2 of Section 5.2, we point out that in master-slave control configuration, the developed controller can make the system exhibit different time-scale dynamics when the system's physical structure and the prescribed (or scheduled) references satisfy certain conditions. In addition,

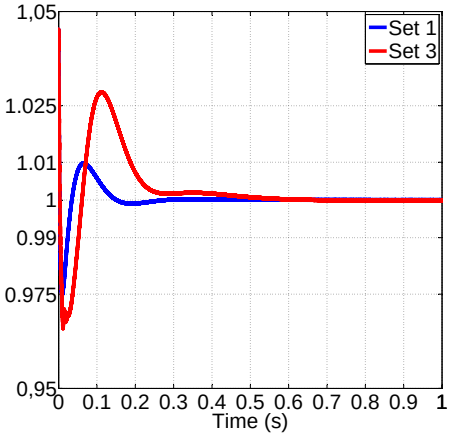

(a) Response of u_{cg_1}.

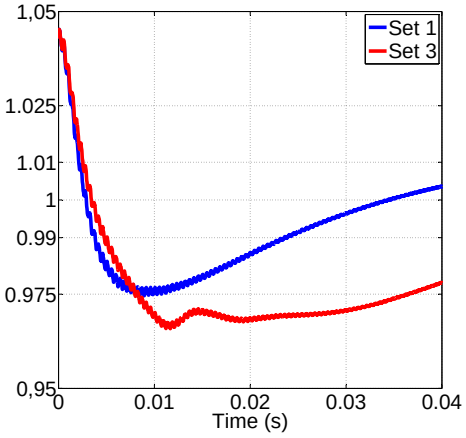

(b) Response of u_{cg_1} during the initial interval.

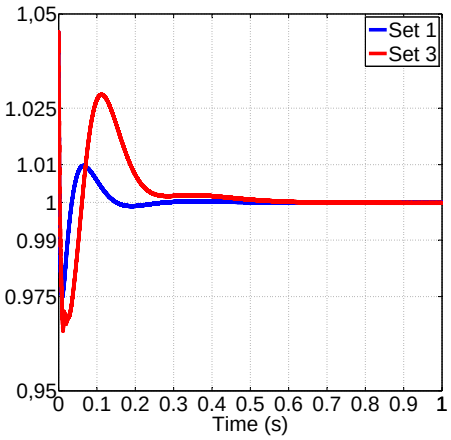

(c) Response of u_{cw_1}.

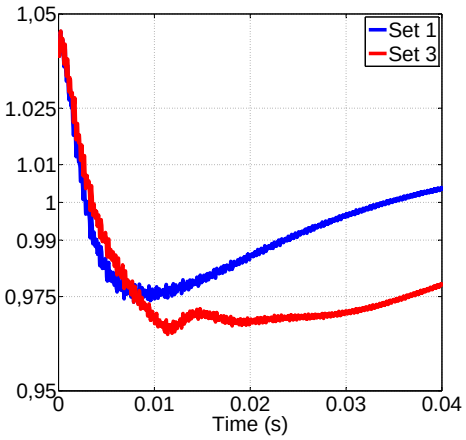

(d) Response of u_{cw_1} during the initial interval.

Figure 5.22: Comparison between Set 1 and Set 3 (1).

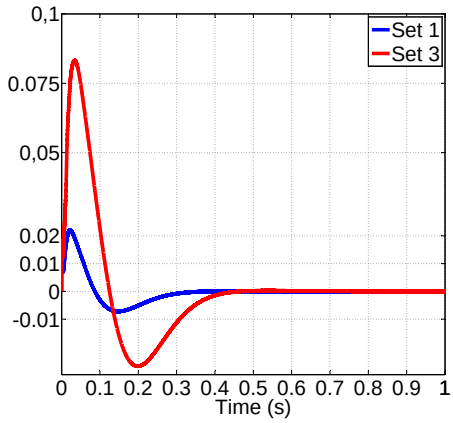

(a) Error between of u_{cg_1} and $u^{re}_{cg_1}$.

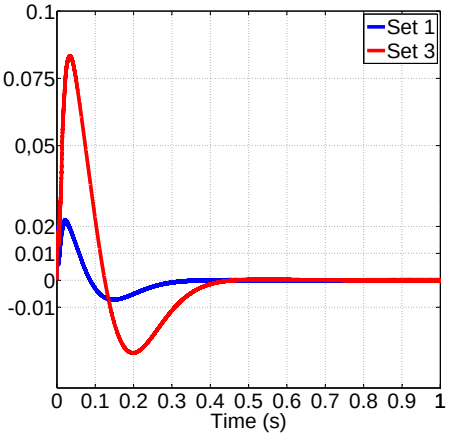

(b) Error between of u_{cw_1} and $u^{re}_{cw_1}$.

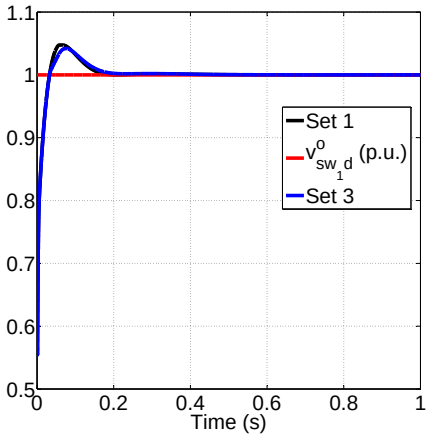

(c) Response of v_{sw_1d}.

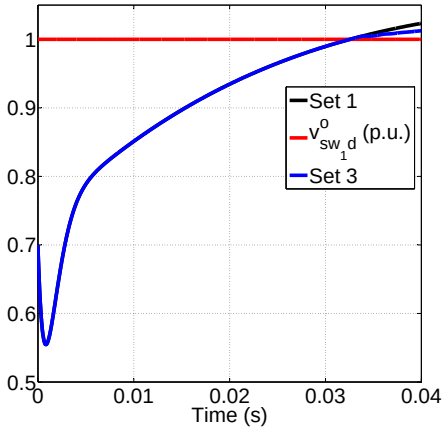

(d) Response of v_{sw_1d} during the initial interval.

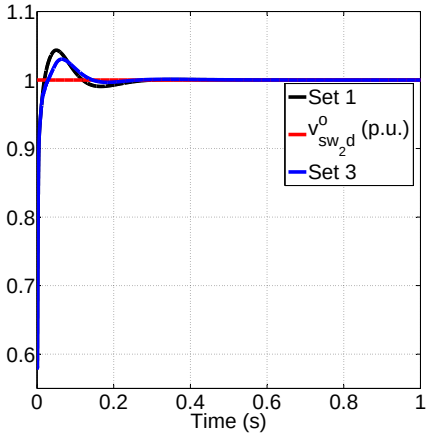

(e) Response of v_{sw_2d}.

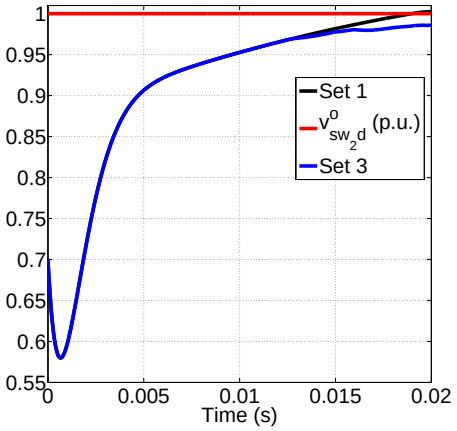

(f) Response of v_{sw_2d} during the initial interval.

Figure 5.23: Comparison between Set 1 and Set 3 (2).

we find that in this control configuration, with the proposed controller, there exist some uncontrolled internal dynamics (for example, the state variables of the DC grid) whose behavior strongly depends on the system inherent characteristics.

Subsequently, we have applied the theoretical results of control induced time-scale separation to droop control configuration. As stated in Lemma 5.3.3 of Section 5.3.3.3, the proposed time-scale separation controller has no specific requirements on the system parameters, topology or those prescribed references. Unlike master-slave control configuration, the dynamics of the DC grid are determined by the droop gains and hence, there is no uncontrolled internal dynamics. The theoretical studies carried out in this chapter have been verified with simulation results where various simulated scenarios have been considered.

Chapter 6

Frequency control using MTDC systems

Contents

As presented in the previous sections, the developed controllers are used to guarantee the operation of the system states around their prescribed references which are given by a higher control level. In this chapter, we will propose a possible method based on frequency control for computing the active power references. The main idea of this approach is to make the non-synchronous systems interconnected via an MTDC system share their primary reserves by modifying their scheduled power references. A DC-voltage-based control scheme, only needing local information, is introduced to regulate the AC frequency, for which a sufficient condition on tuning the control gains are derived to ensure the system stability.

6.1 Introduction and motivation

In an AC system, the frequency, as an indication of power balance, is common everywhere on the time scale of a few milliseconds. With this common frequency, all generating units within the system can sense a power imbalance and adjust their power output to counter this disturbance. This mechanism of restoring power balance is commonly called primary frequency control, and the region of variation of generators' output is referred to as primary reserve. With the current practice of

transferring a scheduled power among the AC areas through HVDC links, the frequencies of the areas are independent of each other, and thus generators in one area are not sensible to other areas' power imbalances. The advantage of this practice is that a disturbance in one area does not affect another, and thus the HVDC link can play the role of a firewall to prevent cascading failure. However, in the case of a severe power imbalance, the generating units within the affected area may not be strong enough to restore the power balance in time, and the resulting frequency excursion may be so large that invasive and expensive corrective measures (e.g. load shedding) have to be triggered. Such undesirable scenarios may be avoided if the HVDC system can be controlled in real time in such a way that the interconnected AC areas can share their primary reserves.

References [Hamzei-nejad 1986, Dai 2010] proposed frequency controllers that modify the active power transferred by an HVDC link. These proposed controllers require other AC areas' frequency measurements. Due to the time-delay of information communication, the controllers may destabilize the overall system. To become independent of remote information, [Rashed 2008] proposes a controller, named the DC-voltage-based controller, which takes actions only based on local information, requiring no communication among the AC areas. The theoretical stability proof in [Rashed 2008] is only valid for the special case of identical parameters of the AC areas, which is unrealistic in practice. In addition, the choice of the control gain in [Rashed 2008] was also rather empirical, and no proper approach to tuning the control gain was given.

In this work, we study a more general case without any restrictions on AC area parameters. A rigorous stability analysis is given to ensure safety and reliability. Moreover, we investigate the feasible region for the control gains based on Lyapunov theory and LMI techniques [Boyd 1994].

6.2 Modeling

The work in this chapter is based on the following consideration:

- We do not distinguish the difference between the SAC and WAC connected VSC terminals. Every converter station is considered to be a black box. Since the control of the VSC terminal has dynamics in the ms range (see the simulation results in the previous sections), much faster than the problem of frequency control, the dynamics of the converter stations are neglected. We assume that any active power references generated by the frequency control can be perfectly tracked by the converter stations.

- The dynamics of the DC grid is neglected where each DC circuit branch is simply represented by an aggregated resistance.

As depicted in Fig. 6.1, we consider a simplified MTDC system consisting of a DC grid, N AC areas, and N VSC converters where P_i^{dc} represent active power injections to the HVDC grid. By convention, if P_i^{dc} is negative, AC area i absorbs

power from the HVDC grid as a consumer. Otherwise, AC area i provides power as a supplier.

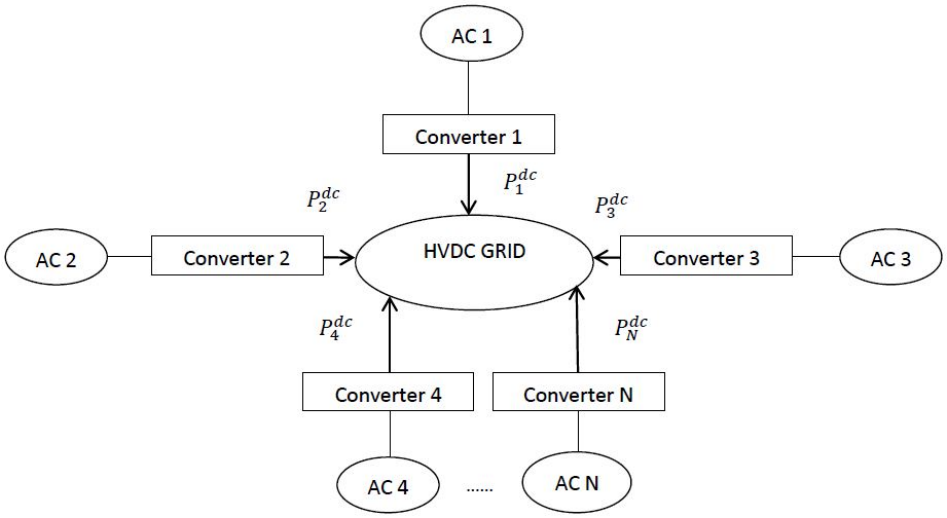

Figure 6.1: Diagram of an MTDC system with N AC areas.

6.2.1 DC grid

Each DC voltage is denoted as V_i. Thanks to VSC converter and PWM technology, all converters can independently control their V_i. The power injected to the DC grid from AC area i, P_i^{dc}, satisfies Ohm's law

$$P_i^{dc} = \sum_{k=1}^{N} \frac{V_i(V_i - V_k)}{R_{ik}} \tag{6.1}$$

where the aggregated resistance R_{ik} represents the transmission line between AC areas i and k. Obviously $R_{ik} = R_{ki}$. If AC areas i and k are not connected directly, R_{ik} is infinity.

6.2.2 AC areas

Each AC area is modeled as an aggregated generator and a load. The equation of motion of the generator is

$$2\pi J_i \frac{df_i}{dt} = \frac{P_{m_i} - P_{l_i} - P_i^{dc}}{2\pi f_{nom,i}} - 2\pi D_{g_i}(f_i - f_{nom,i}) \tag{6.2}$$

where P_{m_i}, J_i and D_{g_i} are the mechanical power input, the moment of inertia and the damping factor of the aggregated generator of area i, respectively. f_i is the frequency of AC area i and $f_{nom,i}$ is its nominal value. P_{l_i} is the power consumed by area i's load. In addition, J_i, D_{g_i} and $f_{nom,i}$ are considered as known parameters.

The primary frequency control is realized by the speed governor of the generator, which modifies P_{m_i} in response to a deviation of f_i from $f_{nom,i}$. This dynamics is modeled as

$$T_{sm,i}\frac{dP_{m_i}}{dt} = P^s_{m_i} - P_{m_i} - \frac{P_{nom,i}}{\sigma_i}\frac{f - f_{nom,i}}{f_{nom,i}} \tag{6.3}$$

where $T_{sm,i}$ is the time constant of the servomotor, $P^s_{m_i}$ is the scheduled value for P_{m_i}, $P_{nom,i}$ is the nominal power of the generator and σ_i is the generator droop.

By combining (6.2) and (6.3), the whole system is represented as

$$\begin{aligned} 2\pi J_i\frac{df_i}{dt} &= \frac{P_{m_i} - P_{l_i} - P^{dc}_i}{2\pi f_{nom,i}} - 2\pi D_{g_i}(f_i - f_{nom,i}) \\ T_{sm,i}\frac{dP_{m_i}}{dt} &= P^s_{m_i} - P_{m_i} - \frac{P_{nom,i}}{\sigma_i}\frac{f_i - f_{nom,i}}{f_{nom,i}} \end{aligned} \tag{6.4}$$

for $i = 1, \cdots, N$. f_i and P_{m_i} are the state variables. By substituting (6.1) into (6.4), V_i explicitly appear in the system model, and they are considered as the control inputs.

6.2.3 Reference operating point

The reference operating point defined here corresponds to the steady state of the system, which is qualified by specific values of input parameters P_{l_i}, $P^s_{m_i}$ and the variables f_i, P_{m_i}, P^{dc}_i, V_i. We here use the same notation $(\cdot)^o$ as in the previous section to denote the reference values of the system variables.

We usually expect that the system would operate in nominal condition and hence, the reference values of f^o_i and $P^o_{m_i}$ are naturally set to their nominal values, i.e.

$$\begin{aligned} f^o_i &= f_{nom,i} \\ P^o_{mi} &= P^o_{m_i} \end{aligned}$$

Since the reference operating point is a steady state, we have

$$\begin{aligned} 0 &= \frac{P^o_{mi} - P^o_{l_i} - P^{dc,o}_i}{2\pi f_{nom,i}} - 2\pi D_{g_i}(f^o_i - f_{nom,i}) \\ 0 &= P^o_{m_i} - P^o_{m_i} - \frac{P_{nom,i}}{\sigma_i}\frac{f^o_i - f_{nom,i}}{f_{nom,i}} \\ P^{dc,o}_i &= \textstyle\sum_{k=1}^{N} \dfrac{V^o_i(V^o_i - V^o_k)}{R_{ik}} \end{aligned} \tag{6.5}$$

V^o_i can be obtained by solving (6.5). Since the above algebraic equations are in quadratic formula, finding the proper solution for V^o_i can be turned into an optimization problem. Here, we will not focus on this issue.

6.3 Control strategy

Consider that the MTDC system initially operates at the reference operating point. Then, one of its AC areas is subjected to a disturbance that takes form of a step load

change, i.e. $P_{l_i} \neq P^o_{l_i}$. It is true that this load change can be satisfied by the primary frequency control of its own area (P_{m_i}). However, in case of a large disturbance, if we rely only on P_{m_i}, the resulting frequency deviation may be so large that it endangers the correct operation of the system. Thus, our objective is to improve the transient frequency profile by calling for other area's primary reserves so that the frequency excursions in area i are less pronounced.

6.3.1 Control law

The control objective is to regulate each converter's DC voltage V_i only based on local measurements f_i, i.e. V_i is a function of f_i only. Therefore, a DC voltage based controller is designed as

$$V_i = V_i^o + \alpha_i(f_i - f_i^o) \tag{6.6}$$

with positive gain $\alpha_i > 0$.

Under this controller, due to the physical coupling of the HVDC grid (6.1), the resulting power injected to DC grid P_i^{dc} can be regulated by controlling V_i. This method leads our whole system to achieve the objective of sharing every area's primary reserve. However, we are not sure whether f_i and P_{m_i} are ultimately bounded around the reference operating point under the control law (6.6) with an arbitrary positive control gain α_i.

6.3.2 Choice of control gains

In this part, we give a detailed analysis for choosing the control gain α_i to guarantee ultimate boundedness of f_i and P_{m_i} under (6.6).

To simplify our problem, at first, we shift the reference values to the origin by introducing the following new variables

$$\begin{aligned} \tilde{P}_i^{dc} &= P_i^{dc} - P_i^{dc,o} \\ \tilde{P}_{li} &= P_{l_i} - P^o_{l_i} \\ \tilde{P}_{mi} &= P_{m_i} - P^o_{mi} \\ \widetilde{V}_i &= V_i - V_i^o \end{aligned} \tag{6.7}$$

Recalling (6.1), $\tilde{P}_i^{dc}$ can be expressed in these new variables as

$$\tilde{P}_i^{dc} = \sum_{k\neq i}^{N} \frac{(\widetilde{V}^2 + 2\widetilde{V}_i V_i^o - \widetilde{V}_i\widetilde{V}_k - \widetilde{V}_i V_k^o - \widetilde{V}_k V_i^o)}{R_{ik}} \tag{6.8}$$

An error system of the original system (6.4) is generated in terms of the new variables by applying (6.5) and (6.8)

$$\begin{aligned} \dot{\tilde{f}}_i =& -a_{1i}\tilde{f}_i + a_{2i}\tilde{P}_{mi} - a_{2i}\tilde{P}_{li} - a_{2i}\cdot \\ & \left(\sum_{k\neq i}^{N} \frac{(\widetilde{V}^2 + 2\widetilde{V}_i V_i^o - \widetilde{V}_i\widetilde{V}_k - \widetilde{V}_i V_k^o - \widetilde{V}_k V_i^o)}{R_{ik}}\right) \\ \dot{\tilde{P}}_{mi} =& -a_{4i}\tilde{f}_i - a_{5i}\tilde{P}_{mi} \end{aligned} \tag{6.9}$$

where $a_{1i} = \frac{D_{g_i}}{J_i}$,$a_{2i} = \frac{1}{4\pi^2 J_i f_{nom,i}}$, $a_{4i} = \frac{P_{nom,i}}{T_{sm,i}\sigma_i f_{nom,i}}$, $a_{5i} = \frac{1}{T_{smi}}$. It is worthwhile to note that a_{1i}, a_{2i}, a_{4i}, a_{5i} are strictly positive, and it can be seen that the control input $\widetilde{V}_i$ explicitly appears in the system (6.9).

As seen in (6.9), $\tilde{P}_{li}$ is viewed as a nonvanishing perturbation which is uniformly bounded if a load demand imbalance exists, i.e. $P_{l_i} - P_{l_i}^o \neq 0$. As a result, the system (6.9) can be considered as a perturbation of the nominal system

$$\begin{aligned}\dot{\tilde{f}}_i =& -a_{1i}\tilde{f}_i + a_{2i}\tilde{P}_{mi} - a_{2i}\cdot \\ & \left(\sum_{k\neq i}^{N} \frac{\widetilde{V}_i^2 + 2\widetilde{V}_i V_i^o - \widetilde{V}_i\widetilde{V}_k - \widetilde{V}_i V_k^o - \widetilde{V}_k V_i^o}{R_{ik}}\right) \\ \dot{\tilde{P}}_{mi} =& -a_{4i}\tilde{f}_i - a_{5i}\tilde{P}_{mi}\end{aligned} \tag{6.10}$$

If the origin of the nominal system (6.10) is asymptotically stable under the control law, then the perturbed system (6.9) is ultimately bounded around the origin [Khalil 1996]. Thus, the problem becomes to investigate a feasible region for α_i such that the origin of the nominal system (6.10) is asymptotically stable under (6.6). In the following part, two methods are devised to search a feasible region for α_i by means of analyzing the stability of the nonlinear system (6.10).

6.3.2.1 First approach - linearization of injected DC power flow

The first approach consists in analyzing the stability of the nonlinear system via linearization. Let us linearize (6.8) around the reference operating point resulting in

$$\begin{aligned}\tilde{P}_i^{dc} &= \sum_{k\neq i}^{N} \frac{2V_i^o - V_k^o}{R_{ik}}\widetilde{V}_i - \sum_{k\neq i}^{N} \frac{V_i^o}{R_{ik}}\widetilde{V}_k \\ &= \sum_{k\neq i}^{N} \frac{V_i^o - V_k^o}{R_{ik}}\widetilde{V}_i + \sum_{k\neq i}^{N} \frac{V_i^o}{R_{ik}}\widetilde{V}_i - \sum_{k\neq i}^{N} \frac{V_i^o}{R_{ik}}\widetilde{V}_k\end{aligned} \tag{6.11}$$

To simplify the notation, we define

$$\begin{aligned}\tilde{f} &= \begin{bmatrix}\tilde{f}_1 & \cdots & \tilde{f}_N\end{bmatrix}^T \\ \tilde{P}_m &= \begin{bmatrix}\tilde{P}_{m1} & \cdots & \tilde{P}_{mN}\end{bmatrix}^T \\ \tilde{P}^{dc} &= \begin{bmatrix}\tilde{P}_1^{dc} & \cdots & \tilde{P}_N^{dc}\end{bmatrix}^T \\ \widetilde{V} &= \begin{bmatrix}\widetilde{V}_1 & \cdots & \widetilde{V}_N\end{bmatrix}^T\end{aligned} \tag{6.12}$$

and then write (6.11) compactly in vector form as

$$\tilde{P}^{dc} = \mathrm{diag}(V_i^o)L\widetilde{V} + \mathrm{diag}(V_i^o)\mathrm{diag}(\sum_{k\neq i}^{N}\frac{1}{R_{ik}})\widetilde{V} - \mathrm{diag}(\sum_{k\neq i}^{N}\frac{V_k^o}{R_{ik}})\widetilde{V} \tag{6.13}$$

where $L \in \mathbb{R}^{N\times N}$ is the weighted Laplacian matrix describing the topology of HVDC grid, defined as

$$[L]_{ik} = \begin{cases} -\dfrac{1}{R_{ik}} & , \quad k \neq i \\ \sum_{j\neq i}^{N} \dfrac{1}{R_{ij}} & , \quad k = i \end{cases}$$

With the new notations

$$V = \mathrm{diag}(V_i^o);\ R = \mathrm{diag}(\sum_{k\neq i}^{N} \frac{1}{R_{ik}});\ V_R = \mathrm{diag}(\sum_{k\neq i}^{N} \frac{V_k^o}{R_{ik}})$$

the nominal system (6.10) can be expressed in matrix form as

$$\begin{bmatrix} \dot{\tilde{f}} \\ \dot{\tilde{P}}_m \end{bmatrix} = \begin{bmatrix} -A_1 & A_2 \\ -A_4 & -A_5 \end{bmatrix} \begin{bmatrix} \tilde{f} \\ \tilde{P}_m \end{bmatrix} - \begin{bmatrix} A_2(VL + VR - V_R) \\ 0 \end{bmatrix} \widetilde{V} \tag{6.14}$$

where $A_1 = \mathrm{diag}(a_{1i})$, $A_2 = \mathrm{diag}(a_{2i})$, $A_4 = \mathrm{diag}(a_{4i})$, $A_5 = \mathrm{diag}(a_{5i})$, $A_\alpha = \mathrm{diag}(\alpha_i)$. In addition, according to the control algorithm given by (6.6), $\tilde{V}$ in (6.14) can be expressed as

$$\widetilde{V} = \begin{bmatrix} A_\alpha & 0 \end{bmatrix} \begin{bmatrix} \tilde{f} \\ \tilde{P}_m \end{bmatrix} \tag{6.15}$$

Substituting the control law (6.15) into (6.14) leads to the following closed-loop system

$$\begin{bmatrix} \dot{\tilde{f}} \\ \dot{\tilde{P}}_m \end{bmatrix} = A \begin{bmatrix} \tilde{f} \\ \tilde{P}_m \end{bmatrix} \tag{6.16}$$

where A is given by

$$A = \begin{bmatrix} -A_1 - A_2(VL + VR - V_R)A_\alpha & A_2 \\ -A_4 & -A_5 \end{bmatrix}$$

A Lyapunov-based method is used to find a feasible region for A_α. Taking

$$W = \tilde{f}^T A_4 \tilde{f} + \tilde{P}_m^T A_2 \tilde{P}_m \tag{6.17}$$

as a Lyapunov function candidate, the derivative of W along the trajectories of (6.16) is

$$\dot{W} = -\tilde{f}^T F_\alpha \tilde{f} - 2\tilde{P}_m^T A_5 A_2 \tilde{P}_m \tag{6.18}$$

where F_α is a symmetric matrix, expressed as

$$F_\alpha = 2A_1A_4 + A_\alpha(LV + RV - V_R)A_2A_4 + A_4A_2(VL + VR - V_R)A_\alpha$$

If there is a region for A_α such that F_α is positive definite, the origin of the closed-loop system (6.16) is then asymptotically stable. Thus, our problem becomes to find

a feasible region for α such that $F_\alpha > 0$. This leads to a linear matrix inequality (LMI) problem. The objective is now to find a diagonal A_α such that the following inequalities

$$\begin{aligned} A_\alpha &> 0 \\ 2A_1A_4 + A_\alpha(LV + RV - V_R)A_2A_4 + A_4A_2(VL + VR - V_R)A_\alpha &> 0 \end{aligned} \tag{6.19}$$

hold. The above LMI problem can be solved for typical values. As seen in (6.19), it is shown that the feasible region for A_α is determined by all the AC areas parameters and the reference operating values of the system variables.

6.3.2.2 Second approach - nonlinear approach

It is well known that the approximation of the nonlinear system (6.10) by its linearized system (6.14) is valid only in a neighbourhood of the origin. Thus, to study the global behaviour of the system under the control law, another approach based on Lyapunov theory is devised to study the stability of the nonlinear system (6.10).

We rewrite $\tilde{P}_i^{dc}$ (6.8) in a vector form as

$$\tilde{P}_i^{dc} = \text{diag}(\widetilde{V}_i)L\widetilde{V} + \text{diag}(\widetilde{V}_i)LV^o + \text{diag}(V_i^o)L\widetilde{V} \tag{6.20}$$

where

$$V^o = \begin{bmatrix} V_1^o & \cdots & V_N^o \end{bmatrix}^T$$

The matrix form of the system (6.10) is given by

$$\begin{bmatrix} \dot{\tilde{f}} \\ \dot{\tilde{P}}_m \end{bmatrix} = \begin{bmatrix} -A_1 & A_2 \\ -A_4 & -A_5 \end{bmatrix} \begin{bmatrix} \tilde{f} \\ \tilde{P}_m \end{bmatrix} - \begin{bmatrix} A_2 \\ 0 \end{bmatrix} \cdot (\text{diag}(\widetilde{V}_i)L\widetilde{V} + \text{diag}(\widetilde{V}_i)LV^o + \text{diag}(V_i^o)L\widetilde{V}) \tag{6.21}$$

Substituting $\widetilde{V}_i = \alpha_i\tilde{f}_i$ and $\text{diag}(\widetilde{V}_i) = A_\alpha\text{diag}(\tilde{f}_i)$ into the above expression, then the closed-loop system is obtained as

$$\begin{bmatrix} \dot{\tilde{f}} \\ \dot{\tilde{P}}_m \end{bmatrix} = \begin{bmatrix} -A_1 & A_2 \\ -A_4 & -A_5 \end{bmatrix} \begin{bmatrix} \tilde{f} \\ \tilde{P}_m \end{bmatrix} - \begin{bmatrix} H_1(\tilde{f}) & 0 \\ 0 & 0 \end{bmatrix} \begin{bmatrix} \tilde{f} \\ \tilde{P}_m \end{bmatrix} - \begin{bmatrix} H_2(\tilde{f}) \\ 0 \end{bmatrix} \tag{6.22}$$

where $H_1(\tilde{f})$ and $H_2(\tilde{f})$ take the form

$$\begin{aligned} H_1(\tilde{f}) &= A_2A_\alpha\text{diag}(\tilde{f}_i)LA_\alpha + A_2\text{diag}(V_i^o)LA_\alpha \\ H_2(\tilde{f}) &= A_2A_\alpha\text{diag}(\tilde{f}_i)LV^o \end{aligned}$$

To investigate the stability of the closed-loop system (6.22), the same Lyapunov function candidate

$$W = \sum_{i=1}^{N} a_{4i}\tilde{f}_i^2 + \sum_{i=1}^{N} a_{2i}\tilde{P}_{mi}^2 \tag{6.23}$$

is chosen as in Section 6.3.2.1. Then, the derivative of Lyapunov function is

$$\dot{W} = -2\tilde{f}^T A_1 A_4 \tilde{f} - \tilde{f}^T A_4 H_1 \tilde{f} - \tilde{f}^T H_1^T A_4 \tilde{f} - \tilde{f}^T A_4 H_2 - H_2^T A_4 \tilde{f} - 2\tilde{P}_m^T A_5 A_2 \tilde{P}_m$$

where

$$\tilde{f}^T A_4 H_1 \tilde{f} = \sum_{i=1}^{N} a_{4i} a_{2i} (\alpha_i \tilde{f}_i^2 + V_i^o \tilde{f}_i) \left(\sum_{k \neq i}^{N} \frac{\alpha_i \tilde{f}_i - \alpha_k \tilde{f}_k}{R_{ik}} \right)$$
$$\tilde{f}^T A_4 H_2 = \sum_{i=1}^{N} a_{4i} a_{2i} \alpha_i \tilde{f}_i^2 \left(\sum_{k \neq i}^{N} \frac{V_i^o - V_k^o}{R_{ik}} \right)$$

To facilitate our analysis, we rewrite $\dot{W}$ as

$$\dot{W} = -M_1 - M_2 - 2\tilde{P}_m^T A_5 A_2 \tilde{P}_m \tag{6.24}$$

where M_1 and M_2 are given by

$$M_1 = \tilde{f}^T A_1 A_4 \tilde{f} + \tilde{f}^T A_4 H_1 \tilde{f} + \tilde{f}^T H_1^T A_4 \tilde{f}$$
$$M_2 = \tilde{f}^T A_1 A_4 \tilde{f} + \tilde{f}^T A_4 H_2 + H_2^T A_4 \tilde{f}$$

It is possible to rewrite M_1 and M_2 in a total sum square form as

$$M_1 = \sum_{i=1}^{N} a_{4i} \left(a_{1i} \tilde{f}_i^2 + 2a_{2i} (\alpha_i \tilde{f}_i^2 + V_i^o \tilde{f}_i) \cdot \left(\sum_{k \neq i}^{N} \frac{\alpha_i \tilde{f}_i - \alpha_k \tilde{f}_k}{R_{ik}} \right) \right)$$
$$M_2 = \sum_{i=1}^{N} a_{4i} \tilde{f}_i^2 \left(a_{1i} + 2a_{2i} \alpha_i \left(\sum_{k \neq i}^{N} \frac{V_i^o - V_k^o}{R_{ik}} \right) \right)$$

As a consequence, we get

$$\begin{aligned} & M_1 + M_2 \\ & = \sum_{i=1}^{N} a_{4i} \left(2a_{1i} \tilde{f}_i^2 + 2a_{2i} \left(\sum_{k \neq i}^{N} \frac{V_i^o - V_k^o}{R_{ik}} \right) \alpha_i \tilde{f}_i^2 \right. \\ & + 2a_{2i} \left(\sum_{k \neq i}^{N} \frac{1}{R_{ik}} \right) \alpha_i^2 \tilde{f}_i^3 - 2a_{2i} \alpha_i \left(\sum_{k \neq i}^{N} \frac{\alpha_k x_k}{R_{ik}} \right) \tilde{f}_i^2 \\ & \left. + 2a_{2i} \left(\sum_{k \neq i}^{N} \frac{1}{R_{ik}} \right) V_i^o \alpha_i \tilde{f}_i^2 \right) - \sum_{i=1}^{N} 2a_{4i} a_{2i} V_i^o \left(\sum_{k \neq i}^{N} \frac{\alpha_k \tilde{f}_k \tilde{f}_i}{R_{ik}} \right) \end{aligned} \tag{6.25}$$

Applying arithmetic geometric mean inequality

$$\left| \frac{\alpha_k \tilde{f}_k \tilde{f}_i}{R_{ik}} \right| \leq \frac{1}{2} \left(\frac{\alpha_k \tilde{f}_i^2}{R_{ik}} + \frac{\alpha_k \tilde{f}_k^2}{R_{ik}} \right) \tag{6.26}$$

to $M_1 + M_2$ in (6.25) yields

$$\begin{aligned} & M_1 + M_2 \\ & \geq \sum_{i=1}^{N} a_{4i} \left(2a_{1i} \tilde{f}_i^2 + 2a_{2i} \left(\sum_{k \neq i}^{N} \frac{V_i^o - V_k^o}{R_{ik}} \right) \alpha_i \tilde{f}_i^2 \right. \\ & + 2a_{2i} \left(\sum_{k \neq i}^{N} \frac{1}{R_{ik}} \right) \alpha_i^2 \tilde{f}_i^3 - 2a_{2i} \alpha_i \left(\sum_{k \neq i}^{N} \frac{\alpha_k \tilde{f}_k}{R_{ik}} \right) \tilde{f}_i^2 \\ & \left. + 2a_{2i} \left(\sum_{k \neq i}^{N} \frac{1}{R_{ik}} \right) V_i^o \alpha_i \tilde{f}_i^2 \right) - \sum_{i=1}^{N} a_{4i} a_{2i} V_i^o \left(\sum_{k \neq i}^{N} \frac{\alpha_k \tilde{f}_i^2}{R_{ik}} + \frac{\alpha_k \tilde{f}_k^2}{R_{ik}} \right) \end{aligned} \tag{6.27}$$

The last term of (6.27) can be written as

$$\begin{aligned}&\textstyle\sum_{i=1}^{N} a_{4i}a_{2i}V_i^o\left(\sum_{k\neq i}^{N}\frac{\alpha_k\tilde{f}_i^2}{R_{ik}}+\frac{\alpha_k\tilde{f}_k^2}{R_{ik}}\right)\\ =&\textstyle\sum_{i=1}^{N} a_{4i}\left(a_{2i}V_i^o\left(\sum_{k\neq i}^{N}\frac{\alpha_k}{R_{ik}}\right)+\alpha_i\left(\sum_{k\neq i}^{N}\frac{a_{4k}a_{2k}V_k^o}{a_{4i}R_{ki}}\right)\right)\tilde{f}_i^2\end{aligned} \tag{6.28}$$

Therefore, M_1+M_2 satisfies

$$\begin{aligned}&M_1+M_2\\ \geq&\textstyle\sum_{i=1}^{N} a_{4i}\left(2a_{1i}+2a_{2i}\left(\sum_{k\neq i}^{N}\frac{V_i^o-V_k^o}{R_{ik}}\right)\alpha_i+2a_{2i}\left(\sum_{k\neq i}^{N}\frac{1}{R_{ik}}\right)\alpha_i^2\tilde{f}_i\right.\\ &\textstyle-2a_{2i}\alpha_i\left(\sum_{k\neq i}^{N}\frac{\alpha_k\tilde{f}_k}{R_{ik}}\right)+2a_{2i}\left(\sum_{k\neq i}^{N}\frac{1}{R_{ik}}\right)V_i^o\alpha_i\\ &\textstyle\left.-a_{2i}V_i^o\left(\sum_{k\neq i}^{N}\frac{\alpha_k}{R_{ik}}\right)-\alpha_i\left(\sum_{k\neq i}^{N}\frac{a_{4k}a_{2k}V_k^o}{a_{4i}R_{ki}}\right)\right)\tilde{f}_i^2\end{aligned} \tag{6.29}$$

Finally, a feasible region for α_i is found, denoted by

$$\begin{aligned}\Omega_{\alpha_i}=&\left\{\alpha_i\in\mathbb{R}\,\middle|\,2a_{1i}+2a_{2i}\left(\sum_{k\neq i}^{N}\frac{V_i^o-V_k^o}{R_{ik}}\right)\alpha_i\right.\\ &+2a_{2i}\left(\sum_{k\neq i}^{N}\frac{1}{R_{ik}}\right)\alpha_i^2\tilde{f}_i-2a_{2i}\alpha_i\left(\sum_{k\neq i}^{N}\frac{\alpha_k\tilde{f}_k}{R_{ik}}\right)\\ &+2a_{2i}\left(\sum_{k\neq i}^{N}\frac{1}{R_{ik}}\right)V_i^o\alpha_i-a_{2i}V_i^o\left(\sum_{k\neq i}^{N}\frac{\alpha_k}{R_{ik}}\right)\\ &\left.-\alpha_i\left(\sum_{k\neq i}^{N}\frac{a_{4k}a_{2k}V_k^o}{a_{4i}R_{ki}}\right)\geq 0\right\}\end{aligned} \tag{6.30}$$

Therefore, for any $\alpha_i\in\Omega_{\alpha_i}$, we have $\dot{W}<0,\forall[\tilde{f},\tilde{P}_m]\neq 0$ and as a conclusion, the origin of the nonlinear system (6.10) is asymptotically stable. In a way, once α_i are determined, we can get an estimation of the region of attraction Ω_c for the state variables

$$\begin{aligned}\Omega_c=&\left\{[\tilde{f},\tilde{P}_m]\in\mathbb{R}^{2N}\,\middle|\,\sum_{k\neq i}\frac{-\alpha_i\tilde{f}_i+\alpha_k\tilde{f}_k}{R_{ik}}\leq\frac{a_{1i}}{\alpha_i a_{2i}}\right.\\ &-\left(\sum_{k\neq i}^{N}\frac{V_i^o-V_k^o}{R_{ik}}\right)-\left(\sum_{k\neq i}^{N}\frac{1}{R_{ik}}\right)V_i^o\\ &\left.-\frac{V_i^o}{2\alpha_i}\left(\sum_{k\neq i}^{N}\frac{\alpha_k}{R_{ik}}\right)-\frac{1}{2a_{4i}a_{2i}}\left(\sum_{k\neq i}^{N}\frac{a_{4k}a_{2k}V_k^o}{R_{ik}}\right),\ i=1,\cdots N.\right\}\end{aligned} \tag{6.31}$$

6.3.3 Algorithm for the definition and verification of control gains and the associated region of attraction

It is not easy to use (6.30) and (6.31) directly to get a feasible region due to their complicated expressions. Though a feasible region can be easily found by the linear method (6.19), we can only approximate the nonlinear system (6.10) by its linearization in a small neighbourhood of the origin, of which we do not know the size. Thus,

Table 6.1: Parameter values of each AC area ('-'means dimensionless).

Parameter	Area					Unit
	1	2	3	4	5	
f_{nom}	50	50	50	50	50	Hz
P_m^s	50	80	50	30	80	MW
P_{nom}	50	80	50	30	80	MW
J	2026	6485	6078	2432	4863	kg m^2
D_g	48.4	146.3	140.0	54.9	95.1	W$\cdot$ s^2
δ	0.02	0.04	0.06	0.04	0.03	-
T_{sm}	1.5	2.0	2.5	2	1.8	s
P_l	100	60	40	50	40	MW

when determining the gains α_i, we need to combine these two methods together. In general, the feasible region obtained by linear method is larger than the nonlinear method. At first, we use linear method to get a feasible value for α_i, then we put it into the nonlinear result (6.30) and (6.31) to check if this value satisfies the nonlinear method's condition such that the system is stable when the state variables are in their domain of interest. For example, the domain of interest of $\tilde{f}_i$ is defined by $\tilde{f}_i \in [-1,\ 1]$. If this is not the case, we choose a smaller value for α_i and verify (6.30) and (6.31) again. We repeat this procedure until a proper α_i^* is obtained.

The feasible region of the control gain α given by this thesis is determined by the choice of Lyapunov function. The one used here has two advantages. First, as seen in (6.18), there is no cross term ($\tilde{f}^T\tilde{P}_m$), which greatly simplifies the calculation. Second, the feasible region thus obtained is not so small. However, the feasible region of the control gain is only a sufficient condition, which guarantees ultimate boundedness of the closed-loop system. Thus, with an α outside this feasible region, the system does not necessarily become unbounded.

6.4 Simulation studies

The controller studied in the previous section is tested by computer simulations. The simulated example concerns an MTDC grid of 5 AC areas, whose parameter values are presented in Table 6.1. The system is supposed to initially operate at the reference operating point. Then at time $t = 2$ s, the load demand of AC area 2 has a step increase by 30%.

Figs. 6.2 and 6.3 illustrate the frequency and the mechanical power response without any controller, i.e. $\alpha_i = 0$. In Fig. 6.2, the minimum value of f_2 is less than 49 Hz, which is beyond frequency safety range 50$\pm$1 Hz, and the final value is 49.5615 Hz. The peak value of P_{m2} is nearly 106 MW and the final value is nearly 97.6 MW.

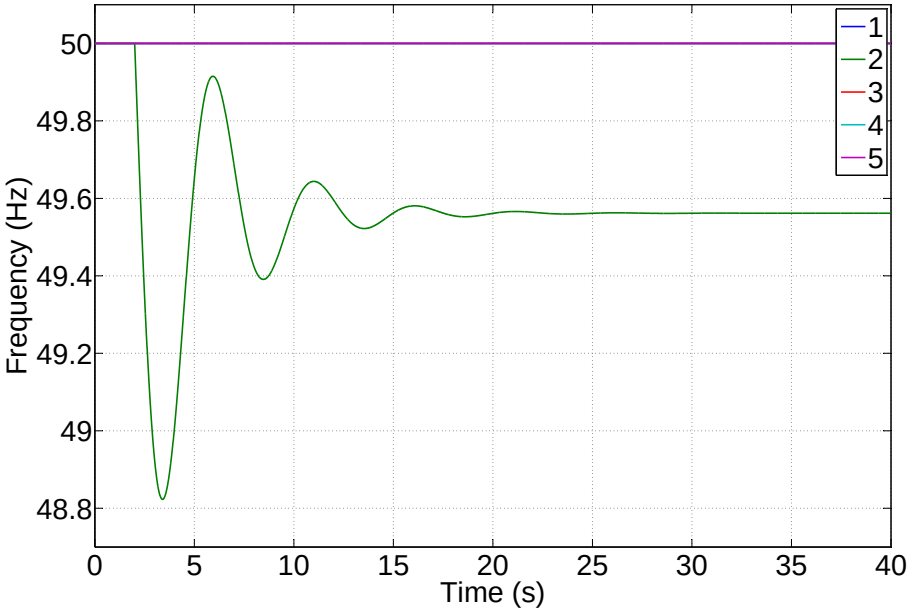

Figure 6.2: Frequencies of 5 AC areas without any controller.

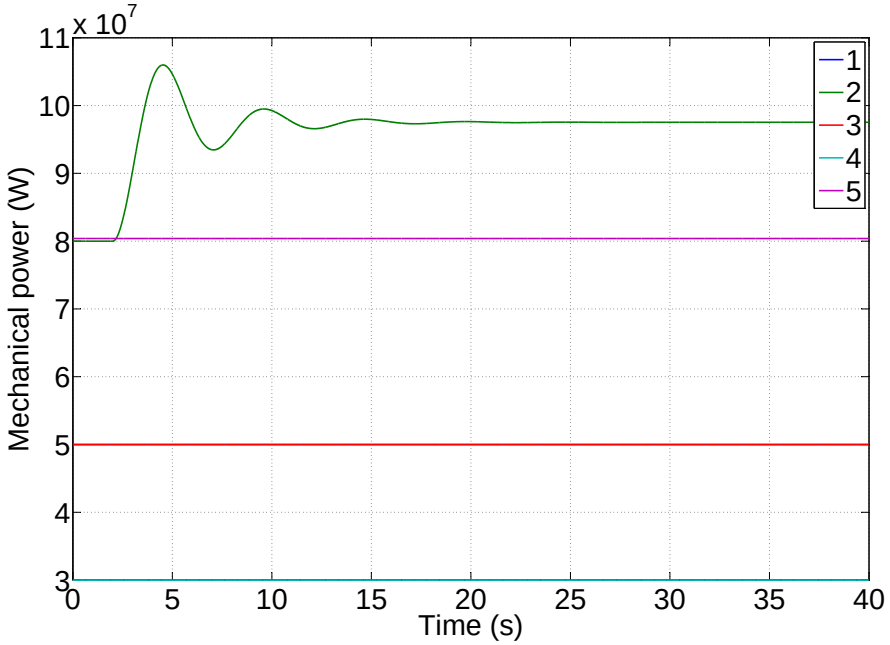

Figure 6.3: Mechanical power inputs of 5 AC areas without any controller.

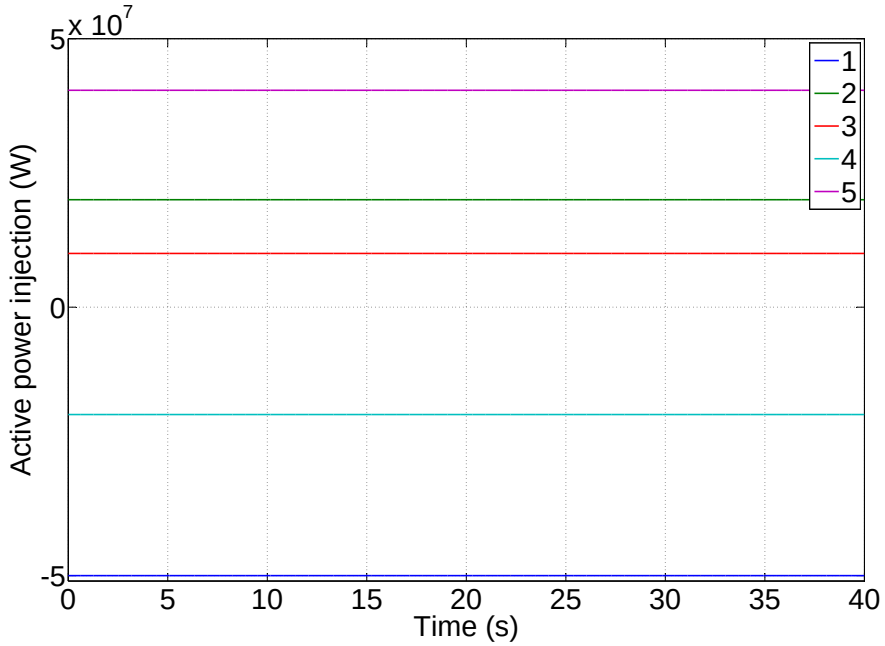

Figure 6.4: Active power injections P_i^{dc} of 5 AC areas without any controller.

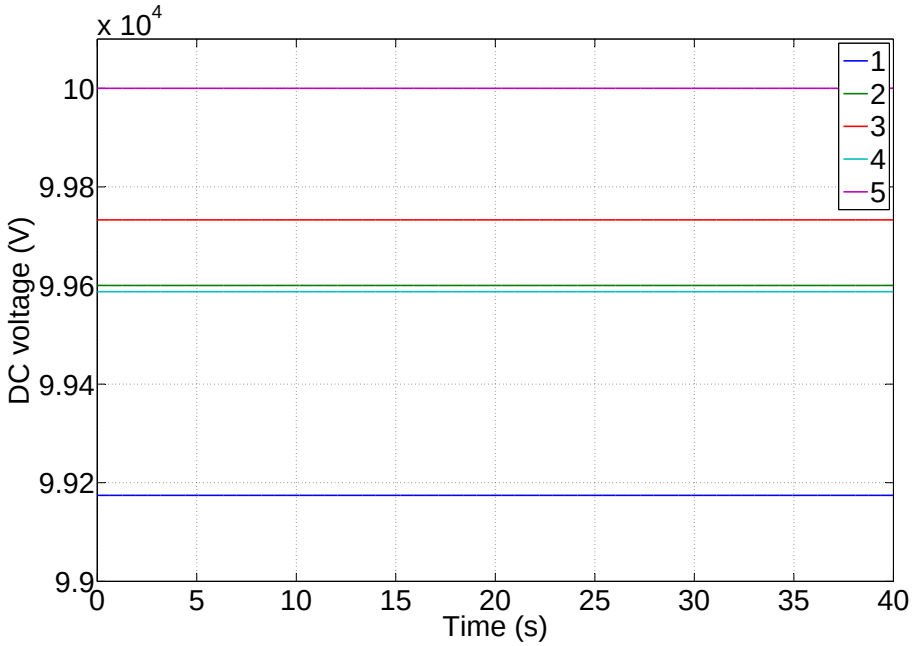

Figure 6.5: DC voltage V_i^{dc} of 5 AC areas without any controller.

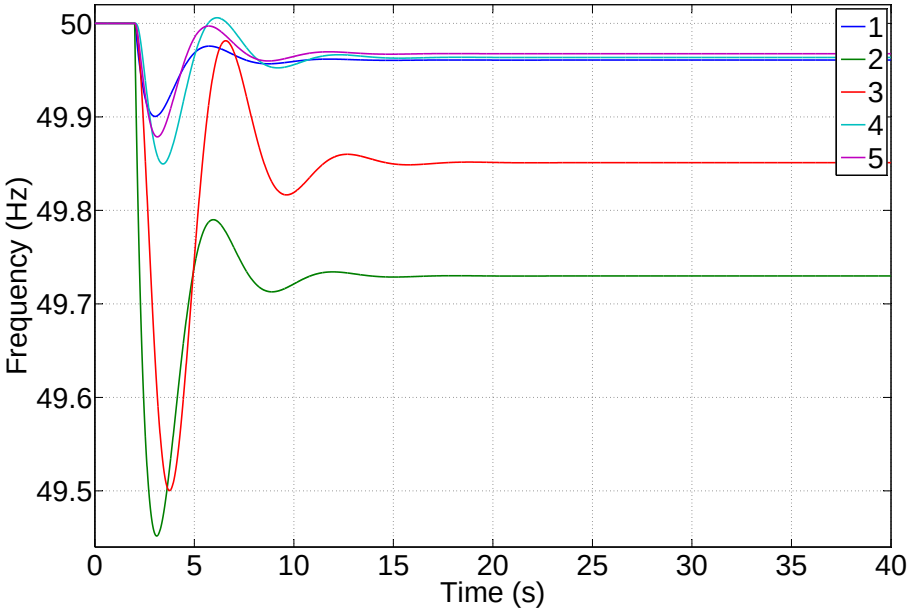

Figure 6.6: Frequencies of 5 AC areas with controller.

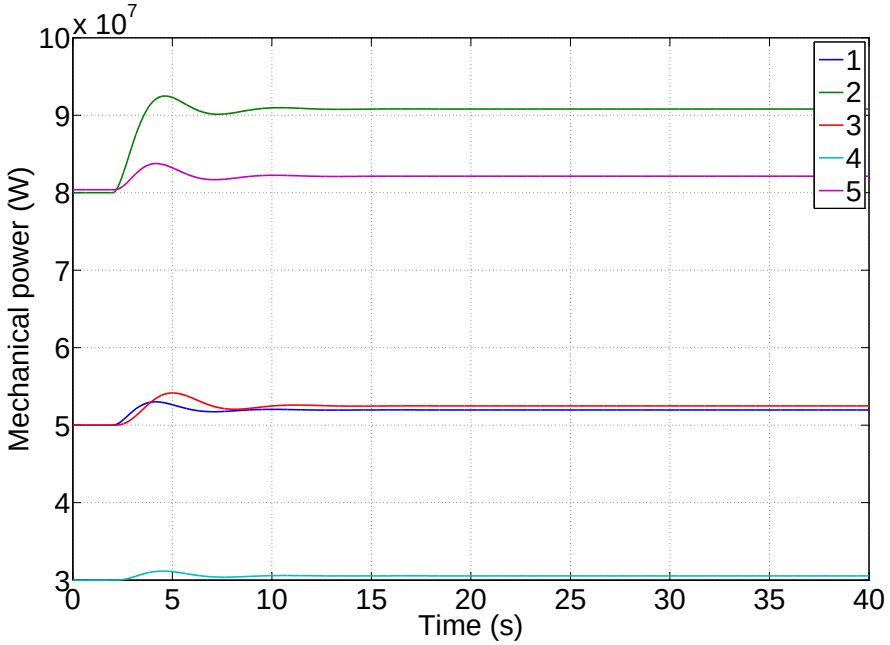

Figure 6.7: Mechanical power inputs of 5 AC areas with controller.

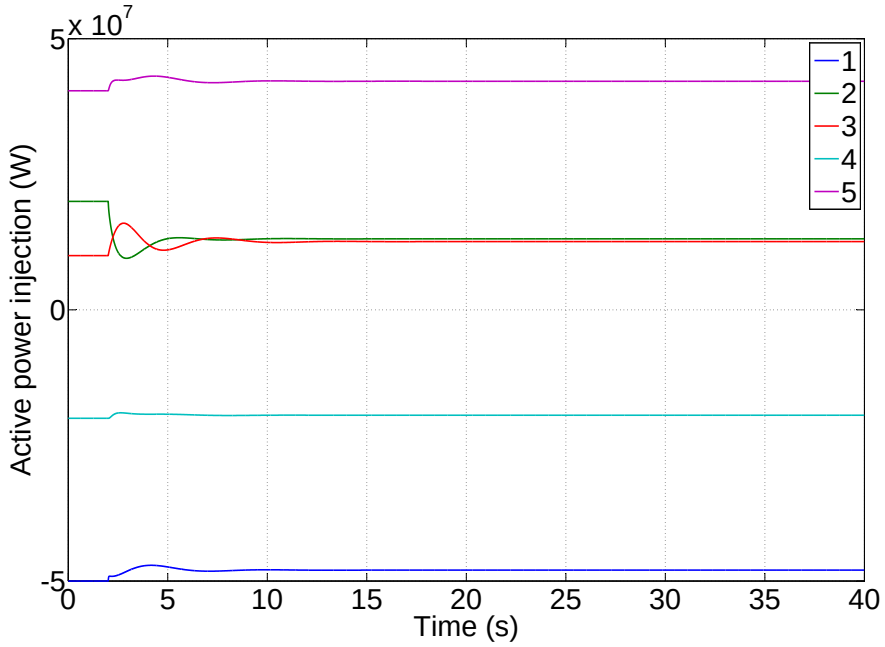

Figure 6.8: Active power injections P_i^{dc} of 5 AC areas with controller.

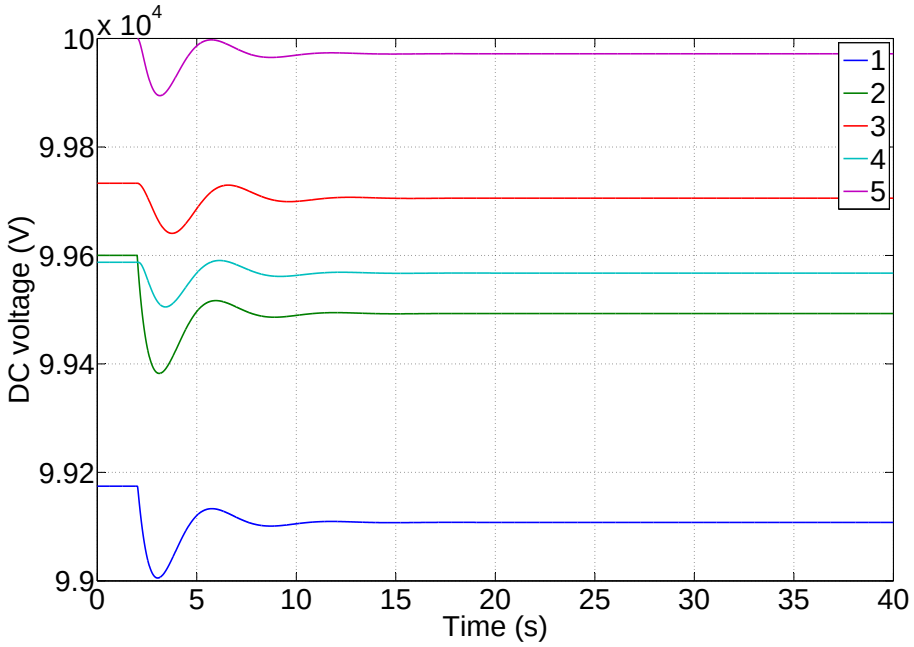

Figure 6.9: DC voltage V_i^{dc} of 5 AC areas with controller.

Figs. 6.6 and 6.7 illustrate the frequency and the mechanical power response

Table 6.2: Values of α_i calculated by LMI.

α_1	α_2	α_3	α_4	α_5
1700	397	185	548	868

when the controller is implanted. Table 6.2 shows the values for α_i calculated by LMI techniques. The proposed α_i are in their feasible region that can make sure that the system is stable. Note that, the minimum value of f_2 is between 49.4515 Hz and 49.452 Hz which is in the safety range and the final value f_2 is 49.7299 Hz. P_{m2} has a peak value of nearly 92.5 MW, and is stabilized at 91 MW. The above results show that our controller makes a significant improvement for f_2 not only in the transient performance but also in the steady-state performance compared to the case without sharing the primary reserves (see Fig. 6.2).

Comparing the trajectories of P_i^{dc} in Figs. 6.4 and 6.8, when the frequency control is applied to counteract the sudden load change of AC area 2, the power injection of every AC area gives a corresponding response, which is sent to their respective converter stations.

6.5 Conclusions

In this chapter, we addressed the problem of developing a frequency controller that provides the active power reference values to the VSC and shares primary reserves between the AC areas connected by an MTDC system. In the case of a power imbalance, the controller reduces the burden of the affected AC area by making the other AC areas collectively react to that disturbance. In addition, the proposed control law is only based on local measurements without needing remote communication, thus avoiding the disadvantages caused by time-delay.

Chapter 7

Conclusions

Contents

7.1 Conclusions

In the last decades, the development of VSC HVDC systems becomes a very important topic in scientific researches. Due to their flexibility, controllability and efficiency, VSC HVDC systems have been greatly promoted in today's electrical networks. In particular, there is a growing need to integrate large-scale offshore renewable energy sources via MTDC systems, whose generation outputs are usually intermittent. Nevertheless, the MTDC technology is not yet mature enough for wide commercial applications. There are still many issues that need to be solved. This dissertation is dedicated to the challenges in the control of MTDC systems.

This thesis started by giving a brief introduction to HVDC technology where the limits of the classical AC transmission technology are shown and the rationale of HVDC systems is discussed. Besides, the comparisons between AC and DC as well as LCC and VSC are also listed. Then, we introduced several existing control structures of VSC HVDC systems according to their research groups in the literature review. Interestingly, we found that most of the control methods only focus on the operating results but neglect related theoretical analysis. As a consequence, extra time-consuming processes are usually needed to accompany these control approaches to achieve good performance. At the end of Chapter 1, we defined the objectives of this thesis: 1) developing new control methods for MTDC systems to improve the overall performance; 2) providing theoretical explanations for the system dynamic behaviors to give new insights into how and why the existing

conventional (or empirical) control structures work; 3) fully developing the potential of MTDC systems for AC frequency regulation; 4) Developing a new control theory named Control Induced Time-Scale Separation. This general control theory was created aiming at the MTDC system, but indeed applies to a very broad class of nonlinear systems, and allows plug-and-play capabilities. In addition, it fits well in a Systems of Systems framework.

In Chapter 2, we first gave an overview of the VSC technology to get a good understanding of the classic operation of VSC HVDC systems. Then, we introduced two different types of AC networks which are distinguished by their Short Circuit Ratio. In line with the control objectives and the type of the connected AC network, possible control modes of a single VSC terminal were discussed, which offer a basic knowledge for the control design of MTDC systems.

In the modeling, the time-averaged modeling method which is the most generally used modeling approach in the context of power systems was chosen and presented in Chapter 3. This modeling approach is much simpler and tractable than the detailed modeling one. In this thesis, the proposed MTDC system consists of N strong AC networks, M weak AC networks and a DC grid. One of the main contributions of this thesis is that a generic topology is considered for the structure of the DC grid, which can be mapped to a weakly connected directed graph. Thus, our research is not only suitable for the radial topology but also for the meshed topology. In addition, all connected AC networks are considered in balanced three-phase condition and hence, Park's transformation is applied to project all three-phase quantities onto a rotating two-axis reference frame. The overall modeling work is divided into three parts: 1) modeling of the strong AC network connected VSC terminals; 2) modeling of the weak AC network connected VSC terminals; 3) modeling of the DC grid. At the end of Chapter 3, an averaged state-space model of high order for the proposed MTDC system was established.

In Chapter 4, two of the most widely used conventional control methods for VSC HVDC systems, namely direct and vector control methods, were discussed. Both advantages and disadvantages of the aforementioned control methods were analyzed. Based on the existing problems of the two control approaches, new improved control strategies were proposed in this dissertation.

In Chapter 5, new control structures by means of different nonlinear control design tools for VSC HVDC systems were developed. We started by applying feedback linearization technique to the development of a nonlinear controller, which can partly transform the nonlinear MTDC model to a linear one. A theoretical analysis of the nonlinear feedback linearization controller was carried out, which indicates that the stability of the equilibrium of the zero dynamics determines the stability of the overall system. Furthermore, a sufficient condition on the system parameters was derived to ensure the stability of the zero dynamics. The performance comparisons between this nonlinear controller and the conventional vector controller were given, which show that the nonlinear control provides much better decoupling characteristics of the DC voltage and the AC $q-$axis current control or the AC voltages v_{sw_jd} and v_{sw_jq} control than the PI controller. Besides, during the simulation process, we

found that when a new operating point of the MTDC systems is to be achieved, it is usually needed to recalculate the proper PI control gains for the conventional vector controller to obtain an optimal performance. However, this is time-consuming and usually requires extra efforts. For the nonlinear feedback controller, we usually have no need to deduce new control gains for different operating conditions. In order to make the system more robust, a sliding mode control technique was applied to develop a novel controller where the uncertainties of the system parameters and other possible exogenous inputs were taken into account. During the design procedure of the feedback linearization controller, we naturally chose the controlled variables as the output. However, the theoretical analysis clearly shows that the MTDC system is not always minimum phase. There exists a restriction on the choice of the prescribed references and the system parameters (see Lemma 4.1.2). To overcome this problem, a passive output was deduced by means of passivity theory so that the MTDC system with the passive output is always minimum phase. Then, a new control strategy based on the input-output feedback linearizaton and the passivity theory was devised. Simulation studies were also carried out to evaluate the performance of the passivity-based state feedback controller.

In Chapter 6, the dynamic behaviors of the proposed MTDC system were analyzed. It is interesting to remark that these dynamics have never been extensively rigorously studied in the literature. The research done on this issue is one of the main contributions of this dissertation summarized as follow:

- **Control induced time-scale separation design for a class of nonlinear systems**

  A control induced time-scale separation method was developed for a class of nonlinear systems, which enables the system to exhibit a multi-time-scale behavior characterized by the presence of fast and slow transients. Based on singular perturbation theory, a detailed theoretical analysis was performed, which shows that the time-scale decomposition of the system dynamics is qualified by the control gains of the driving subsystem. Besides, with the help of the proposed controller, the original system can be divided into two low-order subsystems and then, the behaviors of the system states can be approximated by the solutions of the two simpler subsystems. Furthermore, we gave an analytical expression to illustrate the trade-off between the system performance and the region of attraction.

- **Analysis of the conventional control structures and the dynamics of the MTDC system**

  For an MTDC system, the concept of the conventional vector control method is mainly based on the assertion that the dynamics of the system state variables can be divided into different time scales and hence, the two control loops can be designed independently. However, very few research has ever verified and explained this assertion. In this dissertation, we applied the theoretical results obtained from the study on the time-scale separation controller to

bridge the gap between the practice and the theory where the master-slave and the droop control configurations were studied. From the theoretical analysis of the two control configurations, we identified several points: 1) how and why the system exhibits a multi-time-scale behavior; 2) the rules of tuning the control gains such that parts of those gains regulate the fast transient and the remaining determines the behavior of the slow transient; 3) the existence of uncontrollable state variables when the master-slave control configuration is used. Moreover, we pointed out that the master-slave control configuration based on vector control method is not always applicable for the MTDC system. The stability of the MTDC system with the master-slave control configuration can be ensured only when the system parameters and the scheduled references satisfy certain conditions while for the droop control configuration, there is no special limitation on them.

In Chapter 7, a potential application of MTDC systems was introduced where an AC frequency support strategy via the MTDC system was proposed. This strategy enables the asynchronous AC systems to share their primary reserves via an MTDC system. The control method used in this application, namely the DC-voltage-based controller, is based on local measurements without needing any remote communication, and avoids possible problems caused by time-delay. Simulation studies showed that the proposed control strategy achieves the control objective with satisfactory performances.

7.2 Perspectives for future work

This thesis have met some challenges in the area of MTDC systems. However, there still exist many issues to be investigated.

7.2.1 Further research on the droop control configuration

In Section 5.3, we discussed the dynamic behavior of the MTDC system under the droop control configuration. We found that the choice of the droop gains has great impacts on: 1) the steady-state values of the system variables; 2) the distribution of power sharing between the interconnected AC networks in case of power imbalance; 3) the dynamics of the DC grid. In this thesis, the droop gains are considered constant. It would be interesting to consider the droop gains not as constants but as variables, which could vary according to different operating conditions. For example, each converter terminal has a different capability against the power imbalance. The droop gain of each converter terminal could vary depending on its existing available headroom of the capacity.

7.2.2 Further research on the connection of other types of weak AC systems

One of the most important applications of VSC HVDC systems is to connect island systems. It would be interesting to consider that the MTDC system has one or more converter terminals connected to islands. Moreover, various components related to the island, such as the synchronous generators, the passive loads, can be taken into account. It is worthwhile to note that the passive loads are usually unknown and hence, during the control design for the island connected converter terminal, adaptive control technique could be applied to improve the system performance.

7.2.3 Further research on the operation of MTDC systems

In Section 4.1.4.1, we presented that the MTDC system has plug-and-play capabilities. This ability is very important for the extension of the existing MTDC systems. In this thesis, we provided a qualitative approach to determine whether an AC system could be added or removed. One of possible further work is that a quantitative approach need to be developed from a security point of view.

7.2.4 Further research on system modeling

In this thesis, the ideal three-phase AC source was used for every strong AC network and the controlled three-phase current source was used for every weak AC network. Therefore, we can take the dynamics of the generator and the wind turbine into consideration when modeling an MTDC system. This would help us study the system behaviors and the interactions between AC and DC.

7.2.5 Implementation on a real MTDC system

In this thesis, the developed nonlinear controllers were tested by using SimPowerSystems toolbox of MATLAB/Simulink. From the simulation results, both advantages and disadvantages of each control method are clearly presented. However, due to the limit of the condition, these control methods are not yet implemented on a real MTDC system. It will be interesting to test these proposed controllers on a real MTDC system.

7.2.6 Control induced time-scale separation for the MMC

Compared to the VSC with PMW technology, multilevel modular converter (MMC) has attracted a lot of attention due to its less generated harmonics and losses of the semiconductor devices. Since the MMC has a more complicated structure than the VSC with two (or three) voltage levels, in future work it is possible to apply the obtained theoretical results on the control induced time-scale to analyze the dynamic behavior of MMC in an easy way.

Appendix A

Appendix

A.1 Notations

For a matrix $A \in \mathbb{R}^{n\times m}$, A_{ij} is the element of A in the i^{th} row and the j^{th} column. $A(:,i)$ and $A(j,:)$ denote the i^{th} column and the j^{th} row of A, respectively. A diagonal matrix $A \in \mathbb{R}^{n\times n}$ is represented by $A = \text{diag}(a_i)$, $i = 1,\cdots,n$. $A(l:s,k:h)$ is a submatrix of A where $A(l:s,k:h)_{ij} = A_{(l+i-1)(k+j-1)}$. Given a set of matrix $A_k \in \mathbb{R}^{m_k\times m_k}$, $k = 1,\cdots,n$ and $N = \sum_{k=1}^{n} m_k$, the notation $A = \text{diag}(A_k)$ represents $A \in \mathbb{R}^{N\times N}$ where we have $A(1:m_1, 1:m_1) = A_1$ and $A(\sum_{j=1}^{k-1} m_j + 1 : \sum_{j=1}^{k} m_j, \sum_{j=1}^{k-1} m_j + 1 : \sum_{j=1}^{k} m_j) = A_k$, for $k = 2, \cdots, n$, and the other elements of A are zero. The transpose of A is denoted by A^T. The inverse of A is denoted by A^{-1}. The notation $\text{rank}(A)$ means the rank of A. $0_{n\times m} \in \mathbb{R}^{n\times m}$ represents a zero matrix, with all its elements equal zero. $I_{n\times n} \in \mathbb{R}^{n\times m}$ represents the identity matrix. $0_n \in \mathbb{R}^n$ represents a zero vector, with all its elements equal zero. For $x = [x_1 \ \cdots \ x_n]^T \in \mathbb{R}^n$, $||x|| = \sqrt{x_1^2 + \cdots + x_n^2}$. For a complex number $x \in \mathbb{C}$, the real part of x is denoted as $\text{Re}(x)$ while its imaginary part is denoted as $\text{Im}(x)$. For $A \in \mathbb{R}^{n\times n}$, $||A|| = \sqrt{\lambda_{\max}(A^H A)}$ where A^H is the conjugate transpose of A and $\lambda_{\max}(\cdot)$ represents the maximum eigenvalue of matrix $(\cdot)$. The notation $\mathbb{D}_x \subset \mathbb{R}^n$ denotes the safe operating domain of variable $x \in \mathbb{R}^n$, which is convex. The notation $\bar{x}$ represents the value of x in steady-state condition and the initial value of x is denoted by $x(t_0)$. x^o is the prescribed (or reference value) of the variable x. x^* means the reference trajectory of the variable x. $\hat{x}$ is the estimate of x. Any complex matrix A can be expressed as $A = \mathcal{H}(A) + \mathcal{S}(A)$ where $\mathcal{H}(A) = 1/2(A + A^H)$ is a hermitian matrix and $\mathcal{S}(A) = 1/2(A - A^H)$ is an anti-hermitian matrix. For any matrix A, $\mathcal{R}(A)_l$ is a reduced matrix by deleting the l^{th} row of A. The maximum and the minimum values of a set of variables $(a_1, \cdots, a_m)$ are denoted as $\min(a_1, \cdots, a_m)$ and $\max(a_1, \cdots, a_m)$.

Appendix B

Appendix

B.1 Proof of Lemma 4.1.6

Proof. For any vector $x \in \mathbb{C}^n$, $x \neq 0_n$, we have

$$\begin{aligned}(x^H \mathcal{H}(\Psi) x)^H &= x^H \mathcal{H}(\Psi)^H x \\ &= x^H \mathcal{H}(\Psi) x\end{aligned}$$

Hence, $x^H \mathcal{H}(\Psi) x$ is a real number. Similarly, we can obtain

$$\begin{aligned}(x^H \mathcal{S}(\Psi) x)^H &= x^H \mathcal{S}(\Psi)^H x \\ &= -x^H \mathcal{S}(\Psi) x\end{aligned}$$

Thus, $x^H \mathcal{S}(\Psi) x$ is an imaginary number. So we get $\mathrm{Re}(x^H \Psi x) = x^H \mathcal{H}(\Psi) x$. As a result, $\mathrm{Re}(x^H \Psi x)$ is positive if and only if $x^H \mathcal{H}(\Psi) x$ is positive. □

B.2 Proof of Lemma 4.1.9

Proof. Since Ψ is positive definite, $\mathcal{H}(\Psi)$ is also positive definite and hence there exists an invertible matrix Q such that

$$Q^H \mathcal{H}(\Psi) Q = I_{n \times n}$$

In addition, $Q^H \mathcal{S}(\Psi) Q$ is also an anti-hermitian matrix. Hence, there exists a unitary matrix U such that

$$U^H Q^H \mathcal{S}(\Psi) Q U = \mathrm{diag}(jb_1,\ jb_2,\ \cdot,\ jb_k,\ 0,\ \cdots,\ 0)$$

where $j = \sqrt{-1}$, $b_i \neq 0$ $(i = 1,\ \cdots,\ k)$ are real numbers and $k = \mathrm{rank}(\mathcal{S}(\Psi))$. Moreover, we have

$$U^H Q^H \mathcal{H}(\Psi) Q U = I_{n \times n}$$

Let us denote $P = QU$ and as a consequence, P is invertible. We then have

$$\begin{aligned}P^H \Psi P &= P^H \mathcal{H}(\Psi) P + P^H \mathcal{S}(\Psi) P \\ &= \mathrm{diag}(jb_1 + 1,\ jb_2 + 1,\ \cdot,\ jb_k + 1,\ 1,\ \cdots,\ 1) \triangleq T\end{aligned}$$

Since matrices T and P are invertible and we also have

$$\Psi = (P^H)^{-1} T P^{-1}$$

Ψ is invertible. Moreover, because $\mathcal{H}(T)$ is positive definite, according to Lemma 4.1.6, T is also positive definite. Finally, we get the result that Ψ^{-1} is also positive definite. □

Bibliography

[ABB 2014] ABB. *Lower losses.* http://www.abb.com/industries/db0003db004333/fd32594c4d4dea8cc1257481004a6140.aspx, 2014. (Cited on page 106.)

[Adam 2015] G.P. Adam, I.A. Abdelsalam, K.H. Ahmed and B.W. Williams. *Hybrid Multilevel Converter With Cascaded H-bridge Cells for HVDC Applications: Operating Principle and Scalability.* IEEE Transactions on Power Electronic, vol. 30, no. 1, pages 65–77, Jan 2015. (Cited on page 11.)

[Akhmatov 2014] V. Akhmatov, M. Callavik, C.M. Franck, S.E. Rye, T. Ahndorf, M.K. Bucher, H. Muller, F. Schettler and R. Wiget. *Technical Guidelines and Prestandardization Work for First HVDC Grids.* IEEE Transactions on Power Delivery, vol. 29, no. 1, pages 327–335, Feb 2014. (Cited on page 24.)

[Andersen 2000] B. Andersen and C. Barker. *A new era in HVDC?* IEE Review, vol. 46, no. 2, pages 33–39, Mar 2000. (Cited on page 3.)

[Andersen 2002] B.R. Andersen, L. Xu, P.J. Horton and P Cartwright. *Topologies for VSC transmission.* Power Engineering Journal, vol. 16, no. 3, pages 142–150, Jun 2002. (Cited on pages 2 and 17.)

[Arrillaga 1998] Jos Arrillaga. High voltage direct current transmission. Numeéro 29. Iet, 1998. (Cited on page 4.)

[Asplund 2000] G. Asplund. *Application of HVDC Light to power system enhancement.* In IEEE Power Engineering Society Winter Meeting, volume 4, pages 2498–2503, 2000. (Cited on page 3.)

[Asplund 2007] Gunnar Asplund. *Ultra high voltage transmission.* ABB Review, no. 2, pages 22–27, 2007. (Cited on page 3.)

[Ayodele 2011] TR Ayodele, AA Jimoh, JL Munda and JT Agee. *The influence of wind power on the small signal stability of a power system.* In International conference on renewable energy and power quality, pages 13–15, Las Palmas de Gra Canaria, Spain, April 2011. (Cited on page 8.)

[Bahrman 2007] Michael P Bahrman and Brian K Johnson. *The ABCs of HVDC transmission technologies.* IEEE Power and Energy Magazine, vol. 5, no. 2, pages 32–44, 2007. (Cited on pages 3 and 17.)

[Bajracharya 2008] Chandra Bajracharya, Marta Molinas, Jon Are Suul, Tore M Undeland*et al.* *Understanding of tuning techniques of converter controllers for VSC-HVDC.* In Nordic Workshop on Power and Industrial Electronics, Espoo, Finland, Jun 2008. Helsinki University of Technology. (Cited on pages 12 and 43.)

[Beccuti 2010] G. Beccuti, G. Papafotiou and L. Harnefors. *Multivariable predictive control of voltage source converter HVDC transmission systems.* In IEEE International Symposium on Industrial Electronics (ISIE)„ pages 3145–3152, Jul 2010. (Cited on pages 8 and 9.)

[Beerten 2014] J. Beerten, S. Cole and R. Belmans. *Modeling of Multi-Terminal VSC HVDC Systems With Distributed DC Voltage Control.* IEEE Transactions on Power Systems, vol. 29, no. 1, pages 34–42, Jan 2014. (Cited on pages 11 and 36.)

[Bendtsen 2013] Jan Bendtsen, Klaus Trangbaek and Jakob Stoustrup. *Plug-and-Play Control-Modifying Control Systems Online.* IEEE Transactions on Control Systems Technology, vol. 21, no. 1, pages 79–93, 2013. (Cited on page 132.)

[Bianchi 2011] F.D. Bianchi and O. Gomis-Bellmunt. *Droop control design for multi-terminal VSC-HVDC grids based on LMI optimization.* In 2011 50th IEEE Conference on Decision and Control and European Control Conference (CDC-ECC), pages 4823–4828, Dec. 2011. (Cited on pages 10 and 174.)

[Blasko 1997] V. Blasko and V. Kaura. *A new mathematical model and control of a three-phase AC-DC voltage source converter.* IEEE Transactions on Power Electronics, vol. 12, no. 1, pages 116–123, Jan 1997. (Cited on pages 8, 9 and 41.)

[Bondy 1976] John Adrian Bondy and Uppaluri Siva Ramachandra Murty. Graph theory with applications, volume 6. Macmillan London, 1976. (Cited on page 39.)

[Boyd 1994] S. Boyd, L. El Ghaoui, E. Feron and V. Balakrishnan. Linear matrix inequalities in system and control theory. SIAM, Studies in Applied Mathematics, 1994. (Cited on page 210.)

[Byrnes 1991] Christopher I Byrnes, Alberto Isidori and Jan C Willems. *Passivity, feedback equivalence, and the global stabilization of minimum phase nonlinear systems.* IEEE Transactions on Automatic Control, vol. 36, no. 11, pages 1228–1240, 1991. (Cited on page 101.)

[Carlsson 2002] Lennart Carlsson. *" Classical" HVDC: still continuing to evolve.* Modern power systems, vol. 22, no. 6, pages 19–22, 2002. (Cited on page 4.)

[Carlsson 2003] L Carlsson, G Flisberg and L Weimers. *Recent Evolution in Classic HVDC.* In The 4th International Conference on Power Transmission & Distribution, 2003. (Cited on page 4.)

[Chaudhary 2008] S.K. Chaudhary, R. Teodorescu and P. Rodriguez. *Wind Farm Grid Integration Using VSC Based HVDC Transmission - An Overview.* In IEEE Energy 2030, pages 1–7, Nov 2008. (Cited on pages 8 and 34.)

[Chaudhuri 2013] N.R. Chaudhuri and B. Chaudhuri. *Adaptive Droop Control for Effective Power Sharing in Multi-Terminal DC (MTDC) Grids.* IEEE Transactions on Power Systems, vol. 28, no. 1, pages 21–29, Feb. 2013. (Cited on pages 10 and 174.)

[Chen 2011] Xia Chen, Haishun Sun, Jinyu Wen, Wei-Jen Lee, Xufeng Yuan, Naihu Li and Liangzhong Yao. *Integrating Wind Farm to the Grid Using Hybrid Multiterminal HVDC Technology.* IEEE Transactions on Industry Applications,, vol. 47, no. 2, pages 965–972, Mar 2011. (Cited on page 11.)

[Chen 2013] Wu-Hua Chen, Guo Yuan and Wei Xing Zheng. *Robust Stability of Singularly Perturbed Impulsive Systems Under Nonlinear Perturbation.* IEEE Transactions on Automatic Control, vol. 58, no. 1, pages 168–174, January 2013. (Cited on page 133.)

[Chen 2014] Yijing Chen, Gilney Damm, Abdelkrim Benchaib and Françoise Lamnabhi-Lagarrigue. *Multi-Time-Scale Stability Analysis and Design Conditions of a VSC Terminal with DC Voltage Droop Control for HVDC Networks.* In IEEE Conference on Decision and Control (CDC), Los Angeles, CA, USA, Dec. 2014. IEEE. (Cited on pages 10 and 174.)

[Chung 2000] Se-Kyo Chung. *A phase tracking system for three phase utility interface inverters.* IEEE Transactions on Power Electronics, vol. 15, no. 3, pages 431–438, May 2000. (Cited on page 31.)

[CIGRE 2014] CIGRE. *What is LCC HVDC ?* `http://b4.cigre.org/Menu-links/What-is-SC-B4`, 2014. (Cited on page 4.)

[Cole 2010] Stijn Cole. *Steady-State and Dynamic Modelling of VSC HVDC Systems for Power System Simulation.* PhD thesis, PhD Dissertation, KU Leuven, 2010. (Cited on page 11.)

[Dai 2010] J. Dai, Y. Phulpin, A. Sarlette and D. Ernst. *Impact of delays on a consensus-based primary frequency control scheme for AC systems connected by a multi-terminal HVDC grid.* In Proceedings of the 2010 IREP Symposium - Bulk Power Systems Dynamics and Control - VIII, Buzios, Rio de Janeiro, Brazil, 1-6 August 2010. (Cited on page 210.)

[Dannehl 2009] J. Dannehl, C. Wessels and F.W. Fuchs. *Limitations of Voltage-Oriented PI Current Control of Grid-Connected PWM Rectifiers With LCL Filters.* IEEE Transactions on Industrial Electronics, vol. 56, no. 2, pages 380–388, Feb 2009. (Cited on pages 9, 12, 43 and 47.)

[Daryabak 2014] M. Daryabak, S. Filizadeh, J. Jatskevich, A. Davoudi, M. Saeedifard, V.K. Sood, J.A. Martinez, D. Aliprantis, J. Cano and A. Mehrizi-Sani. *Modeling of LCC-HVDC Systems Using Dynamic Phasors.* IEEE Transactions on Power Delivery, vol. 29, no. 4, pages 1989–1998, Aug 2014. (Cited on page 3.)

[Del Vecchio 2013] D. Del Vecchio and J.E. Slotine. *A Contraction Theory Approach to Singularly Perturbed Systems.* IEEE Transactions on Automatic Control, vol. 58, no. 3, pages 752–757, March 2013. (Cited on page 133.)

[Dodds 2010] S Dodds, B Railing, K Akman, B Jacobson, T Worzyk and B Nilsson. *HVDC VSC (HVDC light) transmission–operating experiences.* Proc. CIGRE Session, Paris, France, pages 1–9, 2010. (Cited on pages 3, 4 and 17.)

[Du 2003] Cuiqing Du. *The control of VSC-HVDC and its use for large industrial power systems.* PhD thesis, Chalmers University of Technology, 2003. (Cited on page 42.)

[Du 2005] Cuiqing Du, Ambra Sannino and Math HJ Bollen. *Analysis of the control algorithms of voltage-source converter HVDC.* In IEEE Power Tech, pages 1–7, Russia, June 2005. (Cited on pages 9 and 34.)

[Durrant 2003] Martyn Durrant, H. Werner and Keith Abbott. *Model of a VSC HVDC terminal attached to a weak AC system.* In IEEE Conference on Control Applications, volume 1, pages 178–182, Jun 2003. (Cited on pages 9, 43 and 47.)

[Durrant 2004] Martyn Durrant, H. Werner and Keith Abbott. *Synthesis of multi-objective controllers for a VSC HVDC terminal using LMIs.* In IEEE Conference on Decision and Control, volume 4, pages 4473–4478, Dec 2004. (Cited on page 109.)

[Durrant 2006] Martyn Durrant, H. Werner and Keith Abbott. *A Comparison of LMI and GA Based Robust Controller Designs for VSC HVDC.* In 45th IEEE Conference on Decision and Control, pages 3990–3995, Dec 2006. (Cited on page 9.)

[Egea-Alvarez 2013] A. Egea-Alvarez, F. Bianchi, A. Junyent-Ferre, G. Gross and O. Gomis-Bellmunt. *Voltage Control of Multiterminal VSC-HVDC Transmission Systems for Offshore Wind Power Plants: Design and Implementation in a Scaled Platform.* IEEE Transactions on Industrial Electronics, vol. 60, no. 6, pages 2381–2391, Jun. 2013. (Cited on page 174.)

[Ekanayake 2009] J.B. Ekanayake. *Multi-terminal DC converters for connecting induction generator based distribution generation.* In International Conference on Industrial and Information Systems (ICIIS), pages 466–471, Dec 2009. (Cited on page 10.)

[Eriksson 2001] Kjell Eriksson. *Operational experience of HVDC LightTM.* In Seventh International Conference on AC-DC Power Transmission, pages 205–210, Nov 2001. (Cited on page 3.)

[Eriksson 2014] R. Eriksson, J. Beerten, M. Ghandhari and R. Belmans. *Optimizing DC Voltage Droop Settings for AC/DC System Interactions*. IEEE Transactions on Power DeliverY, vol. 29, no. 1, pages 362–369, Feb 2014. (Cited on page 10.)

[Escobar 1999] Gerardo Escobar, Arjan J Van Der Schaft and Romeo Ortega. *A Hamiltonian viewpoint in the modeling of switching power converters*. Automatica, vol. 35, no. 3, pages 445–452, 1999. (Cited on page 92.)

[Flourentzou 2009] Nikolas Flourentzou, Vassilios G Agelidis and Georgios D Demetriades. *VSC-based HVDC power transmission systems: an overview*. Power Electronics, IEEE Transactions on, vol. 24, no. 3, pages 592–602, 2009. (Cited on pages 3 and 4.)

[Fu 2014] Jiao Fu, Zhichang Yuan, Yizhen Wang, Shukai Xu, Wei Wei and Yu Luo. *Control strategy of system coordination in Nanao multi-terminal VSC-HVDC project for wind integration*. In IEEE PES General Meeting, pages 1–5, Jul 2014. (Cited on pages 3 and 11.)

[Gavrilovic 1991] A. Gavrilovic. *AC/DC system strength as indicated by short circuit ratios*. In International Conference on AC and DC Power Transmission, pages 27–32, Sep 1991. (Cited on pages 23 and 34.)

[Haileselassie 2008] Temesgen M Haileselassie, Marta Molinas, Tore Undeland*et al.* *Multi-terminal VSC-HVDC system for integration of offshore wind farms and green electrification of platforms in the North Sea*. In Nordic Workshop on Power and Industrial Electronics. Helsinki University of Technology, Jun 2008. (Cited on pages 10 and 11.)

[Haileselassie 2009] T Haileselassie, Tore Undeland and Kjetil Uhlen. *Multiterminal HVDC for offshore wind farms-control strategy*. In Wind Power to the Grid-EPE Wind Energy Conferece, Stockholm, Sweden, 2009. (Cited on page 11.)

[Haileselassie 2012a] Temesgen Mulugeta Haileselassie. *Control, Dynamics and Operation of Multi-terminal VSC-HVDC Transmission Systems*. PhD thesis, Norwegian University of Science and Technology, 2012. (Cited on pages 11 and 40.)

[Haileselassie 2012b] T.M. Haileselassie and K. Uhlen. *Impact of DC Line Voltage Drops on Power Flow of MTDC Using Droop Control*. IEEE Transactions on Power Systems, vol. 27, no. 3, pages 1441–1449, Aug. 2012. (Cited on pages 10, 177 and 181.)

[Hamzei-nejad 1986] A. Hamzei-nejad and C. M Ong. *Coordinating the DC power injections of a multiterminal HVDC system for dynamic control of AC line flows*. IEEE Transactions on Power Systems, vol. PWRS-1, no. 2, May 1986. (Cited on page 210.)

[Hedrick 2005] JK Hedrick and A Girard. *Control of nonlinear dynamic systems: Theory and applications*. Controllability and observability of Nonlinear Systems, 2005. (Cited on page 48.)

[Hernandez-Gomez 2010] M. Hernandez-Gomez, R. Ortega, F. Lamnabhi-Lagarrigue and G. Escobar. *Adaptive PI Stabilization of Switched Power Converters*. IEEE Transactions on Control Systems Technology, vol. 18, no. 3, pages 688–698, May 2010. (Cited on pages 92 and 109.)

[Horn 1985] Roger A Horn and Charles R Johnson. Matrix analysis. Cambridge university press, 1985. (Cited on page 76.)

[IEE 1997] *IEEE Guide for Planning DC Links Terminating at AC Locations Having Low Short-Circuit Capacities*. IEEE Std 1204-1997, 1997. (Cited on page 23.)

[Ilves 2015] K. Ilves, L. Harnefors, S. Norrga and H.-P. Nee. *Analysis and Operation of Modular Multilevel Converters With Phase-Shifted Carrier PWM*. IEEE Transactions on Power Electronics, vol. 30, no. 1, pages 268–283, Jan 2015. (Cited on page 11.)

[Isidori 1995] A. Isidori. Nonlinear control systems, third edition. Springer, 1995. (Cited on pages 48 and 147.)

[Johansson 2004] S.G. Johansson, L. Carlsson and G. Russberg. *Explore the power of HVDC light reg; - a web based system interaction tutorial*. In IEEE PES Power Systems Conference and Exposition, pages 839–842 vol.2, Oct 2004. (Cited on page 3.)

[Johnson 1993] B.K. Johnson, R.H. Lasseter, F.L. Alvarado and R. Adapa. *Expandable multiterminal DC systems based on voltage droop*. IEEE Transactions on Power Delivery, vol. 8, no. 4, pages 1926–1932, Oct 1993. (Cited on page 10.)

[Karaagac 2014] U. Karaagac, S.O. Faried, J. Mahseredjian and A.-A. Edris. *Coordinated Control of Wind Energy Conversion Systems for Mitigating Subsynchronous Interaction in DFIG-Based Wind Farms*. IEEE Transactions on Smart Grid,, vol. 5, no. 5, pages 2440–2449, Sep 2014. (Cited on page 11.)

[Karady 1973] G. Karady and T. Gilsig. *The thyristor valve in HVDC transmission*. IEEE Spectrum, vol. 10, no. 12, pages 36–43, Dec 1973. (Cited on page 3.)

[Karlsson 2003] P. Karlsson and J. Svensson. *DC bus voltage control for a distributed power system*. IEEE Transactions on Power Electronics, vol. 18, no. 6, pages 1405–1412, Nov 2003. (Cited on page 10.)

[Khalil 1987] Hassan K Khalil and Ali Saberi. *Adaptive stabilization of a class of nonlinear systems using high-gain feedback*. IEEE Transactions on Automatic Control, vol. 32, no. 11, pages 1031–1035, 1987. (Cited on page 133.)

[Khalil 1996] H. Khalil. Nonlinear systems. Prentice Hall, New Jersey, 3rd édition, 1996. (Cited on pages 48, 87, 133, 141, 144 and 214.)

[Kim 2010] Dong-Eok Kim and Dong-Choon Lee. *Feedback Linearization Control of Three-Phase UPS Inverter Systems.* IEEE Transactions on Industrial Electronics, vol. 57, no. 3, pages 963–968, Mar 2010. (Cited on page 48.)

[Kimball 2008] Jonathan W Kimball and Philip T Krein. *Singular perturbation theory for DC–DC converters and application to PFC converters.* IEEE Transactions on Power Electronics, vol. 23, no. 6, pages 2970–2981, 2008. (Cited on pages 12 and 133.)

[Kimbark 1971] Edward Wilson Kimbark. Direct current transmission, volume 1. Wiley-Interscience New York, NY, 1971. (Cited on page 4.)

[Kirby 2002] N.M. Kirby, Lie Xu, M. Luckett and W. Siepmann. *HVDC transmission for large offshore wind farms.* Power Engineering Journal, vol. 16, no. 3, pages 135–141, Jun 2002. (Cited on page 8.)

[Kokotovic 1968] P.V. Kokotovic and P. Sannuti. *Singular perturbation method for reducing the model order in optimal control design.* IEEE Transactions on Automatic Control, vol. 13, no. 4, pages 377–384, August 1968. (Cited on page 133.)

[Kokotovic 1976] Petar V Kokotovic*et al. Singular perturbations and order reduction in control theory-an overview.* Automatica, vol. 12, no. 2, pages 123–132, 1976. (Cited on page 133.)

[Kokotovic 1980] Petar V Kokotovic, John J Allemong, James R Winkelman and Joe H Chow. *Singular perturbation and iterative separation of time scales.* Automatica, vol. 16, no. 1, pages 23–33, 1980. (Cited on page 133.)

[Kokotovic 1999] Petar Kokotovic, Hassan K Khali and John O'reilly. Singular perturbation methods in control: analysis and design, volume 25. Siam, 1999. (Cited on page 133.)

[Kong 2014] F. Kong, Z. Hao, S. Zhang and B. Zhang. *Development of a Novel Protection Device for Bipolar HVDC Transmission Lines.* IEEE Transactions on Power Delivery,, vol. 29, no. 5, pages 2270–2278, Oct 2014. (Cited on page 11.)

[Krishnamurthy 2007] Prashanth Krishnamurthy and Farshad Khorrami. *High-gain output-feedback control for nonlinear systems based on multiple time scaling.* Systems & control letters, vol. 56, no. 1, pages 7–15, 2007. (Cited on page 133.)

[Krishnamurthy 2013] Prashanth Krishnamurthy and Farshad Khorrami. *A singular perturbation based global dynamic high gain scaling control design for*

systems with nonlinear input uncertainties. IEEE Transactions on Automatic Control, vol. 58, no. 10, pages 2686–2692, 2013. (Cited on pages 133 and 134.)

[Lamm 1966] A.Uno Lamm. *The peculiarities of high-voltage dc power transmission.* IEEE Spectrum, vol. 3, no. 8, pages 76–84, Aug 1966. (Cited on page 3.)

[Lee 2000] Dong-Choon Lee, G-Myoung Lee and Ki-Do Lee. *DC-bus voltage control of three-phase AC/DC PWM converters using feedback linearization.* IEEE Transactions on Industry Applications, vol. 36, no. 3, pages 826–833, May 2000. (Cited on pages 34 and 48.)

[Lee 2003] Tzann-Shin Lee. *Input-output linearization and zero-dynamics control of three-phase AC/DC voltage-source converters.* IEEE Transactions on Power Electronics, vol. 18, no. 1, pages 11–22, Jan 2003. (Cited on pages 94 and 115.)

[Li 2010] Shuhui Li, T.A. Haskew and Ling Xu. *Control of HVDC Light System Using Conventional and Direct Current Vector Control Approaches.* IEEE Transactions on Power Electronics, vol. 25, no. 12, pages 3106–3118, Dec 2010. (Cited on pages 8 and 9.)

[Li 2014] Xiaolin Li, Zhichang Yuan, Jiao Fu, Yizhen Wang, Tao Liu and Zhe Zhu. *Nanao multi-terminal VSC-HVDC project for integrating large-scale wind generation.* In IEEE PES General Meeting, pages 1–5, Jul 2014. (Cited on pages 3 and 11.)

[Liang 2009] Jun Liang, O. Gomis-Bellmunt, J. Ekanayake and N. Jenkins. *Control of multi-terminal VSC-HVDC transmission for offshore wind power.* In The 13th European Conference on Power Electronics and Applications, pages 1–10, Sep 2009. (Cited on page 10.)

[Liang 2011] Jun Liang, Tianjun Jing, Oriol Gomis-Bellmunt, Janaka Ekanayake and Nicholas Jenkins. *Operation and control of multiterminal HVDC transmission for offshore wind farms.* IEEE Transactions on Power Delivery, vol. 26, no. 4, pages 2596–2604, 2011. (Cited on page 11.)

[Lie 2008] X Lie, B.W. Williams and Y Liangzhong. *Multi-terminal DC transmission systems for connecting large offshore wind farms.* In IEEE Power and Energy Society General Meeting - Conversion and Delivery of Electrical Energy in the 21st Century, pages 1–7, Jul 2008. (Cited on pages 11, 34 and 62.)

[Lindberg 1994] A. Lindberg and L. Lindberg. *Inner current loop for large voltage low switching frequency.* In Fifth International Conference on Power Electronics and Variable-Speed Drives, pages 217–222, Oct 1994. (Cited on pages 8, 9 and 41.)

[Lindberg 1996] A. Lindberg and T. Larsson. *PWM And Control Of Three Level Voltage Source Converters In An Hvdc Back-to-back Station.* In Sixth International Conference on AC and DC Power Transmission, pages 297–302, Apr 1996. (Cited on pages 8, 9 and 41.)

[Livermore 2010] L. Livermore, Jun Liang and J. Ekanayake. *MTDC VSC Technology and its applications for wind power.* In The 45th International Universities Power Engineering Conference (UPEC), pages 1–6, Aug 2010. (Cited on page 8.)

[Long 2007] W. Long and S. Nilsson. *HVDC transmission: yesterday and today.* IEEE Power and Energy Magazine, vol. 5, no. 2, pages 22–31, Mar 2007. (Cited on page 2.)

[Lu 2003] Weixing Lu and Boon-Teck Ooi. *Optimal acquisition and aggregation of offshore wind power by multiterminal voltage-source HVDC.* IEEE Transactions on Power Delivery„ vol. 18, no. 1, pages 201–206, Jan 2003. (Cited on page 10.)

[Lu 2005] Weixing Lu and Boon-Teck Ooi. *Premium quality power park based on multi-terminal HVDC.* IEEE Transactions on Power Delivery„ vol. 20, no. 2, pages 978–983, Apr 2005. (Cited on page 10.)

[Mariethoz 2014] S. Mariethoz, A. Fuchs and M. Morari. *A VSC-HVDC Decentralized Model Predictive Control Scheme for Fast Power Tracking.* IEEE Transactions on Power Delivery„ vol. 29, no. 1, pages 462–471, Feb 2014. (Cited on page 9.)

[Marino 1985] Riccardo Marino. *High-gain feedback in non-linear control systems.* International Journal of Control, vol. 42, no. 6, pages 1369–1385, 1985. (Cited on pages 133 and 134.)

[Marino 1988] R Marino and Petar V Kokotovic. *A geometric approach to nonlinear singularly perturbed control systems.* Automatica, vol. 24, no. 1, pages 31–41, 1988. (Cited on page 133.)

[Marques 2011] M. Marques, R. Castro and M.E. Almeida. *Connection of offshore wind parks: HVAC and HVDC-LCC links with STATCOM.* In The 11th International Conference on Electrical Power Quality and Utilisation (EPQU), pages 1–6, Oct 2011. (Cited on page 5.)

[Martinez 2007] I. Martinez, A.R. Messina and V. Vittal. *Normal Form Analysis of Complex System Models: A Structure-Preserving Approach.* IEEE Transactions on Power Systems, vol. 22, no. 4, pages 1908–1915, November 2007. (Cited on page 133.)

[Middlebrook 1976] R. D. Middlebrook and S. Cuk. *A general unified approach to modeling switching-converter power stages.* In Power Electronics Specialists Conference, pages 73–86, Cleveland, Ohio, 1976. (Cited on page 28.)

[Mier 2012] V Mier, PG Casielles, J Koto and Lorenzo Zeni. *Voltage margin control for offshore multi-use platform integration.* In The International Conference on Renewable Energies and Power Quality (ICREPQ'12), 2012. (Cited on page 10.)

[Mohan 2003] N. Mohan and Tore M Undeland. Power electronics: Converters, applications, and design. John Wiley & Sons Inc, 2003. (Cited on pages 19 and 40.)

[Moharana 2010] A. Moharana and P.K. Dash. *Input-Output Linearization and Robust Sliding-Mode Controller for the VSC-HVDC Transmission Link.* IEEE Transactions on Power Delivery, vol. 25, no. 3, pages 1952–1961, Jul 2010. (Cited on page 48.)

[Nakajima 1999] T. Nakajima and Shoichi Irokawa. *A control system for HVDC transmission by voltage sourced converters.* In IEEE Power Engineering Society Summer Meeting, volume 2, pages 1113–1119, 1999. (Cited on page 10.)

[Narendra 2012] Kumpati S Narendra and Anuradha M Annaswamy. Stable adaptive systems. Courier Corporation, 2012. (Cited on page 109.)

[Network 2012] Renewable Energy Policy Network. *(2011).* Renewables 2011 Global Status Report, 2012. (Cited on page 7.)

[Noguchi 1998] T. Noguchi, H. Tomiki, S. Kondo and I. Takahashi. *Direct power control of PWM converter without power-source voltage sensors.* IEEE Transactions on Industry Applications, vol. 34, no. 3, pages 473–479, May 1998. (Cited on pages 8 and 40.)

[Ohnishi 1991] T. Ohnishi. *Three phase PWM converter/inverter by means of instantaneous active and reactive power control.* In International Conference on Industrial Electronics, Control and Instrumentation, volume 1, pages 819–824, Oct 1991. (Cited on pages 8 and 40.)

[Ooi 1990] B. T Ooi and X. Wang. *Voltage angle lock loop control of the boost type PWM converter for HVDC application.* IEEE Transactions on Power Electronics,, vol. 5, no. 2, pages 229–235, Apr 1990. (Cited on page 8.)

[Ortega 2002] R. Ortega, M.W. Spong, F. Gomez-Estern and G. Blankenstein. *Stabilization of a class of underactuated mechanical systems via interconnection and damping assignment.* IEEE Transactions on Automatic Control, vol. 47, no. 8, pages 1218–1233, August 2002. (Cited on page 132.)

[Parthasarathy 1994] K. R. Parthasarathy. Basic graph theory. Tata McGraw-Hill, 1994. (Cited on pages 38 and 39.)

[Pekarek 2002] S.D. Pekarek, M.T. Lemanski and E.A. Walters. *On the use of singular perturbations to neglect the dynamic saliency of synchronous machines.* IEEE Transactions on Energy Conversion, vol. 17, no. 3, pages 385–391, September 2002. (Cited on page 133.)

[Pena 1996] R. Pena, J.C. Clare and G.M. Asher. *Doubly fed induction generator using back-to-back PWM converters and its application to variable-speed wind-energy generation.* IEE Proceedings - Electric Power Applications, vol. 143, no. 3, pages 231–241, May 1996. (Cited on page 34.)

[Peponides 1982] G. Peponides, P.V. Kokotovic and J. Chow. *Singular perturbations and time scales in nonlinear models of power systems.* IEEE Transactions on Circuits and Systems, vol. 29, no. 11, pages 758–767, November 1982. (Cited on page 133.)

[Perez 2004] M. Perez, R. Ortega and J.R. Espinoza. *Passivity-based PI control of switched power converters.* IEEE Transactions on Control Systems Technology, vol. 12, no. 6, pages 881–890, Nov 2004. (Cited on page 92.)

[Pernebo 2002] Lars Pernebo and Bengt Hansson. *Plug and play in control loop design.* Preprints Reglermöte, 2002. (Cited on page 132.)

[Petersen 2013] I.R. Petersen. *Singular Perturbation Approximations for a Class of Linear Quantum Systems.* IEEE Transactions on Automatic Control, vol. 58, no. 1, pages 193–198, January 2013. (Cited on page 133.)

[Pinto 2011] R.T. Pinto, S.F. Rodrigues, P. Bauer and J. Pierik. *Comparison of direct voltage control methods of multi-terminal DC (MTDC) networks through modular dynamic models.* In Proceedings of the 14th European Conference on Power Electronics and Applications, pages 1–10, Aug 2011. (Cited on page 10.)

[Pinto 2013] R.T. Pinto, P. Bauer, S.F. Rodrigues, E.J. Wiggelinkhuizen, J. Pierik and B. Ferreira. *A Novel Distributed Direct-Voltage Control Strategy for Grid Integration of Offshore Wind Energy Systems Through MTDC Network.* IEEE Transactions on Industrial Electronics, vol. 60, no. 6, pages 2429–2441, Jun 2013. (Cited on pages 10 and 11.)

[Poullain 2001] S. Poullain, F. Heliodore, A. Henni, J.L. Thomas and E. Courbon. *Modelling of the dynamic characteristics of the DC line for VSC transmission scheme.* In Seventh International Conference on AC-DC Power Transmission, pages 305–310, Nov 2001. (Cited on page 3.)

[Prieto-Araujo 2011] E. Prieto-Araujo, F.D. Bianchi, A. Junyent-Ferre and O. Gomis-Bellmunt. *Methodology for Droop Control Dynamic Analysis of Multiterminal VSC-HVDC Grids for Offshore Wind Farms.* IEEE Transactions on Power Delivery, vol. 26, no. 4, pages 2476–2485, Oct 2011. (Cited on pages 10, 11, 36 and 174.)

[Rashed 2008] M. Rashed, S.M.A. El-Anwar and F.M.H. Youssef. *Nonlinear control scheme for VSC-HVDC transmission systems.* In 12th International Middle-East Power System Conference, MEPCON 2008, pages 486–491, March 2008. (Cited on page 210.)

[Reeve 1980] J. Reeve. *Multiterminal HVDC Power Systems.* Power Apparatus and Systems, IEEE Transactions on, vol. PAS-99, no. 2, pages 729–737, Mar 1980. (Cited on page 6.)

[Riverso 2013] S. Riverso, M. Farina and G. Ferrari-Trecate. *Plug-and-Play Decentralized Model Predictive Control for Linear Systems.* IEEE Transactions on Automatic Control, vol. 58, no. 10, pages 2608–2614, October 2013. (Cited on page 132.)

[Rodrigues 2013] S. Rodrigues, R.T. Pinto, P. Bauer and J. Pierik. *Optimal Power Flow Control of VSC-Based Multiterminal DC Network for Offshore Wind Integration in the North Sea.* IEEE Journal of Emerging and Selected Topics in Power Electronics, vol. 1, no. 4, pages 260–268, Dec 2013. (Cited on page 11.)

[Rogersten 2014] R. Rogersten, Lidong Zhang and P. Mitra. *Applying power-synchronization control in a multi-terminal DC system.* In IEEE PES General Meeting | Conference Exposition„ pages 1–5, Jul 2014. (Cited on page 10.)

[Ruan 2007] Si-Ye Ruan, Guo-Jie Li, Xiao-Hong Jiao, Yuan-Zhang Sun and TT Lie. *Adaptive control design for VSC-HVDC systems based on backstepping method.* Electric Power Systems Research, vol. 77, no. 5, pages 559–565, 2007. (Cited on page 109.)

[Rudervall 2000] Roberto Rudervall, JP Charpentier and Raghuveer Sharma. *High voltage direct current (HVDC) transmission systems technology review paper.* Energy Week, vol. 2000, 2000. (Cited on pages 2 and 5.)

[Shi 2015] Xiaojie Shi, Zhiqiang Wang, Bo Liu, Yiqi Liu, L.M. Tolbert and F. Wang. *Characteristic Investigation and Control of a Modular Multilevel Converter-Based HVDC System Under Single-Line-to-Ground Fault Conditions.* IEEE Transactions on Power Electronics„ vol. 30, no. 1, pages 408–421, Jan 2015. (Cited on page 11.)

[Siemens 2005] Siemens. *High Voltage Direct Current-Proven Technology for Power Exchange.* Siemens publication, 2005. (Cited on pages 2 and 17.)

[SIEMENS 2014] SIEMENS. *HVDC benefits.* http://www.energy.siemens.com/br/en/power-transmission/hvdc/applications-benefits.htm, 2014. (Cited on page 6.)

[Simon 1962] Herbert A Simon. *The architecture of complexity.* In the American Philosophical Society, 1962. (Cited on page 133.)

[Slotine 1991] Jean-Jacques E Slotine and Weiping Li. Applied nonlinear control. Prentice-Hall Englewood Cliffs, NJ, 1991. (Cited on page 48.)

[Sood 2010] V. Sood and H. Patel. *Comparison between direct and vector control strategy for VSC-HVDC system in EMTP-RV.* In International Conference on Power Electronics, Drives and Energy Systems (PEDES), pages 1–6, Dec 2010. (Cited on pages 8, 9, 40 and 41.)

[Spong 1994] Mark W Spong. *The control of underactuated mechanical systems.* 1st International Conference on Mechatronics, January 1994. (Cited on pages 132, 134 and 137.)

[Spong 1995] M.W. Spong. *The swing up control problem for the Acrobot.* IEEE Control Systems Magazine, vol. 15, no. 1, pages 49–55, February 1995. (Cited on page 132.)

[Stendius 2006] L. Stendius and P. Jones. *The challenges of offshore power system construction-bringing power successfully to Troll A, one of the worlds largest oil and gas platform.* In The 8th IEE International Conference on AC and DC Power Transmission, pages 75–78, Mar 2006. (Cited on page 3.)

[Stijn 2010] COLE Stijn. *Steady-state and dynamic modelling of VSC HVDC systems for power system Simulation.* PhD thesis, Katholieke University Leuven, Belgium, 2010. (Cited on pages 19 and 40.)

[Teel 2003] A.R. Teel, L. Moreau and D. Nesic. *A unified framework for input-to-state stability in systems with two time scales.* IEEE Transactions on Automatic Control, vol. 48, no. 9, pages 1526–1544, September 2003. (Cited on page 133.)

[Thallam 1992] R.S. Thallam. *Review of the design and performance features of HVDC systems connected to low short circuit ratio AC systems.* IEEE Transactions on Power Delivery,, vol. 7, no. 4, pages 2065–2073, Oct 1992. (Cited on page 23.)

[Thomas 2001] J.L. Thomas, S. Poullain and A. Benchaib. *Analysis of a robust DC-bus voltage control system for a VSC transmission scheme.* In Seventh International Conference on AC-DC Power Transmission, pages 119–124, Nov 2001. (Cited on page 8.)

[Tokiwa 1993] Yukio Tokiwa, Fumitoshi Ichikawa, Kenichi Suzuki, Haruhisa Inokuchi, Syunichi Hirose and Kazuaki Kimura. *Novel control strategies for HVDC system with self-contained converter.* Electrical engineering in Japan, vol. 113, no. 5, pages 1–13, 1993. (Cited on page 10.)

[Trzynadlowski 1996] A.M. Trzynadlowski. *An overview of modern PWM techniques for three-phase, voltage-controlled, voltage-source inverters.* In Proceedings

of the IEEE International Symposium on Industrial Electronics, volume 1, pages 25–39, Jun 1996. (Cited on pages 4 and 19.)

[Van Hertem 2005] D. Van Hertem, J. Verboomen, R. Belmans and W.L. Kling. *Power flow controlling devices: an overview of their working principles and their application range.* In International Conference on Future Power Systems, Nov 2005. (Cited on page 25.)

[Varley 2004] James Varley. *HVDC fifty years on.* Modern Power Systems, vol. 24, pages 18–20, Oct 2004. (Cited on pages 3 and 4.)

[Wang 2011] Feng Wang, Lina Bertling, Tuan Le, Anders Mannikoff and Anders Bergman. *An overview introduction of VSC-HVDC: State-of-art and potential applications in electric power systems.* In Cigrè International Symposium, Bologna, Italy, Sept. 2011., 2011. (Cited on page 4.)

[Wang 2014a] Wenyuan Wang and M. Barnes. *Power Flow Algorithms for Multi-Terminal VSC-HVDC With Droop Control.* IEEE Transactions on Power Systems, vol. 29, no. 4, pages 1721–1730, Jul 2014. (Cited on pages 10, 174 and 181.)

[Wang 2014b] Wenyuan Wang, A. Beddard, M. Barnes and O. Marjanovic. *Analysis of Active Power Control for VSC-HVDC.* IEEE Transactions on Power Delivery, vol. 29, no. 4, pages 1978–1988, Aug 2014. (Cited on page 10.)

[Winkelman 1980] James R Winkelman, Joe H Chow, John J Allemong and Petar V Kokotovic. *Multi-time-scale analysis of a power system.* Automatica, vol. 16, no. 1, pages 35–43, 1980. (Cited on page 133.)

[Wollard 1988] K. Wollard. *Uno Lamm: inventor and activist.* Spectrum, IEEE, vol. 25, no. 3, pages 42–45, Mar 1988. (Cited on page 3.)

[Xiang 2015] B. Xiang, Z. Liu, Y. Geng and S. Yanabu. *DC Circuit Breaker Using Superconductor for Current Limiting.* IEEE Transactions on Applied Superconductivity, vol. 25, no. 2, pages 1–7, Apr 2015. (Cited on page 11.)

[Xin 2010] H. Xin, D. Gan, M. Huang and K. Wang. *Estimating the stability region of singular perturbation power systems with saturation nonlinearities: an linear matrix inequalitybased method.* Control Theory Applications, IET, vol. 4, no. 3, pages 351–361, March 2010. (Cited on page 133.)

[Xu 1998] X Xu, RM Mathur, J Jiang, GJ Rogers and P Kundur. *Modeling of generators and their controls in power system simulations using singular perturbations.* IEEE Transactions on Power Systems, vol. 13, no. 1, pages 109–114, 1998. (Cited on page 133.)

[Xu 2000] X. Xu, R.M. Mathur, J. Jiang, G.J. Rogers and P. Kundur. *Modeling effects of system frequency variations in induction motor dynamics using*

singular perturbations. IEEE Transactions on Power Systems, vol. 15, no. 2, pages 764–770, May 2000. (Cited on page 133.)

[Xu 2005] Lie Xu, B.R. Andersen and P. Cartwright. *VSC transmission operating under unbalanced AC conditions - analysis and control design.* IEEE Transactions on Power Delivery,, vol. 20, no. 1, pages 427–434, Jan 2005. (Cited on page 8.)

[Xu 2007a] Lie Xu, Liangzhong Yao and Christian Sasse. *Grid Integration of Large DFIG-Based Wind Farms Using VSC Transmission.* IEEE Transactions on Power Systems, vol. 22, no. 3, pages 976–984, Aug 2007. (Cited on pages 11 and 34.)

[Xu 2007b] Lie Xu, Dawei Zhi and Liangzhong Yao. *Direct Power Control of Grid Connected Voltage Source Converters.* In IEEE Power Engineering Society General Meeting, pages 1–6, Jun 2007. (Cited on page 9.)

[Xu 2011] L. Xu and L. Yao. *DC voltage control and power dispatch of a multi-terminal HVDC system for integrating large offshore wind farms.* IET Renewable Power Generation,, vol. 5, no. 3, pages 223–233, May 2011. (Cited on page 10.)

[Yang 2011] Chunyu Yang, Qingling Zhang, Jing Sun and Tianyou Chai. *Lur'e Lyapunov Function and Absolute Stability Criterion for Lur'e Singularly Perturbed Systems.* IEEE Transactions on Automatic Control, vol. 56, no. 11, pages 2666–2671, November 2011. (Cited on page 133.)

[Young 1977] Kar-Keung D Young, Petar V Kokotovic and Vadim I Utkin. *A singular perturbation analysis of high gain feedback systems.* In Joint Automatic Control Conference, numéro 14, pages 1270–1277, 1977. (Cited on page 133.)

[Zakaria Moustafa 2008] M.M. Zakaria Moustafa and S. Filizadeh. *Simulation of a VSC transmission scheme supplying a passive load.* In 34th Annual Conference of IEEE Industrial Electronics, pages 942–946, Nov 2008. (Cited on pages 9, 24, 25, 35 and 41.)

[Zervos 2009] A Zervos, C Kjaer, S Azau, J Scola and J Quesada. *Pure power–wind energy targets for 2020 and 2030.* European Wind Energy Association, vol. 250, 2009. (Cited on page 8.)

[Zhang 2010] Lidong Zhang, Lennart Harnefors and H.-P. Nee. *Power-Synchronization Control of Grid-Connected Voltage-Source Converters.* IEEE Transactions on Power Systems, vol. 25, no. 2, pages 809–820, May 2010. (Cited on page 9.)

[Zhang 2011a] Lidong Zhang, Lennart Harnefors and H.-P. Nee. *Interconnection of Two Very Weak AC Systems by VSC-HVDC Links Using Power-Synchronization Control.* IEEE Transactions on Power Systems,, vol. 26, no. 1, pages 344–355, Feb 2011. (Cited on page 9.)

[Zhang 2011b] Lidong Zhang, Lennart Harnefors and H.-P. Nee. *Modeling and Control of VSC-HVDC Links Connected to Island Systems.* Power Systems, IEEE Transactions on, vol. 26, no. 2, pages 783–793, May 2011. (Cited on page 9.)

[Zhang 2011c] Lidong Zhang, H.-P. Nee and Lennart Harnefors. *Analysis of Stability Limitations of a VSC-HVDC Link Using Power-Synchronization Control.* IEEE Transactions on Power Systems,, vol. 26, no. 3, pages 1326–1337, Aug 2011. (Cited on page 12.)

[Zhang 2012] Lirong Zhang, Yi Wang and Heming Li. *Coordinated control of MTDC-based microgrid with wind turbines.* In The 7th International Power Electronics and Motion Control Conference (IPEMC), volume 3, pages 2076–2080, Jun 2012. (Cited on page 10.)

[Zhao 2013] Xiaodong Zhao and Kang Li. *Control of VSC-HVDC for wind farm integration based on adaptive backstepping method.* In IEEE International Workshop on Intelligent Energy Systems (IWIES),, pages 64–69, Nov 2013. (Cited on page 9.)

[Zhi 2007] Dawei Zhi and Lie Xu. *Direct Power Control of DFIG With Constant Switching Frequency and Improved Transient Performance.* IEEE Transactions on Energy Conversion,, vol. 22, no. 1, pages 110–118, Mar 2007. (Cited on page 9.)

[Zhi 2009] Dawei Zhi, Lie Xu and B.W. Williams. *Improved Direct Power Control of Grid-Connected DC/AC Converters.* IEEE Transactions on Power Electronics,, vol. 24, no. 5, pages 1280–1292, May 2009. (Cited on page 9.)

[Zonetti 2014] Daniele Zonetti, Romeo Ortega and Abdelkrim Benchaib. *Modeling and Control of High-Voltage Direct-Current Transmission Systems: From Theory to Practice and Back.* Automatica, 2014. (Cited on page 94.)